

University College London

**The Development of Novel Vorapaxar
Analogues as Topical Protease Activated
Receptor-1 Antagonists for the Treatment of
Idiopathic Pulmonary Fibrosis**

Emily Knight

Submitted in partial fulfilment of the requirements for the degree of

Doctor of Philosophy

Declaration

I, Emily Knight, confirm that the work presented in this thesis is my own. Where information has been derived from other sources, I confirm that this has been indicated in the thesis.

Emily Knight

July 2015

Abstract

The overall aim of this project was to design and synthesise novel Protease Activated Receptor-1 (PAR-1) inhibitors in order to develop a novel treatment for Idiopathic Pulmonary Fibrosis (IPF). After finding the commercially available, allosteric PAR-1 inhibitor, "Q94" inactive and insoluble, focus switched to making novel vorapaxar analogues. A newly published synthetic route towards himbacine was successfully adapted to give vorapaxar analogues with a C-9-keto group. These were shown to have moderate potency against PAR-1 in a FLIPR calcium flux assay. After further synthetic route optimisation and investigation another novel vorapaxar analogue was identified. Compound (-)-**94** was shown to be the most potent of the series of compounds tested, achieving an IC_{50} of 27 nM. In the same assay vorapaxar gave an IC_{50} of 13 nM. This makes (-)-**94** a novel, potent, PAR-1 inhibitor worthy of further investigation and development as a potential IPF drug.

Table of Contents

Declaration.....	2
Abstract.....	3
Table of Contents.....	4
Acknowledgements.....	6
Abbreviations	7
Chapter 1: Introduction	11
Idiopathic Pulmonary Fibrosis	11
Diagnosis, Epidemiology and Pathogenesis	11
Past and Present Treatments	13
Protease Activated Receptor-1.....	18
Activation and Signalling.....	18
PAR-1 and Disease	22
Protease Activated Receptor-1 Inhibitors	24
RWJ-58259.....	24
Atopaxar (E5555).....	27
Vorapaxar (SCH 530348)	31
Other Series.....	39
Allosteric Inhibitors.....	47
Project Aims	52
Chapter 2: Q94 Synthesis and Testing	53
Introduction.....	53
Synthesis.....	53
Biological Results and Discussion.....	54
Conclusions and Updated Aims	56

Chapter 3: Vorapaxar Analogues.....	57
Introduction.....	57
Atopaxar Synthesis.....	57
Vorapaxar Synthesis.....	59
Novel Synthesis of Himbacine	62
Vorapaxar SAR.....	63
New Project Aims	64
Results and Discussion	65
Vorapaxar Analogues with Smaller Head Groups.....	65
Synthesis	65
Biological Results and Discussion.....	68
C-9 Substituted Vorapaxar Analogues.....	71
Synthesis	71
Proof of Concept	77
Computational Modelling	79
Optimisation	84
Biological Testing	92
Investigations Towards an Alternative Route.....	102
Chapter 4: Conclusions and Future Work	107
Experimental	110
Chapter 2.....	110
General Experimental	110
Chapter 3.....	113
General Experimental	113
Biology	191
References.....	193

Acknowledgements

My supervisor, Professor Stephen Caddick, gave me the opportunity to carry out this research, and for that I'd like to thank him. Huge appreciation also goes to our collaborators Professor Rachel Chambers and Graham Inglis who gave useful guidance and enthusiasm during the research.

I'd like to offer thanks for all of the support from the members of the Caddick Group, KLB 230 and KLB 237 labs who gave great encouragement during the lows, and helped celebrate the highs. This made my time in the lab all the more enjoyable. Special thanks go to Vijay Chudasama, Rachel Morgen and Eifion Robinson who gave invaluable advice throughout my research and kindly proof read my thesis. I'd like to thank GSK for allowing me to spend a year researching at the Stevenage site. Consequently, all those in the GSK Fibrosis DPU who welcomed and encouraged me require thanking.

Dr Natalia Smoktunowicz and Dr Manuela Plate deserve my gratitude for their huge assistance with the biological work. Thanks should also go to Dr Abil Aliev and the GSK NMR team for their assistance with NMR. A further thank you goes to Lisa Haigh, Eifion Robinson and Kersti Karu who helped with mass spectrometry throughout my PhD. Finally, thank you to Sam Ranasinghe for support with the FLIPR instrument and Xiao Lewell without whom the computational studies would not have been possible.

Lastly, I'd like to thank my family and friends who have supported me, patiently listened to my rants and believed in me; I don't think I'd have made it without you!

Abbreviations

AC = Adenylate cyclase

ACS = Acute coronary syndrome

$[\alpha]_D$ = Optical rotation

AD-mix- β = A mixture of (DHQD)₂PHAL, potassium osmate, potassium ferricyanide and K₂CO₃

ADME = Absorption, distribution, metabolism and excretion

AECs = Alveolar epithelial cells

AV = Arteriovenous

Bn = Benzyl

b.p. = Boiling point

CAD = Coronary artery disease

CCL2 = Chemokine ligand 2

CYP = Cytochrome P450

cAMP = Cyclic adenosine monophosphate

DA = Diels Alder

DBU = 1,8-Diazabicyclo[5.4.0]undec-7-ene

DCC = *N,N*-Dicyclohexylcarbodiimide

DIPA = Diisopropylamine

DIPEA = Diisopropylethylamine

DL_{CO} = Diffusion capacity

DMAP = 4-*N,N*-Dimethylaminopyridine

DME = Dimethoxyethane

DMF = *N,N*-Dimethylformamide

DMSO = Dimethyl sulfoxide

EDCI = *N*-(3-Dimethylaminopropyl)-*N'*-ethylcarbodiimide hydrochloride

ee = Enantiomeric excess

E_{max} = Maximum agonist effect

ELISA = Enzyme-linked immunosorbent assay

ES = Electrospray

FGFR = Fibroblast growth factor receptor

FLIPR = Fluorescence Imaging Plate Reader
Fmoc = Fluorenylmethyloxycarbonyl
FVC = Forced vital capacity
GPCR = G-Protein Coupled Receptors
G-proteins = Guanine nucleotide-binding proteins
GSK = GlaxoSmithKline
h = Hour(s)
h = Human
H8 = Helix 8
ha = High-affinity
HATU = 1-[Bis(dimethylamino)methylene]-1H-1,2,3-triazolo[4,5-b]pyridinium 3-oxide hexafluorophosphate
H-bond = Hydrogen-bond
HEK = Human embryonic kidney (cells)
HLF = Human lung fibroblasts
HMDS = Hexamethyldisylazane
HPLC = High-performance liquid chromatography
HRCT = High-Resolution Computed Tomography
HRMS = High-resolution mass spectrometry
IC₅₀ = Half maximal inhibitory concentration
ILDs = Interstitial lung diseases
IMDA = Intramolecular Diels-Alder
IP₃ = Inositol trisphosphate
IPF = Idiopathic pulmonary fibrosis
i-PrOH = Isopropanol
IR = Infrared (spectroscopy)
IV = Intravenous
KO*t*-Bu = Potassium *tert*-butoxide
LCMS = Liquid chromatography-mass spectrometry
LDA = Lithium diisopropylamine
LiHMDS = Lithium hexamethyldisylazane

LTMP = Lithium tetramethylpiperidine
LTOT = Long-term oxygen therapy
M = Molecular ion
m = Murine
m- = *meta-*
MACEs = Major adverse cardiovascular events
MDAP = Mass directed auto-purification
2-MeTHF = 2-Methyltetrahydrofuran
MI = Myocardial infarctions
min = Minute(s)
MIRC = Michael-Initiated Ring Closure
MLF = Mouse lung fibroblasts
mRNA = Messenger Ribonucleic acid
mTOR = Mammalian target of rapamycin
m/z = Mass/charge
NAC = *N*-Acetylcysteine
NBS = *N*-Bromosuccinimide
n-BuLi = *normal*-Butyl lithium
NMR = Nuclear magnetic resonance (spectroscopy)
o- = *ortho-*
OCT-2 = Organic cation transporter-2
p- = *para-*
PAR = Protease activated receptor
 pA_2 = Measure of the potency of an antagonist. It is the negative logarithm of the molar concentration of an antagonist that would produce a 2-fold shift in the concentration response curve for an agonist.
PBS = Phosphate buffered saline
PCI = Percutaneous coronary intervention
PdCl₂(dppf) = [1,1'-Bis(diphenylphosphino)ferrocene]dichloropalladium
PDGFR = Platelet-derived growth factor receptor
PD = Pharmacodynamics

Pet. Ether = Petroleum ether

PI = Phosphoinositide

PK = Pharmacokinetics

pK_b = The negative logarithm of the K_b value. K_b is the dissociation constant for a radiolabeled drug determined by saturation analysis. It is the molar concentration of radioligand which, at equilibrium, occupies 50% of the receptors.

PKC = Protein kinase C

PLC- β = Phospholipase C- β

RF = Relative fluorescence

Rt. = Retention time

RT = Room temperature

SAR = Structure activity relationship

sec = Second(s)

$t_{1/2}$ = Half-life

t-BME = *tert*-Butyl methyl ether

t-BuLi = *tert*-Butyl lithium

t-BuOH = *tert*-Butanol

TFA = Trifluoroacetic acid

TGF- β = Transforming growth factor- β

THF = Tetrahydrofuran

TLC = Thin layer chromatography

T_{max} = Time to maximal concentration

TMP = 2,2,6,6-Tetramethylpiperidine

TRAPs = Thrombin Receptor Activating Peptides

UIP = Usual interstitial pneumonia

UV = Ultraviolet

VEGFR = Vascular endothelial growth factor receptor

Chapter 1: Introduction

Idiopathic Pulmonary Fibrosis

Diagnosis, Epidemiology and Pathogenesis

Idiopathic pulmonary fibrosis (IPF) is the most common of the interstitial lung diseases (ILDs); a family of over 200 diseases that affect the interstitial tissue in the lung. It is chronic, progressive and characterised by scarring on the lung that gives rise to a honeycomb like texture and a poor gas exchange surface¹. As the name suggests there is no known cause so it is only diagnosed once other interstitial lung diseases have been ruled out.² However, there are several factors that have been associated with the diagnosis of IPF. Smoking has been shown to increase the risk of IPF, along with a work environment that exposes you to wood, metal, textile or stone dust.³ Finally, it has recently been suggested that some of the cases of IPF could be re-diagnosed as asbestosis.

IPF and asbestosis both show symptoms of shortness of breath during everyday activities, a dry persistent cough and, in some cases, clubbing of the fingers. Further, their progression can both be tracked by a decline in forced vital capacity (FVC). The main difference is that in asbestosis the fibrosis is focussed around asbestos fibres⁵ whilst in IPF there is no obvious cause. IPF can now be diagnosed based on a High-Resolution Computed Tomography (HRCT)² of the lung. This shows a characteristic histopathologic pattern in IPF lungs, known as usual interstitial pneumonia (UIP) (Figure 1). HRCT is a non-invasive scan making it a preferable diagnostic tool, in comparison to diagnosis by lung biopsy. Fortunately, there are certain characteristics that, in some cases, can mark a difference between IPF and asbestosis.^{6,7} Despite this, asbestosis is still often only diagnosed if the patient reports known asbestos exposure.⁸ This neglects the possibility of unknown asbestos exposure.⁹ A study which looked into the regional distribution of IPF and asbestosis diagnosis found that there were higher mortality rates, caused by IPF, in areas with a history of shipyard work. Around shipyards there would be

increased potential for unknown exposure to asbestos.¹⁰ This supports the idea that some of the IPF diagnoses could actually be asbestosis.

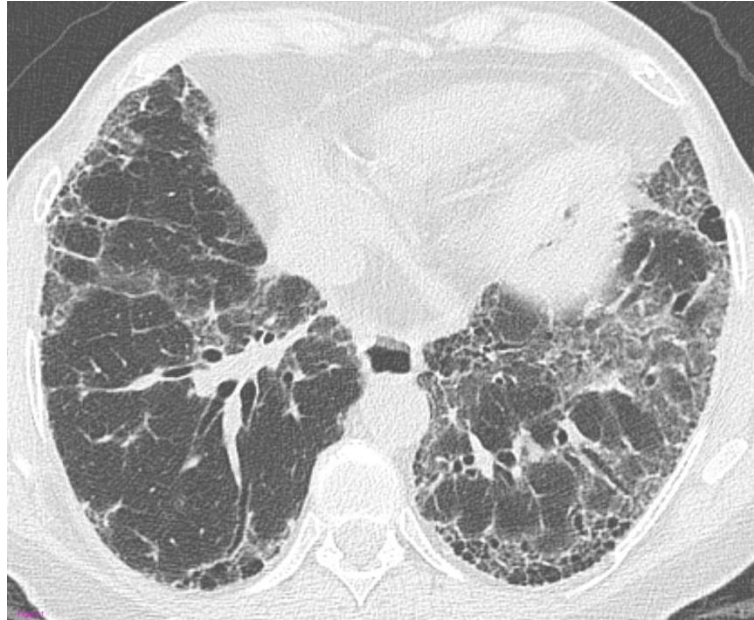


Figure 1: Transverse high-resolution computed tomography (HRCT) image of IPF lung showing the characteristic usual interstitial pneumonia (UIP) pattern.¹¹

The potential mis-diagnosis of asbestosis as IPF highlights two issues. One, that the fibrotic response, seen with IPF, is observed in other related diseases and, two, that IPF is very difficult to diagnose.¹² Consequently, the prevalence of IPF stated in different sources varies. A recent study suggested that there are over 5000 new cases of IPF a year in the UK alone. This may not sound like very many but, considering that the average life expectancy is only 3-5 years (post-diagnosis), it means that more people in the UK will die from IPF per year than from ovarian cancer, leukaemia, lymphoma or several other cancers. Further, the number of diagnoses is still on the increase.¹³

Evidently, IPF is a growing concern. The post-diagnosis life expectancy is shorter than for many cancers whilst the prevalence, in some cases, is greater. Finally, the quality of life for sufferers is very poor. As a consequence, one may expect that there would already be a reasonable treatment for IPF available. Sadly, this is not

the case. Further, IPF research does not receive much in the way of funding, especially in comparison to the billions spent on cancer related studies.¹⁴ Despite this, over the last 15 years there has been a huge increase in the understanding of the pathogenesis of IPF, and consequently, a rise in the number of potential drugs reaching clinical trials.

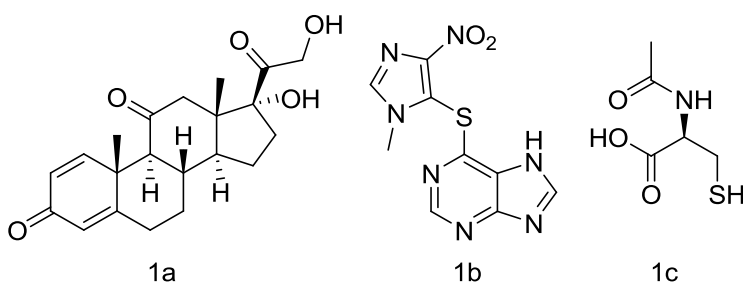
It was previously hypothesised that IPF was initiated by an inflammatory response in the lungs, as is the case for many of the non-IPF ILDs.¹⁵ However, it is now thought that IPF results from an aberrant wound healing process. The type I alveolar epithelial cells (AECs), which line most alveolar surfaces, are thought to be damaged upon lung epithelial injury. In the healthy lung, type I AECs regulate pulmonary structural mesenchymal cells. However, when they are damaged, type II AECs proliferate to cover the basement membrane and avoid alveolar collapse. The type II AECs should then undergo controlled apoptosis or differentiate into type I AECs.¹⁶

It is thought that in the diseased state the type II AECs undergo uncontrolled apoptosis and release pro-fibrotic compounds, such as transforming growth factor- β (TGF- β). The dying type II AECs can also attract fibroblasts which are known to differentiate into α -smooth muscle actin-expressing myofibroblasts. The end result is secretion of collagen, and other extra-cellular matrix proteins, which can be deposited at the site of injury.¹⁷ It is at this stage that the inflammatory response is thought to be initiated, attracting monocytes, macrophages and fibrocytes, which develop the fibrosis further. The dense collection of myofibroblasts and scarring create a “fibroblastic foci” around which, it is thought, AECs remain abnormal, helping to explain the fast rate of disease progression.¹⁸

Past and Present Treatments

In the past, glucocorticoids or immunosuppressive agents had been used to treat IPF, guided by the outdated belief that IPF was initiated by inflammation. Typically

a dual therapy of prednisone (Compounds **1a**) and azathioprine (Compounds **1b**) or a triple therapy of prednisone, azathioprine and *N*-acetylcysteine (NAC) (Compounds **1c**) were given.¹⁹ Prednisone is an immunosuppressing synthetic corticosteroid used to treat certain inflammatory diseases and in high doses certain cancers.²⁰ Azathioprine is an immunosuppressing purine analogue frequently used in organ transplant and for treating auto-immune diseases.²¹ Finally, NAC is a cysteine derivative which in itself is a mucolytic agent but is also a precursor to glutathione.²² Glutathione is an important anti-oxidant agent in the lung that becomes depleted in IPF patients which potentially allows oxidative stress mediated AEC injury. Small scale studies had shown that orally administered NAC increased the concentration of glutathione in the lung.²³



Compounds **1a**, **b** and **c**: Prednisone, Azathioprine and *N*-Acetylcysteine; combine to give the triple therapy.

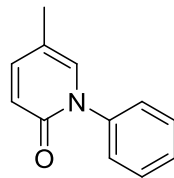
The Idiopathic Pulmonary Fibrosis International Group Exploring *N*-Acetylcysteine I Annual (IFIGENIA) study was the original clinical trial which tested the triple therapy. The triple therapy was compared to the dual therapy because, at the time, that was the standard IPF treatment. It led to a significant reduction in absolute FVC and a decline in diffusion capacity (DL_{CO}) suggesting that it was more effective than the dual therapy.²⁴ Nevertheless, the study was criticised as (i) there was no placebo arm, (ii) the results had not been replicated and (iii) few patients completed the year-long study.²⁵

The prednisone, azathioprine, and *N*-acetylcysteine: a study that evaluates response in idiopathic pulmonary fibrosis (PANTHER-IPF) clinical trial compared

the triple therapy with NAC mono-therapy and to a placebo. The triple therapy arm of this trial was terminated early due to an excess in the number of deaths, hospitalisations, and serious adverse events among patients.²⁶ This was pretty conclusive and stopped the prescription of immunosuppressants to IPF patients. The monotherapy and placebo arms were continued until study completion. Unfortunately, the recent results showed that NAC was no more effective than a placebo for reducing IPF development or decreasing the number of deaths.²⁷

The IFIGENIA study had been the first clinical trial to show a positive result for an IPF treatment. The negative results of the follow-up PANTHER-IPF trial gave the conclusion that immunosuppressants and NAC, like many other drugs that had been trialled for the treatment of IPF, were actually not effective. Warfarin (an anticoagulant) showed increased mortality.²⁸ everolimus [a mammalian target of rapamycin (mTOR) inhibitor] gave increased disease progression²⁹ and bosentan and macitentan (dual endothelin receptor antagonists) showed no significant results in comparison to placebo.³⁰ These are just a few examples of the unsuccessful therapy options trialled; nevertheless, it highlights how difficult IPF is to treat.

Until 2008, there were no drugs registered for the specific treatment of IPF. Patients were either given the dual or triple therapy or long-term oxygen therapy (LTOT). LTOT does nothing to the rate of disease progression but it helps to reduce the hypoxemia and thus increases the patients' quality of life.³¹ The final treatment option was to have a lung transplant which may not always be viable.³² Not only would there be long transplant waiting lists, but IPF is a seriously debilitating disease that usually affects 60-70 year olds. As a consequence, having an operation could be very risky for the patient. In 2008, however, pirfenidone (Compound 2) was registered as the first IPF treatment in Japan.³³



2

Compound 2: Pirfenidone

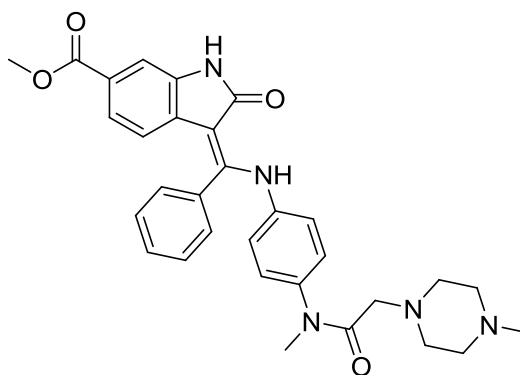
Pirfenidone is a small molecule which acts to reduce fibroblast proliferation, reduce the production of TGF- β , TGF- α and interleukin 1- β and inhibit collagen production promoted by TGF- β . This gives it anti-fibrotic and anti-inflammatory properties.³⁴ It was developed by several companies; InterMune Inc. in the US, Shionogi Ltd. in Japan and GNI Group Ltd in China. Pirfenidone was registered in Japan in 2008, but, was only approved in China and Europe in 2011.^{35,36} The delayed approvals were prompted by the publishing of the results of the phase III, multinational, randomised, double-blind, placebo-controlled trials; Clinical Studies Assessing Pirfenidone in IPF: Research of Efficacy and Safety Outcomes 1 and 2 (CAPACITY 1 and 2), results which prompted the delayed approvals.

The results from the trials were slightly conflicting. CAPACITY 1 met its desired primary end-point, showing that pirfenidone slowed the decline in FVC when compared to placebo. CAPACITY 2, unfortunately, failed to meet this primary end-point, but did show improvements in some of the secondary end-points.³⁷ A final phase III trial was conducted to try and confirm the efficacy of pirfenidone. The Assessment of Pirfenidone to Confirm Efficacy and Safety in Idiopathic Pulmonary Fibrosis (ASCEND) study confirmed that pirfenidone is effective at increasing progression-free survival in IPF patients.³⁸ The supporting data from the extra study was enough to warrant FDA approval in the US.³⁹

The success of the clinical trials and the growing market of pirfenidone should be good news to IPF sufferers. Regrettably, the patients who received the drug on the trial reported no improvements in how they felt. Further, pirfenidone causes gastrointestinal upset and skin photosensitisation. These side-effects were enough

to cause drug discontinuation in some of the study patients.⁴⁰ Clearly, pirfenidone is a step in the right direction but it is not the solution. Inhalable pirfenidone is being investigated to try and overcome the photosensitisation issue but there is still clearly room for improvement.⁴¹

Whilst InterMune were battling to get US approval for pirfenidone,⁴² Boehringer Ingelheim were racing to get their IPF drug to the market. Nintedanib (Compound **3**) targets and inhibits tyrosine kinases that act as growth factor receptors, especially platelet-derived growth factor receptor (PDGFR), fibroblast growth factor receptor (FGFR) and vascular endothelial growth factor receptor (VEGFR).⁴³ These have all been shown to contribute to the pathogenesis of pulmonary fibrosis.⁴⁴ Subsequently, nintedanib has been shown in two parallel, randomised, double-blind, placebo-controlled, phase III clinical trials (INPULSIS-1 and -2) to reduce the rate of decline of FVC over a 52 week trial period.⁴⁵ In other words, both trials met their primary end point, along with most of their secondary end-points.



3

Compound **3**: Nintedanib

Nintedanib, although behind pirfenidone in coming to market, appears to offer superior treatment. Unlike pirfenidone, nintedanib shows no significant side-effects except for diarrhoea. Moreover, in one of the INPULSIS trials, the patients' quality of life was said to be improved, based on a St George's Respiratory Questionnaire.⁴⁶ However, neither drug can claim to reverse the progression of IPF. A small Biotech, Fibrinogen, is planning further phase II trials for FG-3019.

This is after the initial data from one phase II trial which showed FG-3019 to reverse the fibrotic process based on forced vital capacity measurements and quantitative HRCT.⁴⁷ FG-3019 is an antibody which targets connective tissue growth factor (CTGF). CTGF can induce excess fibrosis in combination with TGF- β .⁴⁸ Therefore, inhibiting CTGF can slow down the progression of fibrosis explaining the results seen with FG-3019. This is exciting progress for the field of IPF treatment.

It is clear that there has been an expansion in IPF research. The understanding of how the disease is initiated and develops has advanced considerably. As a result, the standard pharmaceutical treatment that would have been given 10 years ago has been discontinued. In its place many potential drug candidates that target different receptors within the vast and complicated disease pathway have been trialled. As a result, pirfenidone has recently come to market as the first specific IPF drug, whilst nintedanib is likely to be approved for the treatment of IPF in the US within the next year. Despite all of this, there is still room for further research, as evidenced by Fibrinogen investing heavily on their novel antibody treatment, FG-3019.⁴⁹

Protease Activated Receptor-1

Activation and Signalling

The research presented in this thesis pertains to the protease activated receptor-1 (PAR-1). PAR-1 belongs to a family of 7-transmembrane G-Protein Coupled Receptors (GPCRs) which were first cloned in 1991.⁵⁰ There are currently four subclasses known, three of which; PAR-1, PAR-3 and PAR-4, are primarily activated by the protease thrombin.⁵¹ PAR-2, on the other hand, is typically agonised by trypsin. Thrombin has long been known as an important mediator in the coagulation pathway. Activation of this pathway is essential, upon tissue injury, to limit blood loss by promoting the formation of a fibrin clot. It was only in the last 20 years that it was shown that thrombin exhibited its pro-coagulation effects,

along with its inflammation mediation and tissue repair, through the activation of PAR-1. As can be expected, PARs exist throughout the body and some cells express more than one type of PAR. Furthermore, PAR distribution appears to be species specific.

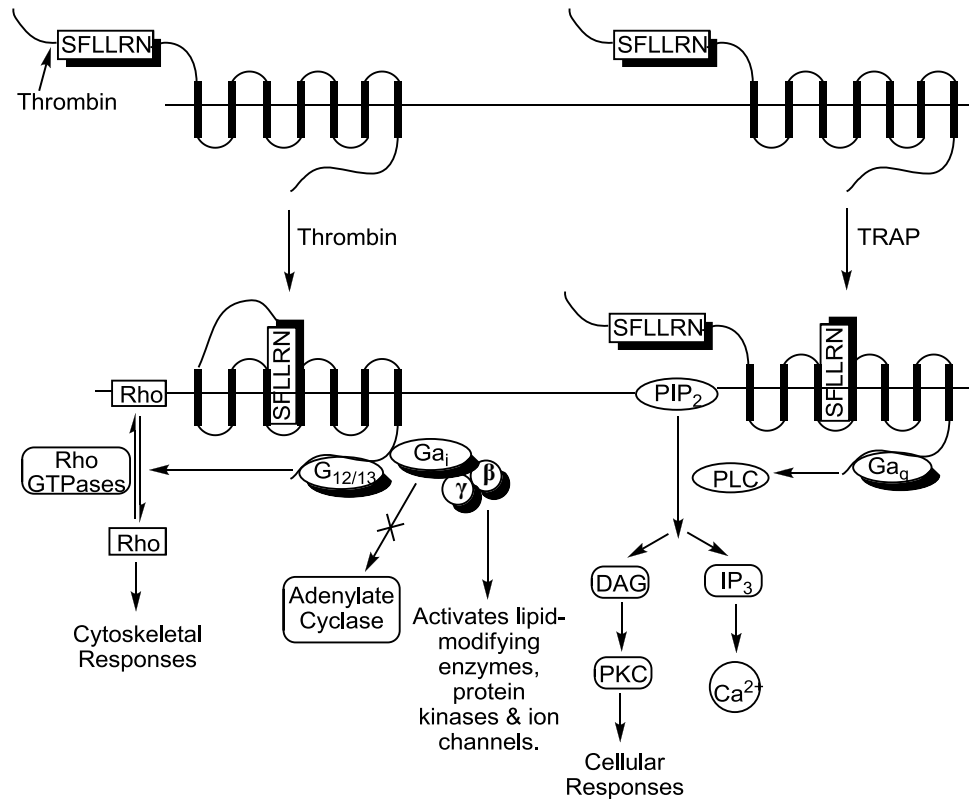


Figure 2: PAR-1 Signalling Pathways. LHS: Thrombin activated PAR-1- G_{12/13} preferentially activated. RHS: TRAP activated PAR-1- G_q preferentially activated All modes of activation are available in both cases.

The discovery of the PARs uncovered a novel mode of receptor activation. In the case of PAR-1, thrombin binds to the specific amino acid sequence LPDR⁴¹-S⁴² found on the N-terminal. Upon binding, it cleaves the amide bond between R⁴¹ and S⁴² leaving a new extracellular N-terminus. This acts as a tethered ligand by wrapping around to the PAR-1 active site (Figure 2).⁵² The affinity and potency of thrombin to PAR-1 is increased by a secondary interaction. This interaction is between the anion-binding exosite I, found on thrombin, and an acidic region, termed the “hirudin-like” domain, found on the PAR-1 N-terminus. Experimentally, PARs can be agonised by short peptide chains which are based around the

specific tethered ligand amino acid sequence. These are known as Thrombin Receptor Activating Peptides (TRAPs). Once activated, PAR-1 can couple to one of three classes of guanine nucleotide-binding proteins (G-proteins); $G_{\alpha_{12/13}}$, G_{α_q} or G_{α_i} . Evidence suggests that the mode of PAR-1 activation can influence which G-protein is coupled. Thrombin activation tends to lead to $G_{\alpha_{12/13}}$ association whilst using TRAP as the agonist will give predominantly G_{α_q} coupling.⁵³

The activated G-proteins can initiate many different signalling pathways (Figure 2). The $G_{\alpha_{12}}$ and $G_{\alpha_{13}}$ subunits stimulate Rho GTPases which can cause shape changes in platelets and increase permeability and migration of endothelial cells. The G_{α_q} subunits can activate phospholipase C- β (PLC- β) causing the hydrolysis of phosphoinositide (PI) and subsequent mobilisation of calcium (Ca^{2+}) stores. In addition protein kinase C (PKC) can be activated by G_{α_q} to give cellular responses such as granule secretion, integrin activation and platelet aggregation. The G_{α_i} subunits act to promote platelet response by inhibiting adenylate cyclase (AC). Further, the $G_{\beta\gamma}$ subunits, which are released from all of the G-protein subtypes, can alone activate a range of lipid-modifying enzymes, protein kinases and ion channels. Finally, the activated PAR-1 itself can cause the liberation of receptor tyrosine kinase ligands which can affect receptors associated with cell growth and differentiation.⁵³

It is becoming increasingly evident that the process of PAR activation is more complicated than originally thought. Although activation can occur *via* the tethered ligand, or using a TRAP, it is now clear that PARs can exist as dimers or oligomers and thus activate their partner intermolecularly or act as co-factors. This in turn can modulate the receptor response often by effecting which signalling pathway is activated. Human (h)PAR-1-PAR-1 homodimerisation has been observed; equally, hPAR-1 can also form heterodimers with hPAR-2, hPAR-3 and hPAR-4.⁵⁴

An experiment was carried out on an hPAR-1 homodimer made up of one signalling deficient receptor and one thrombin-resistant receptor. Normal

downstream signalling was shown when the mutant homodimers were stimulated with thrombin. This means that the thrombin-generated tethered ligand, on the receptor which could not itself signal, must have intermolecularly bound to the tethered ligand active site on the partner receptor to elicit a response. Naturally, the intermolecular agonism was less efficient than the standard intramolecular mechanism of activation; nevertheless, the type of downstream signalling did not appear to be affected.⁵² On the other hand, in the case of hPAR-1-hPAR-2 heterodimerisation, hPAR-2 could also be intermolecularly activated by the PAR-1 tethered ligand but the activated heterodimer conveyed different downstream signalling effects to those seen with monomeric hPAR-1 activation. An example of the modulated signalling can be seen in the pathogenesis of sepsis. In early phase sepsis, thrombin promotes vascular disruption *via* the PAR-1 activation of $G\alpha_{12/13}$ and $G\alpha_q$ signalling; whereas, in late stage sepsis, thrombin activation of PAR-1 results in a PAR-2 downstream effect; Rac1 signalling. This suggests that the heterodimer offers increased functionality for thrombin activated PAR-1.⁵⁵ Heterodimerisation between hPAR-1 and hPAR-3 seems to cause activated PAR-1 to preferentially couple to $G\alpha_{13}$, in other words PAR-3 acts to modulate the activity of PAR-1.⁵⁶ Finally, hPAR-1-hPAR-4 heterodimers appear to allow co-factorisation.⁵⁷

The first example of PARs acting as co-factors was shown in mice. Murine (m) platelets express both mPAR-3 and mPAR-4, but not mPAR-1. PAR-3, like PAR-1, has the “hirudin-like” domain giving it high affinity for thrombin; PAR-4, on the other hand, does not. As a consequence, monomeric PAR-4 can only be activated in the presence of high concentrations of thrombin. However, it has been shown that, whilst mPAR-3 cannot cause thrombin-induced platelet activation and aggregation alone, when it is co-expressed with mPAR-4 low concentrations of thrombin can elicit platelet activation.⁵⁸ It was later shown that thrombin remains bound to the “hirudin-like” site, on cleaved mPAR-3, with its active site free, thus allowing the N-terminus, on the dimerised mPAR-4, to be subsequently cleaved.⁵⁹

On human platelets there are also two types of PAR expressed; hPAR-1 and hPAR-4. These appear to also act as co-factors. Unlike mPAR-3, hPAR-1 can cause platelet activation, independently, at low concentrations of thrombin; whilst, monomeric hPAR-4 still requires high concentrations of thrombin to elicit a response. However, when co-expressed with hPAR-1, activated by thrombin but inhibited by a TRAP mimetic (RWJ-56110; Compound 5), hPAR-4 can be activated with low concentrations of thrombin. During the process of determining the specific contributions of each of the PARs, throughout platelet activation, it was shown that there was a rapid increase of intracellular Ca^{2+} upon thrombin activation of hPAR-1. Interestingly, this was followed by a sustained Ca^{2+} flux response mediated by hPAR-4. Further, hPAR-4 was shown to sustain other secondary signalling responses essential for late phase platelet aggregation.⁵⁷ This suggests that hPAR-4 has the important role of prolonging thrombin induced platelet activation, *via* hPAR-1-hPAR-4 co-factoring, rather than just being a PAR-1 back-up, as was originally hypothesised.⁶⁰

PAR-1 and Disease

The extensive network of PAR-1 signalling pathways associates the receptor with a wide variety of disease states. Some of the lesser explored disease implications include the link between the PAR-1 gene and the genetic disorder 5q syndrome and the role of PAR-1 in cancer and in some neurological disorders.⁵⁰ The most explored medical implication of the PAR-1 cascades involves the formation of thrombi. Thrombi are blood clots that reside in the blood vessels blocking blood flow. They may lead to further complications such as acute coronary syndrome (ACS), atherosclerosis or restenosis; the re-occlusion of blood vessels following invasive surgery.

Anticoagulants such as warfarin, which inhibit thrombin directly, and antiplatelets like aspirin and clopidogrel, which inhibit platelet aggregation, have been used therapeutically to block the formation of thrombi.⁶¹ However, these medicines tend

to be non-selective and thus inhibit the homeostatic function of thrombin causing unwanted side-effects such as excessive off-target bleeding. Consequently, in the last 10 years, there has been a huge drive towards developing PAR-1 antagonists to treat the formation of arterial thrombi. PAR-1 inhibitors are predicted to be selective for a variety of reasons. For one, arterial thrombi are platelet rich giving rise to target selectivity due to the extensive role of PAR-1 in platelet aggregation. Moreover, PAR-1 is up-regulated in atherosclerotic plaques and, following vascular injury, in vascular smooth muscle cells. This increases the concentration of target receptors at the therapeutic site.⁶²

Idiopathic pulmonary fibrosis (IPF) involves lung inflammation and fibrosis following lung injury. It has been shown in knockout mice studies that PAR-1 was associated with fibrosis formation. It was seen that PAR-1 deficient mice were protected from bleomycin-induced pulmonary fibrosis.⁶³ PAR-1 is responsible for the rapid proliferation of fibroblasts along with the overproduction of extracellular matrix proteins.⁶⁴ These are both associated with the pathophysiology of pulmonary fibrosis. Further, as PAR-1 is associated with many activation pathways which give rise to profibrotic effects, such as cell migration and the secretion of profibrotic growth factors and cytokines, it follows that, in the absence of PAR-1, the fibrotic response will not be activated.

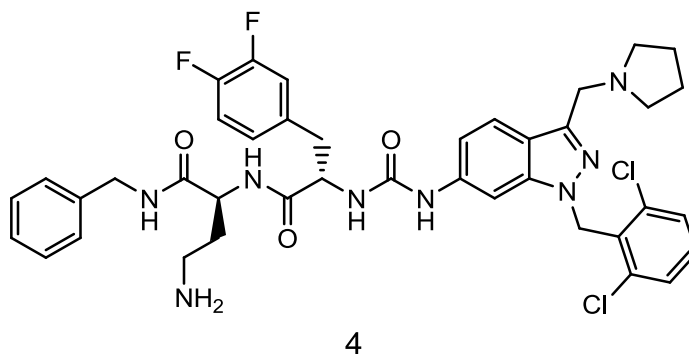
Many of the potential drug candidates for IPF treatment target proteins downstream of PAR-1. However, the knockout mouse study highlights PAR-1 as a potential therapeutic target in itself. This is further supported by a study which showed that P1pal-12 limited the development of bleomycin-induced pulmonary fibrosis in mice.⁶⁵ P1pal-12 is a peptidase that blocks the interaction between PAR-1 and the relevant G-protein, explaining its inhibitory effects. PAR-1 is expressed in endothelium and in smooth muscle, both of which are found in the lung airways. Additionally, primary adult lung fibroblasts, and human pulmonary artery endothelial cells, also express PAR-1. Finally, it has been shown that PAR-1 expression is up-regulated in inflammatory pulmonary diseases.⁶⁶ In combination,

these factors make PAR-1 a promising drug target for the selective treatment of IPF.

Protease Activated Receptor-1 Inhibitors

There have been a number of PAR-1 inhibitors developed; however, to the best of our knowledge, none for the treatment of IPF. PAR-1 inhibitors have been used as research tools to help determine the biological pathways through which PAR-1 gives its effects. Furthermore, several PAR-1 inhibitors have been evaluated in drug trials, predominantly, as target specific arterial antithrombotic agents. The most successful of these inhibitors has recently made it to market. Detailed below are some of the notable, literature PAR-1 inhibitors.

RWJ-58259



Compound 4: RWJ-58259

One of the earliest effective PAR-1 inhibitors was developed by Johnson and Johnson. RWJ-58259 (Compound **4**) was designed as a mimetic for the PAR-1 tethered ligand amino acid sequence, Ser-Phe-Leu-Leu-Arg-Asn (SFLLRN). During the development process, the tethered ligand sequence was computationally modelled to find the lowest energy conformations. The results gave rise to the three-point receptor binding model (Figure 3). This dictated that the distance between the amino terminus, the benzene ring of the phenylalanine and the central carbon of the arginine guanidine group was important.⁶⁷

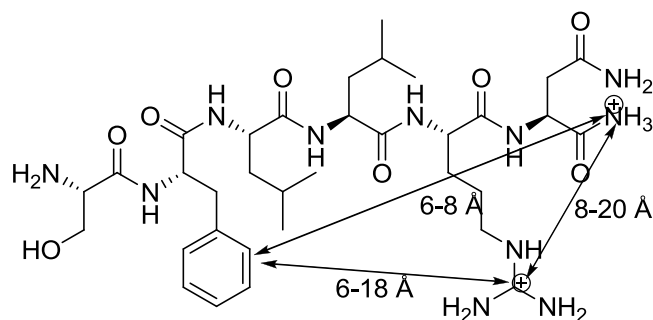
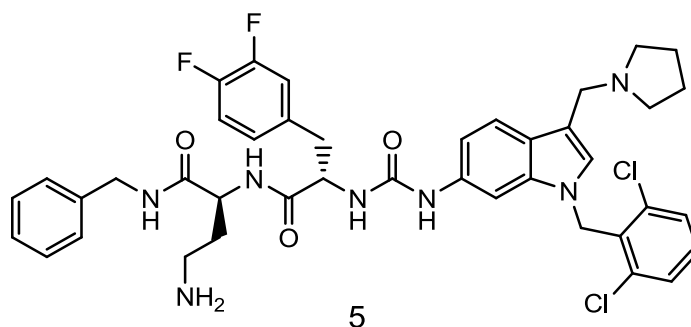


Figure 3: SFLLRN and the three-point binding model.

The series, which culminated in RWJ-58259, started with a 6-amino linked indole scaffold. The indole scaffold displayed a spatial arrangement which fulfilled the three-point receptor binding model.⁶⁷ Following an extensive optimisation programme, which highlighted several significant structure activity relationships, the compound RWJ-56110 (Compound **5**) was deemed a lead compound. Unfortunately, like some of the other early indole compounds, it displayed hypotensive effects when tested in guinea pigs.⁶⁸ This led to the indole being replaced by an indazole to finally give RWJ-58259.



Compound **5**: RWJ-56110

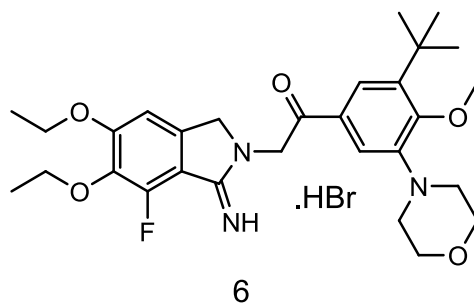
RWJ-56110 and RWJ-58259 showed comparable inhibition of thrombin induced human platelet aggregation (IC_{50} = 34 and 37 μ M respectively). RWJ-58259, however, was better in most other respects. It showed improved PAR-1 binding in a binding assay previously developed by Johnson and Johnson (IC_{50} = 15 μ M), improved potency in a rat aortic smooth muscle cell Ca^{2+} mobilization assay (IC_{50} =

0.07 μM) and in a rat vascular smooth muscle cell proliferation assay ($\text{IC}_{50} = 2.3 \mu\text{M}$).⁶⁹ Importantly, it also showed an improved toxicity profile in relation to the hypotensive effects seen with the indole compounds.

In order to further develop the pre-clinical data profile for RWJ-58259 it was assessed in a number of different animal models. In a rat arterial balloon-injury model it showed a dose dependent reduction in neointimal thickness. On the other hand, the results were insignificant for the arteriovenous (AV) shunt, and the photochemically-induced thrombosis models, when conducted in guinea pigs. This was thought to reflect the additional presence of PAR-3 and PAR-4 found on guinea pig platelets.⁷⁰ Finally, RWJ-58259 was tested using an electrolytic injury-induced carotid thrombosis model in cynomolgus monkeys. Cynomolgus monkeys have a similar PAR-1 expression pattern to humans thus providing a very relevant model. Intravenously administered RWJ-58259 was shown to significantly reduce the time it took to form an occlusive thrombus in this model. Further, there was roughly a three-fold reduction in the relative area made up of platelets. Better still, it did not alter the composition of the blood or effect coagulation.

The positive biological results would lead one to believe that RWJ-58259 would have been a suitable drug candidate. However, it is not orally bio-available which would limit it to use for acute treatments after events such as heart attack or stroke. In addition, there is some evidence to suggest that it has a very short half-life ($t_{1/2}$). It was shown to be rapidly metabolized in an *in vitro* human liver microsome assay giving a $t_{1/2}$ of only 9.2 min. It showed a slightly improved $t_{1/2}$ of 30 min in rats following IV administration.⁷¹ These drawbacks made it unviable as a therapeutic drug. Still, given that it was amongst the first of the PAR-1 inhibitors, it received widespread use as a research tool. It was, and still is, used as a positive control for early stage target validation. Additionally, the development of suitable biological and animal models helped pave the way to better PAR-1 inhibitors.

Atopaxar (E5555)



Compound **6**: Atopaxar

Atopaxar (Compound **6**) is a 2-aminopyrrolidine derivative, developed by Eisai, which displays potent oral PAR-1 inhibition. There does not appear to be significant literature regarding the early development of atopaxar. The structure was claimed in a patent filed in 2002.⁷² It can be assumed that the scaffold, which led to atopaxar, was found *via* a high throughput screen. This is owing to the fact that the 2-aminopyrrolidine scaffold is a common motif found in drug compounds. The patent literature shows thousands of example structures. This suggests that a vast library of 2-aminopyrrolidine derivatives were synthesised and tested allowing the structure activity relationship (SAR) at most positions to be explored before the structure of atopaxar was finally decided upon as a viable drug candidate.

Atopaxar was evaluated in many of the same pre-clinical tests used with RWJ-58259. In most respects it showed a better profile. It inhibited thrombin induced, human platelet, aggregation with an IC_{50} of 64 nM; this makes it 1000 times more efficient than RWJ-58259. Equally, atopaxar was found to inhibit the binding of [³H]-high-affinity (ha) TRAP to PAR-1, in human platelet membranes, with a 1000 times greater potency (IC_{50} = 19 nM). The fact that atopaxar competes with TRAP suggests that it, like RWJ-58259, must bind at or close to the tethered-ligand binding site.

In the rat smooth muscle cell proliferation assay atopaxar exhibited an IC_{50} value of 0.16 μ M.⁷³ This makes it about 15 times more potent than RWJ-58259, in this model. Atopaxar, like RWJ-58259, showed a significant reduction in neointimal

formation in the rat arterial balloon-injury model.⁷⁴ However, unlike RWJ-58259, a 100 mg/kg oral dosing of atopaxar prolonged the arterial occlusion time 2.4-fold, in comparison to the vector alone, in the guinea pig photochemically-induced thrombosis model. Importantly, it gave this result without increasing bleed time or effecting coagulation.⁷⁵ These results led Eisai to believe that atopaxar had the potential to treat arterial thrombosis in humans.

Atopaxar had shown great potential in animal studies. The next stage was to assess the safety and pharmacodynamics (PD) within humans. The first phase I study had three randomly assigned groups of twelve healthy volunteers. The participants of each group received a once daily dose of 50, 100 or 200 mg atopaxar, or the placebo equivalent, over a period of 14 days. The results from this study showed atopaxar to have a T_{max} of 3.5 h, a $t_{1/2}$ of 23 h and to reach a steady state after 11 days. Further, there was significant *ex vivo* platelet aggregation inhibition and no adverse side-effects at all dose concentrations.⁷⁶

A second slightly larger phase I trial was conducted. In this study there were eight randomly assigned groups of eight healthy male volunteers. Five of the groups received a single oral dose of 20, 50, 100, 200 or 400 mg of atopaxar. The final three groups were randomly assigned to receive a once daily oral dose of 50, 100 or 200 mg atopaxar over a period of 10 days. Some of the volunteers, within the repeated dose groups, were randomly assigned to receive a placebo giving a double-blind, placebo-controlled trial. The inhibitory effect on platelet aggregation was determined *ex vivo*. It was found that in all but the 20 mg dosing thrombin induced platelet aggregation was inhibited by over 80%. Furthermore, in the repeated dose groups, it was seen that this inhibitory effect was maintained with subsequent dosing. Even at 24 h after dosing 100% inhibition of platelet aggregation was observed in those receiving repeat doses of 100 or 200 mg atopaxar. This highlighted the long $t_{1/2}$ shown by atopaxar. Importantly, atopaxar again appeared to be well tolerated at all doses and showed no changes in coagulation time and bleeding time.⁷⁷

The success of the phase I trials led Eisai to progress atopaxar to assess it in a larger population in Phase II trials. They completed two dual-arm, multicentre, randomised, double-blind, placebo-controlled studies. The first; Japanese-Lessons From Antagonizing the Cellular Effects of Thrombin (J-LANCELOT) recruited 504 Japanese patients.⁷⁸ One arm of the study was made up of 241 patients who had ACS. The remaining patients had high-risk coronary artery disease (CAD) and were assigned to the second arm. The patients in the J-LANCELOT-ACS arm were randomized into one of four dose groups; placebo, 50, 100 or 200 mg atopaxar. The patients were given once daily dosing, for 12 weeks following a 400 mg load dose or placebo equivalent. The patients in the J-LANCELOT-CAD arm were randomized into the same dosing groups but did not receive the load dose and were treated for 24 weeks rather than for 12. The trial therapy was given in addition to the patients' personal standard of care which, in 75% of the cases, was the dual therapy of aspirin and clopidogrel. In both groups, the primary end-point was the number of bleed events, the secondary end-point was the number of major adverse cardiovascular events (MACEs) and finally, an *ex vivo*, aggregation assessment was performed. The results showed no significant difference in the incidence of bleed events between each of the dose groups suggesting that atopaxar does not cause off target bleeding. There was also no significant difference in the occurrence of MACEs thus, unfortunately, providing no evidence for the efficacy of atopaxar. Finally, the aggregation assessments reflected the positive results found in the phase I trials.

The second phase II trial was conducted outside of Japan, using the same study protocol, but a larger study population; 603 and 720 in the LANCELOT-ACS and LANCELOT-CAD arms respectively. Again, there was no significant difference in the number of bleed events, or MACEs, between all of the dose groups. Of moderate concern was the observation of up-regulated liver enzymes; alanine and aspartate aminotransferase, and dose-related prolongation of the corrected QT interval, seen in both clinical trials. In summary, the results from the phase II trials

highlighted a few potential safety concerns and, due to the insufficient population size, did not show conclusive efficacy. It was concluded that a phase III trial would be needed to determine whether the significant results in the aggregation measurements could correlate to a real clinical effect.

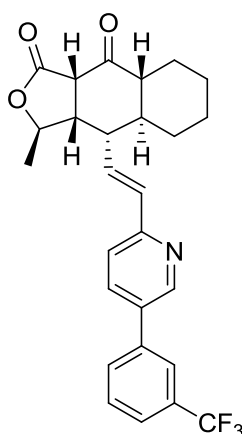
Since the completion of the phase II trials there have been a few further investigations using atopaxar. Two smaller clinical trials have been conducted assessing drug-drug interactions in healthy subjects. The first was between atopaxar and diltiazem (NCT01261156); a drug commonly used to treat hypertension and angina.⁷⁹ More importantly, diltiazem is a mild cytochrome P450 3A4 (CYP3A4) inhibitor. Since, atopaxar is mainly metabolised by CYP3A4, this study was largely focused on the effects diltiazem had on the pharmacokinetics (PK) and PD of atopaxar. The second trial showed the interactions between atopaxar and metformin (NCT01241669); an oral anti-diabetic drug used to treat type II diabetes.⁸⁰ Metformin, is a superior organic cation transporter-2 (OCT-2) substrate.⁸¹ OCT-2 is the major cation transporter protein in the kidney so this study was primarily designed to determine the effects of atopaxar on renal function. However, the study was also being used to determine the effects of atopaxar on metformin PD. The results from these studies, although complete, have yet to be published. However, as patients with ACS or CAD are likely to suffer from hypertension, angina and/or type II diabetes, the results would greatly influence the decisions made by Eisai regarding the progression of atopaxar. The results may even promote a change in utility if atopaxar slowed the clearance of metformin.

The results from the pre-clinical data suggested that, not only did atopaxar inhibit PAR-1 associated platelet aggregation; it also inhibited non-PAR-1 related platelet activation. To gain fuller appreciation of the inhibitory effects of atopaxar an *in vitro* study was conducted. The study used the blood of healthy volunteers, who had several cardiovascular risk factors, and of patients with known CAD. The CAD patients were either receiving a single therapy of aspirin or a dual therapy of aspirin and clopidogrel; the standard treatment options for CAD. The blood was used to

conduct a series of tests for standard platelet biomarkers. It was concluded that atopaxar exhibited moderate inhibition of platelet activation beyond that expected from direct PAR-1 blockade. Additionally, the study showed that atopaxar enhanced the anti-platelet activities of lone aspirin and combined aspirin and clopidogrel therapies. It also provided useful data for the determination of a suitable effective dose were atopaxar to be progressed to phase III clinical trials.⁸²

Despite the completion of additional post-phase II studies in 2012, Eisai discontinued the development of atopaxar. This decision would have been due to a combination of factors. The limited efficacy, shown in the phase II trials, would have left Eisai relying on significant results being shown with a larger study population. These results would be required to prove atopaxar as a useful treatment option. Further, the additional cost and patient compliance implications of having to administer atopaxar as a dual or triple therapy, with aspirin and/or clopidogrel, would have led Eisai to question the marketability. Finally, atopaxar was losing the development race with the third of the notable, literature PAR-1 inhibitors; vorapaxar.

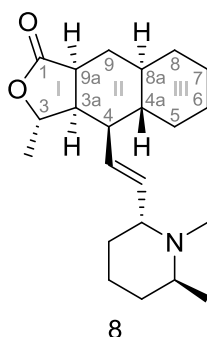
Vorapaxar (SCH 530348)



7

Compound 7: Vorapaxar

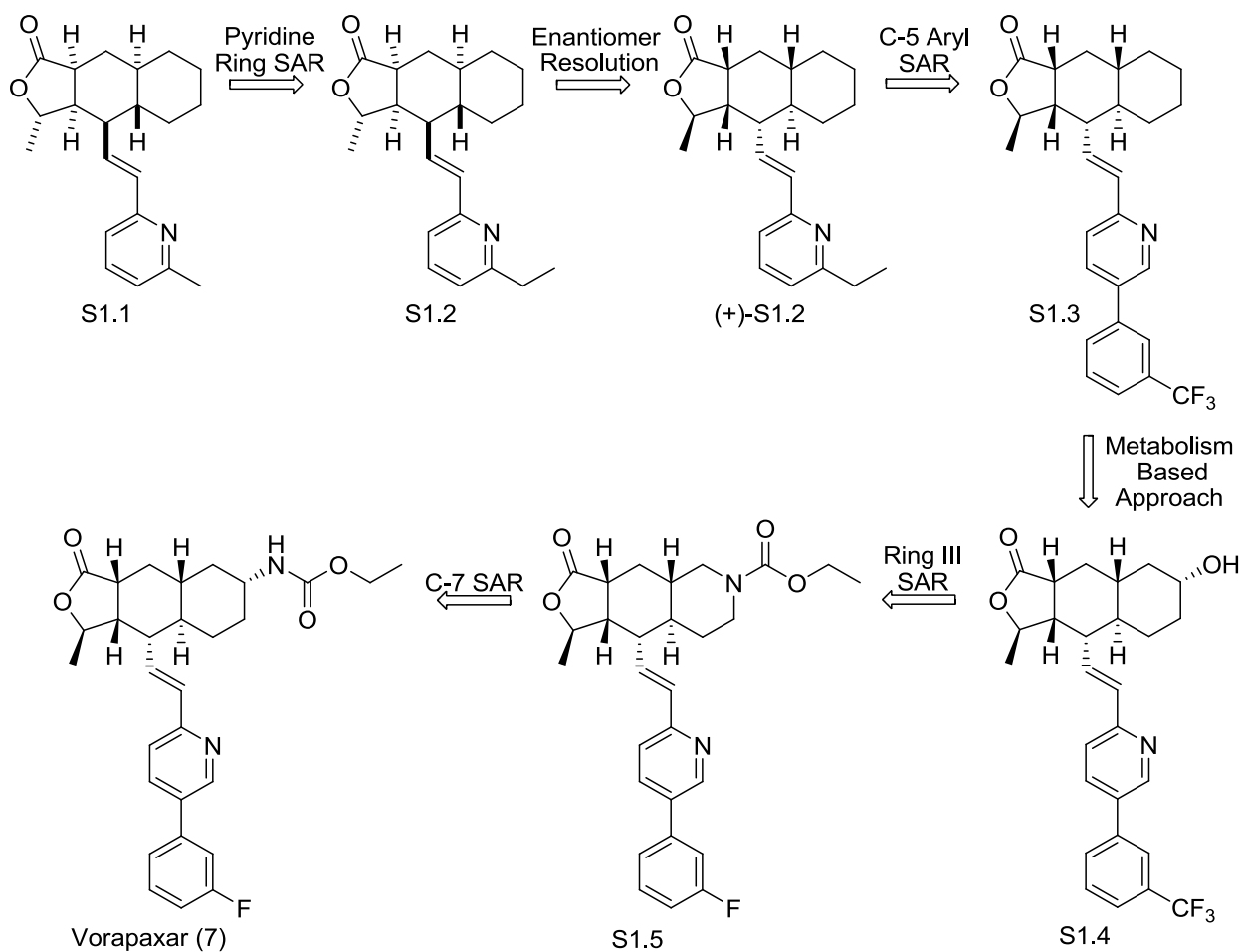
Vorapaxar (Compound **7**) was the first to market oral potent PAR-1 inhibitor. It was initially developed by Schering-Plough before Merck and Co. took them over and thus obtained the patents. Vorapaxar is a derivative of an alkaloid; himbacine (Compound **8**). Schering-Plough had a vast library of himbacine derivatives as they had shown promise for the treatment of Alzheimer's disease.⁸³ Upon screening their compound library against PAR-1, they discovered the further potential of himbacine derivatives. The series was first patented in 1999 (WO99/26943).⁸⁴



Compound **8**: Himbacine

The initial hit (**S1.1**, Scheme 1) was already more potent than RWJ-58259, competing with [³H]-ha TRAP, with an IC₅₀ of 300 nM, as opposed to 15,000 nM. Initial SAR studies, aiming to optimize the substitution on the pyridine ring, gave the ethyl derivative (**S1.2**, Scheme 1) (IC₅₀ = 85 nM). Enantiomer resolution of **S1.1** and **S1.2** provided a hugely significant SAR development. It was shown that the unnatural *ent*-himbacine scaffold was roughly ten times more potent than the natural himbacine structure. The (+)-enantiomers gave IC₅₀ of 150 and 20 nM for the methyl and ethyl derivatives, respectively. On the other hand, the (-)-enantiomers gave IC₅₀ values of 1500 and 400 nM. (+)-**S1.2** showed dose dependent inhibition of TRAP induced platelet aggregation (IC₅₀ = 70 nM) and *ex vivo* platelet aggregation in blood from cynomolgus monkeys dosed, at 10 mg/kg, with IV for 30 min. The compound was showing good potency but had a poor t_{1/2} and was not orally bioavailable.⁸⁵ Therefore, further optimization, to improve the PK, involved exploring the effects of an aromatic group at the pyridine C-5 position. Compound **S1.3** was found to be the most potent of the series (IC₅₀ = 11 nM). It

showed great potency and PK in a number of platelet aggregation and animal studies.⁸⁶ However, a 10 day enzyme induction study highlighted significant liver enzyme induction in rats; notably, CYP2B and CYP1A enzymes showed an increase of 21-fold and 3.6-fold, respectively.⁸⁷



Scheme 1: Development of Vorapaxar.

IC₅₀ (in nM) of the major compounds; **S1.1** = 300, **S1.2** = 85, **(+)-S1.2** = 20, **S1.3** = 11, **S1.4** = 17, **S1.5** = 11 and vorapaxar (**7**) = 8 nM.

In a metabolite study, the liver enzymes were shown to primarily hydroxylate at the C-8 position on ring III. There was also some C-7 hydroxylation product observed. The PAR-1 binding potencies of C-6, C-7 and C-8 hydroxy compounds were investigated giving compound **S1.4** as the most potent (IC₅₀ = 17 nM). Compound **S1.4** was still shown to mildly up-regulate liver enzymes, giving rise to di-

hydroxylated metabolites. Further SAR was completed on ring III; heteroatoms were incorporated in place of C-7 and/or C-8. Compound **S1.5** was found to be very potent ($IC_{50} = 11$ nM), had great oral bioavailability, displayed *ex vivo* platelet aggregation inhibition in a cynomolgus monkey model, was selective over other GPCRs and showed good results in a mouse enzyme induction model and a cynomolgus monkey clearance model.⁸⁸

Finally, additional SAR was completed at the C-7 region to give vorapaxar with a C-7 carbamate. Throughout much of the development process the bi-aryl portion of the compound had a *m*-CF₃ substituent. However, the final drug candidate had a *m*-fluoro substituent as it was shown to reduce the lipophilicity. Vorapaxar bound competitively and with high affinity to PAR-1 ($IC_{50} = 8.1$ nM), it also gave a long disassociation rate ($t_{1/2} = 20$ h). In an *ex vivo*, cynomolgus monkey, platelet aggregation inhibition model it gave 100% inhibition after 24 h, following an oral dosing of 0.1 mg/kg, without increasing bleed times. After 48 h considerable inhibition of platelet aggregation was still observed. Following a 1 mg/kg oral dose, to monkeys, vorapaxar exhibited a T_{max} after 1 h, 86% bioavailability and an elimination $t_{1/2}$ of 13 h. It was shown to selectively inhibit PAR-1 over other GPCRs, thrombin and TRAP over other platelet agonists and importantly gave no evidence for liver enzyme inhibition.⁸⁹

The excellent pre-clinical profile led Merck to progress vorapaxar into clinical trials. A number of phase I studies were completed to assess the safety, PK and PD of vorapaxar in healthy volunteers. In a series of phase I trials, designed to determine a suitable dosing regimen, 50 healthy volunteers were randomly allocated to receive a single, oral dose of 0.25, 1, 5, 10, 20 or 40 mg of vorapaxar, 36 subjects were allocated to receive a once daily dosing of 1, 3 or 5 mg vorapaxar for 28 days and 12 volunteers were allocated to receive a loading dose of 10 or 20 mg vorapaxar followed by a daily dosing of 1 mg for 6 days. In each of the dosing options several subjects were randomly assigned to receive placebo instead. The blood from the volunteers was used to perform several *ex vivo*, TRAP induced,

platelet aggregation studies. Dose-related inhibition was observed; a single, 5 mg, dose gave over 80% inhibition of platelet aggregation, by 12 h after administration. With a 10 mg single dose it only took 2 h to get over 80% inhibition and with the 20 and 40 mg single doses over 80% inhibition was achieved after an hour. Significantly, the inhibition was maintained for at least 72 h whilst full platelet recovery could take several months. The daily dosing studies all gave maintained inhibition of platelet aggregation of over 80% throughout the length of the study and showed up no obvious safety concerns. It was concluded from this series of phase I trials that a daily dosing of at least 1 mg would be sufficient for maintenance therapy. Additionally, a loading dose could be used in cases where a fast onset of action would be required.⁹⁰

A similar set of studies, designed to determine ethnic differences in the PK and PD of vorapaxar, randomised 50 healthy Japanese and Caucasian volunteers to receive a single, oral, dose of 5, 10, 20 or 40 mg vorapaxar and 48 subjects to receive daily, oral, dosing of 0.5, 1 or 2.5 mg of vorapaxar for 28 days. Again, *ex vivo*, TRAP-induced platelet aggregation was monitored, along with several PK, clinical and safety assessments. The platelet aggregation results supported those of the studies above with no variation observed between the ethnic groups. It was concluded that a 40 mg loading dose was best suited to give a fast onset of action, whilst, a 2.5 mg daily dose was thought to be best for chronic treatment. Again, no significant safety concerns were highlighted in this study.⁹¹

The conclusions, regarding the required therapeutic dose, were supported further by a slightly larger phase I study. In this study, 111 healthy volunteers were, again, randomly assigned to receive a single, oral, dose of 5, 10, 20 or 40 mg vorapaxar or a daily, oral, dosing of 0.5, 1 or 2.5 mg of vorapaxar, for 28 days. Again, the platelet aggregation inhibition was consistent with what had been found already providing strong evidence for the efficacy of vorapaxar. This study also noted the rapid absorption and the long mean terminal-phase $t_{1/2}$ which was shown to be 165-311 h.⁹² A further study investigating the effects of food and antacid on the PK

and PD of vorapaxar found that although food delayed the absorption of vorapaxar, it increased the exposure; whilst, antacid decreased the exposure. However, these effects were insignificant in a clinical setting. Thus, it was concluded that vorapaxar would be able to be used without thoughts to meals or antacid usage.⁹³

The results were looking very promising, and there did not seem to be any safety issues; thus Merck carried vorapaxar into phase II clinical trials. The Thrombin-Receptor Antagonist for cardiovascular event reduction in Percutaneous Coronary Interventions (TRA-PCI) (NCT00132912) trial was the largest of the phase II trials and was designed to assess the safety and tolerability of vorapaxar in patients undergoing non-urgent percutaneous coronary intervention (PCI). It was a multi-centre, international, randomised, placebo-controlled, double-blind study involving 1030 patients who were undergoing non-urgent PCI or coronary angiography with planned PCI. The patients were randomly allocated to receive an oral loading dose of 10, 20 or 40 mg vorapaxar or the placebo equivalent. The patients who underwent PCI, the primary PCI cohort, received an oral, daily, maintenance dose of 0.5, 1 or 2.5 mg vorapaxar, or placebo equivalent, for 60 days post-procedure. As with the atopaxar phase II clinical trials, vorapaxar was given in addition to the patients standard medication, often aspirin plus clopidogrel; the primary end-point was the occurrence of clinically significant bleeding events, a safety end-point and the secondary end-point was the number of MACEs, an efficacy end-point. It was concluded from the study that orally dosed vorapaxar was well tolerated and did not increase the number of bleed events when compared with placebo.⁹⁴ This supported the idea that it was safe. Unfortunately, although there was a tendency towards a reduction in the number of MACEs, the study had too few patients to provide statistical significance. Therefore, it was concluded that larger phase III studies would be required to determine if vorapaxar was efficacious.⁹⁴

A smaller study assessed the safety and efficacy of vorapaxar in Japanese patients with non-ST-segment elevation acute coronary syndrome (NSTEMI ACS) was completed. The 117 Japanese patients were scheduled to have PCI and were

given the standard treatment; a cocktail of aspirin, heparin and ticlopidine, accordingly. They were then randomised to receive an oral loading dose of 20 or 40 mg vorapaxar, followed by a daily maintenance dose of 1 or 2.5 mg for 60 days, or the placebo equivalent. The primary and secondary end-points were the same as those in the TRA-PCI study and again no significant increase in the number of bleed events were observed. However, this study showed a significant decrease in the number of myocardial infarctions (MI) occurring throughout the PCI.⁹⁵ This gave the first evidence of a beneficial effect of vorapaxar in humans.

Another phase II study was conducted using Japanese patients who had prior ischemic stroke. In this study, 90 patients, who were already taking daily aspirin, were randomised to, additionally, receive daily, oral, 1 or 2.5 mg dosing of vorapaxar, or placebo, for 60 days. Again, there were no significant differences in the number of bleed events between any of the trial groups.⁹⁶ This further supported the idea that vorapaxar was well tolerated even on top of the standard treatment. Merck clearly concluded that there was sufficient evidence to justify progressing vorapaxar further.

Two large phase III trials were initiated; the Thrombin-Receptor Antagonist for Clinical Event Reduction in Acute Coronary Syndrome (TRACER)⁹⁷ and the Thrombin-Receptor Antagonist in Secondary Prevention of Atherothrombotic Ischemic Events (TRA 2°P)-TIMI 50 trial.⁹⁸ Both studies were multinational, placebo-controlled, double-blind and randomized; they both had an efficacy primary end-point which was the number of MACEs or deaths caused by cardiovascular issues and in both trials vorapaxar was administered on top of the patients' standard treatments. The TRACER study recruited 12,944 patients with NSTEMI ACS and randomly allocated them to receive an oral, load dose of 40 mg vorapaxar, followed by a daily, maintenance dose of 2.5 mg or the placebo equivalent. The study was intended to run for at least a year; or until a certain number of primary end point events had occurred. Instead, the study was terminated early, after only 6 months, for two reasons. Firstly, the set number of

primary end-points had occurred and, more importantly, a significant increase in bleed events (particularly intracranial bleeding) had been observed in the vorapaxar treatment group.⁹⁹ This, added to the fact that there was an insignificant reduction of primary end-points in the vorapaxar group, was a major concern for Merck. Nonetheless, the TRA 2°P-TIMI 50 study was still running.

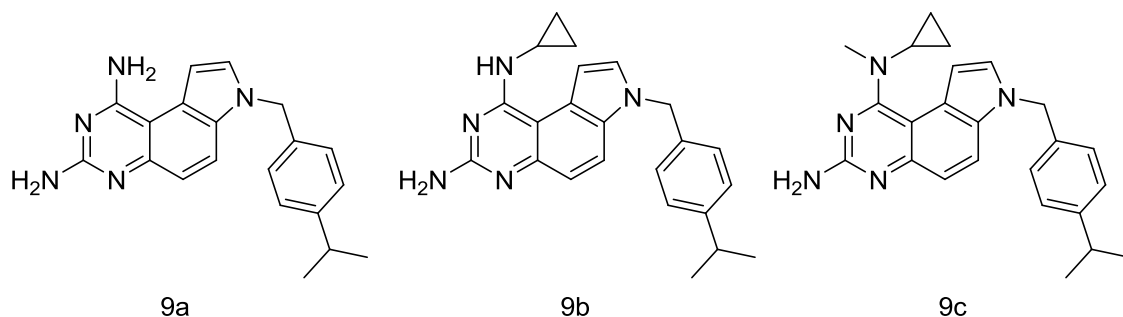
The TRA 2°P-TIMI 50 trial recruited 26,449 patients with stable atherosclerotic vascular disease; typically those who had suffered from myocardial infarction, stroke, or peripheral artery disease within the previous year. The patients were randomly allocated to receive a once daily, oral dose of 2.5 mg vorapaxar, or placebo, on top of their standard treatment; most commonly low-dose aspirin. The treatment was continued on average for 2.5 years. It was found that, similar to the TRACER trial, there was an insignificant reduction in cardiovascular death, MI or stroke. However, a significant reduction in hospitalisation for acute limb ischemia and periphery artery revascularisation was observed. A significant increase in bleed events was also seen in this study. Moreover, the patients with a history of stroke were withdrawn from the study early since the increased bleed events tended to be intracranial.¹⁰⁰

In summary, the two large phase III trials did not yield desirable results for Merck. However, they had already invested heavily in the development of vorapaxar. First, they had taken over Schering-Plough to obtain the licence; then they had carried it through extensive and expensive clinical trials. The problematic phase III results meant that they had a critical decision to make. They could either cut their losses and discontinue development, in the same way that Eisai had, or they could find a suitable patient group with whom vorapaxar was safe and beneficial to use. Merck opted for the second choice. Two years after the completion of the TRA 2°P-TIMI 50 trial, vorapaxar was finally approved as a novel treatment for the reduction of thrombotic cardiovascular events in patients with a history of heart attack or with peripheral arterial disease.¹⁰¹ Significantly, it was not to be prescribed to patients with a history of stroke, transient ischemic attack or intracranial haemorrhage, thus,

vastly reducing the eligible patient population. Vorapaxar is now being marketed as Zontivity.¹⁰²

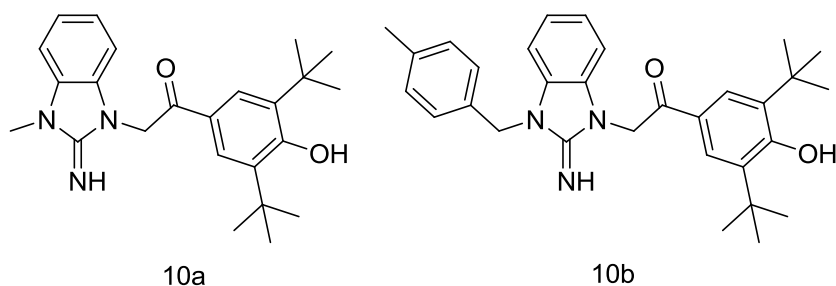
Other Series

The three significant PAR-1 inhibitors detailed above achieved various degrees of clinical success and provided a proof of concept. Detailed below are some of the series which were discontinued along the development process to vorapaxar and atopaxar. In addition, some of the newer series of PAR-1 antagonists, developed by research groups encouraged by the success of vorapaxar, are described. In some cases the compounds offered completely new scaffolds whilst in others inspiration clearly came from RWJ-58259, atopaxar or vorapaxar.



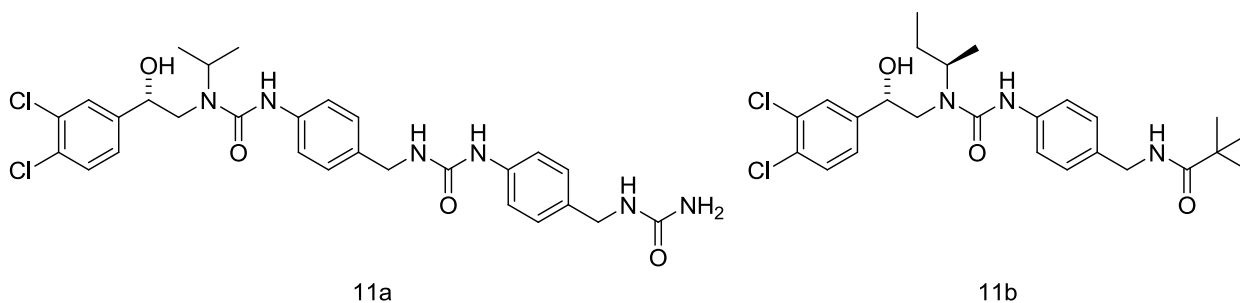
Compounds **9a**, **b** and **c**: Pyrroloquinazoline series hit and optimised leads.

Schering-Plough must have evaluated several scaffolds before they focussed their research efforts on vorapaxar. The pyrroloquinazoline derivative (Compounds **9a**) was discovered in a high-throughput screen and shown to inhibit ha-TRAP from binding to PAR-1 with an IC_{50} of 300 nM. SAR investigations at N1, N3 and N7 gave rise to Compounds **9b** and Compounds **9c** as the most potent of the series. They inhibited ha-TRAP binding with IC_{50} s of 56 and 52 nM, respectively. They inhibited TRAP-induced platelet aggregation with IC_{50} s of 300 and 150 nM, whilst inhibiting thrombin-induced platelet aggregation with IC_{50} s of 3000 and 700 nM.¹⁰³ Clearly the tertiary amine was the more potent compound, but not potent enough for Schering-Plough to develop the series further.



Compounds **10a** and **b**: Benzimidazole series hit and optimised lead.

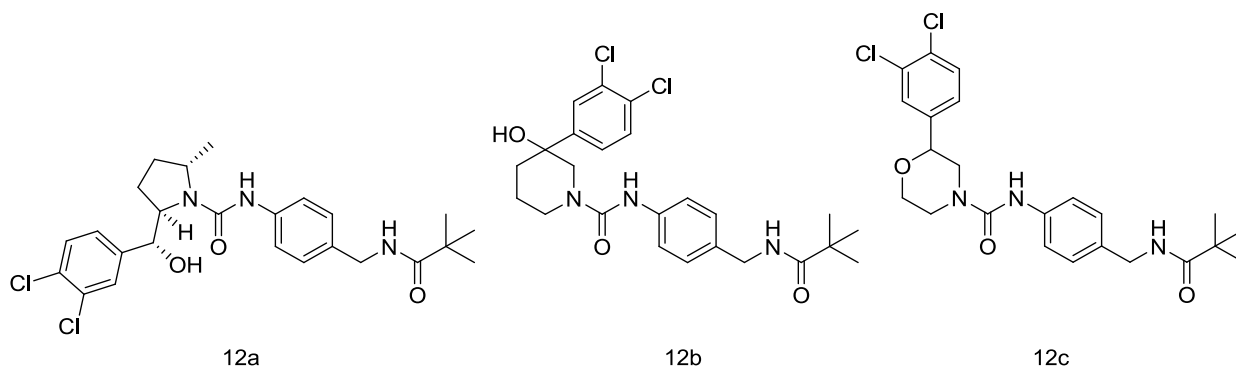
Another series Schering-Plough investigated was based on a benzimidazole derivative, also discovered *via* a high-throughput screen. The initial hit (Compounds **10a**) inhibited [³H]-ha-TRAP in a PAR-1 binding assay ($IC_{50} = 900$ nM). Following minimal optimisation they found Compounds **10b** to be the most potent of the series. It gave a PAR-1 binding IC_{50} of 33 nM and inhibited ha-TRAP induced human platelet aggregation ($IC_{50} = 575$ nM).¹⁰⁴ The structure is quite similar to that of atropaxar with the tri-substituted benzene ring attached to a heteroaromatic core. Consequently, it can be assumed that it binds to PAR-1 in a similar fashion to atropaxar; it potentially would have given a similar development profile, had it not been discontinued.



Compounds **11a** and **b**: Tri-substituted urea series hit and optimised lead.

Before Merck took over Schering-Plough, and the development of vorapaxar, they too were developing their own PAR-1 antagonists. They screened their compound library and discovered a tri-substituted urea (Compounds **11a**). It inhibited the TRAP-stimulated secretion of ³H-serotonin, from human platelets, with an IC_{50} of

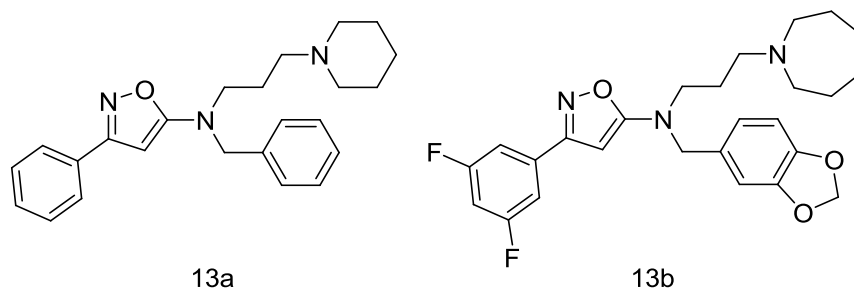
0.6 μM . A SAR profile was developed around Compounds **11a** to give Compounds **11b** as the most potent of the series. It was found that there was very little tolerance on the di-substituted benzene ring, however, simplification by removal of the two terminal ureas led to improved solubility. The potency was not significantly improved but the ligand efficiency was, owing to the reduction in molecular weight. Compounds **11b** showed an IC_{50} of 0.23 μM , in the TRAP-induced serotonin secretion assay, however, when using 1 nM thrombin as the agonist it only gave 38% inhibition. In a PAR-1 binding assay it gave an IC_{50} of 0.12 μM , confirming that it was binding to PAR-1 itself. Finally, it delayed thrombin induced platelet aggregation in a concentration dependant manner.¹⁰⁵ The tri-substituted urea series did not appear to show much potential but it was used to direct future developments.



Compounds **12 a**, **b** and **c**: The most potent compounds from the proline, piperidine and morpholine derived urea series.

Structurally constrained analogues of the tri-substituted urea series were also assessed. Proline, piperidine and morpholine derived ureas were investigated. The best compound from each series (Compounds **12a-c**) gave TRAP-induced serotonin secretion inhibition with IC_{50} s of 0.4, 0.5 and >40 μM , respectively. None of the structurally constrained ureas were developed further. Instead, a library of compounds, relating to the tri-substituted ureas, was screened. This led to the identification of the structurally distinct isoxazole lead (Compounds **13a**) which gave an IC_{50} of 9 μM , in the serotonin secretion assay. After optimization at the *N*-

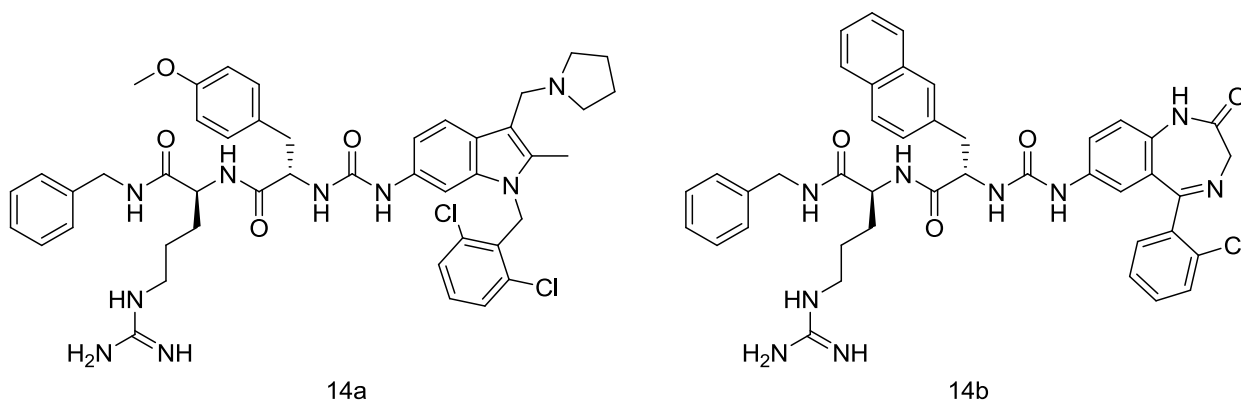
benzyl, tertiary amine and 3-aryl group, Compound **13b** was identified. This showed an IC_{50} of 0.09 μ M in the TRAP induced serotonin secretion assay but, unlike the lead from the tri-substituted series, it also gave full inhibition of thrombin induced serotonin secretion with an IC_{50} of 0.51 μ M. It gave an IC_{50} of 0.15 μ M in the PAR-1 binding assay and inhibited thrombin-induced platelet aggregation at 4 μ M.¹⁰⁶ Despite proving more effective than the tri-substituted urea series, Merck did not appear to progress with the isoxazole series either.



Compounds **13a** and **b**: Isoxazole series hit and optimised lead.

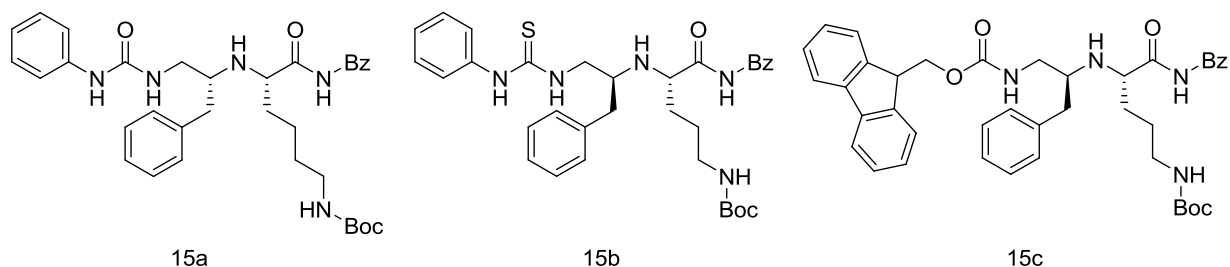
It was clear that some of the big Pharmaceutical companies were interested in PAR-1 antagonists but the series described in more recent publications tended to come from academic research groups. A group in Italy took inspiration from the work that culminated in RWJ-58259. They investigated two different cores to provide peptidomimetics.¹⁰⁷ One set of compounds was based around the indole core which, in the case of the RWJ series, had shown hypotensive effects in guinea pigs. The group added a methyl at the indole 2-position to try and force the pyrrolidine to interact with the receptor more efficiently. The methylated compound (Compounds **14a**) showed about 25% greater inhibition of TRAP-induced platelet aggregation when compared with the equivalent non-methylated RWJ compound, thus suggesting that tighter binding was afforded. The group did not show whether the novel compound reduced the hypotensive effects that led Johnson and Johnson to move away from the indole core. This means that, although they have moderately improved the potency, the compound is still unlikely to be a viable clinical candidate. The second set of compounds the group investigated was based around a 1,4-benzodiazepinone scaffold. Unfortunately, the best compound in this

series (Compounds **14b**) only gave about 30% inhibition of TRAP-induced platelet aggregation at 10 μ M. The loss in activity is possibly due to the lack of a second basic centre; a requirement needed according to the 3 point binding model. This work provided further insight into the agonist binding pocket but is unlikely to lead to any new clinical leads.



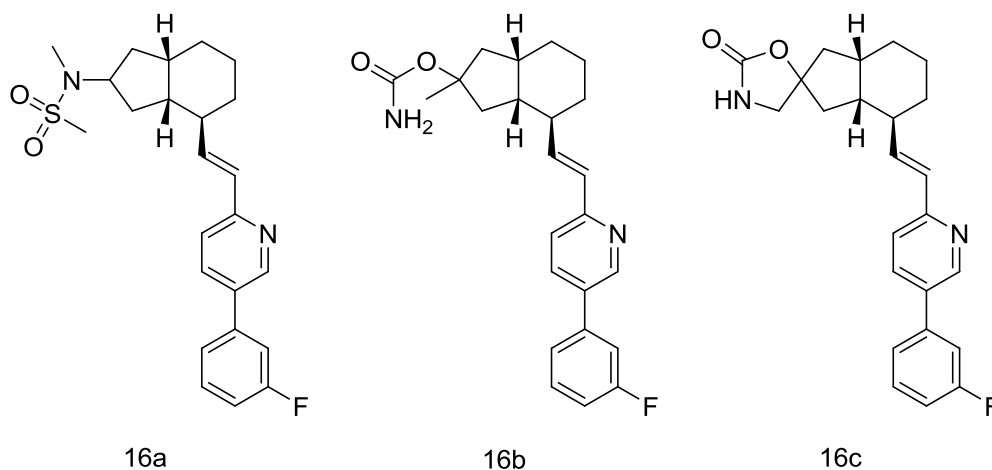
Compounds **14a** and **b**: The most potent compounds from the 2-methylindole and the 1,4-benzodiazepinone series.

More recently, a group from Spain reported the synthesis of a set of urea and thiourea compounds based on diversity orientated synthesis. Their aim was to make small, diverse libraries of different scaffolds which could display aromatic groups and basic groups at variable distances and orientations. This approach resulted in a series of analogues of RWJ-58259 which were less effective at inhibiting TRAP-induced human platelet aggregation. The best of the ureas (Compounds **15a**) gave 38% inhibition; one of the two thioureas (Compounds **15b**) gave 33% inhibition. Finally, the most potent of the compounds synthesised was actually an intermediate in the synthesis; an Fmoc protected amine (Compounds **15c**). It gave 51% inhibition of platelet aggregation, at 10 μ M, whilst RWJ-58259 gave 98% inhibition.¹⁰⁸ Again this work has not provided any major hit compounds but it has further developed the understanding of the binding site and has given structurally simpler and smaller peptidomimetics.



Compounds **15a**, **b** and **c**: The most potent compounds from the urea, thiourea and Fmoc protected amine series.

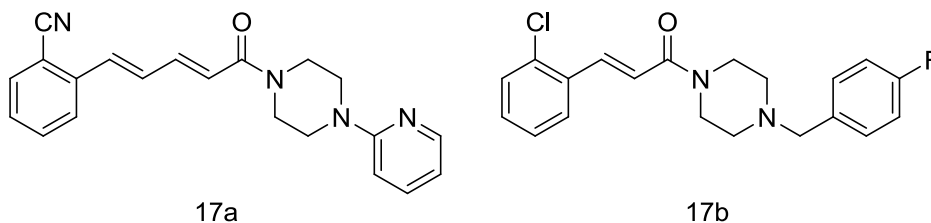
Evidently, RWJ-58259 was used as inspiration for the development of novel potent PAR-1 antagonists. On the other hand, a research group from Korea clearly used vorapaxar as their main influence. During the development of vorapaxar, Schering-Plough obtained a large number of patents covering many thousands of vorapaxar analogues. The analogues typically showed variation of the tricyclic ring; monocyclic and bicyclic variants have been covered (US2007/0232635 A1) along with spirocyclic (US2006/0223808 A1) and oxazoloisoquinoline (WO2007/075809 A2) derivatives to name but a few. This suggested that there was a high degree of tolerance surrounding the tricyclic ring but that obtaining novel analogues could be difficult. Nevertheless, the Korean group developed a series of octahydroindene vorapaxar analogues. Following some SAR profiling, at the C-2 of the octahydroindene motif, the group found that short bulky substitutions, such as the *N*-methylmethanesulfonamide of Compounds **16a**, gave better PAR-1 binding. This led them to make quaternary (Compounds **16b**) and spiro-substituted (Compounds **16c**) octahydroindenes. Compounds **16a**, **b** and **c** proved to be as potent as the parent vorapaxar, achieving PAR-1 binding IC_{50} s of 1.3, 2.7 and 8.6 nM respectively. Equally, they inhibited TRAP-induced platelet aggregation with IC_{50} s of 0.097, 0.10 and 0.21 μ M, compared with vorapaxar which gave an IC_{50} of 0.12 μ M. Functionally the octahydroindenes proved successful; unfortunately, they lacked metabolic stability surviving for no longer than 5 min when incubated with both rat and human liver microsomes.¹⁰⁹ Even so, the group had proved that designing novel PAR-1 inhibitors around the vorapaxar scaffold was both feasible and promising.



Compounds **16a**, **b** and **c**: Tertiary, quaternary and spiro-substituted octahydroindenes.

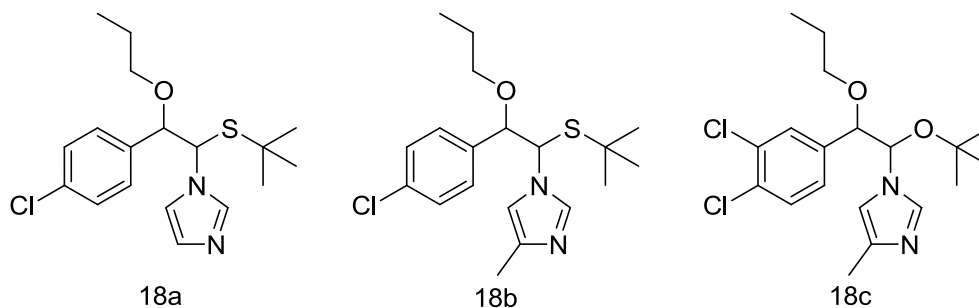
A group in France have explored two novel scaffolds, found *via* a library screening approach, for use as PAR-1 inhibitors. The first was based around a cinnamoylpiperazine motif. Following some optimisation studies they arrived at F16618 and F16357 (Compounds **17a** and **b**, respectively) as the most potent in their series. They had respective binding affinities (pA_2) of 6.49 and 6.67, inhibited TRAP-induced Ca^{2+} flux, measured in a fluorescent imaging plate reader (FLIPR) assay, by 99 and 93% and inhibited TRAP induced human platelet aggregation to give pK_b equalling 5.30 and 5.52, in that order. Finally, in a rat AV shunt model, IV administration increased the re-occlusion time by 58% with Compounds **17a** and 28% with Compounds **17b**. Following an oral dosing of 40 mg/kg the occlusion times were increased by 54% and 59%, correspondingly. Both compounds showed good absorption, distribution, metabolism and excretion (ADME) properties and were investigated further.¹¹⁰ Compounds **17b** was used as a basis for further optimisation; several series, with linker variations, were investigated but none of the resultant compounds appeared to significantly improve upon the original piperazine linker.¹¹¹ Additional biological studies were completed with Compounds **17a**. It was compared to, and investigated in combination with, aspirin and clopidogrel in the rat AV shunt model. Administration with clopidogrel increased the time to occlusion by about 70% whilst giving minimal increase to the systemic

bleed time.¹¹² This suggests that it, like vorapaxar, could be a successful anti-thrombotic agent given alongside aspirin and/or clopidogrel.



Compounds **17a** and **b**: The most potent compounds from the cinnamoylpiperazine series; F16618 and F16357.

The effects of Compounds **17a** on smooth muscle contraction was also investigated. PAR-1 activation can lead to vasoconstriction, under certain pathological conditions, which is thought to be associated with the development of vascular lesions.¹¹³ The group showed that Compounds **17a** competitively inhibited TRAP-induced constriction of both isolated pig coronary artery and rat superior mesenteric artery.¹¹⁴ Similarly, atopaxar had been shown to be able to inhibit the thrombin induced vasoconstriction in a rabbit subarachnoid haemorrhage model.¹¹⁵ The inhibition of vasoconstriction seen with atopaxar may have been enough to protect patients from the significant increase of brain haemorrhage observed with vorapaxar. Consequently, the promising results of this study mean that Compounds **17a** could prove to be a synthetically simpler, potent, orally active PAR-1 inhibitor which shows antithrombotic activity with the added benefits of being able to treat vascular injury provoked vasospasm.

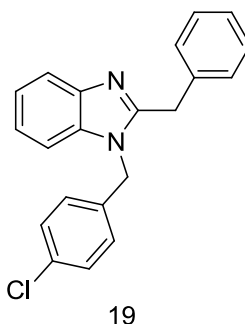


Compounds **18a**, **b** and **c**: Initial hit and optimised leads for the imidazole series.

The second series discovered by the group in France was based on a substituted imidazole. The initial hit (Compounds **18a**) already showed 96% inhibition of TRAP-induced Ca^{2+} release at 10 μM and gave a pK_b of 5.01 in the TRAP-induced human platelet aggregation assay. Still, further optimisation was carried out to obtain Compounds **18b** and **c**. These showed 99 and 81% inhibition in the Ca^{2+} flux assay, pK_b of 5.71 and 5.73 in the platelet aggregation assay and 45 and 43% increase in re-occlusion time, following 1.25 mg/kg IV dosing, in the rat AV shunt model, respectively. They both showed reasonable stability in human liver microsomes but poor stability in rat liver microsomes. Despite the success with the cinnamoylpiperazine compounds, the group claim to be further optimising this series.¹¹⁶ This highlights the continuing interest in PAR-1 antagonists.

Allosteric Inhibitors

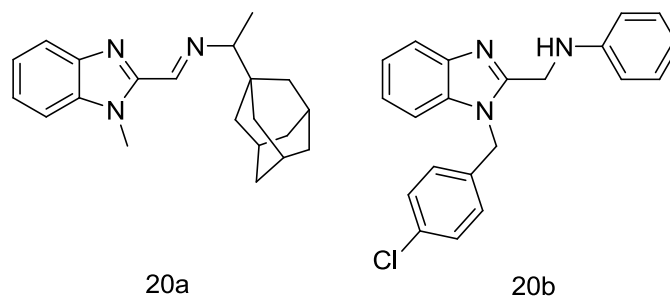
The PAR-1 inhibitors discussed so far are all thought to antagonise the receptor in the extracellular domain, either at the thrombin binding site or at the third extracellular loop where the tethered ligand binds. This makes them non-selective for the type of G-protein inhibited thus causing all pathways downstream of PAR-1 to be blocked. On the other hand, in the last few years some compounds have been found to inhibit $\text{G}\alpha_q$ selectively. These compounds could be the inspiration behind a new, more selective PAR-1 inhibitor.



Compound **19**: Q94

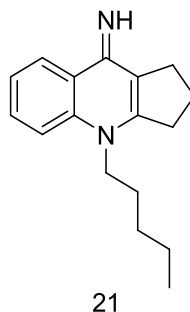
Compound **19**, commonly known in the literature as Q94, appears to be a synthetically simple benzimidazole derivative. It was identified by the company Caden Biosciences in a library screen of compounds supplied by ChemDiv. They screened the compounds in competition with a high-affinity peptide, which mimicked the $G\alpha_q$ C-terminus, using an enzyme-linked immunosorbent assay (ELISA). Q94 blocked the $G\alpha_q$ mimic from binding to activated PAR-1 receptors with an IC_{50} of 916 nM. In addition, Q94 was shown to inhibit TRAP-induced Ca^{2+} flux, in human embryonic kidney (HEK) cells, in a concentration dependent manner; a 10 μ M dose gave full inhibition. This suggested that Q94 could be used to directly inhibit the $G\alpha_q$ subunit. Consequently, it was thought to be the first small molecule to inhibit PAR-1 at the intracellular level with increased selectivity of PAR-1 inhibition.

Caden Biosciences offered a free sample of “Caden Biosciences Q94” to any research group who requested it, and the Chambers group obtained a small batch. They intended to investigate PAR-1 related thrombin mediated signalling in mouse lung fibroblasts (MLF). They were particularly interested in the pathway that led to the release of the chemoattractive chemokine ligand 2 (CCL2). This is because CCL2 levels tend to be up-regulated in patients with ILDs and thus they hoped it could be a good biomarker to assess the clinical progression of IPF. This was the first example of PAR-1 inhibitors being used in relation to IPF. They showed by ELISA that a 10 μ M dose of “Caden Biosciences Q94” was sufficient to fully inhibit thrombin-induced CCL2 production in MLF. Furthermore, 10 μ M of “Caden Biosciences Q94” was shown to cause approximately 70% reduction in thrombin-induced CCL2 mRNA levels.¹¹⁷ They concluded that CCL2 production was one of the downstream effects of activated PAR-1 binding to the $G\alpha_q$ subunit. They also recognised the opportunity for using Q94 as a starting point to develop a selective PAR-1 inhibitor as a clinical candidate for treating inflammatory and fibroproliferative diseases.



Compounds **20a** and **b**: Q94 analogues Q89 and Q109 respectively.

Another group, in Italy, were inspired by the work completed by Chambers *et al.*. Initially, they screened around 10,000 ChemDiv compounds with the same competition ELISA used by Caden Biosciences. From the library screen, they identified Q89 (Compounds **20a**) and used it as a template to find the commercial analogues Q94 (Compound **19**) and Q109 (Compounds **20b**). In the competition ELISA, the three compounds, Q89, Q94 and Q109, gave IC_{50} s of 320, 923 and 817 nM (respectively). It is suggested that they subsequently synthesised the three compounds in-house in order to complete further pharmacological tests. The compounds were assessed in a thrombin-induced Ca^{2+} flux assay in human dermal microvascular endothelial cells-1. Q94 and Q109 showed evidence of allosteric modulation which led to the inhibition of Ca^{2+} release with IC_{50} s of 10.3 and 19.2 nM, respectively. An IC_{50} for the original hit, Q89, was not obtained as they found that it did not reduce the maximum effect (E_{max}) of thrombin. This meant that it would not have an inhibitory effect. The inhibition of the $G\alpha_q$ pathway, observed with Q94 and Q109, was further supported by the fact that they inhibited thrombin-induced inositol trisphosphate (IP_3) accumulation. IP_3 production is another downstream effect observed with the thrombin activation of the $G\alpha_q$ pathway. On the other hand, the group found that Q94 and Q109, in the absence of thrombin, both inhibited cAMP production. Since, cAMP is synthesised by AC, which is in turn inhibited by the coupling of activated PAR-1 to $G\alpha_i$ subunits, it can be concluded that Q94 and Q109 act as allosteric agonists for PAR-1 $G\alpha_i$ signalling.¹¹⁸ This suggests that the benzimidazole derivatives are even more interesting than the Chambers group previously thought.

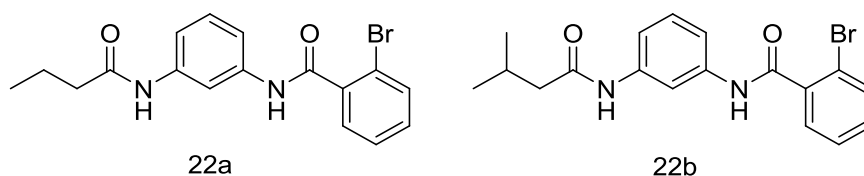


Compound **21**: JF5

Another, intracellular, PAR-1 inhibitor, named JF5 (Compound **21**), was shown, by Flaumenhaft *et al.*, to interact allosterically with the intracellular helix 8 (H8) of the PAR-1 receptor to modulate G-protein binding. It was discovered through a high-throughput screen using a luciferin-luciferase based assay designed to identify compounds which could inhibit TRAP-induced platelet granule secretion. The assay was able to identify allosteric modulators as it is a functional test as opposed to a site-specific binding assay. JF5 was shown to inhibit platelet aggregation which, like granule secretion, is a downstream result of $G\alpha_q$ activation. It was shown to have no effect on platelet shape change, which is caused by $G\alpha_{12/13}$ activation, highlighting the selectivity. Even though JF5 blocks only one of the G-proteins, it was still shown to greatly reduce the accumulation of platelets into thrombi in mice that had laser-induced arterial injury. In this *in vivo* model, JF5 exhibited an IC_{50} of about 1mg/kg. Furthermore, it was shown to more than double the time to 50% maximal platelet accumulation at this dosing.¹¹⁹ This helps to prove the concept that a G-protein selective PAR-1 inhibitor could be of potential use. Unfortunately, JF5 targets many of the GPCRs which have the H8 regions. Thus, although interesting, it is unlikely to be developed into a clinical candidate.

Flaumenhaft *et al.* discovered a second PAR-1 allosteric modulator, based on a 1,3-diaminobenzene scaffold, using the same library screening strategy as before. The initial hit (Compounds **22a**) inhibited dense granule release ($IC_{50} = 1-10 \mu M$), did not inhibit platelet activation caused by other receptors, was reversible and soluble in phosphate buffered saline (PBS); the buffer used for biological assays.

Compounds **22a** was shown to be moderately stable in human plasma with around 80% remaining after 5 h. Unfortunately, in mouse plasma it showed unacceptable stability, thus making it difficult to conduct any *in vivo* studies. Nevertheless, like JF5, it was shown to exhibit non-competitive inhibition of platelet aggregation without inhibiting the ability for the platelets to change shape. Consequently, it can again be assumed that Compounds **22a** blocks $G\alpha_q$ activation and not $G\alpha_{12/13}$. Finally, it was shown to inhibit TRAP-induced surface expression of P-selectin in human platelets ($IC_{50} = 0.26 \mu\text{M}$). P-selectin is a cell adhesion molecule which lines the inner surface of activated platelets. It is released from α -granules, when the platelets become activated, which means that it again is related to $G\alpha_q$ activation.

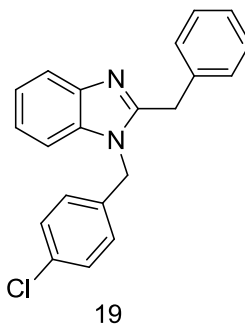


Compounds **22a** and **b**: Initial hit and optimised lead of the 1,3-diaminobenzene series.

Compounds **22a**, termed ML161, was a promising compound in itself but to try and increase the potency, and most importantly to improve the mouse plasma stability, a series of SAR studies were completed. Compound **22b** was the only compound found to have equivalent potency, in the P-selectin assay ($IC_{50} = 0.29 \mu\text{M}$), but improved mouse plasma stability (65% remaining after 5 h). The compounds only differ by the addition of a methyl group β to the left-hand amide. More generally, the results from the SAR studies showed that, on the right-hand side of the 1,3-disubstituted benzene ring, a secondary benzamide (with a small, electron-neutral, or electron withdrawing, *ortho*-substituent) was required. Whilst, on the left-hand side, a secondary amine or amide with a linear, or branched, aliphatic chain (no longer than four carbons) was required.¹²⁰ The group hope to use the more stable analogue to evaluate whether allosteric inhibitors could be used to decrease the risk of haemorrhage related to the use of PAR-1 inhibitors.

Project Aims

The Chambers group were the first to recognise the opportunity for using allosteric antagonists, such as Q94, as a starting point for the development of a selective PAR-1 inhibitor. Consequently, they wanted to advance their understanding of its mechanism of action. They had used up most of their batch of “Caden Biosciences Q94”, thus, in order to further their research, they purchased a new batch of Q94 from ChemDiv. They tested the ChemDiv batch with the CCL2 detecting ELISA but found no activity. Worse still, the “ChemDiv Q94” appeared to precipitate when added to the biological medium. Precipitation had never been seen with “Caden Biosciences Q94”.¹²¹



Compound **19**: “ChemDiv Q94”

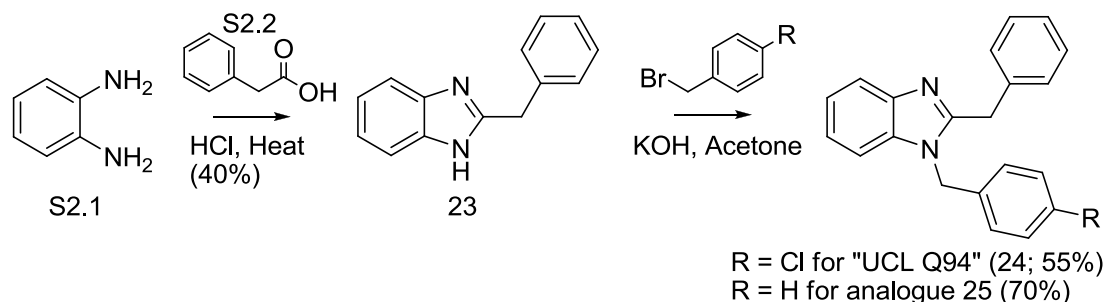
Rachel Chambers started collaborating with us to provide chemistry expertise, before other allosteric antagonists such as Q89, Q109, JF5 and ML161 had been reported on. Accordingly, the initial aim of this project was to validate a suitable synthetic route to Q94 and use it to supply the Chambers group with a pure sample so they could continue with their research. From there, the aim was to synthesise a series of Q94 analogues which could be tested to establish an SAR profile for the benzimidazole series. It was intended that at least one of these analogues would show improved potency and thus potential as a selective PAR-1 inhibitor which could be used for the treatment of IPF.

Chapter 2: Q94 Synthesis and Testing

Introduction

The structure of “ChemDiv Q94” is not complex and so theoretically would be expected to be straightforward to synthesise. It is based around a benzimidazole motif which is frequently found in pharmaceutical agents. In the literature, benzimidazoles are formed by condensing *o*-phenylenediamine with a carboxylic acid in the presence of a strong acid.^{122,123} It has been shown that the benzimidazole core can then be *N*-alkylated with a benzylhalide, in the presence of a base, in a variety of solvents, including ionic liquids.¹²⁴ This two step process should render the synthesis of Q94 and its analogues easy to develop. The synthetic route used by Asteriti *et al.*, for their “in-house” synthesis of Q94, has not been disclosed at this time.

Synthesis



Scheme 2: The synthesis of “UCL Q94” (24) and its analogue (25).

“UCL Q94” (24) was synthesised using the route outlined in Scheme 2. *o*-Phenylenediamine (S2.1) was condensed with benzoic acid (S2.2) in the presence of concentrated hydrochloric acid to give 23 in moderate yield (40%). This was then *N*-alkylated with 4-chlorobenzyl bromide to give 24 in modest yield (55%). The dibenzyl analogue 25 was synthesised in a similar fashion but with a greater yield (70%).

Biological Results and Discussion

The Chambers group had already shown that “Caden Biosciences Q94” had an IC_{50} of 916 nM, when in competition with a $G\alpha_q$ C-terminal mimic.¹¹⁷ In trying to replicate their results with “ChemDiv Q94” they found no activity and observed considerable precipitation into the biological medium. Equally, when testing the newly synthesised batch of “UCL Q94” (**24**) and its analogue (**25**), precipitation, and lack of activity, was again observed. After many attempts to regain the activity observed with “Caden Biosciences Q94” and stop the precipitation seen with “ChemDiv Q94” and “UCL Q94”, the Chambers group had to conclude that the structure of the original batch was probably not consistent with that described. However, this was before the Italian group published their results regarding Q89, Q94 and Q109. The group in Italy claimed to have used both Q94 purchased from ChemDiv and some they had synthesised themselves to get positive results. They had also shown that a batch of Q94 could compete with a $G\alpha_q$ C-terminal mimic to give an IC_{50} of 923 nM. This is comparable to the IC_{50} obtained by the Chambers group with “Caden Biosciences Q94”.

In light of the newly published results, “ChemDiv Q94” was tested again, along with a purchased batch of Q109. The compounds were tested at 3 μ M in a Ca^{2+} flux FLIPR assay using human lung fibroblasts (HLF). The cells were stimulated with 0, 0.3, 3 and 10 nM thrombin solutions. In a similar assay the Italian group had shown Q94 and Q109 to give IC_{50} of 10.3 and 19.2 nM, respectively.¹¹⁸ Unfortunately, as can be seen in Figure 4, our collaborators in the Chambers group saw very little effect.

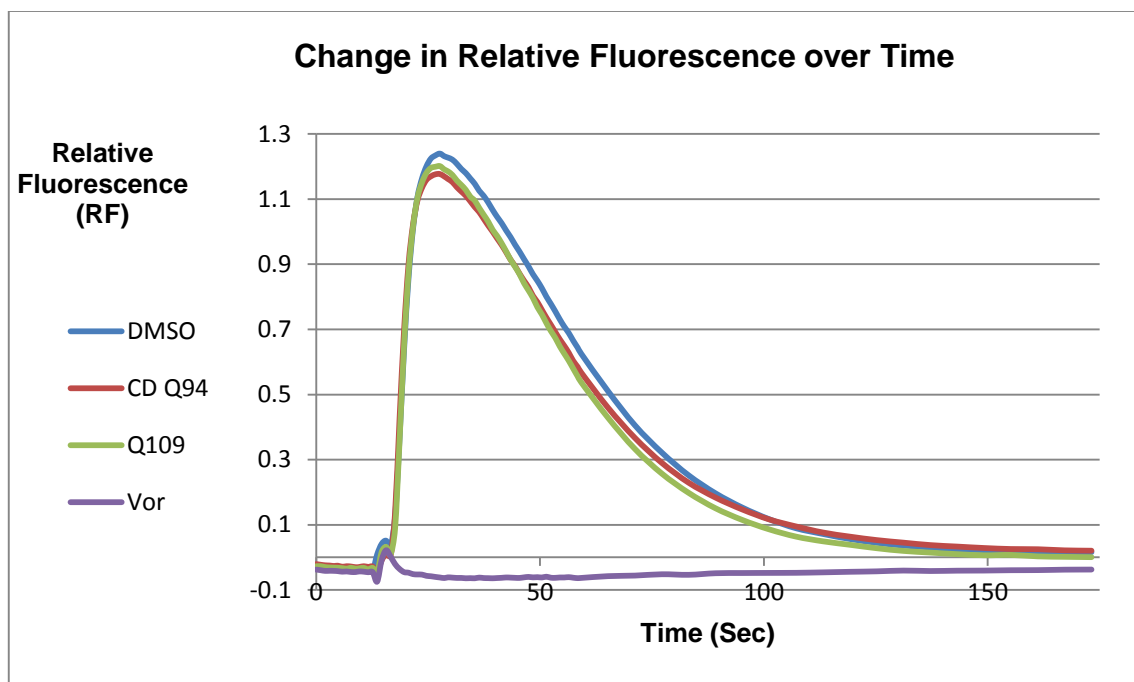


Figure 4: The average (n = 3) relative fluorescence (RF) observed over time (sec) upon the addition of 10 nM thrombin to human lung fibroblasts in buffer pre-incubated with Fluo-4 NW dye mix and 3 μ M antagonist; 0.5% DMSO, ChemDiv Q94, Q109 and vorapaxar.

Figure 4 shows the relative fluorescence (RF) observed over the time course of the Ca^{2+} flux experiment, at the highest thrombin concentration (10 nM). It is seen that there is no fluorescence observed with the positive control (vorapaxar). This supports the idea that the positive control provides full inhibition of PAR-1 because it suggests that no Ca^{2+} was released from the cell. On the other hand, with the negative control (0.5 % dimethylsulfoxide (DMSO) in medium) there is a huge increase in RF following the addition of thrombin. This implies that there was a huge efflux of Ca^{2+} which would have bound to the Fluo-4-NW dye, found in the biological medium, allowing it to fluoresce. Both, “ChemDiv Q94” and Q109, showed similar profiles to the negative control. This again suggests that there was a huge efflux of Ca^{2+} meaning that the effects of thrombin were not inhibited. Further, the percentage inhibition observed with “ChemDiv Q94” and Q109, at lower concentrations of thrombin, was very similar to the percentage inhibition seen with the negative control (Figure 5). In summary, the results obtained did not support the results found by the group in Italy.

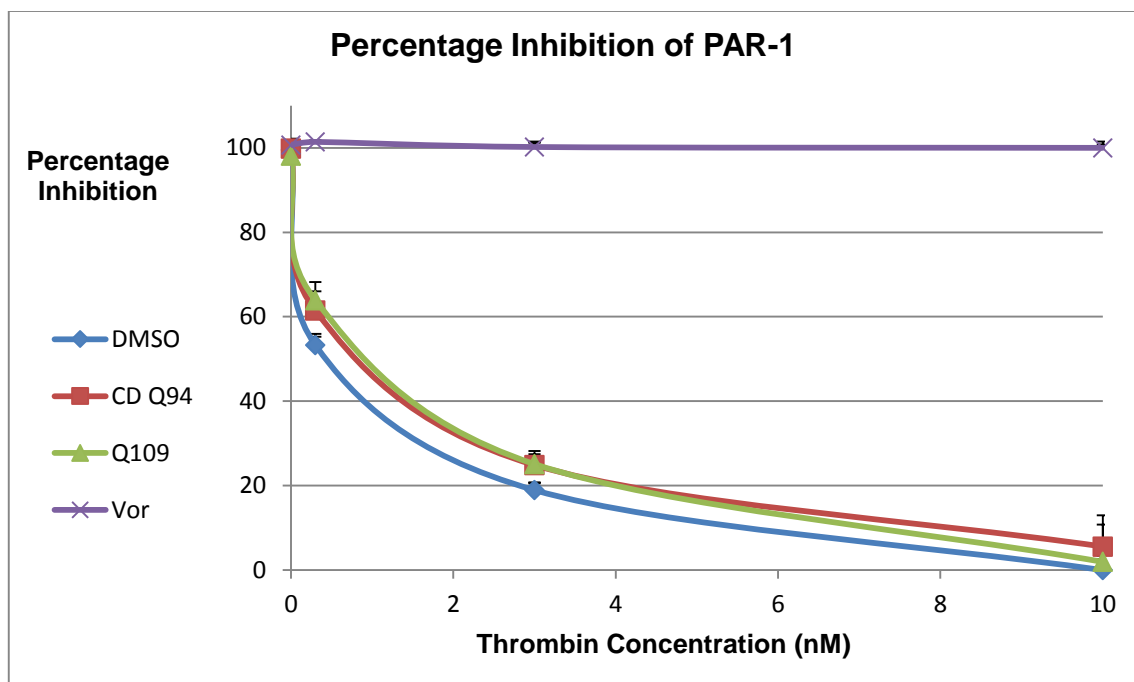


Figure 5: The average (n = 3) percentage inhibition observed upon the addition of thrombin at varying concentrations (0, 0.3, 3 and 10 nM) to human lung fibroblasts in buffer pre-incubated with Fluo-4 NW dye mix and 3 μ M antagonist; 0.5% DMSO, ChemDiv Q94, Q109 and vorapaxar.

Conclusions and Updated Aims

There are two possible conclusions that could be made from this work. Either, “ChemDiv Q94” has a different structure to the one originally proposed, or, the published structure of Q94 is correct but perhaps existed as a salt to increase solubility. Nevertheless; it was concluded that, although what was thought to be Q94 had been successfully synthesised, we were not in a suitable position to use it as a starting point for the development of a novel PAR-1 inhibitor that could be used to treat IPF. As a consequence, the aim of the project was broadened. It was still the plan to design novel PAR-1 inhibitors to be used as potential IPF medicines; but, other sources were investigated to provide the initial inspiration.

Chapter 3: Vorapaxar Analogues

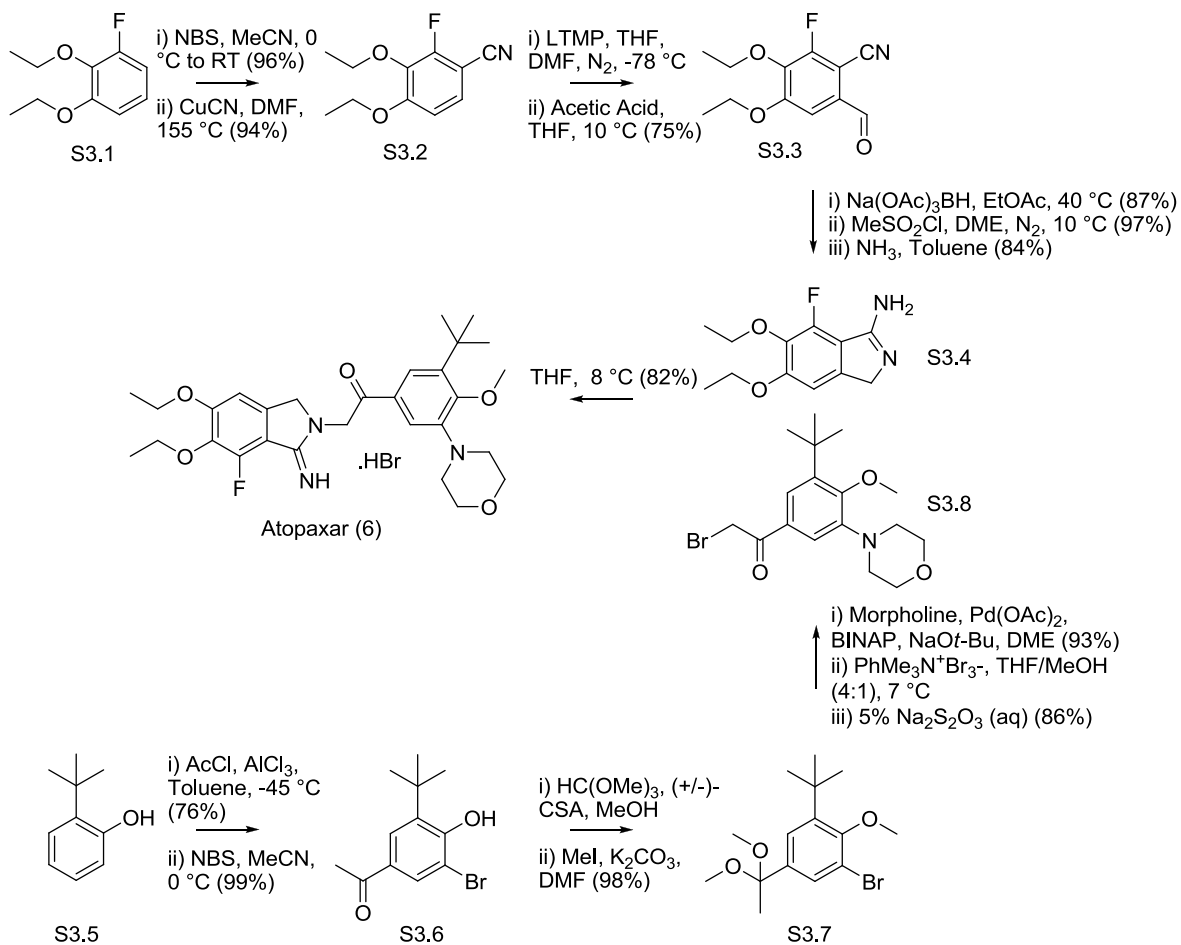
Introduction

The obvious candidates from which to develop novel PAR-1 inhibitors to provide new inspiration were atopaxar and vorapaxar. This is owing to the fact that at the time, the phase II trials assessing atopaxar were coming to an end and the haemorrhage complications seen in the phase III trials of vorapaxar were yet to be published. Both showed considerable promise that they could get to market and both had a wealth of patent literature behind them. Following an extensive literature search it was clear that the main pharmacophores for vorapaxar and atopaxar were the biaryl group and the substituted benzene, respectively. An initial idea was to combine the two groups to give a novel scaffold but it was thought that the resulting compounds would be too lipophilic and thus insoluble. A second idea was to look at cut-down versions of the compounds. Merck, and Lee *et al.*, had shown that this was a successful strategy when applied to vorapaxar; whilst the benzimidazole series developed by Schering-Plough could be seen as atopaxar cut-downs. Therefore, it may be interesting to see how small one could go whilst still achieving potency. Finally, developing SAR around regions of the two molecules which have yet to be explored could be another way of achieving novel, potent PAR-1 inhibitors. The synthesis of atopaxar and vorapaxar were investigated to help direct which would be the best path to novelty to follow.

Atopaxar Synthesis

The synthesis of atopaxar was based around the coupling of the iminoisoindole fragment (**S3.4**) with the 3-*tert*-butyl-4-methoxy-5-morpholinophenyl group (**S3.8**) (Scheme 3).¹²⁵ The iminoisoindole fragment (**S3.4**) was synthesised from commercially available 1,2-diethoxy-3-fluorobenzene (**S3.1**) *via* an 8 step sequence. The fluorobenzene was first selectively brominated adjacent to the fluorine using *N*-bromosuccinimide (NBS). The bromine was subsequently substituted with a cyanide group to afford the aryl cyanide (**S3.2**). This was then

formylated at the C-5 position to give **S3.3**. The aldehyde was reduced and mesylated allowing cyclisation to occur providing the key iminoisoindole fragment; **S3.4**.



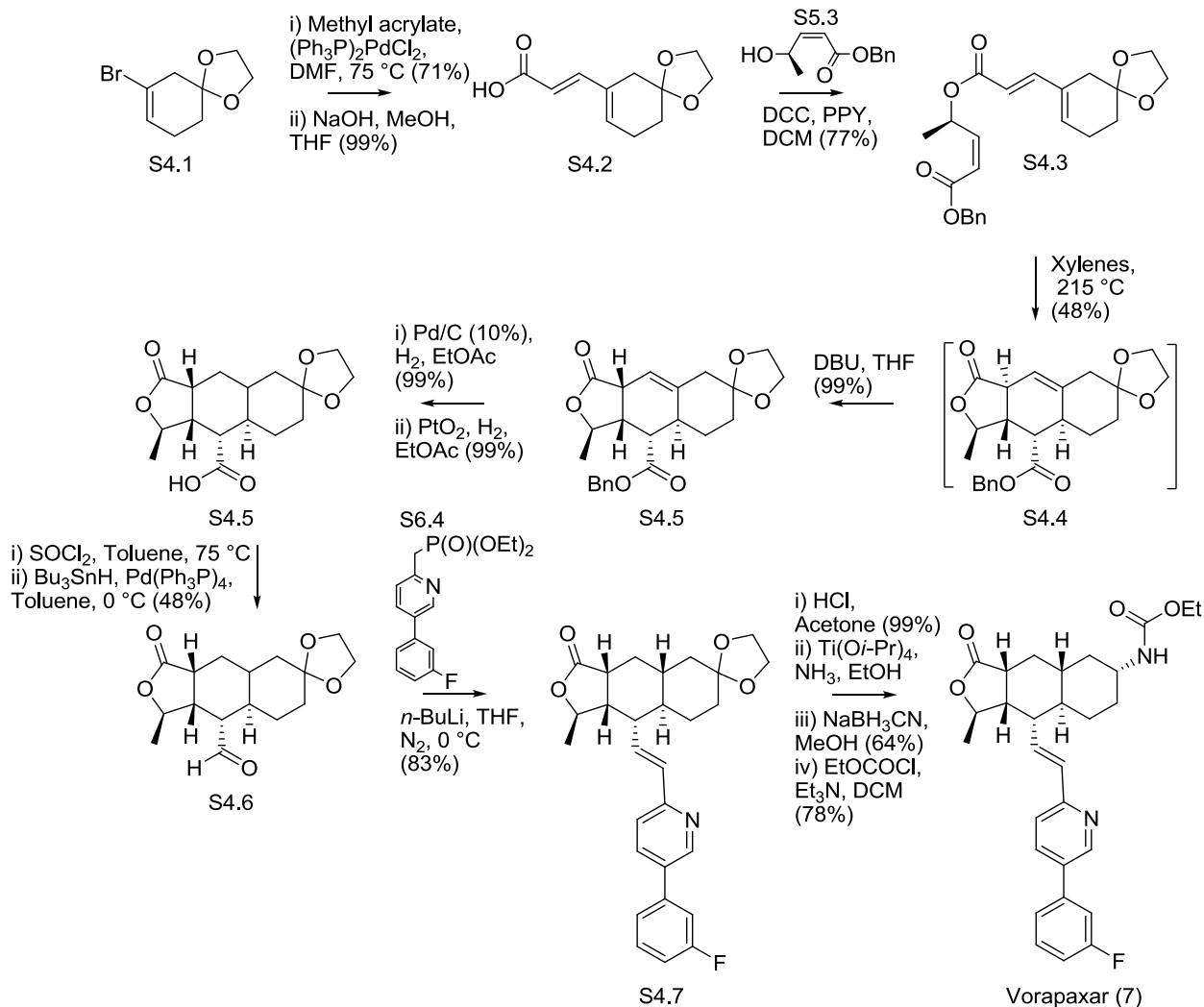
Scheme 3: Eisai's Synthesis of Atopaxar (6)

The 3-*tert*-butyl-4-methoxy-5-morpholinophenyl fragment (**S3.8**) was synthesised from 2-*tert*-butylphenol (**S3.5**) in 7 steps. First it was acylated, under Friedel-Crafts conditions, *para* to the hydroxyl group; next, bromination, *ortho* to the hydroxyl, was achieved to give **S3.6**. The added ketone was then ketal protected prior to methylation of the hydroxyl group giving **S3.7**. Next, palladium catalysed substitution of the C-5 bromine with morpholine was completed. Before the ketone was deprotected, terminal bromination of the ketal group was carried out. The final ketal deprotection gave 3-*tert*-butyl-4-methoxy-5-morpholinophenyl (**S3.8**) which

was coupled to the iminoisoindole fragment (**S3.4**) to give atopaxar (**6**) as a hydrogen bromide salt. The convergent synthetic approach would allow focused compound libraries to be synthesised relatively easily. Reflecting this, the patent literature surrounding atopaxar gave thousands of example compounds. This suggests that many compounds were tested and that the SAR at most positions would have already been explored.

Vorapaxar Synthesis

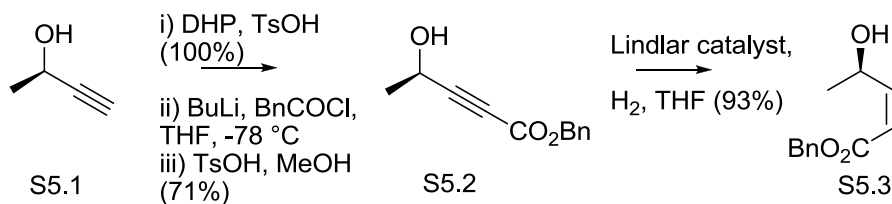
Himbacine is an interesting natural product both pharmaceutically and synthetically; consequently, there are a number of published synthetic routes used to make it. The majority of these revolve around building the tricycle with an intramolecular Diels-Alder (IMDA) reaction.¹²⁶ Vorapaxar was synthesised using a similar IMDA reaction approach (Scheme 4).^{87,89} The synthesis was initiated with a Heck reaction to attach methyl acrylate to the commercially available ketal-protected bromocyclohexenone (**S4.1**). The ester was then hydrolysed to give the dienonic acid (**S4.2**) which was coupled, using *N,N'*-dicyclohexylcarbodiimide (DCC), with (*R,Z*)-benzyl 4-hydroxypent-2-enoate (**S5.3**) to give the IMDA precursor; **S4.3**. The hydroxypentenoate (**S5.3**) was itself made according to Scheme 5.



Scheme 4: Schering Plough's Synthesis of Vorapaxar (7)

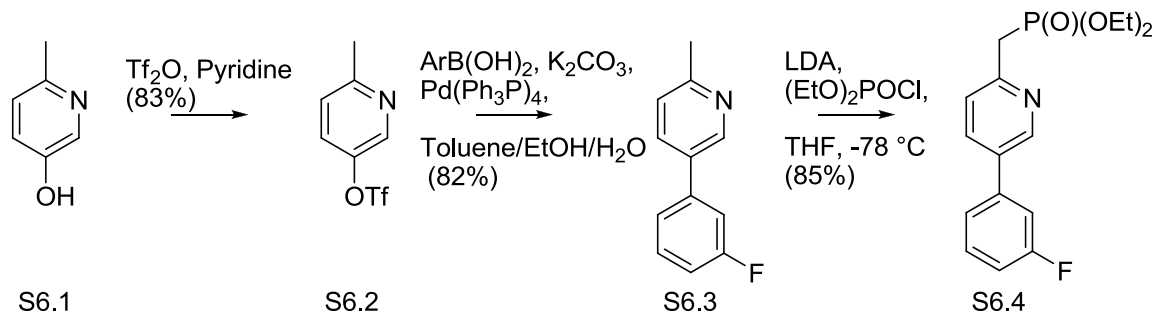
The IMDA precursor (**S4.3**) was cyclised in xylenes at high temperature giving **S4.4**. During this reaction the stereocentres were set by the absolute chirality of the C-3 methyl-substituent. It was thought that the methyl group caused a facial selectivity created by an allylic strain on the dienophile during one of the IMDA transition states. This differentiation was enough to set the stereochemistry at C-3a which in turn set the stereocentres for the rest of the tricycle. The relative stereochemistry between C-3a and C-4 was conveyed due to the *cis*-geometry of the dienophile whilst the exoselective transition state gave the *trans*-configuration

between C-3a and C-9a. Consequently, epimerisation at C-9a was promoted by the addition of DBU to give the desired *cis*-fused lactone (**S4.5**).



Scheme 5: Schering Plough's Synthesis of (*R,Z*)-benzyl 4-hydroxypent-2-enoate

Once the tricycle had been assembled palladium-catalysed hydrogenation removed the benzyl (Bn) group whilst the platinum-catalysed diastereoselective hydrogenation was done to reduce the internal double bond giving **S4.6**. The resulting carboxylic acid (**S4.6**) was converted into an acid chloride before reduction using tributyltin hydride and tetrakis(triphenylphosphine)palladium(0) to give **S4.7**. The resulting aldehyde (**S4.7**) was coupled with a phosphonate ester of the biaryl group (**S6.4**) (made following Scheme 6) in a Horner-Emmons reaction to give **S4.8**. The final steps involved de-protecting the ketal at the C-7 position to give a ketone which in turn was reductively aminated to give a primary amine. Coupling with ethyl chloroformate finally gave vorapaxar (**7**).



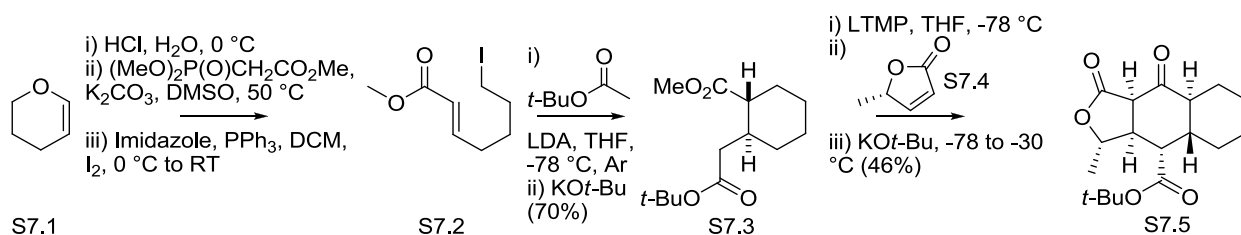
Scheme 6: Schering-Plough's Synthesis of Biaryl Phosphonate Ester

On the face of it, it looks like the synthesis of atopaxar is shorter and simpler than the synthesis of vorapaxar. However, if novel vorapaxar analogues were made with a methylene at C-7 the synthesis would be significantly simplified. Since the C-7

carbamate was installed primarily to block metabolism, analogues without the carbamate tend not to have diminished potency. Consequently, it would not be unreasonable to omit the carbamate if a series of novel vorapaxar analogues were to be investigated.

Novel Synthesis of Himbacine

A recent publication, from Casey *et al.*, described a novel method towards synthesising the himbacine tricycle.¹²⁷ It used a double Michael-Initiated Ring Closure (MIRC) reaction (Scheme 7) rather than the typical intramolecular Diels-Alder seen in most other himbacine syntheses. The first few steps of the synthesis were already established in the literature. It commenced with acid catalysed ring-opening of the commercially available dihydropyran (**S7.1**). In the same pot, the product was subjected to Horner-Emmons reaction conditions to give an α,β -unsaturated ester with a terminal alcohol.¹²⁸ The alcohol was converted into an iodo species (**S7.2**)¹²⁹ before the first of two MIRC reactions was performed.¹³⁰ The resulting racemic cyclodiester (**S7.3**) was then reacted with a stereoisomeric lactone (**S7.4**; itself made in two steps¹³¹) in a second MIRC reaction to give the himbacine tricycle with a ketone at the C-9 position (**S7.5**). It was their intention to continue with this approach to eventually provide a novel, short, enantioselective route to himbacine. However, to the best of our knowledge, there are no examples in the vorapaxar literature with substitutions at C-9. Consequently, this new synthetic route could be used to provide originality. The synthetic route could be adapted to give the *ent*-himbacine tricycle. The C-9 ketone could then be used as a synthetic handle to access novel analogues of vorapaxar and allow the exploration of SAR from ring II.



Scheme 7: Casey *et al*'s Developments Towards a Novel Himbacine Synthesis

Vorapaxar SAR

The potential for using the new synthetic route towards himbacine as a starting point for making novel vorapaxar analogues meant that it was important to fully appreciate the existing SAR knowledge surrounding vorapaxar and its analogues. The SAR studies completed during the development of vorapaxar highlighted several regions which appeared vital for effective PAR-1 binding and selectivity. On the other hand, some of the structural features were shown to merely aid pharmacokinetics or synthesis (Figure 6). It was found that the stereochemistry of the tricycle head group was vital. Having the *ent*-himbacine scaffold hugely increased potency. Conversely, the C-3 methyl group was not required to maintain potency. However, it was kept throughout the vorapaxar development process as it acted as a useful stereocentre to aid the stereospecific synthesis. As previously discussed, the C-7 carbamate must be present for successful oral dosing of vorapaxar as it blocks the metabolic site targeted by liver enzymes during first-pass metabolism.

The SAR studies showed that variation was tolerated on both rings I and III, provided a hydrogen bond acceptor existed at the C-1 position. On the flip side, the *trans*-alkene linker at C-4 appeared essential for potency as it was thought to help orientate the pyridine nitrogen into a beneficial position. The basicity and orientation of the pyridine nitrogen was thought to be important. Thus, attachment at pyridine C-2 was seen to improve potency as it was thought to manipulate the nitrogen into a favourable position. Finally, substitution around the pyridine ring hugely influenced potency.⁸⁶ It was seen that the pyridine C-5 tolerated small alkyl

substitution whilst the C-6 position required aryl substitution. Extension from the pyridine C-3 and C-4 seemed to greatly reduce potency.

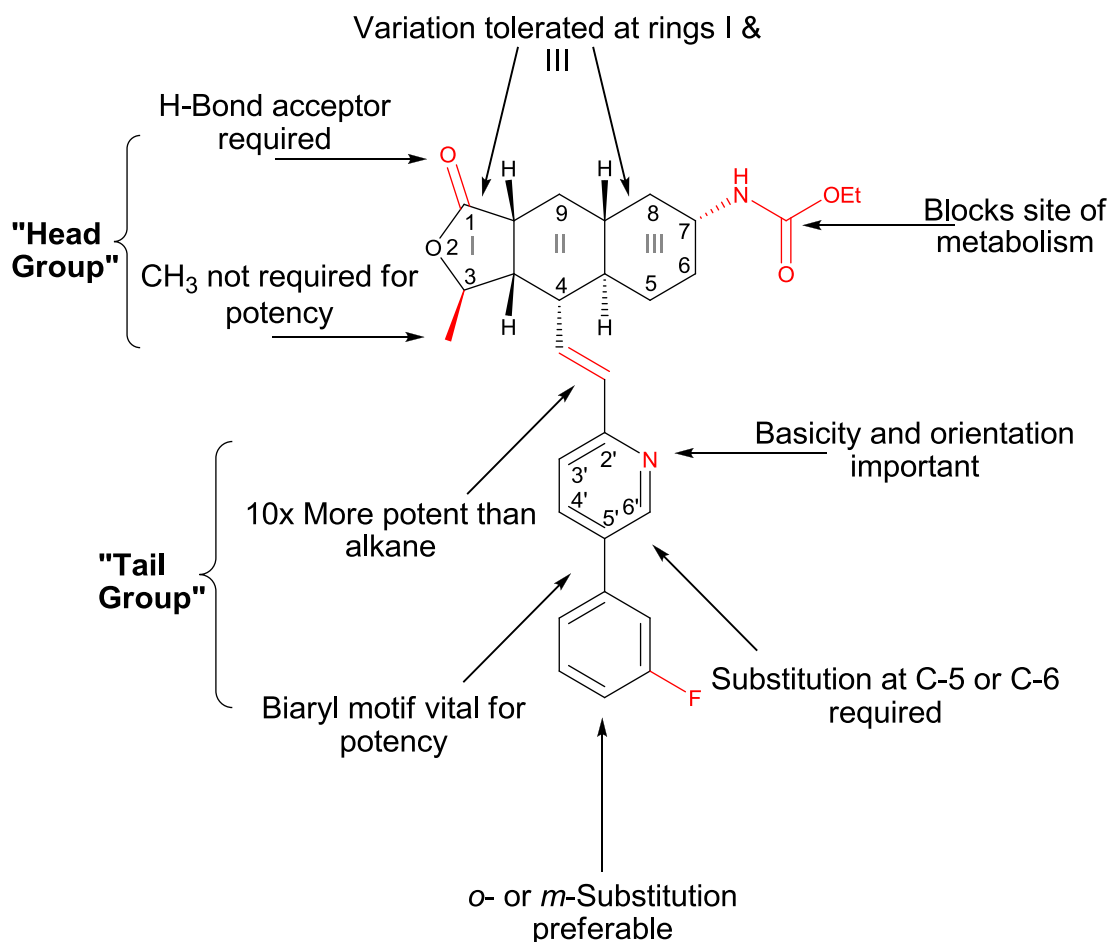


Figure 6: Summary of the Vorapaxar (7) SAR Studies

New Project Aims

Taking inspiration from the newly published synthetic route towards himbacine, it was concluded that novel vorapaxar analogues would be investigated. The first step would be to adapt the synthesis to give the *ent*-himbacine scaffold. It would then be necessary to complete the route to allow the attachment of the biaryl motif. Once full C-9 keto-analogues had been produced biological testing would be

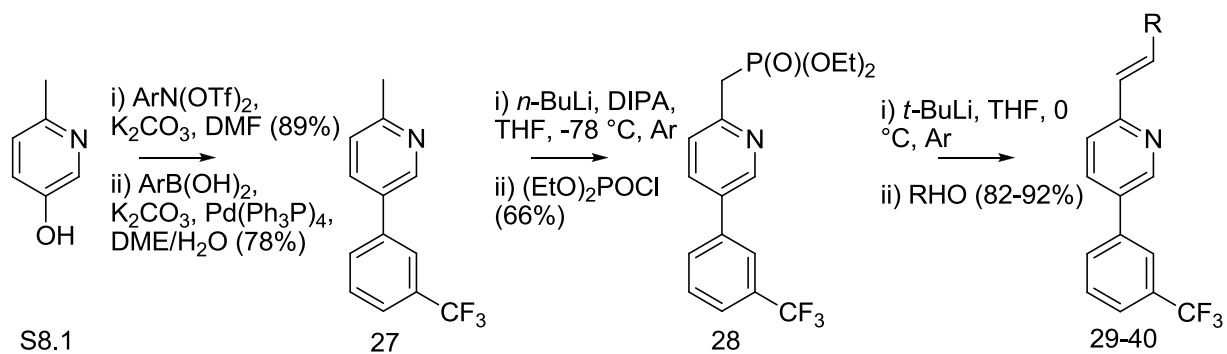
required to provide a proof of concept. It would be necessary to show that growth from the C-9 region would be tolerated. Finally, an SAR profile of different functional groups at this position would be ideal. Alongside this study, it was also hoped that some analogues of vorapaxar with smaller head groups could be profiled.

Results and Discussion

Vorapaxar Analogues with Smaller Head Groups

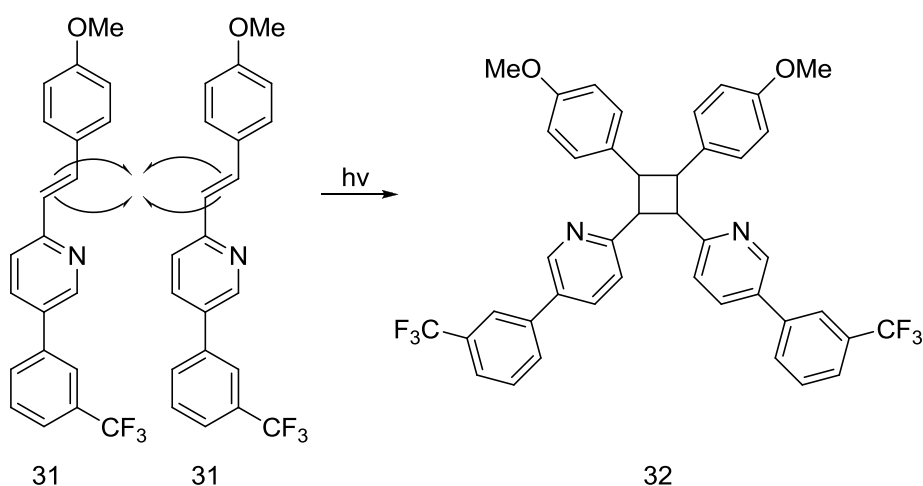
Synthesis

Synthesising vorapaxar analogues with smaller head groups could easily be achieved by coupling a biaryl phosphonate ester with a range of commercially available aldehydes using Horner-Emmons conditions. First the phosphonate ester needed to be synthesised. This was achieved using a similar sequence to that used by Schering-Plough. Initially, commercially available hydroxy-2-methylpyridine (**S8.1**) was converted to the trifluoromethanesulfonate ester using *N,N*-bis(trifluoromethylsulfonyl)aniline and potassium carbonate (K_2CO_3) in DMF to give **26** in good yields (89%). *N,N*-Bis(trifluoromethylsulfonyl)aniline was used instead of triflic anhydride as it is a safer triflating agent. It may not have been used in the original synthesis as it is not so atom efficient and the by-product can be difficult to remove. The next step involved the Suzuki coupling of the triflated starting material with 3-trifluoromethyl phenyl boronic acid. The conditions used for the synthesis of vorapaxar gave little or no yield. However, changing the solvents, from a mixture of toluene, ethanol and water, to dimethoxyethane (DME) and water gave 78% yield in the synthesis of the methyl substituted biaryl **27**. Finally, the methyl group was deprotonated with lithium diisopropylamide (LDA) (prepared *in situ*) and reacted with diethyl chlorophosphate to give the phosphonate ester **28** in reasonable yields (66%).



Scheme 8: Synthesis of Vorapaxar Analogues with Smaller Head Groups (**29-40**)

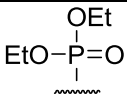
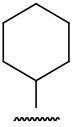
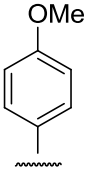
The biaryl phosphonate ester (**28**) was next deprotonated with *tert*-butyl lithium (*t*-BuLi) and coupled with a range of aldehydes (Scheme 8). Coupling with cyclohexanecarboxaldehyde gave the simplest of the analogues. In this reaction the (*E*)-product (**29**) was afforded in excellent yield (89%) whilst a minimal amount of the (*Z*)-product (**30**) was also produced (4%). In order to assess the effects of aryl head groups, *para*-methoxybenzaldehyde was coupled to the deprotonated phosphonate ester. Unfortunately, although the yields were reasonable (54-67%), it appeared that the product (**31**) dimerised about the alkene linker to give the dimer **32** (Scheme 9). This suggested that the compounds could be photosensitive so the subsequent compounds were made in dark conditions.

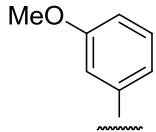
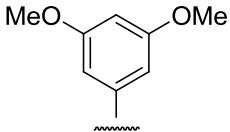
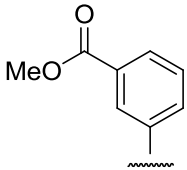
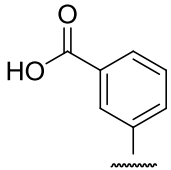
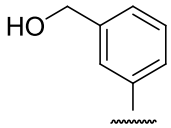
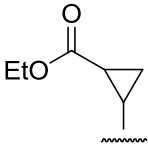
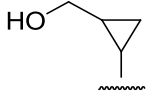
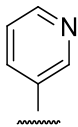


Scheme 9: Dimerisation of Analogue **31** Giving Compound **32**

meta-Methoxybenzaldehyde was coupled to the biaryl functionality in excellent yield (92%) to give **33**. It was hoped that having the methoxy in the *meta*-position would reduce dimerisation because the added electron density in the aryl group would not conjugate onto the alkene. This would make the alkene less electron rich and thus less reactive. The *meta*-methoxy group was also hoped to fulfil the requirement of having a hydrogen bond acceptor at the vorapaxar C-1 position. Consequently, *meta*-dimethoxybenzaldehyde was also coupled giving compound **34** in an 82% yield. In a similar vein, *meta*-carbomethoxybenzaldehyde was coupled because it would also offer a hydrogen bond acceptor. This reaction gave compound **35** in an 84% yield. A portion of **35** underwent base hydrolysis to give the acid product **36** in a 41% yield. A second portion was reduced using lithium aluminium hydride to give the hydroxyl product **37** in 61% yield. With the continuing aim of displaying a hydrogen bond acceptor in place of the vorapaxar C-1 carbonyl, ethyl-2-formyl-1-cyclopropanecarboxylate was coupled to give compound **38** in 83% yield. Again, the hydroxyl product **39** was obtained in 52% yield by reducing a portion of **38** using lithium aluminium hydride. Finally, nicotinaldehyde was coupled giving compound **40** in an 83% yield providing a second pyridine in the compound (Table 1).

Table 1: Vorapaxar Analogues with Smaller Head Groups

Compound	Head Group	Yield	Percentage Inhibition (3 μ M)	Percentage Inhibition (300 μ M)
28		66%	-29	20
29		89%	-21	41
31		62%	-25	13

33		92%	Not Tested	Not Tested
34		82%	-30	74
35		84%	Not Tested	Not Tested
36		41%	Not Tested	Not Tested
37		61%	Not Tested	Not Tested
38		83%	Not Tested	Not Tested
39		52%	Not Tested	Not Tested
40		83%	Insoluble	Insoluble

Biological Results and Discussion

A number of the compounds were tested, in the Ca^{2+} flux FLIPR assay, by our collaborators in the Chambers group. They were tested at concentrations of 3 and 300 μM against varying thrombin concentrations (0, 0.3, 3 and 10 μM). The

compounds were first dissolved in DMSO before they were diluted with biological medium containing the Fluo-4-NW dye which would fluoresce upon binding Ca^{2+} . Compound **40** was found to be insoluble in DMSO so it could not be tested. The insolubility may have been indicative of dimerisation.

The results are given as percentage inhibitions, calculated relative to the positive control (vorapaxar) and the negative control (medium + 0.5% DMSO). The compounds did not give significant inhibition when dosed at 3 μM (Figure 7). In the no thrombin condition, all of the tested compounds (apart from compound **34**) showed a relative inhibition around 100%. This shows that the compounds in themselves did not activate the PAR-1 as there was no activity without thrombin. Compound **34** gave an average relative percentage inhibition of 88%; however, if one looks at the three distinct trial values (99%, 97% and 69%) it could be assumed that the average was skewed by the one outlying data point of 69%. At 0.3 and 3 μM doses of thrombin, the compounds tended to give relative percentage inhibitions which clustered around that of the negative control. At the highest concentration of thrombin, the compounds gave negative relative percentage inhibitions, which in the case of compound **34** reached as low as -30%. This could suggest that the compounds were acting agonistically and adding to the effect of thrombin, although, if this were the case an effect should have been observed at 0 μM thrombin.

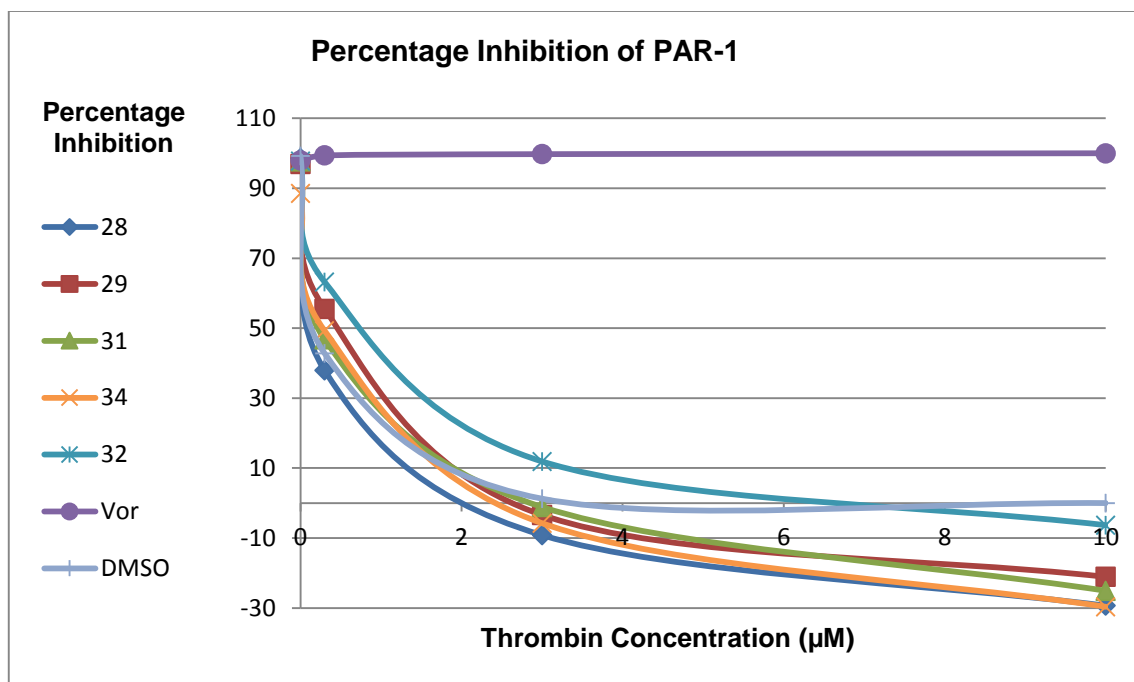


Figure 7 The average (n = 3) relative percentage inhibition observed upon the addition of thrombin at varying concentrations (0, 0.3, 3 and 10 nM) to human lung fibroblasts in buffer pre-incubated with Fluo-4 NW dye mix and 3 µM antagonist; 0.5% DMSO, Compounds **28**, **29**, **31**, **34**, dimer **32** and vorapaxar.

Testing the compounds at 300 µM showed slightly more promising results (Figure 8); compound **29** gave a relative percentage inhibition of 41% and better still compound **34** showed a 74% inhibition. Unfortunately, at this concentration, compounds **29**, **31** and **34** precipitated in the biological medium. This would have affected the passage of light through the wells and thus affected the results. This may have been the cause of the 26% relative inhibition seen with compound **34** at 0 µM thrombin. As a consequence, the results were inconclusive. In addition, because it was very difficult to tell whether the compounds had dimerised prior to or during the biological testing the rest of the analogues were not assessed.

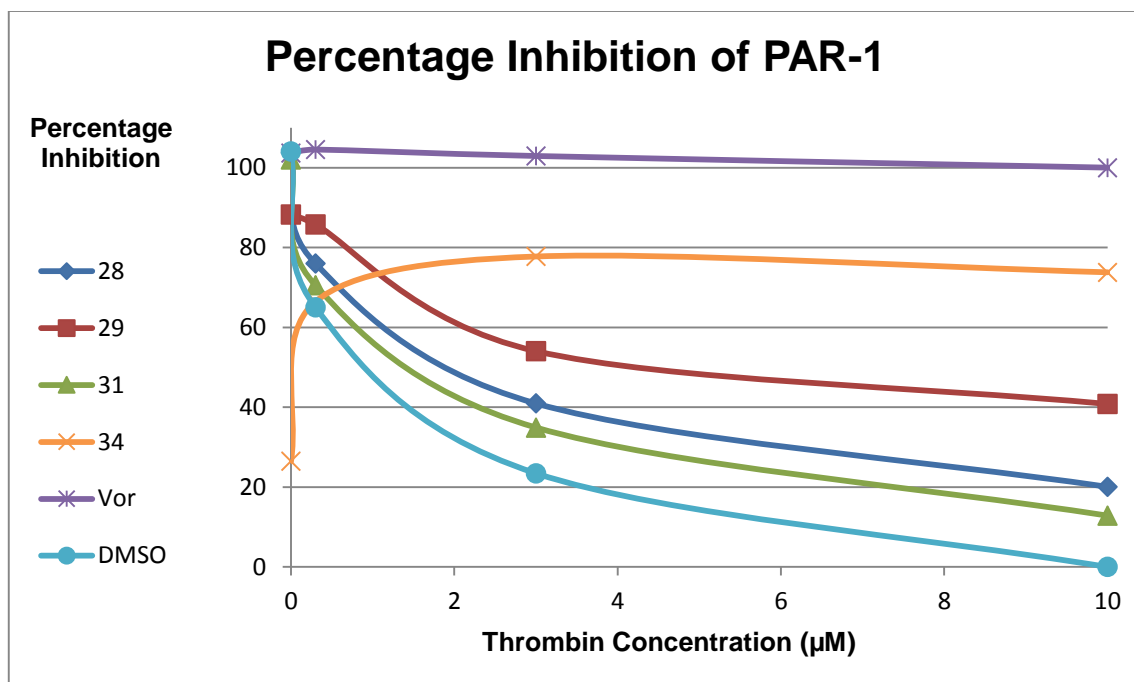


Figure 8: The average ($n = 3$) relative percentage inhibition observed upon the addition of thrombin at varying concentrations (0, 0.3, 3 and 10 nM) to human lung fibroblasts in buffer pre-incubated with Fluo-4 NW dye mix and 300 μM antagonist; 0.5% DMSO, Compounds **28**, **29**, **31**, **34** and vorapaxar.

In conclusion, although the vorapaxar analogues with smaller head groups were easy to synthesise and were given in good to excellent yields they suffered from dimerisation, poor solubility and lacked potency in the Ca^{2+} flux FLIPR assay. Consequently, this avenue of investigation was discontinued and all hope was pinned on the C-9 carbonyl derivatives of vorapaxar.

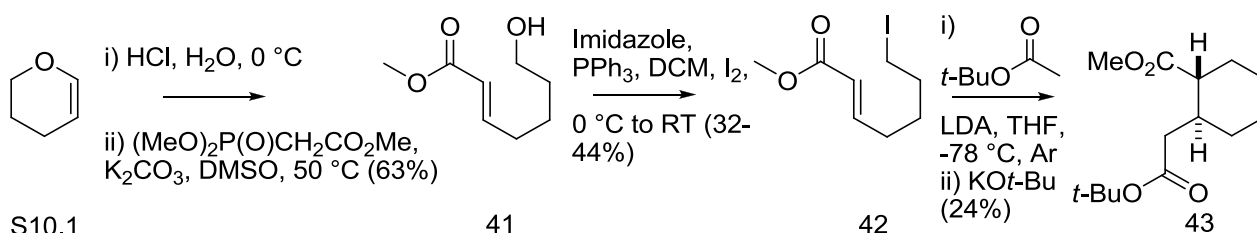
C-9 Substituted Vorapaxar Analogues

Synthesis

The first step towards the substituted C-9 vorapaxar analogues was to adapt the new himbacine synthesis, published by Casey *et al.*,¹²⁷ to give the *ent*-himbacine scaffold. It was decided that the C-7 carbamate found on vorapaxar would not be necessary. In the short term, the missing carbamate should make little difference to the potency of the compounds. In the long run omitting the carbamate would facilitate the topical administration of the compounds. They could be inhaled

straight into the lungs and to the site of the IPF lesions and then be quickly metabolised upon reaching the blood. This would avoid off-target effects as the drug would not be able to affect PAR-1s found at other sites.

The initial stage of the synthesis followed the steps used by Casey *et al.* to give the racemic cyclodiester (**43**) (Scheme 10). Commercially available 3,4-dihydro-2H-pyran (**S10.1**) was hydrolysed in H₂O, catalysed by HCl. The resultant tetrahydropyranol was then treated with K₂CO₃ and DMSO in the same pot to give an aldehyde which could undergo a Horner-Emmons reaction with trimethyl phosphonoacetate. Methyl 7-hydroxyhept-2-enoate (**41**) was obtained in a reasonable yield (63% over the two steps). The terminal hydroxyl group was displaced using imidazole, triphenylphosphine and iodine (I₂) to give compound **42** as the major product in low to moderate yields (32-44%).

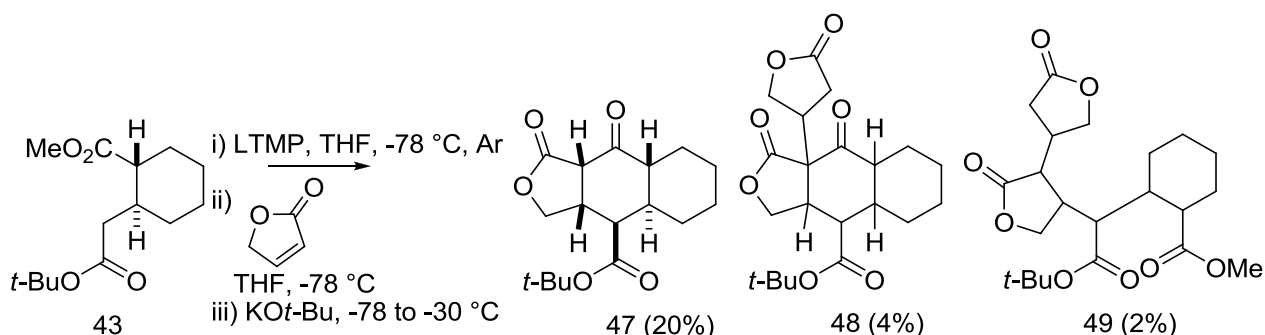


Scheme 10: Racemic Diester (**43**) Synthesis

The next step was to react **42** in a MIRC. LDA (made *in situ*) was used to deprotonate *tert*-butyl acetate. This then underwent Michael addition to **42** as it was added to the solution. Casey *et al.* suggested that the subsequent addition of potassium *tert*-butoxide (KO*t*-Bu) acted to destabilise the resulting lithium enolate allowing the final cyclisation. However, it was found that the addition of KO*t*-Bu, before or after the Michael addition, made very little difference to the yields of the reaction. In all cases the yields of **43** were typically low. This was partly because purification was particularly problematic. Purification by distillation was shown to be ineffective as the by-products appeared to distill at a similar temperature. Consequently, purification by flash column chromatography had to be relied upon. Unfortunately, monitoring the progression of the purification was very difficult

because **43** was optically inactive but co-eluted on thin layer chromatography (TLC) with both optically active and optically inactive by-products. The best method for identifying **43** was found to be by TLC stained with potassium permanganate. However, the major differential between **43** and the by-products was only the rate at which they stained. This made it quite difficult to tell which column fractions contained product and which contained impurity. In the end the best purification method was found to be reverse-phase column chromatography which still gave very close running impurities.

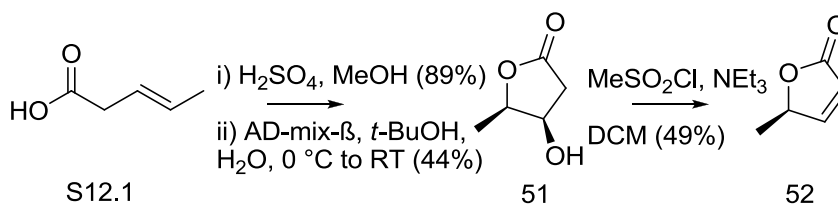
Despite the difficult purifications **43** was eventually isolated in 20-30% yield. With the diester in hand the tricycle synthesis could be completed. Initially the reaction was trialed with commercially available 2(5*H*)-furanone. **43** was deprotonated with lithium tetramethylpiperidine (LTMP) (made *in situ*). For the best results, it was found that the LTMP should be made with freshly distilled 2,2,6,6-tetramethylpiperidine (TMP), using flame-dried glassware and with the lithiation occurring at 0 °C (after the addition of *n*-butyl lithium (*n*-BuLi) at -78 °C). Following the deprotonation of **43**, back at -78 °C, furanone was added promoting the Michael addition. Casey *et al.* next added KO*t*-Bu before warming the reaction to -30 °C to allow the final intramolecular Claisen condensation. It was initially thought that the KO*t*-Bu was essential for the reaction to progress however it was later found that, in our hands, the reaction proceeded more efficiently without it.



Scheme 11: Racemic Tricycle Synthesis giving Compounds **47**, **48** and **49**

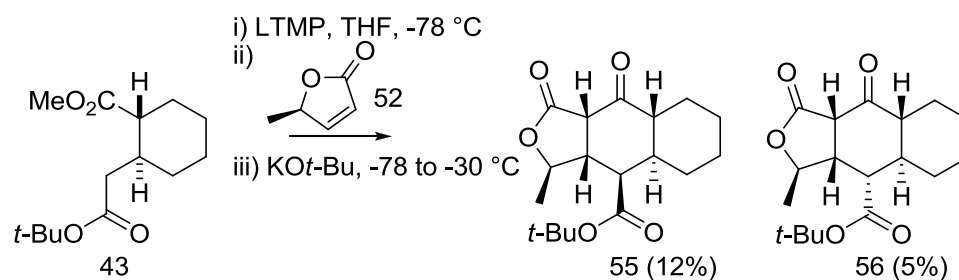
In the early trials of this reaction, excess furanone was used which resulted in double addition side products both on the cyclised and uncyclised scaffolds (Compounds **48** and **49**). This resulted in poor yields for the desired tricycle products. The major product was compound **47** which was obtained in 20% yield (Scheme 11). This unfortunately had the undesired stereochemistry at C-4. Nevertheless, with some working conditions for the reaction in hand it was important to trial the reaction with enantiocontrol.

It was believed that the *ent*-himbacine tricycle scaffold could be made by using an enantiomerically pure furanone in the tricycle synthesis. It was hoped that an *R*-methyl group at the furanone C-5 would set the stereochemistry of the tricycle in a similar vein to that seen by Casey *et al.*. The enantiomerically pure furanone was made from pent-3-enoic acid (**S12.1**) which was first esterified using sulfuric acid (H₂SO₄) in methanol (MeOH) to give methyl pent-3-enoate (**50**) in good yield (89%). Next, a Sharpless asymmetric dihydroxylation, using AD-mix-β in a 50:50 mixture of *tert*-butanol (*t*-BuOH) and H₂O, gave the dihydroxylated product which spontaneously cyclised to give the dihydrofuranone **51** in a moderate yield (44%). Finally, treatment with triethylamine (NEt₃) and methanesulfonyl chloride (MeSO₂Cl) in dichloromethane (CH₂Cl₂) gave the dehydration product **52**; again, in moderate yields (49%) (Scheme 12). It was found that the products were relatively volatile so in later syntheses **51** was extracted into CH₂Cl₂ which was only partially evaporated away before the dehydration step. Unfortunately, the yield was still not significantly improved with a 27% yield across the two steps.



Scheme 12: Stereospecific Furanone (**52**) Synthesis

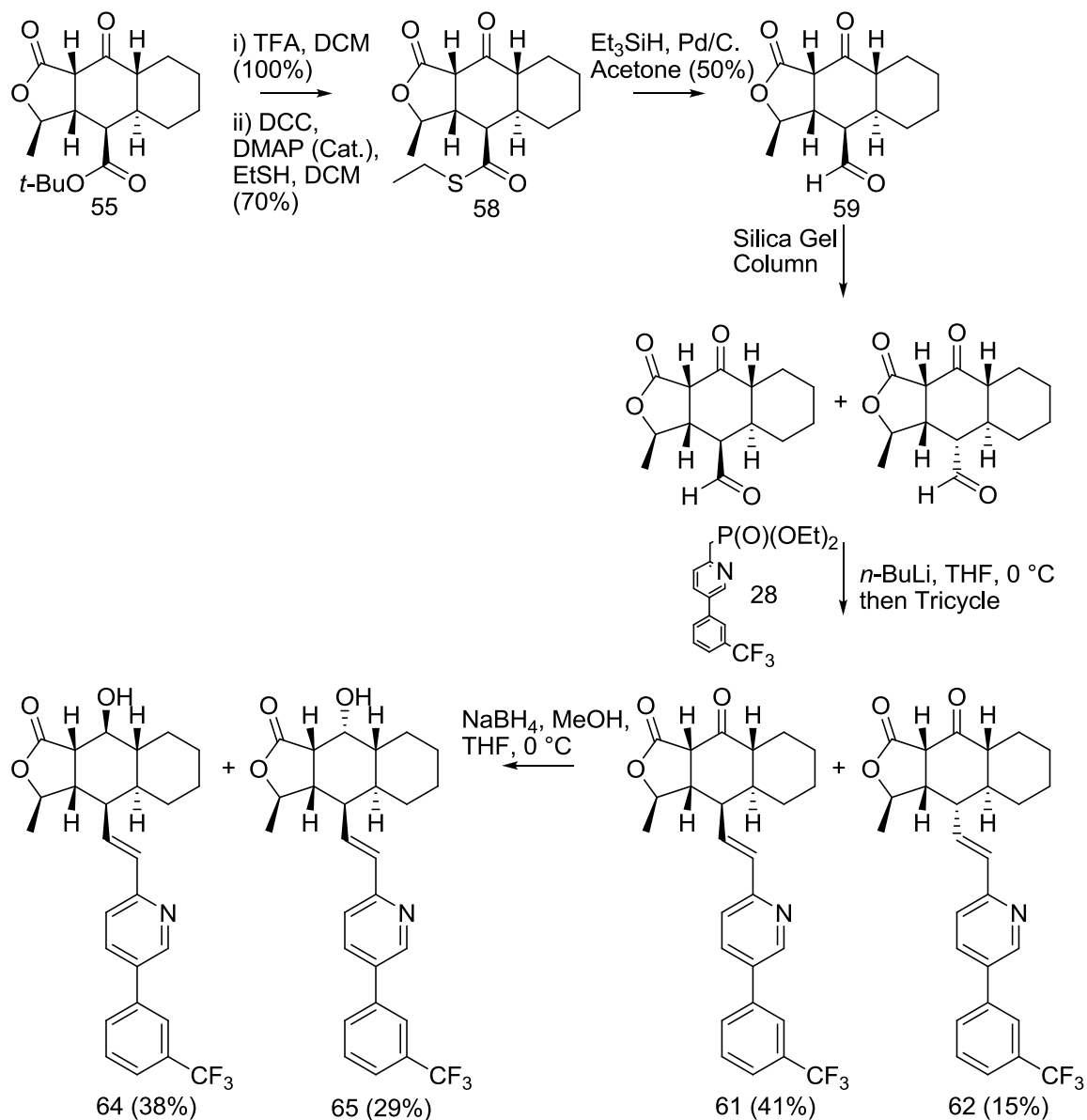
The tricycle synthesis was completed using **52**. Casey *et al.* used 0.5 equivalents of the methylfuranone to achieve a degree of kinetic resolution on the racemic diester. They showed a threefold selectivity for the desired diester enantiomer. In the 2-furanone investigations it had been found that using 0.5 or 1 equivalents made little difference to the stereoselectivity but using 4 equivalents led to further addition of the furanone to C-9a. As a consequence, the stereoselective tricycle synthesis was carried out with 0.5-0.7 equivalents of **52**. Using the conditions acquired on request from Casey *et al.* tricycle **55** was obtained in a 12% yield whilst the desired tricycle, **56**, was only given in a 5% yield (Scheme 13). There was again about 25% of starting material returned and small amounts of other isomers made. This made it difficult to purify, which impacted further on the yields.



Scheme 13: Synthesis of Chiral Tricycles Giving Compounds **55** and **56**

Casey *et al.* did not develop the synthesis past the *tert*-butyl tricycle so with the desired enantiomerically pure tricycle in hand it was next necessary to convert the C-4 *tert*-butyl ester into an aldehyde so the vorapaxar biaryl motif could be attached. One option would have been to follow the protocol used in the vorapaxar synthesis. However, this used tributyltin hydride which is very toxic. Instead, the first step was to de-protect the *tert*-butyl group using trifluoroacetic acid (TFA) and CH₂Cl₂. This was done with 100% conversion to give the carboxylic acid **57**. This was then coupled with ethanethiol, using DCC and catalytic 4-dimethylaminopyridine (DMAP) as the coupling reagents, to give the thioester **58** in around 70% yield. The resulting thioester was then reduced using triethylsilane and catalytic palladium on carbon to give the aldehyde **59** in moderate yields (50%). These were mild reducing conditions¹³² which did not appear to attack the lactone

ring. Further, upon silica gel column chromatography purification, the aldehyde partially epimerised at the C-4 position (Scheme 14). This meant that the more readily available but undesired C-4 epimer could be used to form a portion of the desired epimer via this pathway.



Scheme 14: Vorapaxar Analogue Synthesis Giving Compounds **61**, **62**, **64** and **65**

The final step was to couple **28** with **59**. **28** was deprotonated with *n*-BuLi before **59** was added to allow the Horner-Emmons reaction to proceed in a reasonable

yield. Since the aldehyde epimerised to give inseparable isomers of **59** the Horner-Emmons reaction gave compound **61** in a 41% yield and compound **62** in a 15% yield. Compounds **61** and **62** were readily separable. Further, analytical chiral high-performance liquid chromatography (HPLC) of **61** gave two peaks of 95% and 5%. This suggests that the asymmetric synthesis gave an enantiomeric excess (ee) of 90%.

Since more of **61** had been synthesised, a portion of it was reduced with sodium borohydride to convert the C-9 ketone into a C-9 hydroxyl giving (9*R*)-hydroxy-compound **64** and and the (9*S*)-hydroxy-compound **65** in 38% and 29% yield, respectively. It was thought that the hydroxyl products would be important for SAR purposes as the sp² carbon on the ketone would give a different tricycle ring configuration in comparison to the sp³ carbon observed with the hydroxyl-analogues.

Proof of Concept

The completed stereospecific C-9-substituted vorapaxar analogues were tested in the Ca²⁺ flux FLIPR assay in order to prove that they could actually be used to inhibit the PAR-1. The compounds were tested using HLF and 10 nM thrombin as the agonist. The positive control was a sample of RWJ-58259 (synthesised by a colleague within the group) whilst the negative control was DMSO in biological medium. Each compound was tested 6 times across two different days. In the first instance all of the compounds were tested across a concentration range of 0.0003-30 μM. If the compound did not show full antagonism by 30 μM on the second round of testing it was tested at concentrations ranging from 0.003 μM to 300 μM.

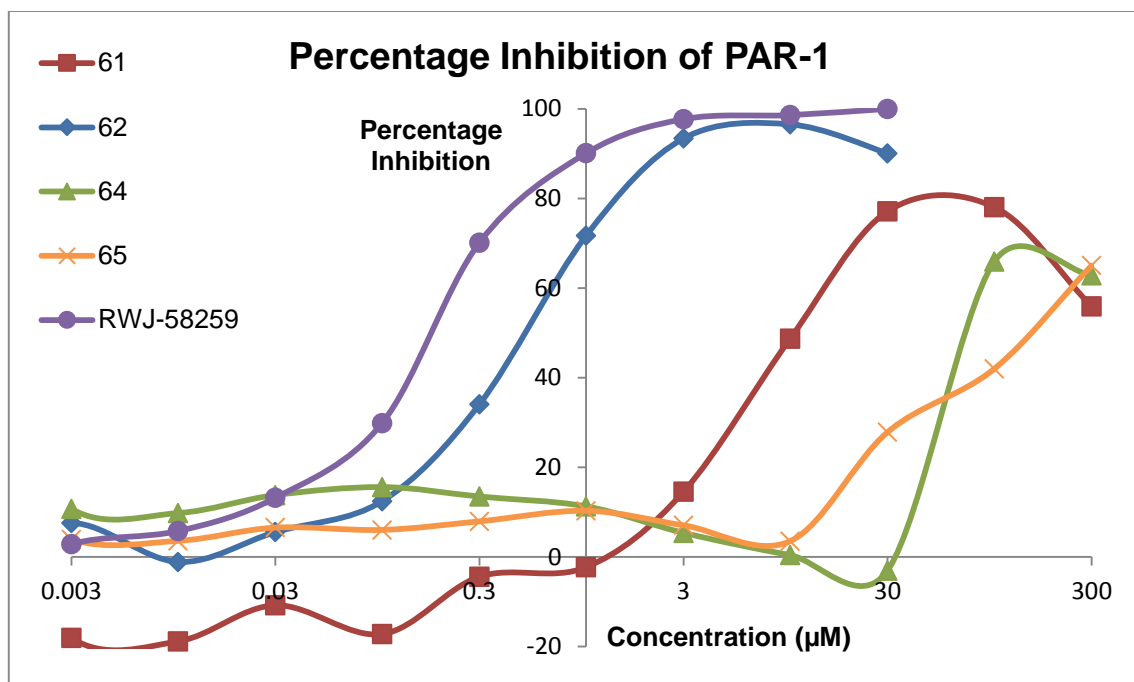


Figure 9: The average (n = 6) percentage inhibition observed upon the addition of thrombin (10 nM) to human lung fibroblasts in buffer pre-incubated with Fluo-4 NW dye mix and 0.0003 - 30 µM antagonist; Compounds **61**, **62**, **64**, **65** and RWJ-58259

The results from the Ca²⁺ flux FLIPR assay suggested that the C-9-substituted vorapaxar analogues were tolerated in PAR-1 and gave dose-dependent inhibition. Unfortunately, none of the compounds were as potent as the RWJ-58259 sample (IC₅₀ = 0.19 µM) which in turn would make them much less potent than vorapaxar. Interestingly, the hydroxyl-analogues were less potent (IC₅₀: **64** = 80 µM and **65** = 150 µM) than the keto-analogues (IC₅₀: **62** = 0.5 µM and **61** = 10 µM). This suggests that the ring configuration promoted by the sp² C-9 was preferred. However, the hydroxyl compounds were only made from **61**, the least potent of the two keto-analogues. This was because, with only 14 mg of compound **62**, there was insufficient material to give useful quantities of the hydroxy-compounds. Therefore, one of the questions that needed to be addressed going forward was whether the hydroxyl-analogues derived from **62** were in fact more potent than those derived from **61**. All the same, this study gave proof of concept and opened the avenue for the development of more novel vorapaxar analogues that would hopefully give greater potency.

Computational Modelling

The strength of binding of vorapaxar to PAR-1 was clearly of interest to other people in the scientific community. Shortly after our proof of concept study had been completed a paper was published with the crystal structure of vorapaxar bound to PAR-1.¹³³ This highlighted some interesting details with regards to the mode of binding. It was shown that vorapaxar bound very close to the extracellular surface in a tunnel made up of residues from the transmembrane segments. The binding site appeared to only have a small opening to the extracellular surface so it was hypothesised, in the paper, that vorapaxar got into the binding site by diffusing across the lipid bilayer.

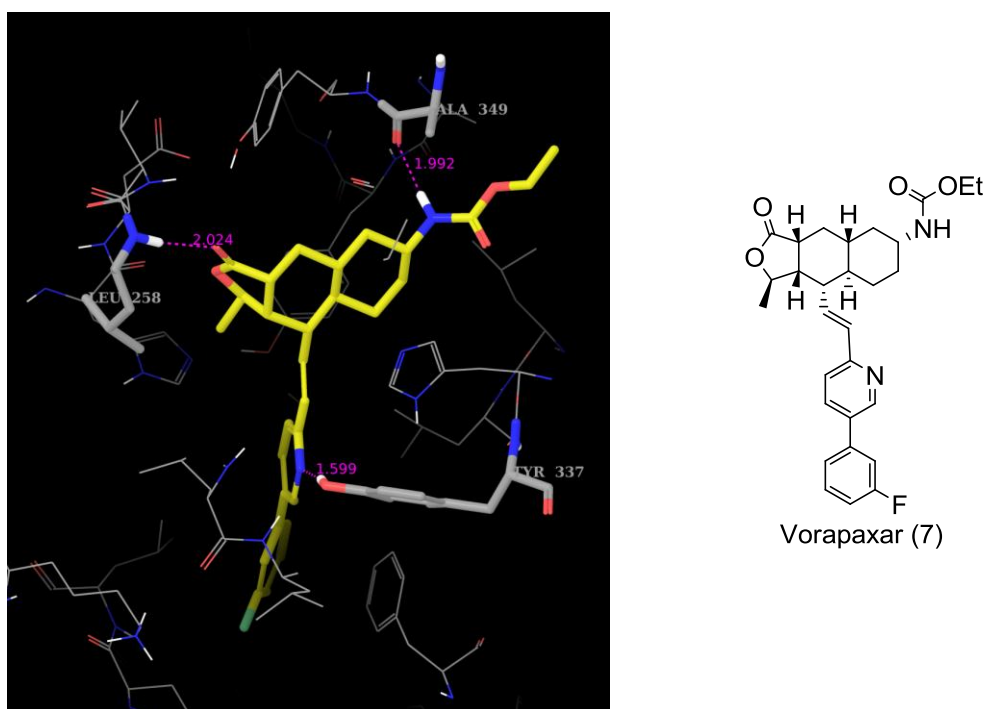


Figure 10: Computational Model of Vorapaxar (7) Binding PAR-1 Based on Published Crystal Structure¹³³

The published crystal structure allowed the established SAR of vorapaxar and the results from our proof of concept study to be rationalised using computational modelling. Vorapaxar was docked, by our collaborators at GSK, into a computational model of the vorapaxar binding site on PAR-1 (Figure 10). The key hydrogen bonds (H-bond) seen support the SAR profile of vorapaxar. The basic

nitrogen on the pyridine appeared to form a strong H-bond to the tyrosine-OH whilst the C-1 carbonyl was calculated to form an H-bond with the leucine-NH. This helped to explain the observed importance of the pyridine and C-1 carbonyl groups. The third H-bond appeared to be between the NH on the carbamate and the carbonyl on a PAR-1 alanine. This was interesting because the SAR profile suggested that the carbamate was not important for the potency of vorapaxar. If the H-bond shown in the computational model was a true H-bond then it would be expected to influence the potency. Typically each additional H-bond a ligand can form with the receptor will lead to an increase in the potency. Despite this one unexpected H-bond, the computational modelling appeared to be a useful tool.

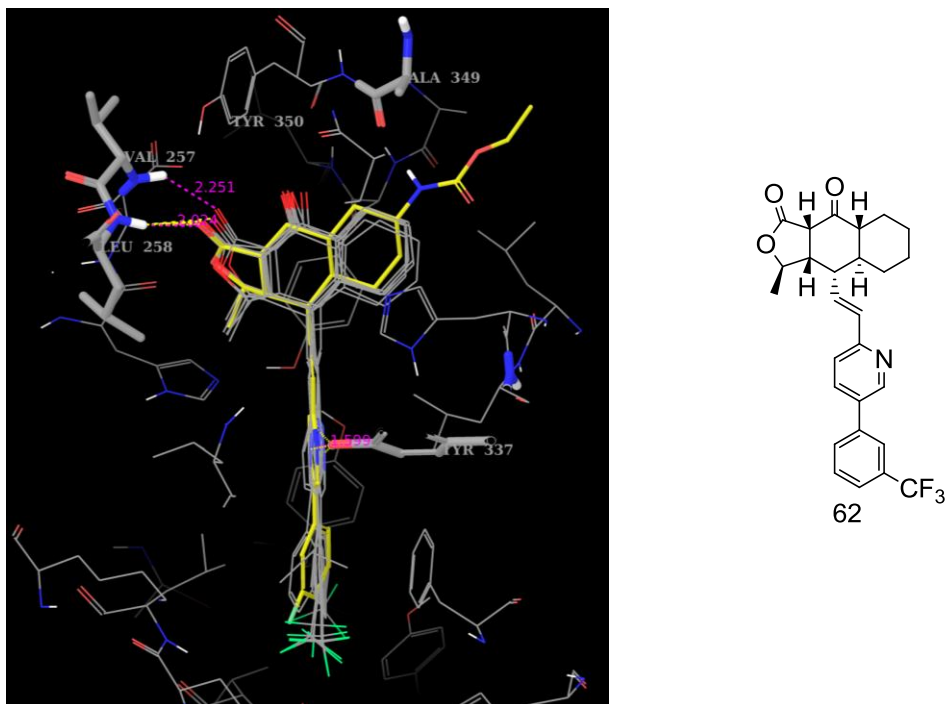


Figure 11: Computational Model of **62** Binding PAR-1 Based on Published Crystal Structure

The stereospecific C-9-substituted vorapaxar analogues, which had already been tested in the proof of concept study, were docked into the same computational model. The closed, tunnel-shaped binding pocket should have meant that there was very little room to expand from the C-9 position. This may have explained the reduction in potency observed with the C-9-substituted analogues in comparison to

vorapaxar. In theory, the additional bulk of the carbonyl could have pushed the analogues deeper into the pocket disrupting the H-bond network. However, it can be seen from the model that **62**, the most potent of the tested compounds, docked in a very similar fashion to vorapaxar (Figure 11). Again, the pyridine nitrogen was shown to form an H-bond with the tyrosine-OH and the C-1 carbonyl was seen to be H-bonding with the leucine-NH. The additional C-9 carbonyl did not appear to be affecting the mode of binding at all making it difficult to rationalise the considerable difference in potency between **62** and vorapaxar.

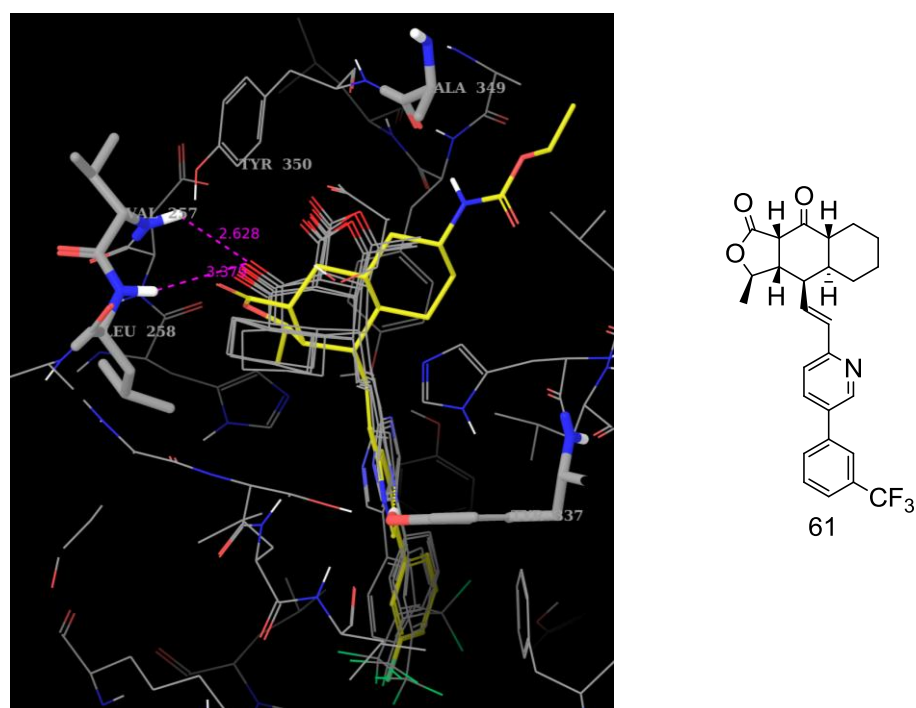


Figure 12: Computational Model of **61** Binding PAR-1 Based on Published Crystal Structure

The computational modelling was much more powerful in helping to explain the differences in potencies across the tested compounds. Whilst **62** docked in a very similar fashion to vorapaxar, **61**, the 4R-epimer of **62**, seemed to bind with the tricycle rotated by 180°. This meant that the C-1 carbonyl was no longer able to form the favourable H-bond, instead the C-9 carbonyl now appeared to be forming a weak, bifurcated H-bond with the leucine and valine-NH (Figure 12). The loss of

one of the key interactions would be sufficient to explain the 10 fold decrease in potency observed between **61** and **62**.

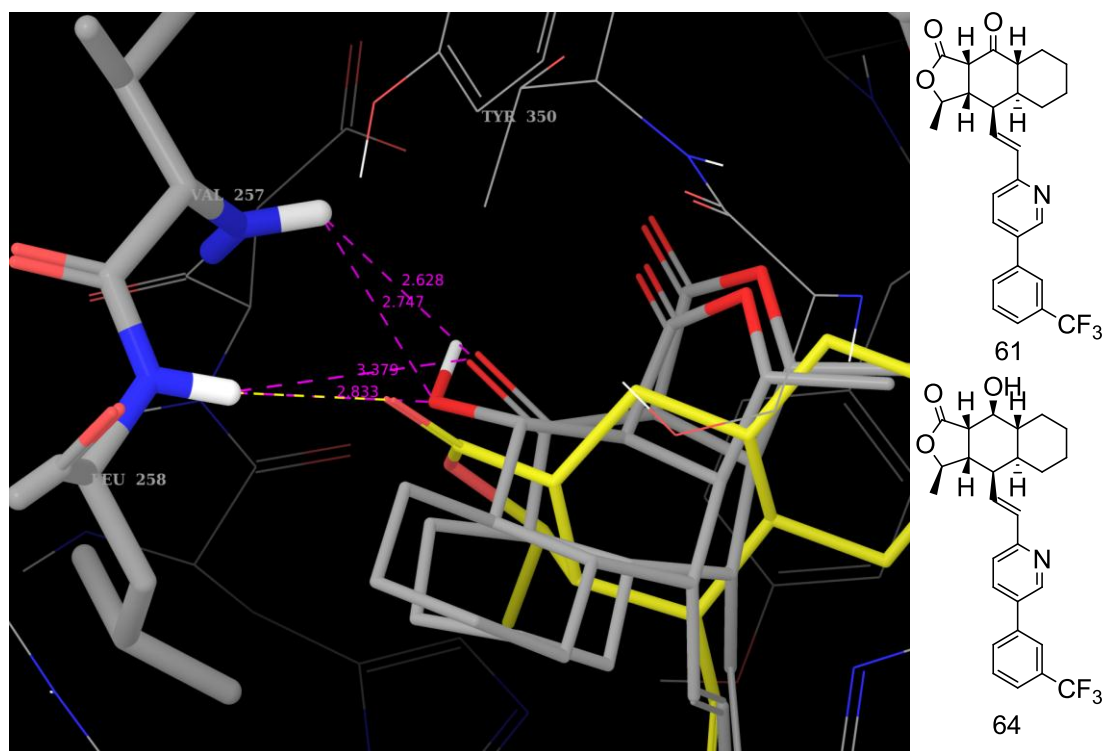


Figure 13: Computational Model Comparing the Docking of **61** and **64** to PAR-1

The fact that the C-9-hydroxyl compounds had only been made from the less potent **61** meant that they also docked with the tricycle rotated by 180°. However, comparing the docking pose of **61** to its hydroxyl derivative, **64**, (Figure 13) gave an indication as to why the hydroxyl compounds were less potent. Reducing the carbonyl group removed the easily accessible H-bond acceptor which was forming the bifurcated H-bond. Instead, a third H-bond donor was created causing potential clash between the C-9-hydroxyl and the PAR-1 leucine and valine-NH. Nevertheless, there was still possibility for an H-bond to form between the leucine and valine NH and the oxygen on the hydroxyl group. This could then explain the difference in potencies between the two hydroxyl compounds. It can be seen from Figure 14 that the hydroxyl group on compound **64** is closer to the H-bond donors on the leucine and valine. As a consequence, it could be proposed that **64** would

make stronger H-bond interactions than compound **65**. This would reflect in the relative potencies observed with the two compounds.



Figure 14: Computational Model Comparing the Docking of **64** and **65** to PAR-1

In addition to using the computational modelling for rationalising observed results it was hoped that it would be possible to use it as a predictive tool. Looking at other residues in the binding pocket would highlight regions on the molecule that could be altered to make the C-9-substituted compounds more potent. Figure 15 shows that in the region of the pyridine there are two other tyrosines close enough to form H-bonds. In theory, having a pyrimidine instead of a pyridine could lead to a second H-bond to the biaryl portion of the compounds and thus an increase in potency. Testing this experimentally would help to justify the strength of the predictability of the computational model.

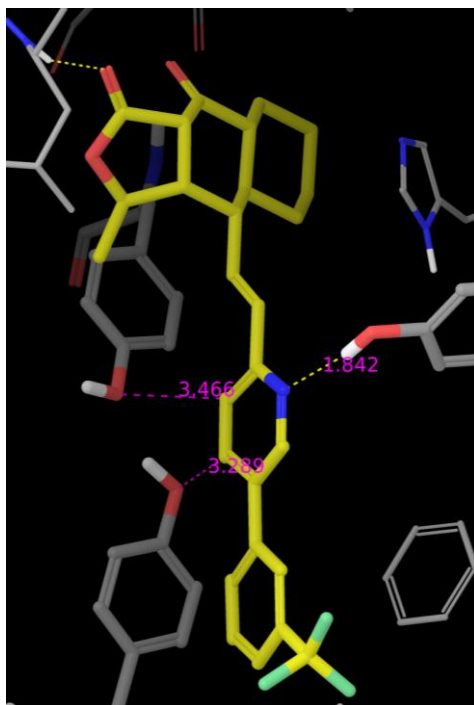


Figure 15: Using Computational Modelling as a Predictive Tool

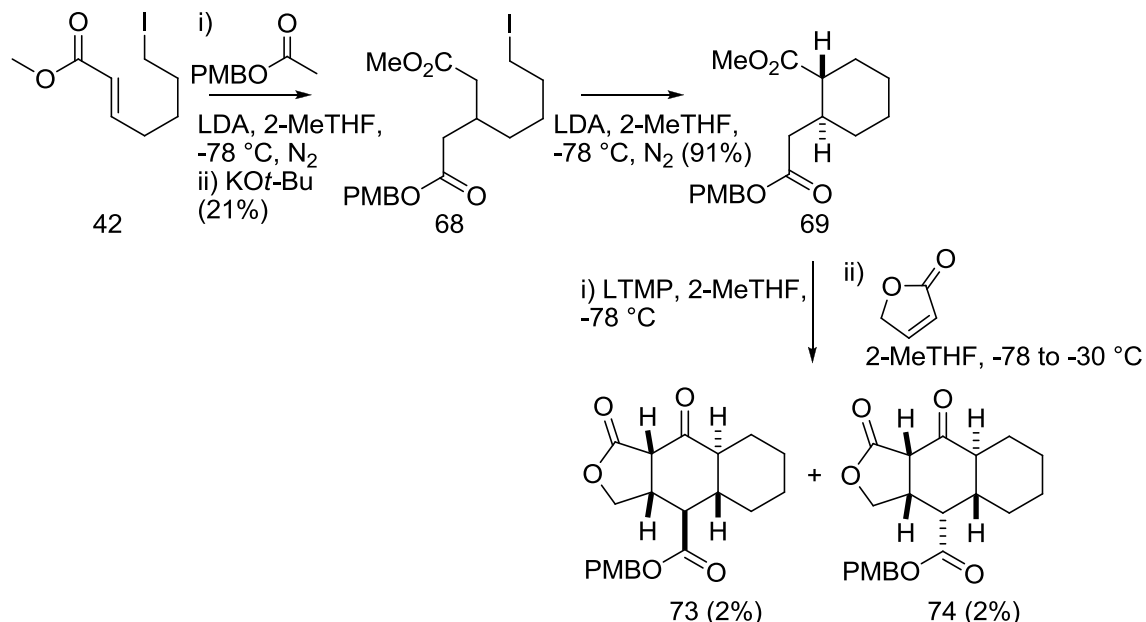
Optimisation

The synthesis of the stereospecific C-9-substituted vorapaxar analogues highlighted several issues with the chosen route. In fact the synthesis was much more troublesome than would have been predicted from the paper published by Casey *et al.* As a consequence, several different approaches were investigated to try and achieve greater overall yields of the desired keto-vorapaxar analogues. It was hoped that enough could be made to provide a stock batch which could be diversified ready for SAR profiling.

The starting materials being used to make the tricyclic were needed in large quantities so it seemed appropriate to try and optimise these steps. Of the early steps, the iodination was the lowest yielding transformation. The Appel-like reaction was very effective in converting the terminal hydroxy-group into a terminal iodine. However, the reaction created large amounts of triphenylphosphine oxide which co-eluted with the desired product. This necessitated multiple purifications by silica gel column chromatography which greatly reduced product recovery.

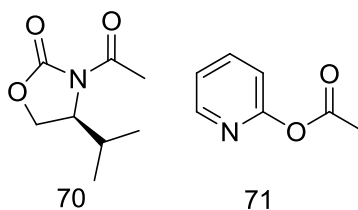
Consequently, the reaction was trialled in a different solvent; *tert*-butylmethylether (*t*-BME). The reaction appeared to progress just as efficiently but the triphenylphosphine oxide crashed out into the *t*-BME allowing the majority of it to be filtered off. This meant that only one round of column chromatography was required and a larger proportion of the product was recovered.

The improvements made to the iodination were useful but there were definitely more significant issues that needed to be addressed. One of these issues was the poor yields and purification complications seen during the diester synthesis. It was thought that changing the ester protection group could provide a UV active product which would be easier to identify during purification and thus improve the yields. *para*-Methoxybenzyl acetate was trialled in the diester synthesis. The *p*-methoxybenzyl group was successful in giving traceable products but it also gave a large number of impurities which made purification difficult. The major product from this reaction was the uncyclised diester **68**. Despite being the major product, **68** was still only obtained in a low 21% yield. Fortunately, simply treating **68** with LDA gave cyclisation to **69** in excellent (91%) yield (Scheme 15).



Scheme 15: *p*-Methoxybenzyl Protected Tricycle Synthesis Giving Compounds **73** and **74**

The *p*-methoxybenzyl group still gave lots of impurities and required two steps to get to the diester. Clearly, it was not the best choice of protection group. As a consequence, it was hoped that the tris(triethylsilyl)silyl (“supersilyl”) group could be used as an alternative to make a suitable acetate for the diester synthesis. The “supersilyl” group had been shown to be a suitable carboxylic acid protecting group which was UV-active, stable and suitable for providing selectivity in aldol reactions.¹³⁴ Regrettably, despite several conditions being trialled, the “supersilyl” acetate was not successfully synthesised. On the other hand, an Evan’s auxiliary was easily acetylated using acetyl chloride and *n*-BuLi in 2-methyltetrahydrofuran (2-MeTHF) to give (*S*)-3-acetyl-4-isopropylloxazolidin-2-one (**70**) in 89% yield. The diester synthesis was trialled with **70** with the hope that it could direct the transition state to get an enantioenriched diester. In turn, it was hoped that this would direct the subsequent tricycle synthesis and improve the yield of the desired tricycle scaffold. Unfortunately, the diester formation reaction did not work when **70** was used. Equally, the diester synthesis did not work when trialled with pyridin-2-yl acetate (**71**) which had been made in a 33% yield by reacting pyridin-2-one with acetyl chloride in the presence of pyridine. It was unfortunate that the pyridine protected diester could not be synthesised because it had been shown that pyridinyl esters can be reduced directly into aldehydes in a similar fashion to the sulfonate ester reduction.¹³⁵ This would have decreased the number of synthetic steps required following the synthesis of the tricycle and thus increased the overall yield.



Compounds **70** and **71**: Acetates Trialled in Diester Synthesis

Since most of the protected acetates had not been successfully turned into the relevant diester only the *p*-methoxybenzyl protected diester could be taken forward

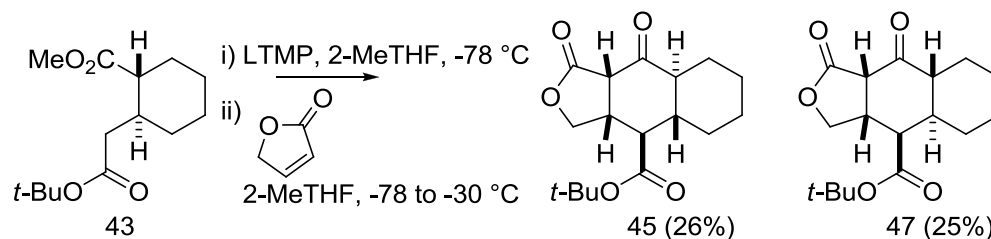
for the tricycle synthesis. Compound **69** was reacted using the established tricycle synthesis conditions but gave very poor yields. The two tricycles **73** and **74** were obtained in only 2% yield each (Scheme 15). Additionally, they were derived from the (1*S*,2*R*)-diester. This meant that not only was a very small amount of material isolated it was of the wrong relative stereochemistry. It was concluded that it would be best to resort back to the *t*-butyl protecting group despite the issues associated with its use.

In addition to continuing with the *t*-butyl protection group, the use of the commercially available 2-(5*H*)-furanone was returned to in an attempt to simplify the tricycle synthesis. Using 2-(5*H*)-furanone avoided the three extra, low yielding, steps required to make the stereospecific furanone. Obviously, using the commercial furanone would lead to the synthesis of racemic compounds. This is because the double bond could easily be approached from both sides without the added steric bulk of the methyl group creating a bias. The racemic products would need to be separated so it was hoped that this could be completed using chiral column chromatography.

LTMP is one of the strongest bases available and since it was required for the initial deprotonation other choices of base were not explored as they simply would not have been strong enough. However, a few adaptations were made to the original synthetic route proposed by Casey *et al.*. The use of KO*t*-Bu following deprotonation with LTMP was found to be unnecessary. The reaction solvent was switched from tetrahydrofuran (THF) to 2-MeTHF. This was only done to allow the reaction solvent to be used directly for extraction following work-up. Finally, during the initial lithiation of TMP, the reaction mixture was warmed to 0 °C to aid the formation of LTMP. Otherwise, the reaction conditions were fairly close to those provided by Casey *et al.*.

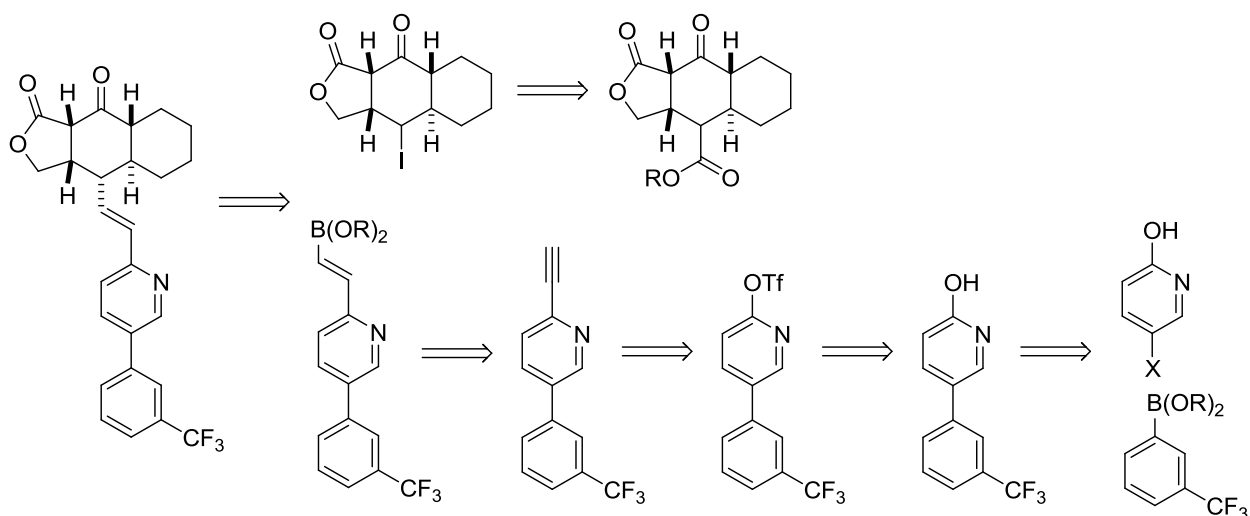
These optimisations led to minor improvements in the yields. In the most successful attempt of the racemic tricycle synthesis both enantiomers of the diester

reacted efficiently. In this case the major products were **45** and **47** which were made in 26% and 25% yields respectively (Scheme 16). Evidently, the furanone seemed to add preferentially to give the relative *R*-stereochemistry at C-4 no matter which enantiomer of **43** reacted. Either way, the combined yield was only 51% which was disappointing considering Casey *et al.* obtained a 53% yield of **47** alone. The still comparatively poor yields could be accounted for by the considerable amount of returned starting material along with the presence of some uncyclised product and a small amount of the *S*-C-4 product (compound **75** in the experimental section).



Scheme 16: Optimised Racemic Tricycle Synthesis Giving Compounds **45** and **47**

Since the tricycle synthesis was still low yielding and problematic, despite optimisation, the idea of using a different coupling method to attach the biaryl motif was investigated. It was hoped that a coupling method which required fewer synthetic steps on the tricycle portion could be used. One way of achieving this would be to functionalise the biaryl motif to give an allyl boronic ester or acid whilst converting the *t*-butyl ester on the tricycle into a halogen allowing the final coupling to be done with a Suzuki reaction. There was literature evidence to suggest that an ester could be directly replaced by an iodine in a one pot, two step, reaction.¹³⁶ Consequently, it was thought that the biggest challenge would be to furnish the biaryl portion with an allyl boronic ester or acid.



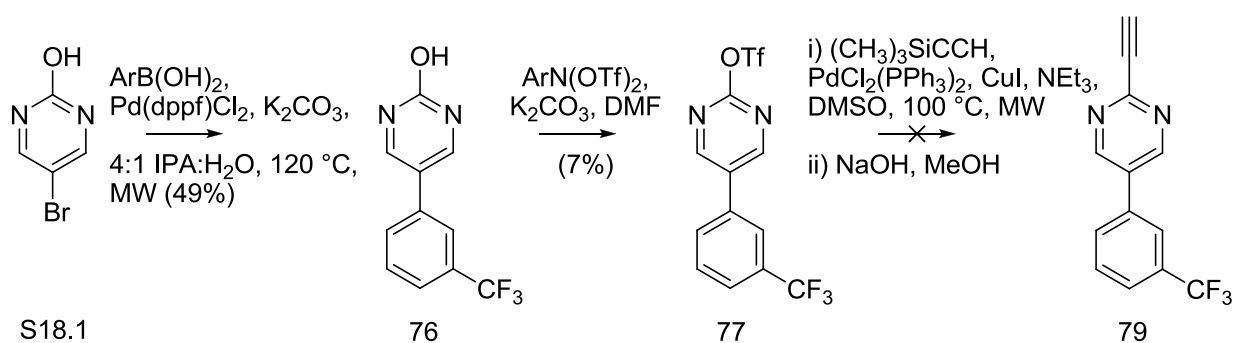
Scheme 17: Retro-Synthetic Analysis of Suzuki Coupled Analogues

Alkynes can be borylated to give *trans*-allyl boronic acids,¹³⁷ thus it was hoped that a Sonogashira reaction could be used to install an alkyne onto the biaryl motif. There was literature precedent which suggested that using trimethylsilyl acetylene for the Sonogashira followed by a basic work-up could give the required terminal alkyne.¹³⁸ Since the biaryl portion was originally constructed using a Suzuki reaction it would be necessary to consider the order of the reactions to selectively install the alkyne onto the pyridine at the 2-position and the second aryl group at the 5-position. Therefore it was hoped that the Sonogashira could be carried out on a triflate group which could be installed after the addition of the aryl group with a Suzuki reaction (Scheme 17).

The investigations for the Suzuki coupled analogue route were carried out using a pyrimidine rather than the pyridine found on the vorapaxar biaryl portion. It was thought that using a pyrimidine had the potential to increase potency whilst introducing another degree of novelty to the vorapaxar analogues. This was based on the predictions from the computational modelling which suggested that there was the potential to form a second H-bond to the biaryl portion.

The initial Suzuki reaction for the trial route was found to be successful using 5-bromopyrimidin-2-ol, (3-(trifluoromethyl)phenyl)boronic acid, [1,1'-bis

diphenylphosphino)ferrocene]dichloropalladium ($\text{PdCl}_2(\text{dppf})$) and K_2CO_3 in a 4:1 mix of isopropanol (*i*-PrOH) and H_2O at $120\text{ }^\circ\text{C}$ in a microwave. It gave compound **76** in a 49% yield. The triflation was subsequently attempted using both *N,N*-bis(trifluoromethylsulfonyl)aniline and triflic anhydride as the triflating reagents. The former gave 7% of the desired biaryl-triflate **77**, whilst the latter gave nothing upon purification. It was presumed that the product was very unstable. However, the small amount of product retrieved was trialled in the Sonogashira reaction (Scheme 18).

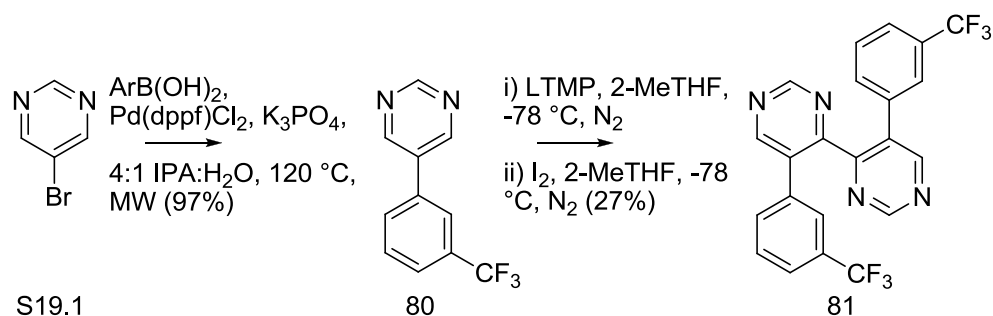


Scheme 18: Towards a Biaryl Boronate Ester

Compound **77** was heated to $100\text{ }^\circ\text{C}$ in a microwave for 10 min with ethynyltrimethylsilane, bis(triphenylphosphine)palladium(II) chloride ($\text{PdCl}_2(\text{PPh}_3)_2$), copper(I) iodide and NEt_3 in DMSO to give the desired Sonogashira product **78** (in experimental section), based on LCMS analysis. The trimethylsilyl group was then removed using methanolic sodium hydroxide. Unfortunately, the desired alkyne product **79** was only assumed to have been produced based on an LCMS analysis as it was lost upon isolation. This route was proving very problematic so another approach was trialled.

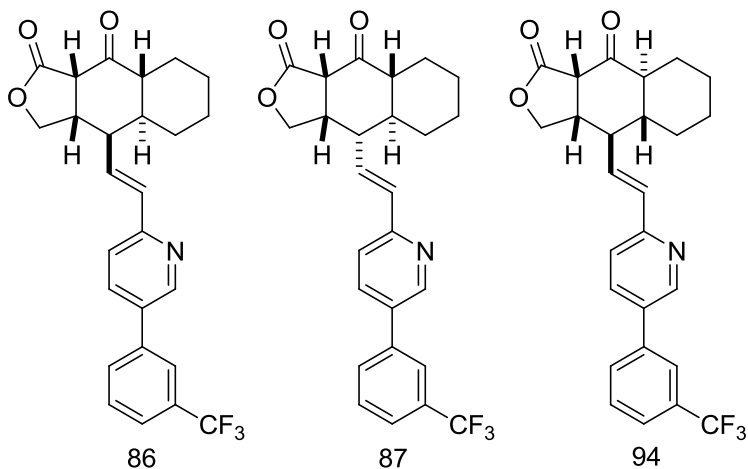
Instead of carrying out a Sonogashira reaction on a potentially unstable triflate it was hoped that a halogen could be introduced following the initial Suzuki reaction. Consequently, pyrimidine **80** was synthesised in 97% yield using similar Suzuki conditions as before. The yield was greatly increased as there was no longer a

hydroxyl-group present which made work-up and purification much easier. In the literature it had been shown that LTMP could be used to deprotonate at the 2-position of a pyridine ready for the addition of an iodine.¹³⁹ This was trialled; unfortunately, the 2-iodobiaryl was not afforded. Instead, the 4,4-dimer **81** was produced (Scheme 19). This general approach to the novel vorapaxar analogues seemed to be producing more problems than it was resolving so, in the interests of time, these investigations were discontinued.



Scheme 19: Towards a Biaryl Boronate Ester - Undesired Dimerisation Giving **81**

Resorting back to the reaction scheme established with the enantiomerically pure tricycles, the bulk of the racemic tricycles were taken through to the final compound. This gave **86**, **87** and **94**. The 4*S* derivative of **94** was not isolated because aldehyde **93** did not epimerise to the same extent as aldehyde **84**. The racemic compounds were supplied to our collaborators at GSK who found that the enantiomers could be very easily separated using chiral purification techniques. 10-14 mg of each enantiomer was isolated.

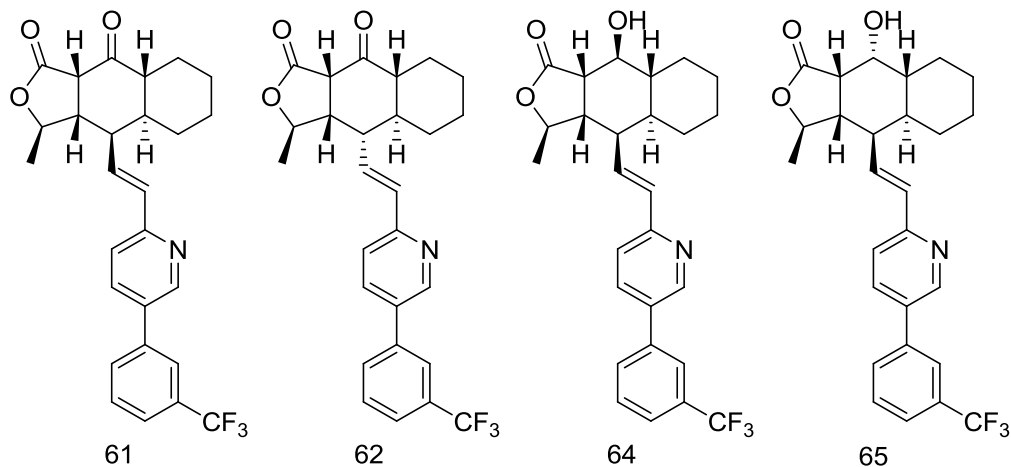


Compounds **86**, **87** and **94**

Both compounds **45** and **47** were taken through to the fully furnished tricycle because it was thought that **94** would take up a similar configuration to the desired vorapaxar like tricycle. If this were to be the case then **94** would be more potent than the compounds derived from **47** whilst being an unexplored tricycle scaffold. Consequently, in order to test this hypothesis, the next stage was to trial the racemic and enantiomerically pure compounds in the Ca^{2+} flux FLIPR assay.

Biological Testing

The synthesis of **62**; the novel keto-analogue of vorapaxar which had shown the greatest potency of all the compounds tested in the proof of concept studies, was never achieved on large scale. Equally, the racemic version (**87**), which should have been easier to make, was also not obtainable in large quantities. Starting the synthetic route on a 40 g scale led to no more than 100 mg of each of the final racemic products. This meant that it was not a viable option to explore the potential of the additional ketone as a synthetic handle. It had been hoped that an array of analogues could be made to establish SAR at the C-9 position. Poor yields in a difficult synthesis meant that this was not possible. However, whilst trying to optimise the route, a new tricycle scaffold was developed (**94**). Based on modelling it was hypothesised that **94** would be at least as potent as **62**, if not more so.



Compounds **61**, **62**, **64** and **65**: Enantiomerically Pure Compounds Tested in the Proof of Concept Study

The biological testing in the proof of concept study allowed the comparison of the potencies when the C-4 biaryl portion was positioned in the *R* or *S* configurations. In addition, the *R* and *S* C-9 hydroxy-analogues of **61**; **64** and **65** respectively, were compared. These initial studies confirmed that having the biaryl group in the 4*S* orientation gave a more potent compound. Furthermore, having the C-9 ketone was shown to be more potent than when it had been reduced to give a hydroxyl group at the C-9 position. The second round of testing allowed the analysis of the racemic analogues along with their chirally purified derivatives and showed the first assessment of **94**, the analogue with the novel tricycle scaffold.

The first question to answer was whether the racemic compounds actually caused a significant drop in potency. Using the same FLIPR assay as that used in the proof of concept study racemic compounds, **86** and **87**, were shown to have IC_{50} values of 2.6 and 1.3 μ M, respectively. This made them more potent than all but one of the enantiomerically pure compounds used in the proof of concept study. Only compound **62** was more potent ($IC_{50} = 0.5 \mu$ M) than the racemic compounds. This is interesting because the belief throughout the development of vorapaxar was that having a specific enantiomer was essential for activity. Further, having the biaryl portion extending from C-4 with *S*-stereochemistry was also seen as crucial. However, in the racemic examples there was negligible difference between the

potencies even though one had a relative *S*-C-4 and the other a relative *R*-C-4. This would suggest that the enantiomeric pairings contributed to balance the disfavoured orientation. A final conclusion that can be made from these results is that the C-3 methyl group does not appear to be essential. With all this said, the dose-response curves given by **86** and **87** (Figure 16) are not clean sigmoidal curves which reach 100% inhibition so any IC₅₀ values taken from them may be inaccurate.

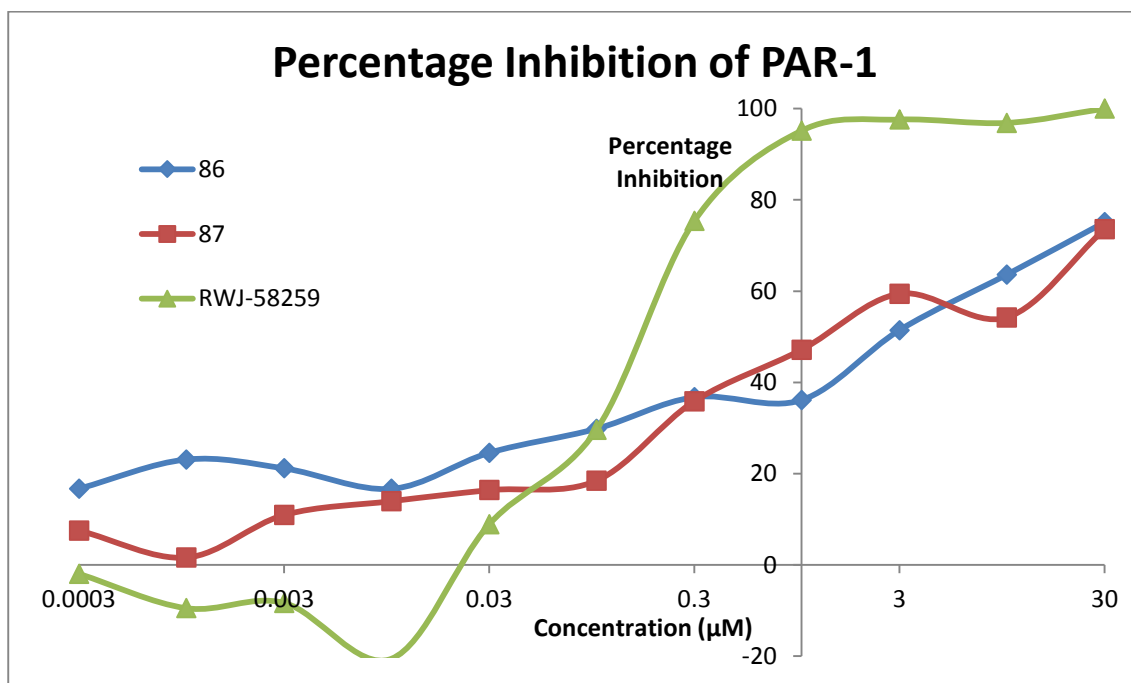


Figure 16: The average (n = 5) percentage inhibition observed upon the addition of thrombin (10 nM) to human lung fibroblasts in buffer pre-incubated with Fluo-4 NW dye mix and 0.0003-30 μM antagonist; Compounds **86**, **87** and RWJ-58259

Separating out the enantiomeric pairs allowed a clearer picture of how each enantiomer affected the potency of the racemic mixtures. As can be seen from Figure 17, racemic-**86** and the positive enantiomer derived from it had very similar dose-response profiles, thus giving similar IC₅₀ values (ca. 2.5 μM). However, the negative enantiomer showed a noticeable decrease in potency (IC₅₀ ≈ 15 μM). Although it was expected that one of the enantiomers would show decreased potency it is odd that the dose-response curve for the racemic compound did not lie between the curves of the two resulting compounds. This may be a result of

experimental variation in the assay. Nevertheless, in all cases the potency is much lower than the tool compound RWJ-58259 which in turn makes them significantly less potent than vorapaxar. Consequently, the slightly unexpected results were not investigated.

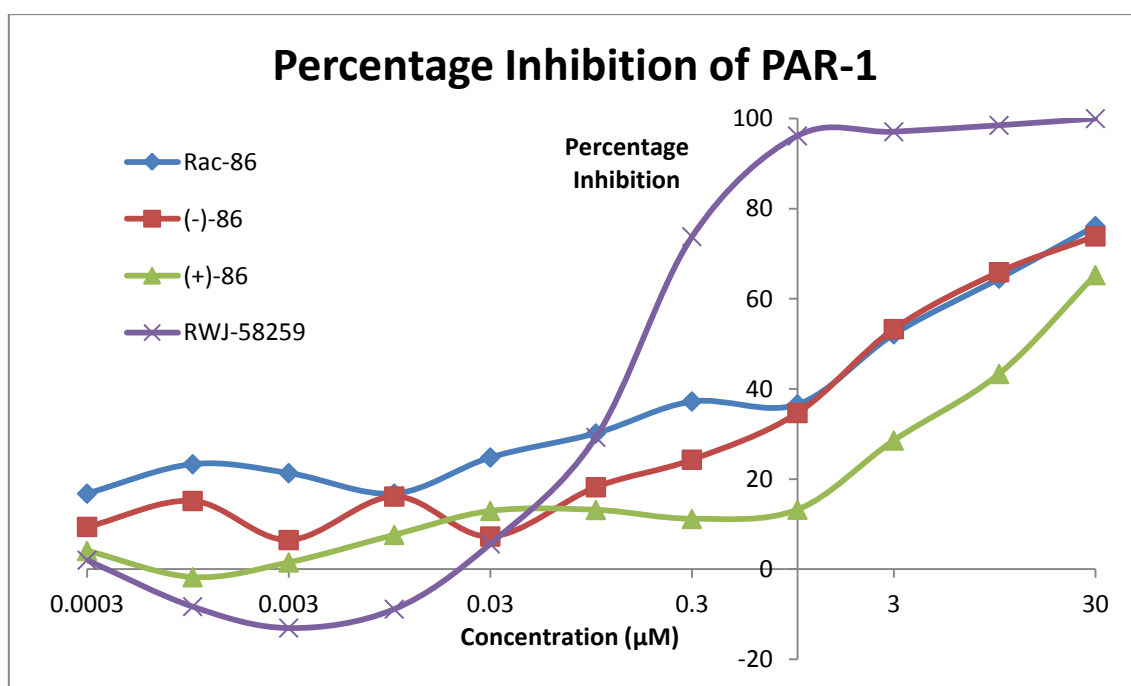
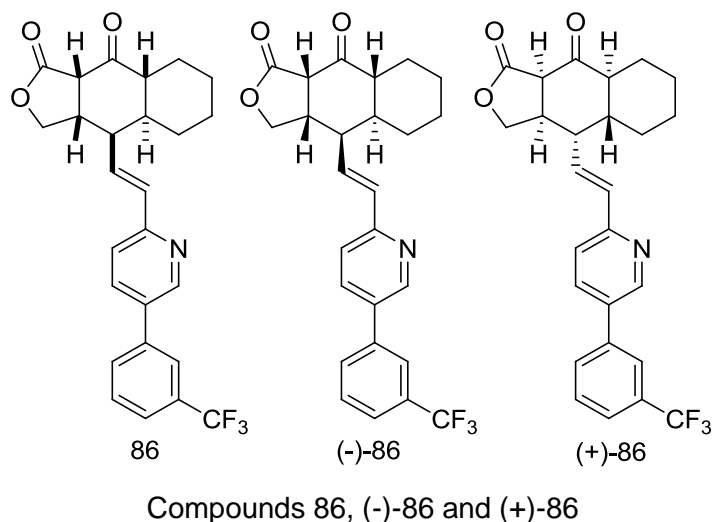
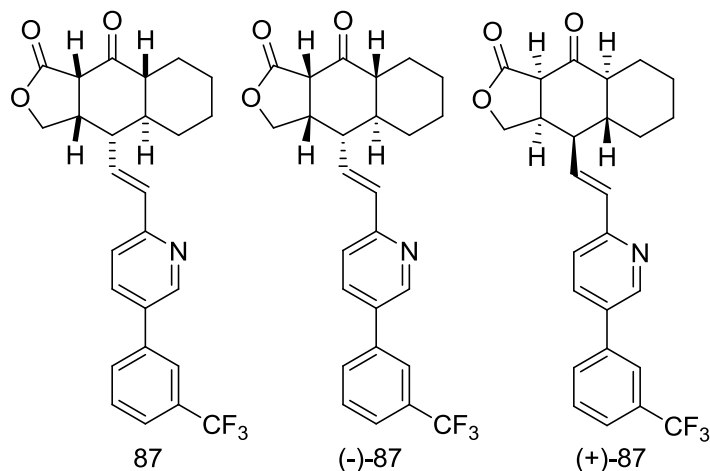


Figure 17: The average (n = 5 or 6) percentage inhibition observed upon the addition of thrombin (10 nM) to human lung fibroblasts in buffer pre-incubated with Fluo-4 NW dye mix and 0.0003-30 µM antagonist; Compounds *rac*-**86**, (+)-**86**, (-)-**86** and RWJ-58259

Figure 18 shows the equivalent results for **87** and its enantiomeric derivatives. These results are more in line with what would be expected. The dose-response curve for the racemic compound falls between that of the positive and negative enantiomers. In all cases the curves are still relatively shallow and do not reach 100% inhibition. It is hard to say whether this is a real indication of how the compound is interacting within the receptor or if it is a consequence of giving a percentage inhibition relative to the positive control; RWJ-58259. This means that despite (-)-**87** being twice as potent ($IC_{50} = 0.10 \mu\text{M}$) as RWJ-58259 ($IC_{50} = 0.19 \mu\text{M}$) it might be inadvisable to draw firm conclusions.



Compounds 87, (-)-87 and (+)-87

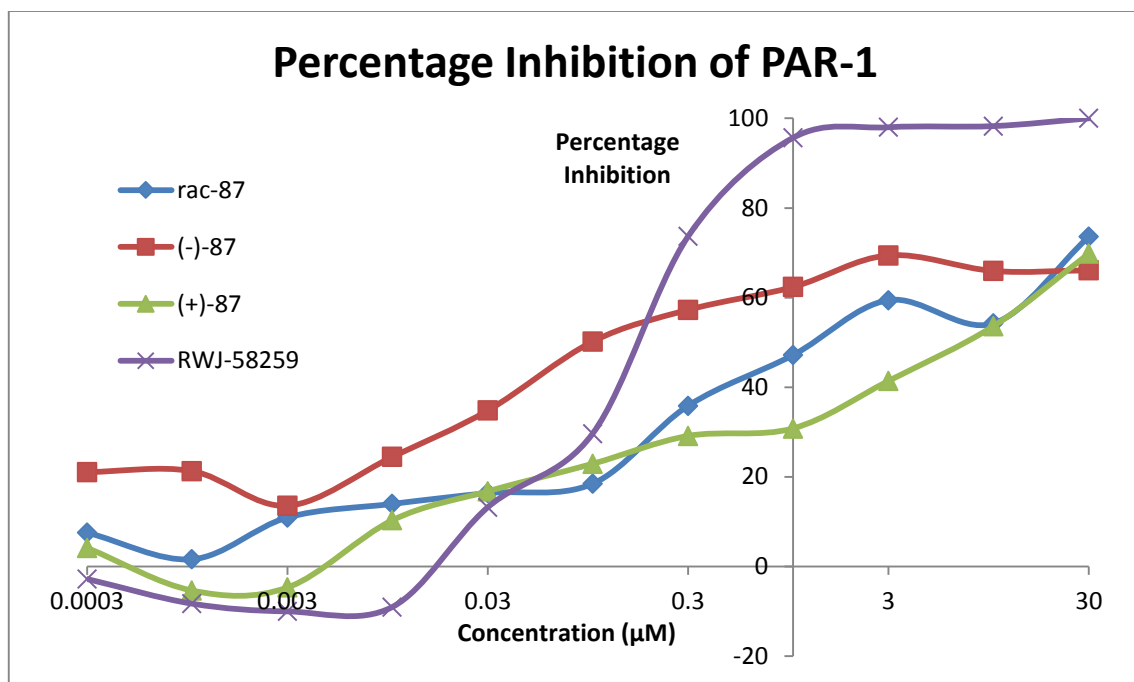
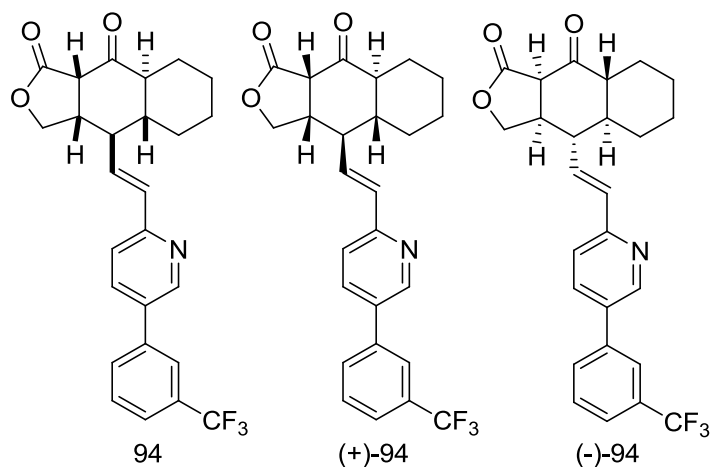


Figure 18: The average (n = 5 or 6) percentage inhibition observed upon the addition of thrombin (10 nM) to human lung fibroblasts in buffer pre-incubated with Fluo-4 NW dye mix and 0.0003-30 µM antagonist; Compounds *rac-87*, (+)-**87**, (-)-**87** and RWJ-58259

The results so far have helped us to answer the question of whether racemic compounds are less potent than enantiopure ones. The evidence suggests that compounds with *S*-stereochemistry at C-4 show a significant difference in the potencies of racemic and enantiopure compounds. On the other hand, having *R*-stereochemistry at C-4 appears to impact on the potency itself so greatly that enantiopure compounds tend to be no more active than the racemic ones. With this in mind, the next question that needed to be answered was whether the novel tricycle scaffold, given in compound **94**, actually led to greater potency than the established scaffolds of **62** and **87**.



Compounds 94, (+)-94 and (-)-94

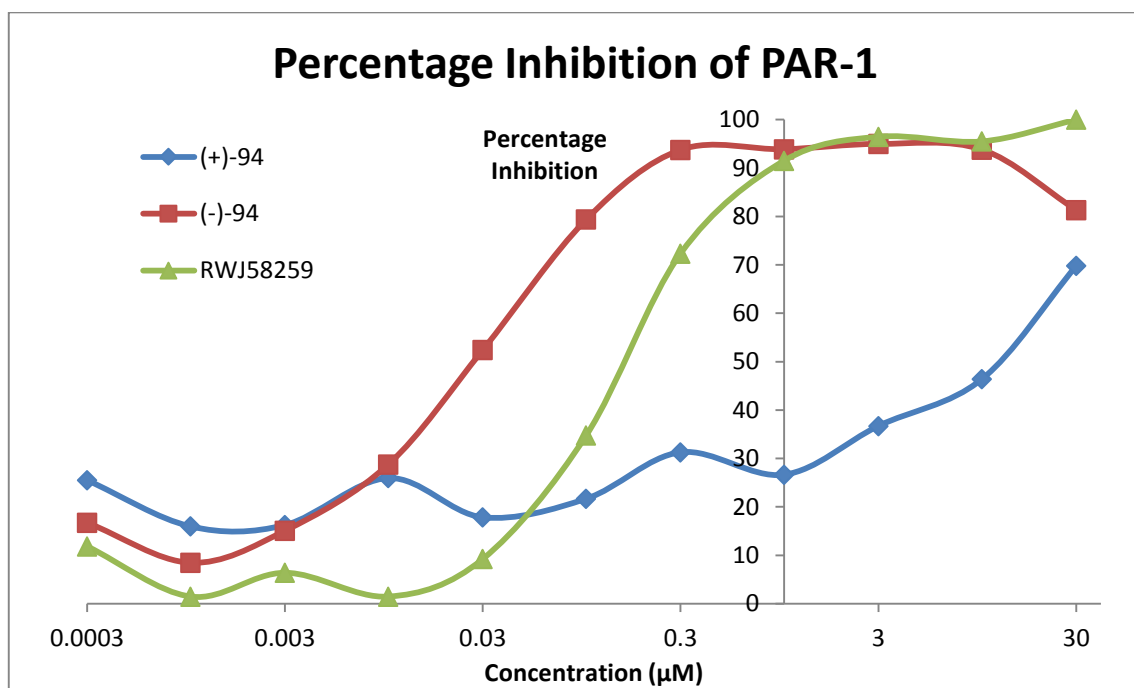


Figure 19: The average (n = 6) percentage inhibition observed upon the addition of thrombin (10 nM) to human lung fibroblasts in buffer pre-incubated with Fluo-4 NW dye mix and 0.0003-30 µM antagonist; Compounds (+)-**94**, (-)-**94** and RWJ-58259

Figure 19 shows the percentage inhibitions of (+)-**94**, (-)-**94** and RWJ-58259. In this case there is a huge difference in the potencies of the enantiomeric pair derived from racemic-**94**. More significantly, the dose-response curve for compound (-)-**94** is considerably left-shifted indicating a high potency. Compound (-)-**94** gave an IC₅₀ of 0.027 µM. This is the best potency of all of the compounds developed so far. It is

10 times that of RWJ-58259 and approaching the level of potency described for vorapaxar. This means that, as predicted, the novel tricycle scaffold was in fact more potent than the established scaffold more analogous to that used in vorapaxar. Conversely, its enantiomeric pair gave an IC₅₀ of 13 μM. This is one of the worst potencies of all of the C-9 ketone compounds. In this case having the enantiopure compound was definitely important.

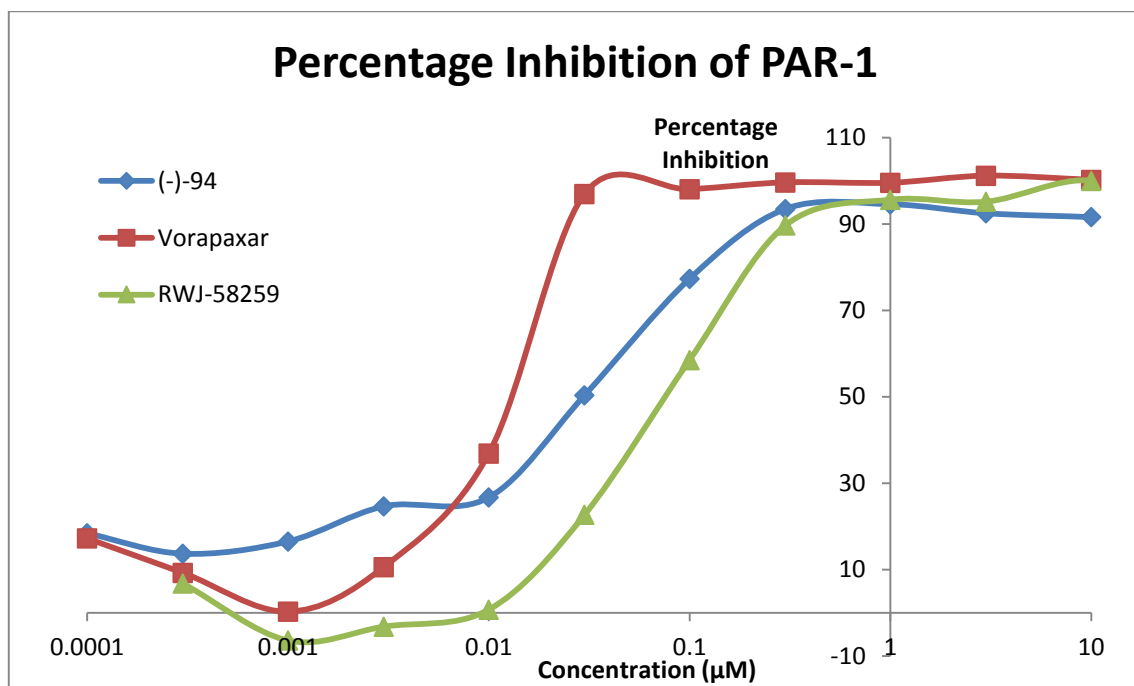


Figure 20: The average (n = 5 or 6) percentage inhibition observed upon the addition of thrombin (10 nM) to human lung fibroblasts in buffer pre-incubated with Fluo-4 NW dye mix and 0.0001-10 μM antagonist; Compounds (-)-**94**, vorapaxar and RWJ-58259

Considering compound (-)-**94** appeared to be approaching similar potencies to vorapaxar it seemed prudent to directly compare the two in the same assay. Figure 20 shows the results of these investigations. Clearly, vorapaxar is still more potent with an IC₅₀ of 0.013 μM (in this assay). However, it is clear that the sigmoidal curve of (-)-**94**, in comparison to that of vorapaxar, is still relatively shallow. This suggests that the shallow dose-response curve is a property of this class of compounds. If it was a direct result of using RWJ-58259 as the comparison when calculating the relative percentage inhibitions then vorapaxar would also have a shallow curve, but it does not.

In order to confirm that using the positive control as the comparator when calculating the relative percentage inhibition made little difference to the results a compound baseline was determined. This was done using compound **62** because in the proof of concept study it had been shown to have moderate potency whilst giving a good sigmoidal dose-response curve. Further, as the most potent compound of the series, (-)-**94** was used to obtain a compound baseline. In order to give the baseline, the assay was completed using the same method as before but without the addition of the agonist; thrombin. This gave a clearer idea of what the compound was doing to the cells in the absence of thrombin.

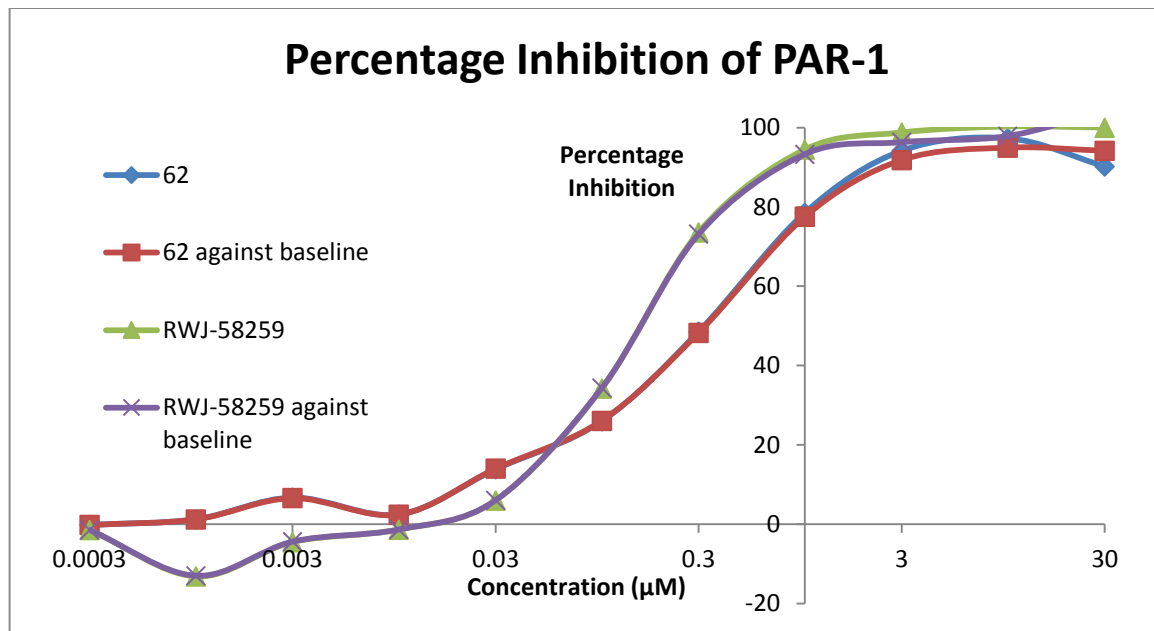


Figure 21: The average (n = 8) percentage inhibition observed upon the addition of thrombin (10 nM) to human lung fibroblasts in buffer pre-incubated with Fluo-4 NW dye mix and 0.0003-30 µM antagonist; Compounds **62** and RWJ-58259, against a compound baseline or simply against the positive control (RWJ-58259).

Figure 21 and Figure 22 show that using the baseline to calculate the relative percentage inhibition gives very similar results as when the strongest inhibition elicited by the positive control is used for the calculations. This would suggest that the shallow dose-response curve, seen with this series of compounds, is a result of how they interact with PAR-1. In some of the cases, such as with *rac*-**87**, (+)-**87**

and (-)-**87**, the fact that 100% inhibition was not reached could suggest that they were acting as partial agonists. On the other hand, some of the compounds, namely **62** and (-)-**94**, did reach 100% inhibition so the partial agonist argument cannot be used. However, a recent paper by Fallahi-Sichani *et al.* suggests that variation in dose-response curve shape can be indicative of cell-to-cell variability. They based their study on drugs targeting the Akt/PI3K/mTOR pathway which tended to give shallower dose-response curves.¹⁴⁰ Since PAR-1 is upstream of the Akt/PI3K/mTOR pathway a similar effect may be occurring with these compounds.

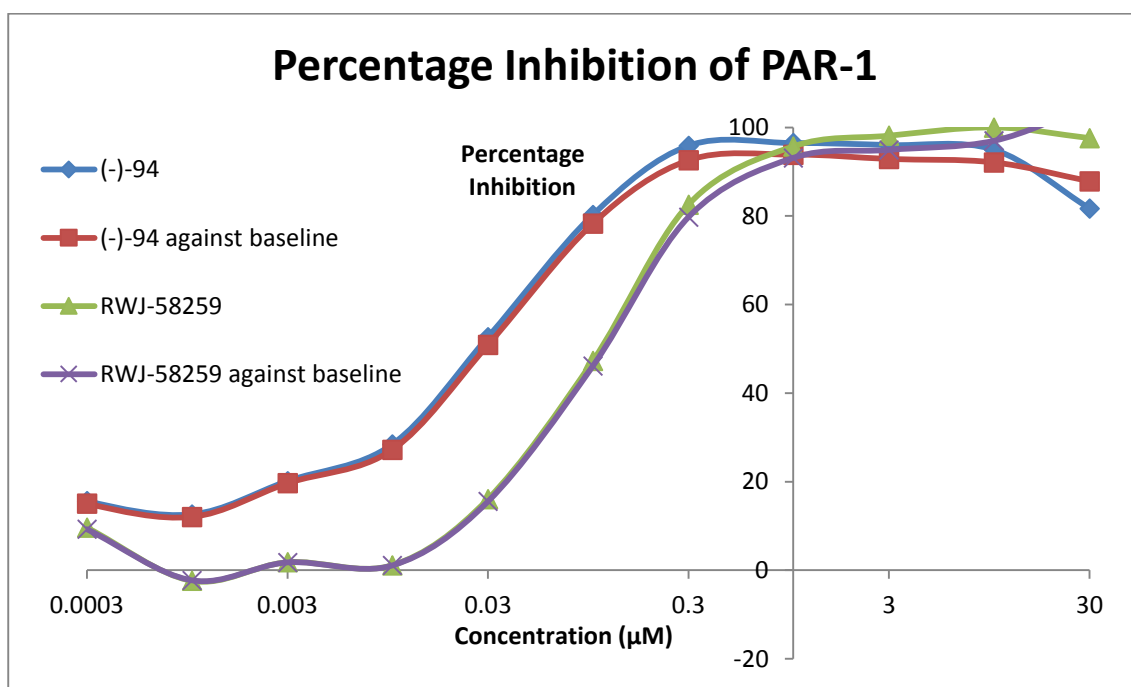


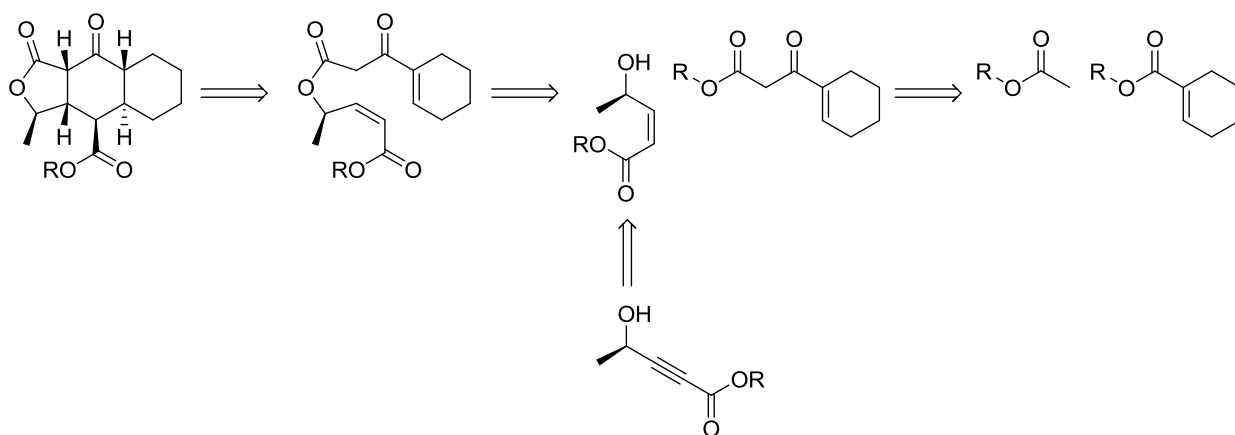
Figure 22: The average (n = 12) percentage inhibition observed upon the addition of thrombin (10 nM) to human lung fibroblasts in buffer pre-incubated with Fluo-4 NW dye mix and 0.0003-30 µM antagonist; Compounds (-)-**94** and RWJ-58259, against a compound baseline or simply against the positive control (RWJ-58259).

In summary, despite not being able to fulfil the early aim of testing a wide array of analogues, with different functional groups attached to C-9, several significant conclusions were made. The proof of concept study had already told us that the C-9 ketone was tolerated. However, the further investigations confirmed that losing the methyl group at C-3 was not an issue and that enantiomerically pure

compounds were only beneficial if the compound tricycle was suitable. This led to the identification of a new, more potent tricycle; the tricycle used in compound **94**.

Investigations Towards an Alternative Route

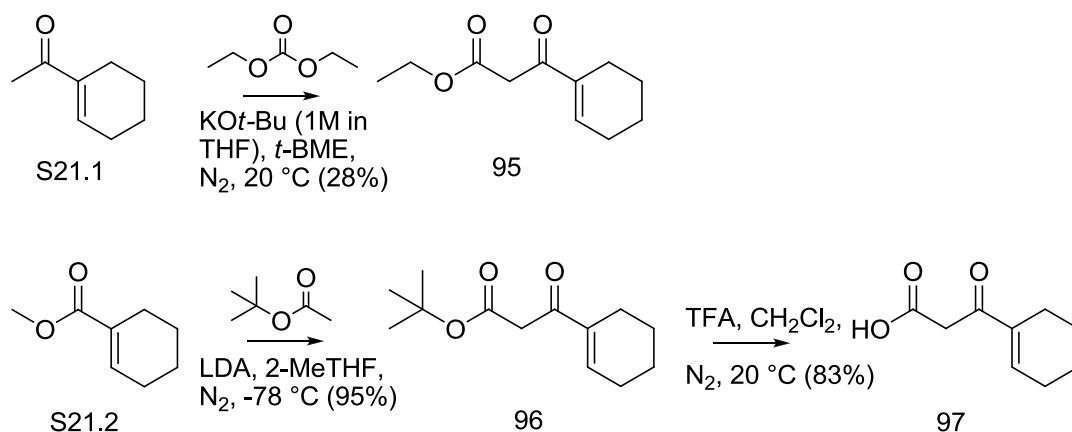
Even though a suitable synthesis for the novel C-9-keto-tricycle had been established it was still low yielding. It was still a desirable aim to obtain sufficient material to make a series of analogues with variation at the C-9 position. Consequently some investigations were made into an alternative, potentially higher yielding route. A variation on the IMDA reaction used for the synthesis of vorapaxar was investigated. It was thought that if the IMDA could be done on an α,β -ketoester the desired C-9-ketone would already be installed (Scheme 20). The dieneophile could be constructed using the same methodology developed for the synthesis of vorapaxar to give the enantiopure hydroxy-pentynoate species.¹⁴¹ This could either undergo stereospecific hydrogenation prior to being coupled to the α,β -ketoester or after the coupling had occurred. The α,β -ketoester could be made *via* a Claisen condensation between an alkyl acetate and a cyclohexenecarboxylate.



Scheme 20: Retro-Synthetic Analysis of α,β -Ketoester IMDA

The Claisen condensation was first trialled to give ethyl 3-cyclohexenyl-3-oxopropanoate (**95**) but the yields were poor (0-28%). The best conditions found

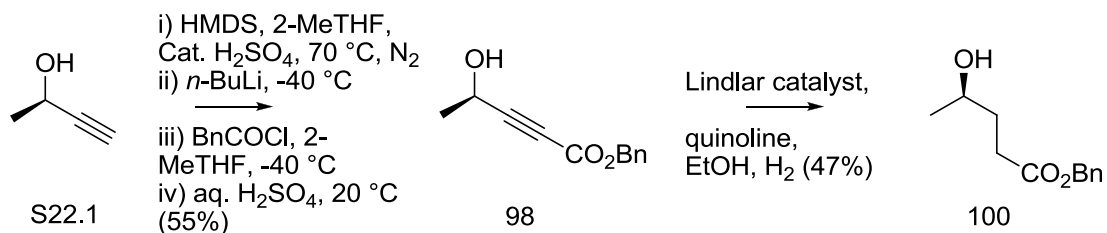
involved condensing 1-(cyclohex-1-en-1-yl)ethanone (**S21.1**) and diethyl carbonate using $\text{KO}t\text{-Bu}$ as the base (Scheme 21). On the other hand, condensing *tert*-butyl acetate deprotonated with LDA with methyl cyclohex-1-enecarboxylate (**S21.2**) gave *tert*-butyl 3-cyclohexenyl-3-oxopropanoate (**96**) with yields as high as 95% (Scheme 21). The difference in yields is likely to be a reflection of the difference of stabilities. Nevertheless, the two different α,β -ketoesters were taken forward. The α,β -ketoesters needed to be coupled to an enantiopure hydroxy-pentynoate. Therefore, (*R*)-benzyl 4-hydroxypent-2-ynoate (**98**) was obtained in a moderate yield (55%) using a similar protocol as that used in the vorapaxar synthesis (Scheme 22).



Scheme 21: Synthesis of the α,β -Ketoesters **95**, **96** and **97**

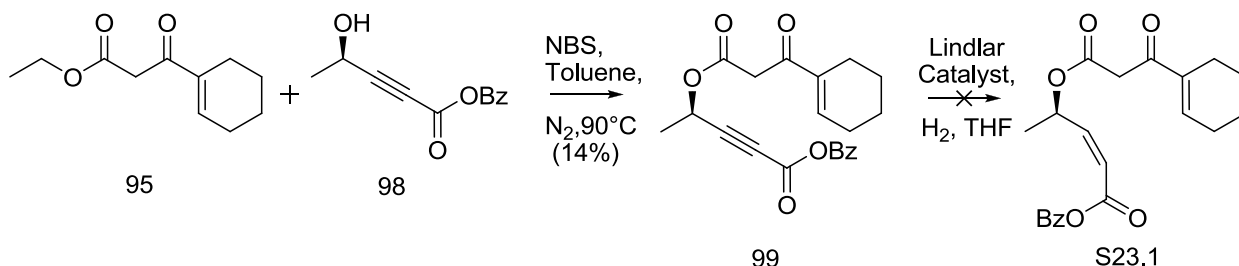
With **98** in hand, a portion of **96** was deprotected using a 1:1 TFA/ CH_2Cl_2 mix to give 3-cyclohexenyl-3-oxopropanoic acid (**97**) in an 83% yield (Scheme 21). **97** was then coupled to **98** using 1-[bis(dimethylamino)methylene]-1H-1,2,3-triazolo[4,5-b]pyridinium 3-oxid hexafluorophosphate (HATU) and diisopropylethylamine (DIPEA) in dimethylformamide (DMF). The coupling was very low yielding giving the coupled product **99** in only a 6% yield. An alternative coupling was trialled; **95** was reacted with **98** in an NBS catalysed transesterification reaction. This gave **99** in a slightly improved but still disappointing 14% yield (Scheme 23). The low yields of the coupling could be explained by the instability of **95** and **97**. The transesterification reaction was

tried with NEt_3 as the coupling reagent but it gave benzyl 3-cyclohexenyl-3-oxopropanoate (**101**) as opposed to the desired product.



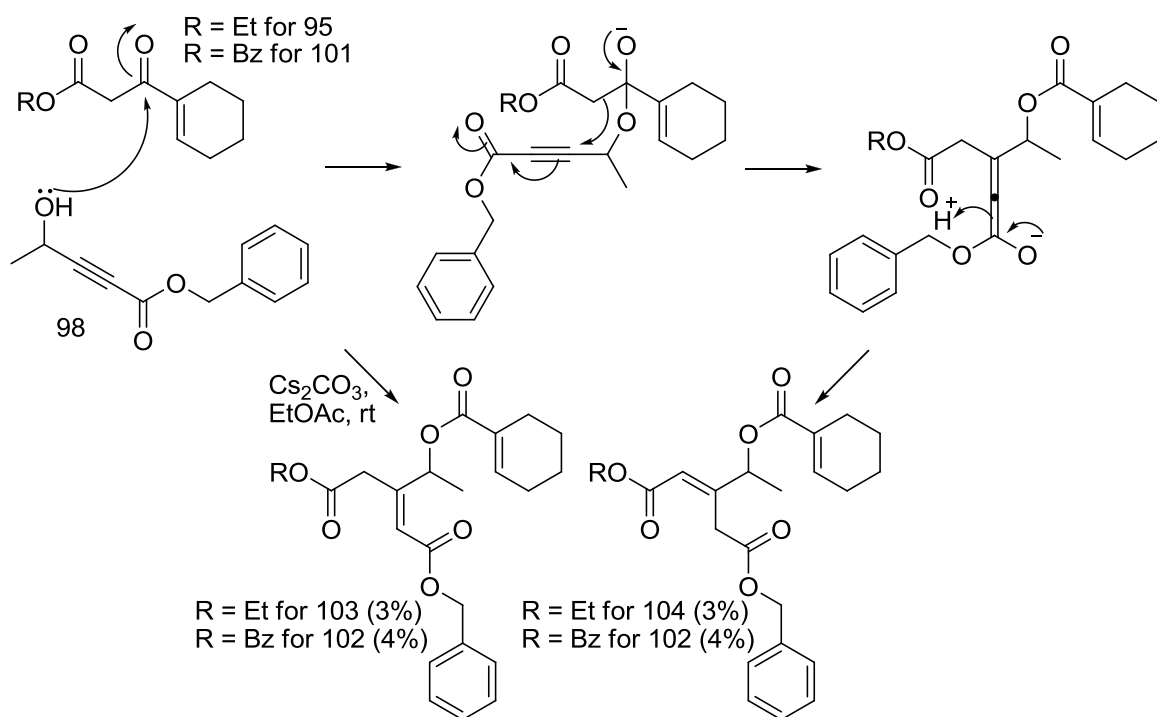
Scheme 22: Synthesis of (*R*)-Benzyl 4-hydroxypent-2-ynoate (**98**) and Undesired **100**

Nevertheless, the successfully coupled material was taken forward. Combined batches of **99** were subjected to Lindlar catalyst conditions to promote stereospecific hydrogenation. Unfortunately, this was unsuccessful (Scheme 23). The failed hydrogenation was probably due to the very small scale on which it was trialled. This in turn was due to the insufficient material made in the coupling trials. In order to avoid the coupling step the Diels-Alder (DA) reaction was trialled intermolecularly instead. The idea would be to deprotect the ester and couple it to give the lactone following the DA. It had been shown that caesium carbonate (Cs_2CO_3) could be used to initiate similar DA reactions with α,β -ketoesters¹⁴² so this was trialled. The hydroxyalkyne, **98**, was used because attempts at mild reduction to the alkene had resulted in full reduction to **100**. Consequently, it was hoped that the double bond that would remain following the DA could be more easily reduced on the cyclised product.



Scheme 23: Synthesis of IMDA Pre-cursor **99**

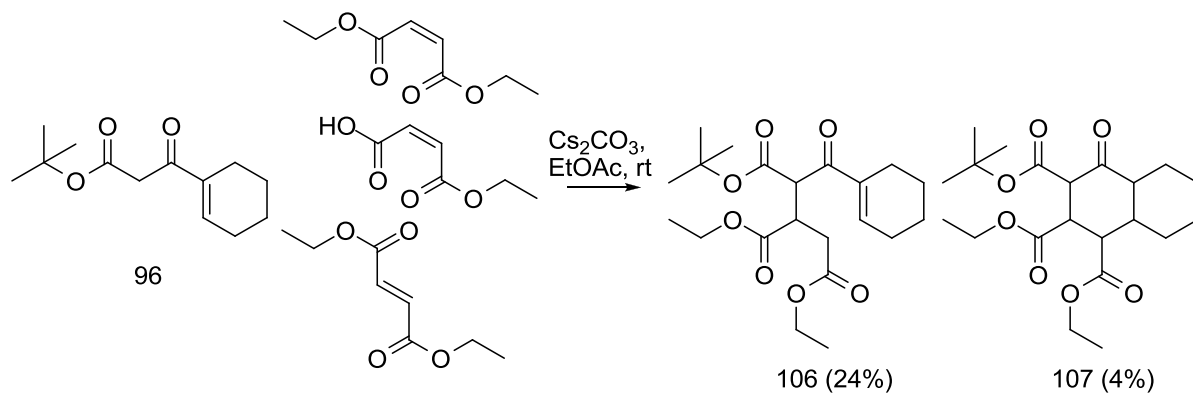
Reacting a couple of different α,β -ketoesters with the hydroxyalkyne in the presence of Cs_2CO_3 gave some interesting results. Sadly, the desired DA reaction did not occur. Instead, an interesting transformation which appeared to require the migration of an acetate group to give a tri-substituted alkene took place (Scheme 24). Using **101** gave compound **102** as a single symmetrical product. On the other hand, reacting **95** under the same conditions gave two major products; **103** and **104**, which were only separable using chiral column chromatography. It was believed that the reaction was initiated by the hydroxy group attacking the β -ketone. Consequently, a series of trial reactions, excluding a free hydroxyl group, were completed to see if the DA could be promoted.



Scheme 24: Mechanism of Hydroxyalkyne Reacting with α,β -Ketoesters.

Compound **96** was reacted with diethyl fumarate, diethyl maleate, maleic acid monoethyl ester and maleic acid using Cs_2CO_3 in ethyl acetate (EtOAc) at RT. The maleic acid reaction did not work at all whilst the other three substrates reacted to give the same addition product, **106**. The reaction also gave a minimal amount of the fully cyclised DA product, **107**, in a 2% yield (Scheme 25). This suggested that

although the DA reaction was feasible it was not the predominant reaction pathway. Compound **106** was treated with a selection of strong bases (LiHMDS, LDA and LTMP) to try and drive the cyclisation but this was unsuccessful. Once again this route appeared to be causing more issues than it was solving so due to time constraints no further investigations were completed.



Scheme 25: Trial Diels-Alder Reactions

Chapter 4: Conclusions and Future Work

The overall aim of this project was to design and synthesise novel PAR-1 inhibitors in order to develop a novel treatment for IPF. Originally the commercially available, allosteric PAR-1 inhibitor, “Q94” was going to act as a starting point for development. Unfortunately, after failing to replicate literature results and finding “Q94” inactive and insoluble, new inspiration was required. Examining the literature identified atopaxar and vorapaxar as potent PAR-1 inhibitors which were, at the time, being tested in clinical trials. Vorapaxar had been developed from the natural product, tricyclic, himbacine. From the literature search a novel synthesis towards himbacine had also been found. The route was incomplete and left a ketone on the central ring of the tricycle. It was hypothesised that the novel synthetic route could be adapted to make novel analogues of vorapaxar. Further, the novel analogues could be used to examine the SAR from the central ring of the tricycle; a previously unexplored region of the molecule.

The published novel synthetic route towards himbacine was successfully adapted to give the desired C-9-keto-*ent*-himbacine tricycle. This was not achieved without difficulty. Nevertheless, some of the earlier synthetic steps were improved upon and several lessons were learnt along the way about the tricycle synthesis. It was found that obtaining pure starting material for the tricycle synthetic step was obviously essential but unexpectedly problematic; purification at this step led to a marked drop in the overall yield. Further, the tricycle synthesis itself was never completed to meet the published yields giving another reduction to the overall yield of the route. Nonetheless, having synthesised the tricycle, the route had to be completed to be able to furnish the tricycle with the characteristic biaryl group found on vorapaxar. This was done with much greater success. In four steps the C-4 ester was replaced with the biaryl group to give the desired vorapaxar analogue; each step typically achieved around 90% yield.

Alongside the initial investigations, into the novel tricycle synthesis, the biaryl group was attached to a series of smaller, monocyclic or aromatic groups. Some of these

compounds were tested against PAR-1 in a biological assay and were found to be inactive and in some cases insoluble. Fortunately, the novel vorapaxar analogues with the full tricycle were tested and were shown to have some potency against PAR-1. The hypothesis that vorapaxar analogues with a C-9-keto-group could be used as a starting point for developing novel PAR-1 inhibitors was proven correct.

The next step was to synthesise more of the keto-compound in order to be able to use it to make a series of compounds with extension from C-9 to enable the exploration of the SAR from this point. However, due to continued problems with the low yielding synthetic route time was taken to try and establish a better, higher yielding route. This did not prove successful but it did identify a new, more potent tricycle scaffold. Compound (-)-**94** was shown to be the most potent of the series of compounds tested, achieving an IC_{50} of 27 nM. In the same assay vorapaxar gave an IC_{50} of 13 nM.

If future work were to be done, apart from further investigations into improving or changing the synthetic route, compound (-)-**94** should be fully assessed. It has been shown to have great potency in one biological assay but to test it in other assays would be ideal to see if the potency holds up. Further, obtaining DMPK data and assessing receptor selectivity would be essential to determine if it would be a suitable drug candidate. In addition, synthesising enough of compound (-)-**94** to allow exploration of SAR from the C-9 position would be desirable. Investigating the extent to which you can grow upwards using reactions such as reductive amination, acetylation and the addition of organometallic compounds. Equally, replacing the ketone with a thioketone or fluorinating at the C-9 position would be interesting (Figure 23).

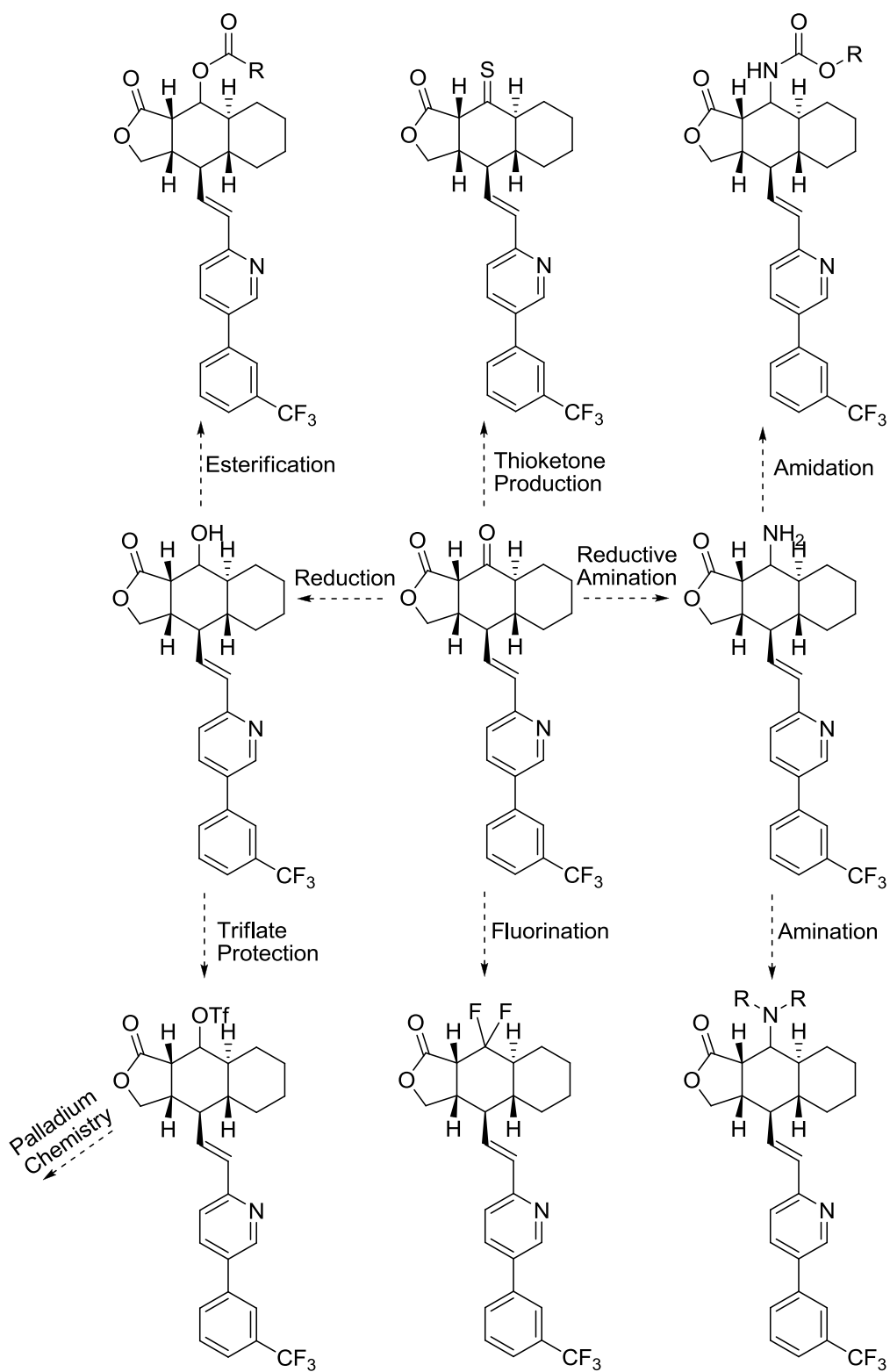


Figure 23: Scope of Transformations to Allow Exploration of SAR from C-9

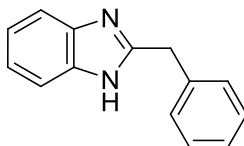
Experimental

Chapter 2

General Experimental

All solvents employed in this study were reagent grade. All reagents were purchased from Sigma-Aldrich, UK and Alfa Aesar, UK and used as received unless otherwise stated. All reactions were magnetically stirred and monitored by thin layer chromatography (TLC) on pre-coated silica gel plates (254 μm). Silica plates were initially examined under UV light and then developed using aqueous basic potassium permanganate stain. Flash chromatography was carried out with silica gel (33-70 μm) supplied by Merck Co.. Quoted yields refer to chromatographically and spectroscopically pure compounds unless otherwise stated. ^1H NMR spectra were recorded at either 500 MHz with a DRX500 or at 600 MHz with a Bruker AMX600. ^{13}C NMR spectra were recorded at 150 MHz. Chemical shifts (δ values) are reported in parts per million (ppm) whilst coupling constants are reported in Hertz (Hz).

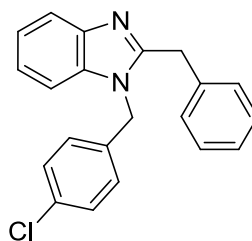
2-Benzyl-1*H*-benzimidazole¹²³ (**23**)



Benzoic acid (0.63 g, 4.60 mmol) was added to a solution of 1,2-phenylenediamine (0.50 g, 4.60 mmol) in conc. HCl (37%) (5 mL) and H₂O (5 mL). The reaction mixture was refluxed for 16 h. Once cool the solution was basified with solid NaOH (pH ~ 9) to form a precipitate. This was filtered under vacuum, washed with H₂O and dissolved in CH₂Cl₂ (10 mL). The filtrate was extracted with CH₂Cl₂ (3 x 20 mL). The combined organic layers were dried (MgSO₄), filtered and concentrated *in vacuo*. Purification by flash column chromatography (0-25% EtOAc/CH₂Cl₂) and recrystallisation (EtOAc) gave 2-benzyl-1*H*-benzimidazole (**23**) (363 mg, 1.74

mmol, 38%) as pearlescent needles; Rf. 0.45 (30% EtOAc in CH₂Cl₂); m.p. 182-183 °C (lit. 182 °C¹⁴³); ¹H NMR (600 MHz, MeOH-d₄) δ 7.48 (2H, bs, 2 x CHCN), 7.31-7.28 (4H, m, 2 x CHCCH₂ & 2 x CHCHCCH₂), 7.24-7.20 (1H, m, CHCHCHCCH₂), 7.20-7.16 (2H, m, 2 x CHCHCN), 4.21 (2H, s, CH₂); ¹³C NMR (150 MHz, MeOH-d₄) δ 155.2 (NCCH₂), 138.3 (CH₂CCH), 129.8 (2 x CHCCH₂), 129.8 (2 x CHCHCCH₂), 128.0 (CHCHCHCCH₂), 123.3 (2 x ArCH), 36.1 (CH₂Ph), Note: Four of the benzimidazole C are not observed due to peak broadening caused by tautomerisation. In CDCl₃ two more benzimidazole-CH are seen as a broad peak at 115.0 ppm; IR (thin film) 3048 (br) (ArC-H), 1536 (ArC-C), 1494 (ArC-C), 1455 (ArC-C), 1435 (ArC-C), 1272 (C-N), 1024 (C-N), 767, 744, 721, 694 cm⁻¹; m/z (ES+) 209 (100%, [M+H]⁺); HRMS (ES+) calcd for C₁₄H₁₃N₂ [M+H]⁺ 209.1079, observed 209.1077. Data agrees with that reported by Algul *et al.*¹²³ and Matsushita *et al.*¹⁴⁴

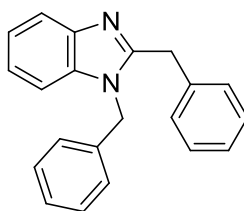
2-Benzyl-1-(4-chlorobenzyl)-1*H*-benzimidazole¹¹⁷ (**24**)



Solid KOH (26.9 mg, 0.48 mmol) and 1-(bromomethyl)-4-chlorobenzene (98.6 mg, 0.48 mmol) were added to a solution of 2-benzylbenzimidazole (**23**) (100 mg, 0.48 mmol) in acetone (4 mL). The reaction mixture was stirred at 20 °C for 16 h before the solvents were removed *in vacuo*. The residue was dissolved in CH₂Cl₂ (10 mL) and sat. aq. Na₂CO₃ (10 mL). The aqueous layer was extracted with CH₂Cl₂ (2 x 20 mL). The combined organic layers were dried (MgSO₄), filtered and concentrated *in vacuo*. Purification by flash column chromatography (0-20% EtOAc/CH₂Cl₂); then (0-20% Et₂O/Pet. Ether) and recrystallisation (20% Et₂O/Pet. Ether) gave 2-benzyl-1-(4-chlorobenzyl)-1*H*-benzimidazole (**24**) (88 mg, 0.26 mmol, 55%) as colourless solid; Rf. 0.41 (30% EtOAc/CHCl₃); m.p. 108-109 °C; ¹H NMR (600 MHz, CDCl₃) δ 7.81 (1H, d, *J* = 7.9, CHCN), 7.28 (1H, dt, *J* = 7.5, 1.1,

CHCN), 7.25 (2H, d, $J = 7.5$, 2 x CHCCH₂C), 7.23-7.17 (6H, m, CHCHCN, 2 x CHCCI, 2 x CHCHCCH₂C and CHCHCHCCH₂C), 7.14 (1H, d, $J = 7.9$, CHCHCN), 6.81 (2H, d, $J = 8.7$ Hz, 2 x CHCHCCI), 5.15 (2H, s, CH₂N), 4.25 (s, 2 H, CH₂Ar); ¹³C NMR (150 MHz, CDCl₃) δ 153.4 (NCCH₂), 142.8 (ArC), 136.0 (CCH₂CCH), 135.7 (ArC), 134.3 (NCH₂C), 133.8 (CCI), 129.2 (2 x CHCCI), 129.0 (2 x CHCCH₂C), 128.6 (2 x CHCHCCH₂C), 127.6 (2 x CHCHCCI), 127.2 (*p*-Bn-CHCHCHCCH₂), 122.9 (ArCH), 122.4 (ArCH), 119.9 (ArCH), 109.6 (ArCH), 46.7 (CH₂N), 34.7 (CH₂Ph); IR (thin film) 3061 (ArC-H), 2925 (ArC-H), 1651 (ArC-C), 1605 (ArC-C), 1492 (ArC-C), 1460 (C-H), 1403 (C-H), 1332 (C-N), 1286 (C-N), 1249 (C-N), 1161 (C-H), 1091, 1014, 804, 742 (C-Cl), 722, 696 cm⁻¹; m/z (ES+) 333 (100%, [M+H]⁺); HRMS (ES+) calcd for C₂₁H₁₈N₂³⁵Cl [M+H]⁺ 333.1159, observed 333.1135. Mass spec data agrees with that obtained from the vendor for the commercial compound.

1,2-Dibenzyl-1*H*-benzimidazole¹⁴⁵ (**25**)



Solid KOH (32.5 mg, 0.58 mmol) and benzylbromide (69.0 μ L, 0.58 mmol) were added to a solution of 2-benzylbenzimidazole (**23**) (121 mg, 0.58 mmol) in acetone (4 mL). The reaction mixture was stirred at 20 °C for 3 h before the solvents were removed *in vacuo*. The residue was dissolved in CH₂Cl₂ (10 mL) and sat. aq. Na₂CO₃ (10 mL). The aqueous layer was extracted with CH₂Cl₂ (2 x 20 mL). The combined organic layers were dried (MgSO₄), filtered and concentrated *in vacuo*. Purification by flash column chromatography (0-20% EtOAc/CH₂Cl₂) and recrystallisation (CH₂Cl₂) gave 1,2-dibenzyl-1*H*-benzimidazole (**25**) (121 mg, 0.41 mmol, 70%) as colourless crystals; m.p. 126-127 °C; ¹H NMR (600 MHz, CDCl₃) δ 7.81 (1H, d, $J = 7.9$ Hz, CHCN), 7.29-7.24 (6H, m, CHCN, 2 x CHCCH₂N, 2 x CHCHCCH₂ and CHCHCHCCH₂N), 7.23-7.18 (5H, m, 2 x CHCHN, 2 x CHCCH₂

and CHCHCHCCH₂), 6.94-6.91 (2H, m, 2 x CHCHCCH₂N), 5.19 (2H, s, CH₂N), 4.26 (s, 2 H, CH₂); ¹³C NMR (150 MHz, CDCl₃) δ 153.5 (NCCH₂), 142.8 (C-N), 136.2 (CH₂C), 135.9 (NCH₂C), 135.9 (C-N), 129.0 (2 x CHCHC), 129.0 (2 x CHCCH₂N), 128.6 (2 x CHC), 128.0 (CHCHCHCCH₂N), 127.1 (CHCHCHC), 126.3 (2 x CHCHCCH₂N), 122.7 (CHCHCN), 122.3 (CHCHCN), 119.7 (CHCN), 109.8 (CHCN), 47.2 (NCH₂), 34.7 (CH₂); IR (thin film) 3061 (ArC-H), 3030 (ArC-H), 2930 (C-H), 1607 (ArC-C), 1508 (ArC-C), 1494 (ArC-C), 1454 (C-H), 1406 (ArC-C), 1356 (C-H), 1331 (C-N), 1285 (C-N), 1249 (C-N), 1159 (C-H), 1030, 912, 857, 742, 721, 694 cm⁻¹. Data agrees with that reported by Cetinkaya *et al.*¹⁴⁵

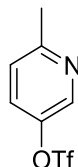
Chapter 3

General Experimental

All solvents employed in this study were reagent grade. All reagents were purchased from Sigma-Aldrich, UK and Alfa Aesar, UK and used as received unless otherwise stated. All reactions were magnetically stirred and monitored by thin layer chromatography (TLC) on pre-coated silica gel plates (254 μm) and/or by LCMS. Silica plates were initially examined under UV light and then developed using aqueous basic potassium permanganate stain. LCMS analysis was conducted on either System A, an Acquity UPLC BEH C18 column (2.1 mm × 50 mm ID, 1.7 μm packing diameter) eluting with 0.1% formic acid in H₂O (solvent A) and 0.1% formic acid in acetonitrile (MeCN) (solvent B), using the following elution gradient 0.0–1.5 min 3–100% B, 1.5–1.9 min 100% B, 1.9–2.0 min 3% B, at a flow rate of 1 mL min⁻¹ at 40 °C. The UV detection was an averaged signal from wavelength of 210 to 350 nm, and mass spectra were recorded on a mass spectrometer using alternate-scan electrospray positive and negative mode ionization (ES +ve and ES -ve); or System B, an Acquity UPLC BEH C18 column (50 mm × 2.1 mm ID, 1.7 μm packing diameter) eluting with 10 mM ammonium bicarbonate ((NH₄)HCO₃) in H₂O adjusted to pH10 with ammonia solution (solvent A) and MeCN (solvent B) using the following elution gradient 0–1.5 min 1–97% B, 1.5–1.9 min 97% B, 1.9–2.0 min 100% B at a flow rate of 1 mL min⁻¹ at 40 °C.

Flash chromatography was carried out with silica gel (33-70 μm) supplied by Merck Co.. Automated column chromatography was performed using pre-packed silica gel columns on a Flashmaster II. The Flashmaster II is an automated multiuser flash chromatography system, available from Argonaut Technologies Ltd, which utilizes disposable, normal phase, SPE cartridges (2–100 g). Mass-directed auto-preparative HPLC (MDAP) was conducted on either System A, a Sunfire C18 column (150 mm \times 30 mm ID, 5 μm packing diameter) at ambient temperature eluting with 0.1% formic acid in H_2O (solvent A) and 0.1% formic acid in MeCN (solvent B), using an appropriate elution gradient over 25 min at a flow rate of 40 mL min^{-1} and detecting at 210–350 nm at room temperature; or System B, an XBridge C18 column (100mm \times 30mm i.d. 5 μm packing diameter) at ambient temperature eluting with 10 mM Ammonium Bicarbonate in water adjusted to pH 10 with Ammonia solution (solvent A) and MeCN (solvent B), using an appropriate elution gradient over 25 min at a flow rate of 40 mL min^{-1} and detecting at 210–350 nm at room temperature. Quoted yields refer to chromatographically and spectroscopically pure compounds unless otherwise stated. ^1H NMR spectra were recorded at either 500 MHz with a DRX500 or at 600 MHz with a Bruker AMX600. ^{13}C NMR spectra were recorded at 101 MHz or 150 MHz. Chemical shifts (δ values) are reported in parts per million (ppm) whilst coupling constants are reported in Hertz (Hz).

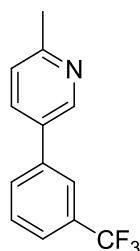
6-Methylpyridin-3-yl trifluoromethanesulfonate⁸⁷ (26)



Solid K_2CO_3 (3.80 g, 27.5 mmol) and *N,N*-bis(trifluoromethylsulfonyl)aniline (3.28 g, 9.17 mmol) were added to a stirred solution of 5-hydroxy-2-methylpyridine (1.00 g, 9.17 mmol) in DMF (20 mL). The reaction mixture was stirred at 25 $^\circ\text{C}$ for 2 h before being added to H_2O (50 mL) and extracted into Et_2O (1 \times 100 mL). The organic layer was washed (brine), dried (Na_2SO_4), filtered and concentrated *in vacuo* to yield a crude pale yellow oil. Purification by flash column chromatography

(0-10% Et₂O/CH₂Cl₂) yielded 6-methylpyridin-3-yl trifluoromethanesulfonate (**26**) (1.87 g, 7.71 mmol, 85%) as a colourless oil; Rf. 0.66 (10% Et₂O/CH₂Cl₂); ¹H NMR (600 MHz, CDCl₃) δ 8.46 (1H, d, *J* = 2.6, CHN), 7.51 (1H, dd, *J* = 8.6, 2.6, CHCOTf), 7.26 (1H, d, *J* = 8.6, CHCMe), 2.60 (3H, s, CH₃); ¹³C NMR (150 MHz, CDCl₃) δ 159.1 (COTf), 145.1 (CMe), 142.0 (CHN), 129.3 (CHCOTf), 124.4 (CHCMe), 118.8 (q, *J* = 319.5, CF₃), 24.1 (CH₃); IR (thin film) 1595 (ArC-C), 1481 (ArC-C), 1425 (ArC-C), 1250 (ArC-N), 1207 (C-O), 1158 (C-O), 1137 (C-F), 1020 (S=O), 879 (S-O), 833, 708 cm⁻¹; m/z (ES+) 241 (100%, [M+H]⁺); HRMS (EI) calcd for C₇H₇NO₃SF₃ [M+H]⁺ 242.00987, observed 242.00960. Data agrees with that reported by Clasby *et al.*⁸⁷

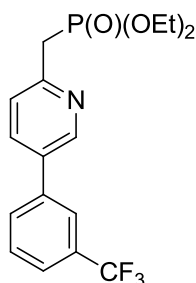
2-Methyl-5-(3-(trifluoromethyl)phenyl)pyridine⁸⁷ (**27**)



Tetrakis(triphenylphosphine)palladium(0) (445 mg, 0.39 mmol) and 3-trifluoromethylphenyl boronic acid (1.85 g, 9.74 mmol) were added to a stirred, degassed solution of 6-methylpyridin-3-yl trifluoromethanesulfonate (**26**) (1.86 g, 7.70 mmol), aq. K₂CO₃ (2 M, 22 mL) and DME (30 mL) under Ar. The reaction mixture was stirred at 100 °C for 1 h before the DME was removed *in vacuo*. The residue was diluted with EtOAc, washed (brine), dried (Na₂SO₄), filtered and concentrated *in vacuo* to yield crude product. Purification by flash column chromatography (0-20% EtOAc/Pet. Ether) yielded 2-methyl-5-(3-(trifluoromethyl)phenyl)pyridine (**27**) (1.58 g, 6.66 mmol, 86%) as a colourless, crystalline solid; Rf. 0.28 (40% EtOAc/Pet. Ether); ¹H NMR (600 MHz, CDCl₃) δ 8.73 (1H, d, *J* = 2.3, CHN), 7.79 (1H, s, CHCCF₃), 7.78 (1H, dd, *J* = 8.3, 2.3, CHCCHN), 7.74 (1H, d, *J* = 7.9, CHCCHCCF₃), 7.64 (1H, d, *J* = 7.9, CHCCF₃), 7.59 (1H, t, *J* = 7.9, CHCHCCF₃), 7.27 (1H, d, *J* = 7.9, CHCMe), 2.62 (3H, s, CH₃); ¹³C NMR (150 MHz, CDCl₃) δ 158.2 (CMe), 147.5 (CHN), 138.9 (CCHCCF₃), 135.0

(CHCCHN), 132.6 (CCHN), 131.6 (q, $J = 32.2$, CCF₃), 130.4 (CHCCHCCF₃), 129.7 (CHCHCCF₃), 124.6 (q, $J = 3.6$, CHCHCCF₃), 123.9 (q, $J = 3.6$, CCHCCF₃), 123.5 (CHCMe), 124.2 (d, $J = 271.8$, CF₃), 24.3 (CH₃); IR (thin film) 2928 (C-H), 1602 (ArC-C), 1582 (ArC-C), 1438 (ArC-C), 1335 (ArC-N), 1267 (ArC-N), 1166 (C-H), 1125 (C-F), 1075, 801, 715, 700 cm⁻¹; m/z (ES⁺) 238 (100%, [M+H]⁺); HRMS (ES⁺) calcd for C₁₃H₁₁NF₃ [M+H]⁺ 238.0831, observed 238.0844. Data agrees with that reported by Clasby *et al.*⁸⁷

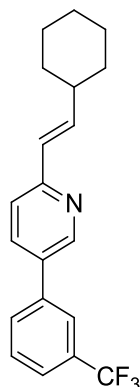
Diethyl (5-(3-(trifluoromethyl)phenyl)pyridin-2-yl)methylphosphonate⁸⁷
(28)



t-BuLi (1.6 M in pentane) (10.4 mL, 16.7 mmol) was added dropwise to a stirred solution of 2-methyl-5-(3-(trifluoromethyl)phenyl)pyridine (**27**) (1.58 g, 6.66 mmol) and diisopropylamine (DIPA) (1.00 mL, 7.33 mmol) in anhydrous THF (30 mL) at -78 °C, under Ar. The reaction mixture was stirred for 15 min at -78 °C before diethyl chlorophosphate (1.00 mL, 6.70 mmol) was added dropwise. The reaction mixture was stirred for a further 45 min and then quenched with sat. aq. NH₄Cl (20 mL). An extraction into EtOAc (2 x 40 mL) was done and the combined organic layers were dried (MgSO₄), filtered and concentrated *in vacuo* to yield a crude brown oil. Purification by flash column chromatography (0-100% EtOAc/CH₂Cl₂) yielded diethyl (5-(3-(trifluoromethyl)phenyl)pyridin-2-yl)methylphosphonate (**28**) (1.88 g, 5.04 mmol, 75%) as an orange oil; R_f. 0.07 (50% EtOAc/CH₂Cl₂); ¹H NMR (600 MHz, CDCl₃) δ 8.75 (1H, d, $J = 2.3$, CHN), 7.85 (1H, dd, $J = 8.2, 2.3$, CHCCHN), 7.79 (1H, s, CCHCCF₃), 7.74 (1H, d, $J = 7.9$, CHCCHCCF₃), 7.64 (1H, d, $J = 7.5$, CHCHCCF₃), 7.59 (1H, t, $J = 7.5$, CHCHCCF₃), 7.48 (1H, dd, $J = 8.2, 2.3$, CHCN), 4.11 (2H, q, $J = 6.8$, OCH₂CH₃), 4.10 (2H, q, $J = 6.8$, OCH₂CH₃), 3.46

(1H, d, $J = 22.2$, CH_2P), 1.29 (6H, t, $J = 6.8$, 2 x OCH_2CH_3); ^{13}C NMR (150 MHz, CDCl_3) δ 152.5 (d, $J = 8.3$, CN), 147.9 (d, $J = 2.4$, CHN), 138.5 (d, $J = 1.2$, CCHCCF_3), 135.2 (d, $J = 3$, CHCCHN), 133.7 (d, $J = 3.6$, CCHN), 131.6 (q, $J = 31.6$, CCF_3), 130.5 (CHCCHCCF_3), 129.7 (CHCHCCF_3), 124.9 (q, $J = 3.6$, CHCHCCF_3), 124.5 (d, $J = 4.8$, CHCN), 123.9 (d, $J = 4.2$, CCHCCF_3), 124.1 (d, $J = 272.4$, CF_3), 62.5 (d, $J = 6.6$, 2 x OCH_2CH_3), 36.4 (d, $J = 135.3$, CH_2P), 16.5 (d, $J = 6.0$, 2 x OCH_2CH_3); IR (thin film) 2984 (C-H), 2910 (C-H), 1598 (ArC-C), 1561 (ArC-C), 1480 (ArC-C), 1440 (ArC-C), 1335 (C-N), 1261 (C-N), 1165 (P=O), 1123 (C-F), 1025, 963 (P-O) cm^{-1} ; m/z (ES+) 374 (98%, $[\text{M}+\text{H}]^+$); HRMS (ES+) calcd for $\text{C}_{17}\text{H}_{20}\text{NO}_3\text{F}_3\text{P}$ $[\text{M}+\text{H}]^+$ 374.1133, observed 374.1130. Data agrees with that reported by Clasby *et al.*⁸⁷

2-(2-Cyclohexylvinyl)-5-(3-(trifluoromethyl)phenyl)pyridine (29)

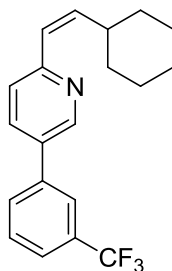


t-BuLi (1.6 M in pentane) (175 μL , 0.28 mmol) was added dropwise to a stirred solution of diethyl (5-(3-(trifluoromethyl)phenyl)pyridin-2-yl)methylphosphonate (**28**) (100 mg, 0.27 mmol) in anhydrous THF (2 mL) at 0 $^{\circ}\text{C}$, under Ar. The reaction mixture was stirred for 10 min at 0 $^{\circ}\text{C}$ before cyclohexanecarboxaldehyde (32.7 μL , 0.27 mmol) in anhydrous THF (2 mL) was added. The reaction mixture was stirred for a further 3 h at 0 $^{\circ}\text{C}$ and then quenched with sat. aq. NH_4Cl (5 mL). An extraction into EtOAc (2 x 10 mL) was completed and the combined organic layers were dried (MgSO_4), filtered and concentrated *in vacuo* to yield a crude orange oil. Purification by flash column chromatography (0-10% Et_2O /Pet. Ether) yielded (*E*)-2-(2-cyclohexylvinyl)-5-(3-(trifluoromethyl)phenyl)pyridine (**29**) (79.4 mg, 0.24

mmol, 89%) as a white solid and (*Z*)-2-(2-cyclohexylvinyl)-5-(3-(trifluoromethyl)phenyl)pyridine (**30**) (3.7 mg, 0.01 mmol, 4%) as a pale yellow solid.

Data for (*E*)-2-(2-cyclohexylvinyl)-5-(3-(trifluoromethyl)phenyl)pyridine (**29**): Rf. 0.44 (30% Et₂O/Pet. Ether); ¹H NMR (600 MHz, CDCl₃) δ 8.76 (1H, d, *J* = 1.9, *CHN*), 7.81 (1H, dd, *J* = 8.3, 2.3, *CHCCHN*), 7.80 (1H, s, *CCHCCF₃*), 7.75 (1H, d, *J* = 7.5, *CHCCHCCF₃*), 7.65-7.62 (1H, m, *CHCHCCF₃*), 7.60-7.57 (1H, m, *CHCHCCF₃*), 7.35 (1H, d, *J* = 8.3, *CHCN*), 6.77 (1H, dd, *J* = 15.8, 7.2, *CHCH=CH*), 6.50 (1H, d, *J* = 15.8, *CH=CHC*), 2.22 (1H, dtd, *J* = 10.7, 7.2, 3.6, *CHCH=CH*), 1.86 (2H, d, *J* = 11.7, 2 x *CHCH^eH*), 1.79 (2H, td, *J* = 12.9, 3.3, 2 x *CH₂CH^eH*), 1.69 (1H, td, *J* = 12.8, 3.4, *CH^eH*), 1.34 (2H, tq, *J* = 12.4, 3.4, 2 x *CHCH^aH*), 1.23 (2H, dq, *J* = 12.4, 3.0, 2 x *CH₂CH^aH*), 1.2 -1.17 (1H, m, *CH^aH*); ¹³C NMR (150 MHz, CDCl₃) δ 156.1 (CN), 147.9 (CHN), 142.4 (CHCH=CH), 138.8 (CCHCCF₃), 134.9 (CHCCHN), 133.0 (CCHN), 131.6 (q, *J* = 31.6, CCF₃), 130.2 (CHCCHCCF₃), 129.7 (CHCHCCF₃), 127.0 (CH=CHC), 124.6 (q, *J* = 3.0, CHCHCCF₃), 123.7 (q, *J* = 3.0, CCHCCF₃), 124.1 (d, *J* = 273.6, CF₃), 121.2 (CHCN), 41.2 (CHCH=CH), 32.7 (2 x CHCH₂), 26.2 (CH₂), 26.1 (2 x CH₂CH₂); IR (thin film) 3007 (C-H), 2925 (C-H), 2852 (C-H), 1650 (C=C), 1592 (ArC-C), 1555 (ArC-C), 1477 (ArC-C), 1442 (ArC-C), 1334 (ArC-N), 1265 (ArC-N), 1165 (C-F), 1124, 1097, 1075, 1048, 970, 799, 699 cm⁻¹; m/z (ES+) 332 (100%, [M+H]⁺); HRMS (ES+) calcd for C₂₀H₂₁NF₃ [M+H]⁺ 332.1626, observed 332.1621.

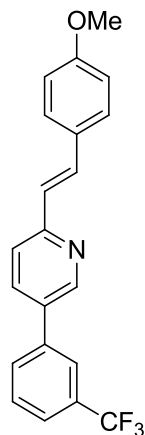
Data for (*Z*)-2-(2-cyclohexylvinyl)-5-(3-(trifluoromethyl)phenyl)pyridine (**30**):



Rf. 0.53 (30% Et₂O/Pet. Ether); ¹H NMR (600 MHz, CDCl₃) δ 8.85 (1H, d, *J* = 1.9, *CHN*), 7.85 (1H, dd, *J* = 8.3, 2.3, *CHCCHN*), 7.84 (1H, s, *CCHCCF₃*), 7.78 (1H, d, *J*

= 7.9, CHCCHCCF₃), 7.65 (1H, d, *J* = 7.5, CHCCHCCF₃), 7.60 (1H, t, *J* = 7.9, CHCCHCCF₃), 7.32 (1H, d, *J* = 8.3, CHCN), 6.40 (1H, d, *J* = 12.0, CH=CHC), 5.76 (1H, dd, *J* = 11.7, 10.2, CHCH=CH), 3.11 (1H, bq, *J* = 10.9, CHCH=CH), 1.80 (2H, bd, *J* = 12.0, 2 x CHCH^aH), 1.75 (2H, td, *J* = 13.2, 3.2, 2 x CH₂CH^aH), 1.69 (1H, bd, *J* = 12.8, CH^aH), 1.34 (2H, tq, *J* = 12.8, 3.4, 2 x CH₂CH^aH), 1.24-1.14 (3H, m, 2 x CHCH^aH, CH^aH); ¹³C NMR (150 MHz, CDCl₃) δ 156.6 (CN), 147.8 (CHN), 143.9 (CHCH=CH), 138.8 (CCHCCF₃), 134.5 (CHCCHN), 132.5 (CCHN), 131.7 (q, *J* = 32.2, CCF₃), 130.3 (CHCCHCCF₃), 129.7 (CHCHCCF₃), 126.1 (CH=CHC), 124.7 (q, *J* = 3.6, CHCHCCF₃), 123.8 (q, *J* = 3.6, CCHCCF₃), 123.7 (CHCN), 124.1 (d, *J* = 272.4, CF₃), 37.2 (CHCH=CH), 33.0 (2 x CHCH₂), 26.2 (CH₂), 25.8 (2 x CH₂CH₂); IR (thin film) 2924 (C-H), 2852 (C-H), 1644 (C=C), 1593 (ArC-C), 1479 (ArC-C), 1444 (ArC-C), 1336 (ArC-N), 1267 (ArC-N), 1167 (C-F), 1128, 1098, 1076, 1047, 803, 700 cm⁻¹; m/z (ES⁺) 332 (100%, [M+H]⁺); HRMS (ES⁺) calcd for C₂₀H₂₁NF₃ [M+H]⁺ 332.1626, observed 332.1621.

(E)-2-(4-Methoxystyryl)-5-(3-(trifluoromethyl)phenyl)pyridine (31)

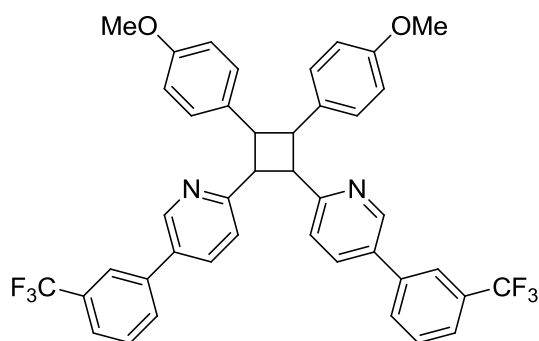


t-BuLi (1.6 M in pentane) (175 μL, 0.28 mmol) was added dropwise to a stirred solution of diethyl (5-(3-(trifluoromethyl)phenyl)pyridin-2-yl)methylphosphonate (**28**) (100 mg, 0.27 mmol) in anhydrous THF (2 mL) at 0 °C, under Ar. The reaction mixture was stirred for 10 min at 0 °C before 4-methoxybenzaldehyde (32.8 μL, 0.27 mmol) in anhydrous THF (2 mL) was added. The reaction mixture was stirred for a further 3 h at 0 °C and then quenched with sat. aq. NH₄Cl (5 mL). An extraction into EtOAc (2 x 10 mL) was completed and the combined organic layers

were dried (MgSO_4), filtered and concentrated *in vacuo* to yield a crude orange oil. Purification by flash column chromatography (0-20% $\text{Et}_2\text{O}/\text{Pet. Ether}$) yielded ((*E*)-2-(4-methoxystyryl)-5-(3-(trifluoromethyl)phenyl)pyridine (**31**) as a white solid (52 mg, 0.15 mmol, 54%); Rf. 0.31 (30% $\text{Et}_2\text{O}/\text{Pet. Ether}$); $^1\text{H NMR}$ (600 MHz, CDCl_3) δ 8.83 (1H, d, $J = 1.9$, CHN), 7.87 (1H, dd, $J = 8.1, 2.1$, CHCCHN), 7.84 (1H, s, CCHCCF₃), 7.79 (1H, d, $J = 7.5$, CHCCHCCF₃), 7.64-7.68 (2H, m, CH=CH & CHCCF₃), 7.61 (1H, t, $J = 7.5$, CHCHCCF₃), 7.56 (2H, d, $J = 8.7$, 2 x CHCHCOMe), 7.47 (1H, d, $J = 8.3$, CHCN), 7.11 (1H, d, $J = 16.2$, CH=CH), 6.93 (2H, d, $J = 8.7$, 2 x CHCHCOMe), 3.85 (3H, s, OCH₃); $^{13}\text{C NMR}$ (150 MHz, CDCl_3) δ 160.2 (COMe), 155.7 (CN), 148.0 (CHN), 138.7 (CCHCCF₃), 135.1 (CHCCHN), 133.2 (CHCH=CH), 133.1 (CCHN), 131.7 (q, $J = 32.8$, CCF₃), 130.2 (CHCCHCCF₃), 129.7 (CHCHCCF₃), 129.4 (CCH=CH), 128.7 (2 x CHCCH=CH), 125.0 (CH=CHC), 124.7 (q, $J = 3.8$, CHCHCCF₃), 123.7 (q, $J = 3.6$, CCHCCF₃), 121.9 (CHCN), 122.3 (d, $J = 273.0$, CF₃), 114.4 (2 x CHCOMe), 55.5 (OCH₃); m/z (CI) 356 (100%, $[\text{M}+\text{H}]^+$); HRMS (CI) calcd for $\text{C}_{21}\text{H}_{16}\text{F}_3\text{NO}$ $[\text{M}+\text{H}]^+$ 356.12568, observed 356.124318.

In the presence of light **31** dimerised to form 6,6'-(3,4-bis(4-methoxyphenyl)cyclobutane-1,2-diyl)bis(3-(3-(trifluoromethyl)phenyl)pyridine) (**32**).

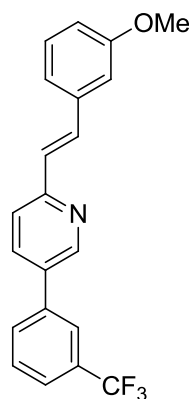
Data for **32**:



Rf. 0.14 (30% $\text{Et}_2\text{O}/\text{Pet. Ether}$); $^1\text{H NMR}$ (600 MHz, CDCl_3) δ 8.74 (2H, d, $J = 1.9$, 2 x CHN), 7.74 (2H, s, 2 x CHCCHN), 7.69 (2H, d, $J = 7.5$, 2 x CHCCHCCF₃), 7.63 (2H, dd, $J = 8.3, 2.3$, 2 x CHCCHN), 7.60 (2H, d, $J = 7.9$, 2 x CHCCF₃), 7.55 (2H, t, $J = 7.5$, 2 x CHCHCCF₃), 7.14 (4H, d, $J = 8.7$, 4 x CHCHCOMe), 7.09 (2H, d, $J =$

7.9, 2 x *CHCN*), 6.68 (4H, d, $J = 8.7$, 4 x *CHCHCOMe*), 4.88 (2H, dd, $J = 10.0$, 7.3, 2 x cyclobutane-*CH*), 4.72 (2H, dd, $J = 10.0$, 7.3, 2 x cyclobutane-*CH*), 3.69 (6H, s, 6 x *OCH*₃); ¹³C NMR (150 MHz, CDCl₃) δ 160.2 (2 x CN), 157.9 (2 x COMe), 147.3 (2 x CHN), 138.8 (2 x CCHCCF₃), 134.3 (2 x CHCCHN), 132.5 (2 x CCHN), 132.4 (2 x CCHCHCOMe), 131.5 (q, $J = 32.8$, 2 x CCF₃), 130.3 (2 x CHCCHCCF₃), 129.6 (2 x CHCHCCF₃), 129.2 (4 x CHCHCOMe), 124.6 (q, $J = 3.6$, 2 x CHCHCCF₃), 123.8 (q, $J = 3.8$, 2 x CCHCCF₃), 123.7 (2 x CHCN), 124.1 (d, $J = 272.4$, 2 x CF₃), 113.5 (4 x CHCOMe), 55.2 (2 x OCH₃), 49.1 (2 x cyclobutane-*CH*), 45.2 (2 x cyclobutane-*CH*); *m/z* (ES-) 709 (100%, [M+H]⁺); HRMS (ES-) calcd for C₄₂H₃₁F₆N₂O₂ [M-H]⁺ 709.2290, observed 709.2286.

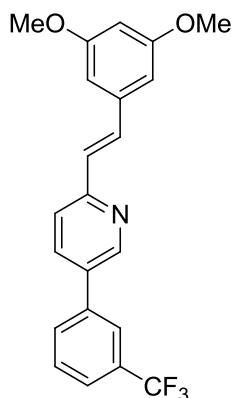
(*E*)-2-(3-Methoxystyryl)-5-(3-(trifluoromethyl)phenyl)pyridine (33)



t-BuLi (1.6 M in pentane) (200 μ L, 0.32 mmol) was added dropwise to a stirred solution of diethyl (5-(3-(trifluoromethyl)phenyl)pyridin-2-yl)methylphosphonate (**28**) (109 mg, 0.29 mmol) in anhydrous THF (1.3 mL) at 0 °C, under Ar. The reaction mixture was stirred for 10 min at 0 °C before 3-methoxybenzaldehyde (35.5 μ L, 0.29 mmol) was added. The reaction mixture was stirred for a further 1 h at 0 °C and then quenched with sat. aq. NH₄Cl (5 mL). An extraction into EtOAc (2 x 10 mL) was completed and the combined organic layers were dried (MgSO₄), filtered and concentrated *in vacuo* to yield a crude orange oil. Purification by flash column chromatography (0-20% Et₂O/Pet. Ether) yielded ((*E*)-2-(3-methoxystyryl)-5-(3-(trifluoromethyl)phenyl)pyridine (**33**) (95.1 mg, 0.27 mmol, 92%) as a waxy solid; ¹H NMR (600 MHz, CDCl₃) δ 8.85 (1H, d, $J = 2.3$, *CHN*), 7.89 (1H, dd, $J = 8.1$, 2.3,

CHCCHN), 7.84 (1H, s, CCHCCF₃), 7.79 (1H, d, *J* = 7.5, CHCCHCCF₃), 7.66 (1H, d, *J* = 7.9, CHCCF₃), 7.66 (1H, d, *J* = 15.8, CH=CH) 7.62 (1H, t, *J* = 7.5, CHCHCCF₃), 7.51 (1H, d, *J* = 8.3, CHCN), 7.31 (1H, t, *J* = 7.9, CHCHCOMe), 7.23 (1H, d, *J* = 15.8, CH=CH), 7.21 (1H, d, *J* = 7.5, CHCCHCOMe), 7.15 (1H, s, CCHCOMe), 6.88 (1H, dd, *J* = 7.9, 2.3, CHCHCOMe), 3.86 (3H, s, OCH₃); ¹³C NMR (150 MHz, CDCl₃) δ 160.0 (COMe), 155.2 (CN), 148.1 (CHN), 138.6 (CCHCCF₃), 138.0 (CCH=CH), 135.1 (CHCCHN), 133.6 (CCHN), 133.5 (CH=CH), 131.7 (q, *J* = 32.2, CCF₃), 130.3 (CHCCHCCF₃), 129.9 (CHCHCOMe), 129.8 (CHCHCCF₃), 127.6 (CH=CH), 124.8 (q, *J* = 3.6, CHCHCCF₃), 123.8 (q, *J* = 4.2, CCHCCF₃), 124.1 (d, *J* = 273.0, CF₃), 122.2 (CHCN), 120.1 (CHCCHCOMe), 114.6 (CHCHCOMe), 112.3 (CCHCOMe), 55.4 (OCH₃); *m/z* (ES+) 356 (100%, [M+H]⁺); HRMS (ES+) calcd for C₂₁H₁₆F₃NO [M+H]⁺ 356.1262, observed 356.1272.

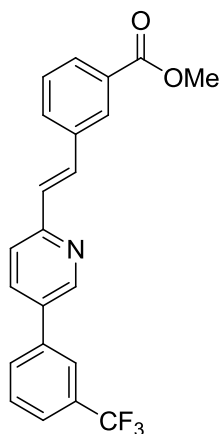
(*E*)-2-(3,5-Dimethoxystyryl)-5-(3-(trifluoromethyl)phenyl)pyridine (34)



t-BuLi (1.6 M in pentane) (200 μL, 0.32 mmol) was added dropwise to a stirred solution of diethyl (5-(3-(trifluoromethyl)phenyl)pyridin-2-yl)methylphosphonate (**28**) (109 mg, 0.29 mmol) in anhydrous THF (1.3 mL) at 0 °C, under Ar. The reaction mixture was stirred for 10 min at 0 °C before 3,5-dimethoxybenzaldehyde (48.5 μL, 0.29 mmol) in anhydrous THF (2 mL) was added. The reaction mixture was stirred for a further 1 h at 0 °C and then quenched with sat. aq. NH₄Cl (5 mL). An extraction into EtOAc (2 x 10 mL) was completed and the combined organic layers were dried (MgSO₄), filtered and concentrated *in vacuo* to yield a crude orange oil. Purification by flash column chromatography (0-10% EtOAc/Pet. Ether) yielded

((*E*)-2-(3,5-dimethoxystyryl)-5-(3-(trifluoromethyl)phenyl)pyridine (**34**) (92.0 mg, 0.24 mmol, 82%) as a fluorescent yellow solid; ¹H NMR (600 MHz, CDCl₃) δ 8.85 (1H, d, *J* = 1.9, CHN), 7.90 (1H, dd, *J* = 8.1, 1.9, CHCCHN), 7.84 (1H, s, CCHCCF₃), 7.79 (1H, d, *J* = 7.5, CHCCHCCF₃), 7.67 (1H, d, *J* = 7.9, CHCCF₃), 7.60-7.64 (2H, m, CH=CH & CHCHCCF₃), 7.52 (1H, d, *J* = 8.3, CHCN), 7.22 (1H, d, *J* = 16.2, CH=CH), 6.77 (2H, d, *J* = 1.9, 2 x CHCOMe), 6.45 (1H, d, *J* = 1.9, CHCOMe), 3.85 (6H, s, 2 x OCH₃); ¹³C NMR (150 MHz, CDCl₃) δ 161.1 (2 x COMe), 155.1 (CN), 148.0 (CHN), 138.5 (CCHCOMe), 135.2 (CHCCHN), 133.7 (CCHCCF₃ & CH=CH), 131.7 (q, *J* = 31.6, CCF₃), 130.3 (CHCCHCCF₃ & CCHN), 129.8 (CHCHCCF₃), 127.7 (CH=CH), 124.9 (q, *J* = 3.6, CHCHCCF₃), 123.8 (q, *J* = 3.6, CCHCCF₃), 124.1 (d, *J* = 273.0, CF₃), 122.2 (CHCN), 105.3 (2 x CHCOMe), 101.1 (CHCOMe), 55.5 (2 x OCH₃); *m/z* (ES⁺) 386 (100%, [M+H]⁺); HRMS (CI) calcd for C₂₂H₁₈F₃NO₂ [M+H]⁺ 386.13624, observed 386.13763.

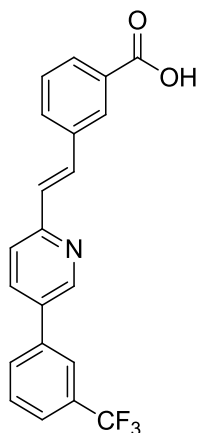
(*E*)-Methyl 3-(2-(5-(3-(trifluoromethyl)phenyl)pyridin-2-yl)vinyl)benzoate (35**)**



t-BuLi (1.6 M in pentane) (580 μL, 0.924 mmol) was added dropwise to a stirred solution of diethyl (5-(3-(trifluoromethyl)phenyl)pyridin-2-yl)methylphosphonate (**28**) (312.8 mg, 0.84 mmol) in anhydrous THF (1.3 mL) at 0 °C, under Ar. The reaction mixture was stirred for 10 min at 0 °C before methyl 3-formylbenzoate (137.9 mg, 0.84 mmol) was added. The reaction mixture was stirred for a further 1 h at 0 °C and then quenched with sat. aq. NH₄Cl (5 mL). An extraction into EtOAc (2 x 10

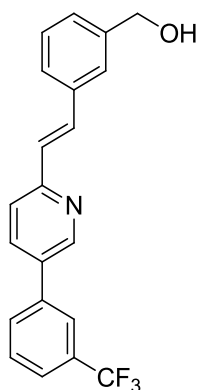
mL) was completed and the combined organic layers were dried (MgSO₄), filtered and concentrated *in vacuo* to yield a crude orange oil. Purification by flash column chromatography (0-20% EtOAc/Pet. Ether) yielded (*E*)-methyl 3-(2-(5-(3-(trifluoromethyl)phenyl)pyridin-2-yl)vinyl)benzoate (**35**) (272 mg, 0.71 mmol, 84%) as a pale yellow solid; ¹H NMR (600 MHz, CDCl₃) δ 8.86 (1H, d, *J* = 2.3, CHN), 8.31 (1H, s, CCHCCOOMe), 7.98 (1H, d, *J* = 7.5, CHCHCCOOMe), 7.91 (1H, dd, *J* = 7.9, 2.3, CHCCHN), 7.85 (1H, s, CCHCCF₃), 7.80 (1H, d, *J* = 7.9, CHCCHCCF₃), 7.77 (1H, d, *J* = 7.5, CHCCHCCOOMe), 7.74 (1H, d, *J* = 15.8, CH=CH), 7.67 (1H, d, *J* = 7.9, CHCCF₃), 7.62 (1H, t, *J* = 7.5, CHCHCCF₃), 7.51 (1H, d, *J* = 8.3, CHCN), 7.47 (1H, app. t, *J* = 7.9, CHCHCCOOMe), 7.31 (1H, d, *J* = 15.8, CH=CH), 3.96 (3H, s, OCH₃); ¹³C NMR (150 MHz, CDCl₃) δ 167.0 (C=O), 154.9 (CN), 148.2 (CHN), 138.5 (CCHCCF₃), 137.0 (CCHCCOOMe), 135.2 (CHCCHN), 133.8 (CCHN), 132.4 (CH=CH), 131.8 (CHCCHCCOOMe), 131.7 (q, *J* = 32.8, CCF₃), 130.8 (CCOOMe) 130.3 (CHCCHCCF₃), 129.8 (CHCHCCF₃), 129.5 (CHCHCCOOMe), 129.0 (CHCHCCOOMe), 128.5 (CH=CH), 128.1 (CCHCCOOMe), 124.9 (q, *J* = 3.6, CHCHCCF₃), 123.8 (q, *J* = 3.6, CCHCCF₃), 124.1 (d, *J* = 272.4, CF₃), 122.5 (CHCN), 52.4 (OCH₃); *m/z* (ES+) 384 (100%, [M+H]⁺); HRMS (CI) calcd for C₂₂H₁₆F₃NO₂ [M+H]⁺ 384.12059, observed 384.121101.

(*E*)-3-(2-(5-(3-(Trifluoromethyl)phenyl)pyridin-2-yl)vinyl)benzoic acid (36)



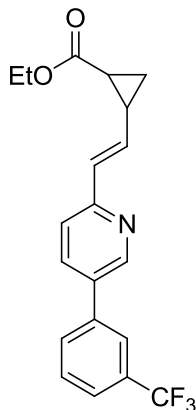
A solution of (*E*)-methyl 3-(2-(5-(3-(trifluoromethyl)phenyl)pyridin-2-yl)vinyl)benzoate (**35**) (83.0 mg, 0.22 mmol) in EtOH (0.5 mL) and aq. NaOH (1M, 1 mL) was refluxed at 80 °C for 40 min. Once cool the solution was acidified with conc. HCl, cooled to 0 °C and the precipitate was filtered and dried under vacuum to yield (*E*)-3-(2-(5-(3-(trifluoromethyl)phenyl)pyridin-2-yl)vinyl)benzoic acid (**36**) (33.2 mg, 0.09 mmol, 41%) as a white solid; ¹H NMR (600 MHz, MeOH-d₄) δ 9.10 (1H, d, *J* = 1.9, CHN), 8.85 (1H, dd, *J* = 8.7, 2.3, CHCCHN), 8.48 (1H, d, *J* = 8.7, CHCN), 8.37 (1H, s, CCHCCOOH), 8.17 (1H, s, CCHCCF₃), 8.12 (1H, d, *J* = 7.9, CHCCHCCF₃), 8.06-8.10 (2H, m, CHCHCCOOH & CH=CH), 8.00 (1H, d, *J* = 8.3, CHCCHCCOOH), 7.86 (1H, d, *J* = 7.9, CHCCF₃), 7.81 (1H, t, *J* = 7.9, CHCHCCF₃), 7.61 (1H, t, *J* = 7.7, CHCHCCOOH), 7.51 (1H, d, *J* = 16.6, CH=CH), 3.95 (1H, s, OH); ¹³C NMR (150 MHz, MeOH-d₄) δ 169.0 (C=O), 151.0 (CN), 144.8 (CHCCHN), 141.8 (CH=CH), 140.8 (CHN), 137.7 (CCHN), 136.5 (CCHCCOOH), 136.2 (CCHCCF₃), 133.3 (CHCCHCCOOH), 133.1 (CCOOH), 132.7 (CHCCOOH), 133.0 (q, *J* = 32.8, CCF₃), 132.2 (CHCCHCCF₃), 131.7 (CHCHCCF₃), 130.6 (CHCHCCOOH), 130.4 (CCHCCOOH), 127.6 (q, *J* = 3.6, CHCHCCF₃), 125.6 (CHCN), 125.1 (q, *J* = 4.2, CCHCCF₃), 125.4 (d, *J* = 271.2, CF₃), 120.2 (CH=CH); *m/z* (ES⁺) 370 (100%, [M+H]⁺).

(*E*)-(3-(2-(5-(3-(Trifluoromethyl)phenyl)pyridin-2-yl)vinyl)phenyl)methanol (37**)**



LiAlH₄ (1.0 M in THF) (220 μ L, 0.22 mmol) was added dropwise to a stirred solution of (*E*)-methyl 3-(2-(5-(3-(trifluoromethyl)phenyl)pyridin-2-yl)vinyl)benzoate (**35**) (86.2 mg, 0.22 mmol) in anhydrous THF (1 mL) under Ar. The reaction mixture was stirred for 40 min and then quenched with aq. NaOH (1M). An extraction into EtOAc (2 x 10 mL) was completed and the combined organic layers were dried (MgSO₄), filtered and concentrated *in vacuo* to yield a crude orange oil. Purification by flash column chromatography (0-20% EtOAc/CH₂Cl₂) yielded (*E*)-(3-(2-(5-(3-(trifluoromethyl)phenyl)pyridin-2-yl)vinyl)phenyl)methanol (**37**) (47.3 mg, 0.13 mmol, 61%) as a waxy pale yellow solid; ¹H NMR (600 MHz, CDCl₃) δ 8.85 (1H, d, *J* = 1.9, CHN), 7.90 (1H, dd, *J* = 8.3, 2.3, CHCCHN), 7.84 (1H, s, CCHCCF₃), 7.80 (1H, d, *J* = 7.5, CHCCHCCF₃), 7.71 (1H, d, *J* = 16.2, CH=CH), 7.67 (1H, d, *J* = 7.5, CHCCF₃), 7.64 (1H, bs, CHCCH₂OH), 7.62 (1H, t, *J* = 7.5, CHCHCCF₃), 7.54 (1H, d, *J* = 7.9, CHCCHCCH₂OH), 7.50 (1H, d, *J* = 7.9, CHCN), 7.40 (1H, t, *J* = 7.5, CHCHCCH₂OH), 7.33 (1H, d, *J* = 7.5, CHCCH₂OH), 7.26 (1H, d, *J* = 16.2, CH=CH), 4.76 (2H, d, *J* = 4.9, CH₂OH), 1.78 (1H, bt, *J* = 4.9, OH); ¹³C NMR (150 MHz, CDCl₃) δ 155.2 (CN), 148.1 (CHN), 141.5 (CCH₂OH) 138.6 (CCHCCF₃), 136.9 (CCHCCH₂OH), 135.2 (CHCCHN), 133.6 (CCHN), 133.3 (CH=CH), 131.7 (q, *J* = 32.2, CCF₃), 130.3 (CHCCHCCF₃), 129.8 (CHCHCCF₃), 129.2 (CHCHCCH₂OH), 127.6 (CH=CH), 127.3 (CHCCH₂OH), 126.8 (CHCCHCCH₂OH), 125.6 (CHCCH₂OH), 124.8 (q, *J* = 3.6, CHCHCCF₃), 123.8 (q, *J* = 3.6, CCHCCF₃), 124.1 (d, *J* = 273.6, CF₃), 122.3 (CHCN), 65.4 (CH₂); *m/z* (ES⁺) 356 (100%, [M+H]⁺); HRMS (CI) calcd for C₂₁H₁₆F₃NO [M+H]⁺ 356.12568, observed 356.126750.

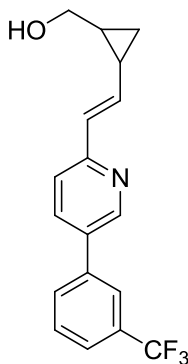
(E)-Ethyl 2-(2-(5-(3-(trifluoromethyl)phenyl)pyridin-2-yl)vinyl)cyclopropanecarboxylate (38)



t-BuLi (1.6 M in pentane) (463 μ L, 0.74 mmol) was added dropwise to a stirred solution of diethyl (5-(3-(trifluoromethyl)phenyl)pyridin-2-yl)methylphosphonate (**28**) (252 mg, 0.68 mmol) in anhydrous THF (2 mL) at 0 °C, under Ar. The reaction mixture was stirred for 10 min at 0 °C before ethyl 2-formyl-1-cyclopropanecarboxylate (89.5 μ L, 0.68 mmol) was added. The reaction mixture was stirred for a further 1 h at 0 °C and then quenched with sat. aq. NH₄Cl (5 mL). An extraction into EtOAc (2 x 10 mL) was completed and the combined organic layers were dried (MgSO₄), filtered and concentrated *in vacuo* to yield a crude orange oil. Purification by flash column chromatography (0-20% EtOAc/Pet. Ether) yielded (E)-ethyl 2-(2-(5-(3-(trifluoromethyl)phenyl)pyridin-2-yl)vinyl)cyclopropanecarboxylate (**38**) (203 mg, 0.56 mmol, 83%) as a pale yellow solid; ¹H NMR (600 MHz, CDCl₃) δ 8.75 (1H, d, *J* = 2.3, CHN), 7.83 (1H, dd, *J* = 8.1, 2.4, CHCCHN), 7.80 (1H, s, CCHCCF₃), 7.76 (1H, d, *J* = 7.5, CHCCHCCF₃), 7.65 (1H, d, *J* = 7.5, CHCHCCF₃), 7.60 (1H, t, *J* = 7.5, CHCHCCF₃), 7.27 (1H, d, *J* = 7.9, CHCN), 6.68 (1H, d, *J* = 15.4, CH=CH), 6.37 (1H, dd, *J* = 15.4, 9.4, CH=CH), 4.16 (2H, q, *J* = 6.9, CH₂CH₃), 2.25 (1H, dddd, *J* = 9.4, 9.0, 5.8, 3.8, CHCH=CH), 1.87 (1H, ddd, *J* = 8.5, 5.1, 3.8, CHCOOEt), 1.54 (1H, ddd, *J* = 9.0, 5.1, 4.7, cyclopropane-CHH), 1.28 (3H, t, *J* = 7.2, CH₂CH₃), 1.19 (1H, ddd, *J* = 8.6, 5.9, 4.7, cyclopropane-CHH); ¹³C NMR (150 MHz, CDCl₃) δ 173.3 (C=O), 154.8 (CN), 148.0 (CHN), 138.6 (CCHCCF₃), 136.1 (CH=CH), 135.1 (CHCCHN), 133.4 (CCHN),

131.6 (q, $J = 32.2$, CCF_3), 130.2 (CHCCHCCF_3), 129.7 (CHCHCCF_3), 129.3 ($\text{CH}=\text{CH}$), 124.7 (q, $J = 3.0$, CHCHCCF_3), 123.8 (q, $J = 3.6$, CCHCCF_3), 124.1 (d, $J = 272.4$, CF_3), 121.5 (CHCN), 60.9 (CH_2CH_3), 25.6 ($\text{CHCH}=\text{CH}$), 22.8 (CHCOOEt), 16.4 (cyclopropyl- CH_2), 14.4 (CH_2CH_3); m/z (ES+) 362 (100%, $[\text{M}+\text{H}]^+$); HRMS (CI) calcd for $\text{C}_{20}\text{H}_{18}\text{F}_3\text{NO}_2$ $[\text{M}+\text{H}]^+$ 362.13624, observed 362.137134.

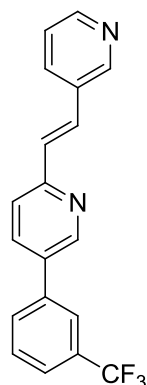
(E)-(2-(2-(5-(3-(Trifluoromethyl)phenyl)pyridin-2-yl)vinyl)cyclopropyl)methanol (39)



LiAlH_4 (1.0 M in THF) (340 μL , 0.34 mmol) was added dropwise to a stirred solution of (*E*)-ethyl 2-(2-(5-(3-(trifluoromethyl)phenyl)pyridin-2-yl)vinyl)cyclopropanecarboxylate (**38**) (123 mg, 0.34 mmol) in anhydrous THF (1 mL) under Ar. The reaction mixture was stirred for 1 h and then quenched with aq. NaOH (1M). An extraction into EtOAc (2 x 10 mL) was completed and the combined organic layers were dried (MgSO_4), filtered and concentrated *in vacuo* to yield a crude orange oil. Purification by flash column chromatography (0-50% EtOAc/Pet. Ether) yielded (*E*)-(2-(2-(5-(3-(trifluoromethyl)phenyl)pyridin-2-yl)vinyl)cyclopropyl)methanol (**39**) (56.2 mg, 0.18 mmol, 52%) as a pale yellow solid; ^1H NMR (600 MHz, CDCl_3) δ 8.74 (1H, d, $J = 2.4$, CHN), 7.81 (1H, dd, $J = 8.2, 2.4$, CHCCHN), 7.80 (1H, s, CCHCCF₃), 7.75 (1H, d, $J = 7.7$, CHCCHCCF₃), 7.64 (1H, d, $J = 7.7$, CHCHCCF₃), 7.59 (1H, t, $J = 7.7$, CHCHCCF₃), 7.26 (1H, d, $J = 8.2$, CHCN), 6.61 (1H, d, $J = 15.4$, CH=CH), 6.40 (1H, dd, $J = 15.4, 9.4$, CH=CH), 3.55-3.64 (2H, m, CH_2OH), 1.61-1.64 (1H, m, CHCH=CH), 1.39-1.45 (2H, m, CHCOOH & OH), 0.87-0.93 (2H, m, cyclopropane- CH_2); ^{13}C NMR (150 MHz, CDCl_3) δ 155.3 (CN), 147.9 (CHN), 139.0 (CH=CH), 138.7 (CCHCCF₃), 135.1

(CHCCHN), 133.0 (CCHN), 131.6 (q, $J = 32.8$, CCF₃), 130.2 (CHCCHCCF₃), 129.7 (CHCHCCF₃), 127.2 (CH=CH), 124.6 (q, $J = 3.6$, CHCHCCF₃), 123.7 (q, $J = 3.6$, CCHCCF₃), 124.1 (d, $J = 272.4$, CF₃), 121.1 (CHCN), 66.2 (CH₂OH), 24.2 (CCH₂OH), 20.7 (CHCH=CH), 12.8 (cyclopropyl-CH₂); m/z (ES+) 320 (100%, [M+H]⁺); HRMS (CI) calcd for C₁₈H₁₆F₃NO [M+H]⁺ 320.12568, observed 320.126290.

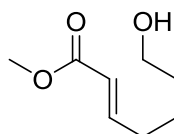
(E)-2-(2-(Pyridin-3-yl)vinyl)-5-(3-(trifluoromethyl)phenyl)pyridine (40)



t-BuLi (1.6 M in pentane) (193 μ L, 0.31 mmol) was added dropwise to a stirred solution of diethyl (5-(3-(trifluoromethyl)phenyl)pyridin-2-yl)methylphosphonate (**28**) (106 mg, 0.28 mmol) in anhydrous THF (1.3 mL) at 0 °C, under Ar. The reaction mixture was stirred for 10 min at 0 °C before nicotinaldehyde (26.6 μ L, 0.28 mmol) was added. The reaction mixture was stirred for a further 1 h at 0 °C and then quenched with sat. aq. NH₄Cl (5 mL). An extraction into EtOAc (2 x 10 mL) was completed and the combined organic layers were dried (MgSO₄), filtered and concentrated *in vacuo* to yield a crude orange oil. Purification by flash column chromatography (0-30% EtOAc/Pet. Ether) yielded (*E*)-2-(2-(pyridin-3-yl)vinyl)-5-(3-(trifluoromethyl)phenyl)pyridine (**40**) (75.6 mg, 0.23 mmol, 83%) as a pale yellow solid; ¹H NMR (600 MHz, CDCl₃) δ 8.87 (1H, d, $J = 2.3$, CHNC), 8.84 (1H, s, CHNCH), 8.55 (1H, d, $J = 4.5$, CHNCH), 7.97 (1H, d, $J = 7.9$, CHCHCHN), 7.93 (1H, dd, $J = 8.3, 2.3$, CHCCHN), 7.85 (1H, s, CCHCCF₃), 7.80 (1H, d, $J = 7.5$, CHCCHCCF₃), 7.72 (1H, d, $J = 15.8$, CH=CH), 7.69 (1H, d, $J = 8.3$, CHCCF₃), 7.63 (1H, t, $J = 8.3$, CHCHCCF₃), 7.52 (1H, d, $J = 8.3$, CHCN), 7.38 (1H, dd, $J = 7.9$,

4.9, CHCHN), 7.31 (1H, d, $J = 15.8$, CH=CH); ^{13}C NMR (150 MHz, CDCl_3) δ 154.3 (CN), 148.7 (CHCHN), 148.5 (CHNCH), 148.2 (CCHN), 138.4 (CCHCCF₃), 135.3 (CHCCHN), 134.3 (CHCHCHN), 134.2 (CCHNC), 132.7 (CHCH=CH), 131.8 (q, $J = 32.2$, CCF₃), 130.3 (CHCCHCCF₃), 129.8 (CHCHCCF₃), 129.5 (CH=CH & CH=CH), 125.0 (q, $J = 3.6$, CHCHCCF₃), 124.1 (CHCHN), 123.9 (q, $J = 3.8$, CCHCCF₃), 124.1 (d, $J = 272.4$, CF₃), 122.7 (CHCN); m/z (ES+) 327 (100%, [M+H]⁺); HRMS (CI) calcd for C₁₉H₁₃F₃N₂ [M+H]⁺ 327.11036, observed 327.111715.

Methyl 7-hydroxyhept-2-enoate¹⁴⁶ (**41**)

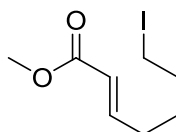


Conc. HCl (37%) (0.34 mL, 11.2 mmol) was added to a stirred solution of 3,4-dihydro-2H-pyran (22.5 mL, 247 mmol) in H₂O (30 mL) at 0 °C. The reaction mixture was stirred at 0 °C for 2 h before solid K₂CO₃ (34.2 g, 247 mmol), methyl 2-(dimethoxyphosphoryl)acetate (20 mL, 124 mmol) and DMSO (60 mL) were added. The reaction mixture was stirred in air at 50 °C for 6 h. Once cool the solution was partitioned between *t*-BME (250 mL) and H₂O (100 mL). The organic layer was dried (hydrophobic frit) and concentrated *in vacuo* to yield a crude colourless liquid. Purification by automated column chromatography (0-100% EtOAc/cyclohexane) yielded methyl 7-hydroxyhept-2-enoate (**41**) (11.5 g, 72.6 mmol, 59%) as a colourless oil, in a 1:5 ratio of *Z*:*E* isomers; Rf. 0.46 (45% EtOAc/Pet. Ether); ^1H NMR (400 MHz, Acetone- d_6) δ 6.95 (1H, dt, $J = 15.6, 7.0$, *E*-AcCH=CH), 6.31 (0.2H, dt, $J = 11.5, 7.6$, *Z*-AcCH=CH), 5.85 (1H, dt, $J = 15.7, 1.6$, *E*-AcCH=CH), 5.79 (0.2 H, dt, $J = 11.5, 1.6$, *Z*-AcCH=CH), 3.68 (3H, s, *E*-COOCH₃), 3.67 (0.6H, s, *Z*-COOCH₃), 3.51-3.60 (3.6H, m, *E*-CH₂OH, *Z*-CH₂OH, *E*-OH & *Z*-OH), 2.64-2.71 (0.4H, m, *Z*-CH₂), 2.23-2.29 (2H, m, *E*-CH₂), 1.53-1.58 ppm (4.8H, m, 2 x *E*-CH₂ & 2 x *Z*-CH₂); ^{13}C NMR (150 MHz, CDCl_3) δ 167.3 (*E*-C=O), 167.0 (*Z*-C=O), 150.6 (*Z*-AcCH=CH), 149.3 (*E*-AcCH=CH), 121.3 (*E*-AcCH=CH), 119.7 (*Z*-AcCH=CH), 62.7

(*E*-CH₂OH), 62.6 (*Z*-CH₂OH), 51.6 (*E*-COOCH₃), 51.2 (*Z*-COOCH₃), 32.2 (*E*-CH=CHCH₂), 32.0 (*Z*-CH₂CH₂OH), 32.0 (*E*-CH₂CH₂OH), 28.6 (*Z*-CH=CHCH₂), 25.2 (*Z*-CH₂), 24.3 (*E*-CH₂); IR (thin film) 3397 (br) (O-H), 2940 (C-H), 2865 (C-H), 1722 (C=O), 1656 (C=C), 1438 (C-H), 1274 (C-O), 1202 (C-O), 1035 (C-O), 984 (=C-H) cm⁻¹; m/z (ES+) 159 (100%, [M+H]⁺); HRMS (CI) calcd for C₈H₁₅O₃ [M+H]⁺ 159.10212, observed 159.10254. Data agrees with that reported by Nieto *et al.*¹⁴⁶ and Tufariello *et al.*¹⁴⁷

A single fraction containing pure *E*-product was concentrated *in vacuo* to give (*E*)-methyl 7-hydroxyhept-2-enoate (**41**) (340 mg, 2.15 mmol, 2% yield) as a colourless oil; ¹H NMR (400 MHz, Acetone-*d*₆) δ 6.95 (1H, dt, *J* = 15.6, 6.9, AcCH=CH), 5.86 (1H, dt, *J* = 15.6, 1.5, AcCH=CH), 3.68 (3H, s, COOCH₃), 3.54-3.60 (2H, m, CH₂OH), 3.48 (1H, t, *J* = 5.0, OH), 2.23-2.30 (2H, m, CH₂), 1.53-1.59 ppm (4H, m, 2 x CH₂); ¹³C NMR (100 MHz, Acetone-*d*₆) δ 166.2 (C=O), 149.2 (AcCH=CH), 120.9 (AcCH=CH), 61.2 (CH₂OH), 50.5 (COOCH₃), 32.2 (CH=CHCH₂), 31.6 (CH₂CH₂OH), 24.4 (CH₂); IR (thin film) 3390 (br) (O-H), 2938 (C-H), 2865 (C-H), 1720 (C=O), 1655 (C=C), 1436 (C-H), 1271 (C-O), 1199 (C-O), 1031 (C-O), 982 (=C-H) cm⁻¹; m/z (ES+) 159 (100%, [M+H]⁺); HRMS (CI) calcd for C₈H₁₅O₃ [M+H]⁺ 159.1017, observed 159.1016. Data agrees with that reported by Nieto *et al.*¹⁴⁶

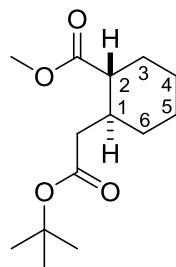
(*E*)-Methyl 7-iodohept-2-enoate¹⁴⁸ (**42**)



Solid I₂ (18.3 g, 72.1 mmol) was added to a stirred solution of methyl 7-hydroxyhept-2-enoate (**41**) (1:5 *Z*:*E* isomers) (11.4 g, 72.1 mmol), PPh₃ (22.7 g, 86.0 mmol) and imidazole (9.81 g, 144 mmol) in 2-MeTHF (200 mL) at 0 °C, under N₂. The reaction mixture was stirred at 20 °C for 2 h before being filtered under vacuum to remove precipitated triphenylphosphine oxide. The filtrate solvents were concentrated *in vacuo* to yield a crude colourless oil with white precipitate.

Purification by automated column chromatography (0-25% EtOAc/cyclohexane) yielded still crude colourless oil with white precipitate. A second purification by automated column chromatography (0-25% EtOAc/cyclohexane) yielded (*E*)-methyl 7-iodohept-2-enoate (**42**) (6.14 g, 22.9 mmol, 32%) as a colourless oil; R_f 0.38 (20% EtOAc/cyclohexane); ¹H NMR (400 MHz, Acetone-*d*₆) δ 6.94 (1H, dt, *J* = 15.6, 7.0, AcCH=CH), 5.88 (1H, dt, *J* = 15.6, 1.6, AcCH=CH), 3.69 (3H, s, COOCH₃), 3.32 (2H, t, *J* = 7.0, CH₂l), 2.30 (2H, tdd, *J* = 7.3, 7.0, 1.6, CH₂), 1.87 (2H, tt, *J* = 7.7, 7.0, CH₂), 1.62 (2H, tt, *J* = 7.7, 7.3, CH₂); ¹³C NMR (100 MHz, Acetone-*d*₆) δ 166.1 (C=O), 148.5 (AcCH=CH), 121.3 (AcCH=CH), 50.6 (COOCH₃), 32.9 (CH₂), 30.6 (CH₂), 28.7 (CH₂), 6.2 (CH₂l); IR (thin film) 2937 (C-H), 2858 (C-H), 1719 (C=O), 1656 (C=C), 1434 (C-H), 1270 (C-O), 1177 (C-H), 1038 (C-O), 974, 845, 718 cm⁻¹; m/z (ES⁺) 269 (100%, [M+H]⁺); HRMS (CI) calcd for C₈H₁₄IO₂ [M+H]⁺ 269.0033, observed 269.0038. Data agrees with that reported by Zhou *et al.*¹⁴⁸

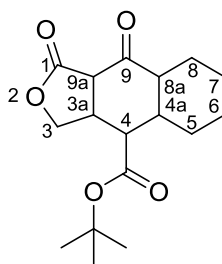
(1*R,2*S**)-Methyl 2-(2-(*tert*-butoxy)-2-oxoethyl)cyclohexanecarboxylate (43)**



n-BuLi (1.6 M in hexanes) (70.0 mL, 112 mmol) was added to a stirred solution of DIPA (15.7 mL, 112 mmol) in anhydrous THF (30 mL) at -78 °C, under Ar. The solution was stirred at -78 °C for 20 mins. A solution of *tert*-butyl acetate (15.0 mL, 112 mmol) was added and stirring continued for 30 min at -78 °C. Next, a solution of (*E*)-methyl 7-iodohept-2-enoate (**42**) (13.7 g, 51 mmol) in anhydrous THF (15 mL) was added. The reaction mixture was stirred for a further 30 min at -78 °C. Finally, solid KO*t*-Bu (12.6 g, 112 mmol) was added and stirring continued for a further 1 h at -78 °C. The reaction mixture was quenched with sat. aq. NH₄Cl (100

mL) and diluted with H₂O (50 mL). An extraction into EtOAc (2 x 100 mL) was completed and the combined organic layers were dried (MgSO₄), filtered and concentrated *in vacuo* to yield a crude pale yellow liquid. Multiple purifications by flash column chromatography (0-2% Et₂O/CH₂Cl₂), (0-10% Et₂O/Pet. Ether) and (0-2% Et₂O/toluene) yielded (1*R**,2*S**)-methyl 2-(2-(*tert*-butoxy)-2-oxoethyl)cyclohexanecarboxylate (**43**) (3.1 g, 12 mmol, 24%) as a colourless liquid; bp. 110-115 °C (at 2.1 mbar); ¹H NMR (600 MHz, CDCl₃) δ 3.66 (3H, s, COOCH₃), 2.26 (1H, d, *J* = 10.9, CHHCOO^tBu), 2.12 (1H, dt, *J* = 11.2, 3.6, C²H), 2.05-1.98 (2H, m, C¹H & CHHCOO^tBu), 1.89 (1H, qd, *J* = 1.9, 13.2, C³HH), 1.84 (1H, dd, *J* = 2.1, 13.0, C⁶HH), 1.74 (1H, dtd, *J* = 12.8, 3.4, 1.1, C⁴HH), 1.72-1.68 (1H, m, C⁵HH), 1.47 (1H, td, *J* = 12.4, 2.6, C³HH), 1.43 (9H, s, C(CH₃)₃), 1.30 (1H, tq, *J* = 12.8, 3.4, C⁵HH), 1.21 (1H, tq, *J* = 13.2, 3.8, C⁴HH), 1.04 (1H, dq, *J* = 13.2, 3.4, C⁶HH); ¹³C NMR (150 MHz, CDCl₃) δ 176.1 (C=OCOMe), 171.8 (C=OCO^tBu), 80.4 (C(CH₃)₃), 51.7 (CH₃), 49.0 (C²H), 40.9 (CH₂COO^tBu), 36.3 (C¹H), 31.3 (C⁶H), 30.0 (C³H), 28.2 (C(CH₃)₃), 25.5 (C⁵H), 25.4 (C⁴H); IR (thin film) 2982 (C-H), 2930 (C-H), 2854 (C-H), 1713 (C=O), 1451 (C-H), 1366 (C-O), 1247 (C-O), 1151, 1108, 1025, 845 cm⁻¹; m/z (ES+) 257 (100%, [M+H]⁺); HRMS (CI) calcd for C₁₃H₁₁O₃ [M-OMe]⁺ 225.14907, observed 225.14872.

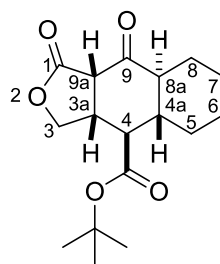
***rac-tert*-Butyl 1,9-dioxododecahydronaphtho[2,3-*c*]furan-4-carboxylate (**44**)**



t-BuLi (2.5 M in hexane) (3.43 ml, 8.58 mmol) was added dropwise to a stirred solution of distilled TMP (1.46 ml, 8.58 mmol) in anhydrous THF (10 mL) at -78 °C, under Ar. The solution was warmed to 0 °C and then re-cooled to -78 °C. A solution of (1*R**,2*S**)-methyl 2-(2-(*tert*-butoxy)-2-oxoethyl)cyclohexanecarboxylate (**43**) (1.00 g, 3.90 mmol) in anhydrous THF (10 mL) was added, via cannular, and

stirring continued for 45 min at -78 °C. Next, a solution of 2(5*H*)-furanone (0.41 mL, 0.59 mmol) in anhydrous THF (5 mL) was added, via cannular, and stirring continued for 1 h at -78 °C. Finally, solid KO*t*-Bu (962 mg, 8.58 mmol) was added. The reaction mixture was warmed to -40 °C, stirred for a further 3 h and then quenched with sat. aq. NH₄Cl (20 mL). An extraction into EtOAc (2 x 40 mL) was completed and the combined organic layers were dried (MgSO₄), filtered and concentrated *in vacuo* to yield a crude yellow oily solid. Multiple purification by flash column chromatography yielded (3*aS**,4*R**,4*aS**,8*aS**,9*aS**)-*tert*-butyl 1,9-dioxododecahydronaphtho[2,3-*c*]furan-4-carboxylate (**45**) (40 mg, 0.13 mmol, 3%), (1*R**,2*R**)-methyl 2-((*R**)-2-*tert*-butoxy-2-oxo-1-((*R**)-5-oxotetrahydrofuran-3-yl)ethyl)cyclohexanecarboxylate (**46**) (38 mg, 0.11 mmol, 3%), (3*aS**,4*R**,4*aR**,8*aR**,9*aS**)-*tert*-butyl 1,9-dioxododecahydronaphtho[2,3-*c*]furan-4-carboxylate (**47**) (240 mg, 0.78 mmol, 20%), a mixture of two undetermined stereoisomers in a ratio of 1:0.9 of *rac*-methyl 2-(2-*tert*-butoxy-1-(2,5'-dioxooctahydro-3,3'-bifuran-4-yl)-2-oxoethyl)cyclohexanecarboxylate (**48**) (50 mg, 0.12 mmol, 4%) and a 1:0.9 mixture of (3*aS**,4*S**,4*aR**,8*aR**,9*aR**)-*tert*-butyl 1,9-dioxo-9a-((*R**)-5-oxotetrahydrofuran-3-yl)dodecahydronaphtho[2,3-*c*]furan-4-carboxylate and (3*aS**,4*S**,4*aR**,8*aR**,9*aS**)-*tert*-butyl 1,9-dioxo-9a-((*S**)-5-oxotetrahydrofuran-3-yl)dodecahydronaphtho[2,3-*c*]furan-4-carboxylate (**49**) (24 mg, 0.06 mmol, 2%) as white solids.

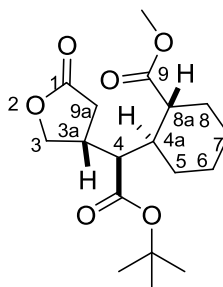
Data for (3*aS**,4*R**,4*aS**,8*aS**,9*aS**)-*tert*-butyl 1,9-dioxododecahydronaphtho[2,3-*c*]furan-4-carboxylate (**45**):



¹H NMR (600 MHz, CDCl₃) δ 4.22 (1H, d, *J* = 3.8, C³HH), 4.21 (1H, s, C³HH), 3.49 (1H, d, *J* = 7.5, C^{9a}H), 3.15 (1H, ddd, *J* = 11.5, 7.5, 3.8, C^{3a}H), 2.41 (1H, t, *J* = 11.5, C⁴H), 2.14-2.10 (1H, m, C⁸HH), 2.01-1.96 (1H, m, C^{8a}H), 1.82-1.66 (4H, m, C^{4a}H,

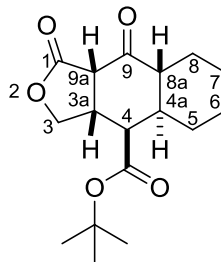
C^5HH , C^6HH & C^7HH), 1.48 (9H, s, $C(CH_3)_3$), 1.46-1.41 (1H, m, C^8HH), 1.25-1.12 (3H, m, C^5HH , C^6HH & C^7HH); ^{13}C NMR (150 MHz, $CDCl_3$) δ 201.9 ($C^9=O$), 172.4 ($C=OO^tBu$), 171.5 ($C^1=O$), 82.5 ($C(CH_3)_3$), 70.5 (C^3H_2), 53.3 ($C^{9a}H$), 51.3 ($C^{8a}H$), 51.0 (C^4H), 42.8 ($C^{4a}H$), 42.8 ($C^{3a}H$), 31.5 (C^8H_2), 28.2 ($C(CH_3)_3$), 25.1 (C^5H_2), 25.0 (C^6H_2), 24.8 (C^7H_2); IR (thin film) 2974 (C-H), 2929 (C-H), 2856 (C-H), 1795 (C=O), 1715 (C=O), 1367 (C-H), 1244 (C-O), 1157, 1021, 845 cm^{-1} ; m/z (ES+) 326 (100%, $[M+NH_4]^+$); HRMS (EI) calcd for $C_{17}H_{24}O_5$ $[M+H]^+$ 308.1618, observed 308.1613.

Data for (1*R**,2*R**)-methyl 2-((*R**)-2-*tert*-butoxy-2-oxo-1-((*R**)-5-oxotetrahydrofuran-3-yl)ethyl)cyclohexanecarboxylate (**46**):



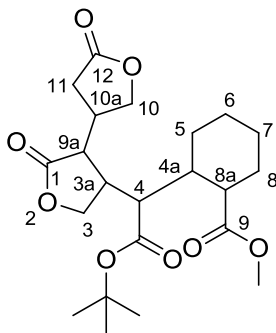
1H NMR (600 MHz, $CDCl_3$) δ 4.47 (1H, t, $J = 8.8$, C^3HH), 3.81 (1H, t, $J = 8.8$, C^3HH), 3.69 (3H, s, OCH_3), 2.97 (1H, ddq, $J = 11.3$, 10.2, 8.8, $C^{3a}H$), 2.59 (1H, dd, $J = 17.5$, 10.2, $C=OCHH$), 2.46 (1H, td, $J = 11.7$, 3.8, $C^{8a}H$), 2.39 (1H, dd, $J = 11.3$, 2.6, C^4H), 2.37 (1H, dd, $J = 17.5$, 10.2, $C=OCHH$), 2.00 (1H, br. dt, $J = 13.2$, 3.0, C^8HH), 1.81-1.72 (4H, m, $C^{4a}H$, C^5HH , C^6HH & C^7HH), 1.45 (9H, s, $C(CH_3)_3$), 1.36 (1H, qd, $J = 12.8$, 3.4, C^8HH), 1.25-1.17 (2H, m, C^6HH & C^7HH), 1.03 (1H, bqd, $J = 12.0$, 3.8, C^5HH); ^{13}C NMR (150 MHz, $CDCl_3$) δ 176.4 ($C^1=O$), 175.9 ($C=OOMe$), 171.3 ($C=OO^tBu$), 81.9($C(CH_3)_3$), 72.5 (C^3H_2), 51.8 (C^4H), 51.8 (OCH_3), 47.4 ($C^{8a}H$), 39.9 ($C^{4a}H$), 35.0 ($C^{3a}H$), 32.3 ($C=OCH_2$), 31.3 (C^8H_2), 28.2 ($C(CH_3)_3$), 25.8 (C^5H_2), 25.8 (C^6H_2), 25.7 (C^7H_2); IR (thin film) 2933 (C-H), 2830 (C-H), 1778 (C=O), 1721 (C=O), 1369 (C-H), 1260 (C-O), 1165, 1148, 1112, 1080, 1048 cm^{-1} ; m/z (ES+) 371 (100%, $[M+MeOH]^+$).

Data for (3*aS**,4*R**,4*aR**,8*aR**,9*aS**)-*tert*-butyl 1,9-dioxododecahydronaphtho[2,3-*c*]furan-4-carboxylate (**47**):



^1H NMR (600 MHz, CDCl_3) δ 4.39 (1H, dd, $J = 9.2, 8.4$, C^3HH), 3.94 (1H, dd, $J = 10.2, 9.2$, C^3HH), 3.71 (1H, d, $J = 9.0$, C^{9a}H), 3.25 (1H, ddd, $J = 10.2, 9.0, 8.4$, C^{3a}H), 2.65 (1H, td, $J = 11.9, 3.8$, C^{8a}H), 2.53 (1H, d, $J = 4.5$, C^4H), 2.04-1.90 (1H, m, C^8HH), 1.88-1.82 (1H, m, C^{4a}H), 1.84-1.75 (3H, m, C^5HH , C^6HH & C^7HH), 1.50 (9H, s, $\text{C}(\text{CH}_3)_3$), 1.49-1.41 (1H, m, C^8HH), 1.35-1.16 (3H, m, C^5HH , C^6HH & C^7HH); ^{13}C NMR (150 MHz, CDCl_3) δ 203.9 ($\text{C}^9=\text{O}$), 172.1 ($\text{C}=\text{OO}^t\text{Bu}$), 171.8 ($\text{C}^1=\text{O}$), 82.5 ($\text{C}(\text{CH}_3)_3$), 69.5 (C^3H_2), 52.9 (C^{9a}H), 48.2 (C^{8a}H), 44.9 (C^4H), 40.5 (C^{4a}H), 40.3 (C^{3a}H), 31.4 (C^8H_2), 28.3 ($\text{C}(\text{CH}_3)_3$), 25.9 (C^5H_2), 25.7 (C^6H_2), 25.1 (C^7H_2); IR (thin film) 2926 (C-H), 2850 (C-H), 1778 (C=O), 1715 (C=O), 1698 (C=O), 1365 (C-H), 1204 (C-O), 1138, 1002, 845 cm^{-1} ; m/z (ES+) 326 (100%, $[\text{M}+\text{NH}_4]^+$); HRMS (ES $^-$) calcd for $\text{C}_{17}\text{H}_{23}\text{O}_5$ $[\text{M}-\text{H}]^+$ 307.1546, observed 307.1545.

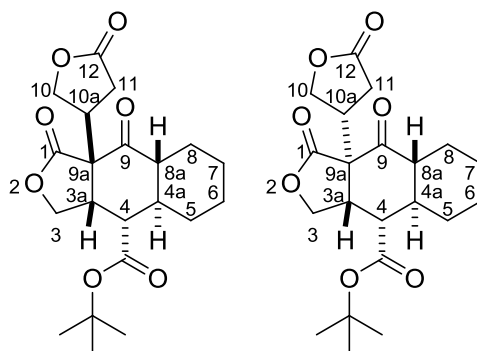
Data for *rac*-methyl 2-(2-*tert*-butoxy-1-(2,5'-dioxooctahydro-3,3'-bifuran-4-yl)-2-oxoethyl)cyclohexanecarboxylate (**48**):



^1H NMR (600 MHz, CDCl_3) δ 4.54 (1H, dd, $J = 9.6, 7.7$, C^3HH), 4.54 (1H, dd, $J = 8.8, 8.3$, C^3HH), 4.44 (1H, dd, $J = 7.9, 1.9$, C^{10}HH), 4.42 (1H, dd, $J = 7.5, 1.9$, C^{10}HH), 4.33 (1H, dd, $J = 8.8, 8.3$, C^3HH), 4.29 (1H, dd, $J = 9.6, 8.5$, C^3HH), 4.05 (1H, dd, $J = 10.0, 4.7$, C^{10}HH), 4.00 (1H, dd, $J = 10.0, 5.1$, C^{10}HH), 3.68 (6H, s, 2 \times OCH_3), 2.87 (1H, dddd, $J = 9.4, 8.5, 7.7, 7.2$, C^{3a}H), 2.84 (1H, dddd, $J = 9.4, 8.3,$

7.7, 7.2, C^{3a}H), 2.63-2.73 (4H, m, 2 x C¹¹HH & 2 x C^{10a}H), 2.60-2.49 (6H, m, 2 x C^{4a}H, 2 x C^{9a}H & 2 x C¹¹HH), 2.47 (1H, dd, *J* = 7.2, 2.6, C⁴H), 2.45 (1H, dd, *J* = 7.5, 2.6, C⁴H), 2.04-1.99 (2H, m, 2 x C⁸HH), 1.83-1.78 (4H, m, 2 x C⁶HH & 2 x C⁷HH), 1.78-1.71 (2H, m, 2 x C⁵HH), 1.46 (18H, d, *J* = 1.5, 2 x C(CH₃)₃), 1.43-1.34 (2H, m, 2 x C⁸HH), 1.27-1.16 (4H, m, 2 x C⁶HH & 2 x C⁷HH), 1.05 (2H, qd, *J* = 12.7, 3.2, 2 x C⁵HH); ¹³C NMR (150 MHz, CDCl₃) δ 176.1 (C¹⁰=O), 175.9 (C¹⁰=O), 175.9 (C=OOMe), 175.8 (C=OOMe), 175.5 (C¹=O), 175.3 (C¹=O), 171.2 (C=OO^tBu), 171.1 (C=OO^tBu), 82.6 (2 x C(CH₃)₃), 70.7 (C¹⁰H₂), 70.7 (C¹⁰H₂), 70.6 (C³H₂), 70.3 (C³H₂), 52.0 (C⁴H), 52.0 (C⁴H), 51.3 (OCH₃), 50.9 (OCH₃), 47.5 (C^{9a}H), 47.4 (C^{9a}H), 44.9 (C^{10a}H), 44.2 (C^{10a}H), 39.5 (C^{4a}H), 39.2 (C^{4a}H), 39.2 (2 x C^{8a}H), 37.1 (C^{3a}H), 37.0 (C^{3a}H), 33.0 (C¹¹H), 31.6 (C¹¹H), 31.1 (C⁸H₂), 28.3 (C(CH₃)₃), 28.3 (C(CH₃)₃), 26.6 (C⁵H₂), 26.5 (C⁵H₂), 25.7 (C⁶H₂), 25.6 (C⁶H₂), 25.6 (C⁷H₂), 25.5 (C⁷H₂).

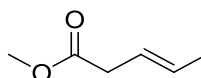
Data for (3a*S**,4*S**,4a*R**,8a*R**,9a*R**)-*tert*-butyl 1,9-dioxo-9a-((*R**)-5-oxotetrahydrofuran-3-yl)dodecahydronaphtho[2,3-*c*]furan-4-carboxylate and (3a*S**,4*S**,4a*R**,8a*R**,9a*S**)-*tert*-butyl 1,9-dioxo-9a-((*S**)-5-oxotetrahydrofuran-3-yl)dodecahydronaphtho[2,3-*c*]furan-4-carboxylate (1:0.9) (**49**):



¹H NMR (600 MHz, CDCl₃) δ 4.52 (1H, dd, *J* = 9.4, 7.5, C¹⁰HH), 4.47 (1H, dd, *J* = 10.5, 7.2, C³HH), 4.45 (1H, dd, *J* = 10.9, 7.9, C³HH), 4.41 (1H, dd, *J* = 9.8, 7.9, C¹⁰HH), 4.33 (1H, dd, *J* = 9.4, 8.3, C¹⁰HH), 4.24 (1H, dd, *J* = 10.9, 2.3, C³HH), 4.22 (1H, dd, *J* = 10.9, 2.6, C³HH), 4.17 (1H, dd, *J* = 10.2, 7.2, C¹⁰HH), 3.13 (1H, dddd, *J* = 9.2, 8.7, 8.3, 7.5, C^{10a}H), 3.08 (1H, dddd, *J* = 9.4, 7.9, 7.8, 7.2, C^{10a}H), 2.89-2.84 (3H, m, 2 x C⁴H), 2.80 (1H, ddd, *J* = 8.7, 6.8, 2.3, C^{3a}H), 2.73 (1H, dd, *J* =

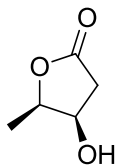
17.7, 7.9, C¹¹HH), 2.63 (1H, dd, $J = 17.5, 9.2$, C¹¹HH), 2.58 (1H, dd, $J = 17.7, 9.4$, C¹¹HH),), 2.46 (1H, ddd, $J = 12.8, 11.7, 3.4$, C^{8a}H), 2.40 (1H, ddd, $J = 12.8, 11.7, 3.4$, C^{8a}H), 2.32 (1H, dd, $J = 17.7, 8.7$, C¹¹HH), 2.32-2.26 (2H, m, 2 x C⁸HH), 1.88-1.83 (4H, m, 2 x C⁶HH & 2 x C⁷HH), 1.82-1.77 (2H, m, 2 x C⁵HH), 1.74-1.67 (2H, m, 2 x C^{4a}H), 1.47 (9H, s, C(CH₃)₃), 1.46 (9H, s, C(CH₃)₃), 1.30-1.17 (6H, m, 2 x C⁵HH, 2 x C⁶HH & 2 x C⁷HH), 1.11-1.03 (2H, m, 2 x C⁸HH); ¹³C NMR (150 MHz, CDCl₃) δ 203.7 (C⁹=O), 203.4 (C⁹=O), 175.1 (C¹⁰=O), 174.9 (C¹⁰=O), 171.1 (C¹=O), 171.1 (C¹=O), 171.0 (C=OO^tBu), 170.9 (C=OO^tBu), 83.9 (2 x C(CH₃)₃), 69.5 (C¹⁰H₂), 69.3 (C¹⁰H₂), 68.7 (C³H₂), 68.6 (C³H₂), 56.5 (C^{9a}H), 56.4 (C^{9a}H), 48.8 (C⁴H), 48.7 (C⁴H), 48.3 (C^{8a}H), 48.3 (C^{8a}H), 42.5 (C^{3a}H), 42.5 (C^{3a}H), 42.0 (C^{10a}H), 41.5 (C^{10a}H), 41.5 (C^{4a}H), 41.4 (C^{4a}H), 31.4 (2 x C⁵H₂), 31.1 (C¹¹H), 30.8 (C¹¹H), 28.1 (2 x C(CH₃)₃), 27.8 (C⁸H₂), 27.5 (C⁸H₂), 25.9 (C⁶H₂), 25.8 (C⁶H₂), 25.7 (2 x C⁷H₂).

Methyl pent-3-enoate¹⁴⁹ (50)



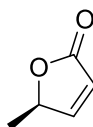
Conc. H₂SO₄ (0.75 mL) was added to a stirred solution of pent-3-enoic acid (1.40 mL, 13.8 mmol) in MeOH (10 mL). The reaction mixture was stirred at 20 °C for 12 h before being neutralised with sat. aq. NaHCO₃. An extraction into CH₂Cl₂ (3 x 20 mL) was completed and the combined organic layers were dried (Na₂SO₄), filtered and concentrated *in vacuo* to yield methyl pent-3-enoate (**50**) (1.39 g, 1.22 mmol, 89%) as a colourless oil which was used with no further purification; ¹H NMR (500 MHz, CDCl₃) δ 5.62-5.50 (2H, m, CH=CH & CH=CH), 3.68 (3 H, s, OCH₃), 3.02 (2H, s, CH₂CH=CH), 1.71-1.68 (3H, m, CH=CHCH₃); ¹³C NMR (126 MHz, CDCl₃) δ 172.7 (C=O), 129.5 (CH₂CH=CH), 122.7 (CH=CHCH₃), 51.8 (OCH₃), 38.0 (CH₂CH=CH), 18.0 (CH=CHCH₃); IR (thin film) 2978 (C-H), 1788, 1734 (C=O), 1716, 1376 (C-H), 1352 (C-H), 1335 (C-H), 1201 (C-O), 1146 (C-O), 1108, 1016, 908, 885, 701, 690 cm⁻¹. Data agrees with that reported by Scarborough.¹⁴⁹

4-Hydroxy-5-methyldihydrofuran-2-(3H)-one¹⁵⁰ (51)



AD-mix- β (10.0 g) was added to a stirred solution of methyl pent-3-enoate (**50**) (860 mg, 7.53 mmol) in a 1:1 mix of *t*-BuOH (22 mL) and H₂O (22 mL) at 0 °C. The reaction mixture was stirred at RT for 4 days, quenched with solid Na₂SO₃ and diluted with H₂O (50 mL). An extraction into CH₂Cl₂ (5 x 50 mL) was completed and the combined organic layers were dried (Na₂SO₄), filtered and concentrated *in vacuo* to yield 4-hydroxy-5-methyldihydrofuran-2-(3H)-one (**51**) (376 mg, 3.24 mmol, 43%) as a colourless oil; ¹H NMR (600 MHz, CDCl₃) δ 4.56 (1H, dq, *J* = 6.4, 3.8, CHCH₃), 4.45 (1H, ddd, *J* = 5.6, 3.8, 1.1, CHOH), 2.80 (1H, dd, *J* = 17.7, 5.6, CH^{cis}H), 2.56 (1H, dd, *J* = 17.7, 1.1, CHH^{trans}), 1.44 (3H, d, *J* = 6.4, CH₃); ¹³C NMR (126 MHz, CDCl₃) δ 80.8 (CHCH₃), 69.3 (CHOH), 39.4 (CH₂), 13.8 (CH₃). Data agrees with that reported by Takahata *et al.*¹⁵⁰

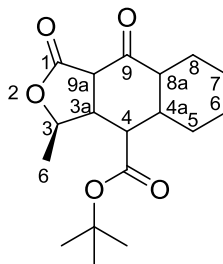
5-Methyl-2(5*H*)-furanone¹⁵¹ (**52**)



NEt₃ (994 μ L, 7.12 mmol) and MeSO₂Cl (289 μ L, 3.73 mmol) were added to a stirred solution of 4-hydroxy-5-methyldihydrofuran-2-(3H)-one (**51**) (394 mg, 3.39 mmol) in CH₂Cl₂ (10 mL) at 0 °C. The reaction mixture was stirred at RT for 1 h, quenched with sat. aq. NH₄Cl (5 mL) and diluted with H₂O (10 mL). An extraction into CH₂Cl₂ (3 x 20 mL) was completed and the combined organic layers were dried (MgSO₄), filtered and concentrated *in vacuo* to yield a crude oil. Purification by flash column chromatography (0-10% EtOAc/Pet. Ether) yielded 5-methyl-2(5*H*)-furanone (**52**) (162 mg, 1.65 mmol, 49%) as a colourless oil; ¹H NMR (600 MHz, CDCl₃) δ 7.45 (1H, dd, *J* = 5.6, 1.2, CH=CH), 6.10 (1H, dd, *J* = 5.6, 1.9, CH=CHC=O), 5.14 (1H, qdd, *J* = 6.8, 1.9, 1.2, CHCH₃), 1.45 (3H, d, *J* = 6.8, CH₃); ¹³C NMR (126 MHz, CDCl₃) δ 173.1 (C=O), 157.4 (CH=CH), 121.3 (CH=CHC=O), 79.7 (CHCH₃), 18.9 (CH₃); IR (thin film) 2983 (C-H), 2936 (C-H), 1750 (C=O), 1736

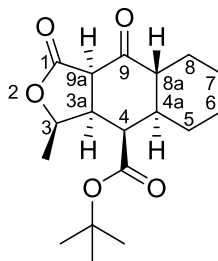
(C=O), 1322 (C-O), 1166, 1105, 1075, 958, 941, 891, 816 cm^{-1} ; m/z (CI) 99 (100%, $[\text{M}+\text{H}]^+$). Data agrees with that reported by Takadoi *et al.*¹⁵¹

***tert*-Butyl 3-methyl-1,9-dioxododecahydronaphtho[2,3-*c*]furan-4-carboxylate¹²⁷ (53)**



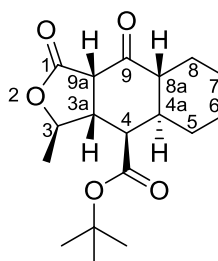
n-BuLi (2.5 M in hexane) (3.60 ml, 9.00 mmol) was added dropwise to a stirred solution of distilled TMP (1.54 mL, 9.00 mmol) in anhydrous THF (10 mL) at $-78\text{ }^{\circ}\text{C}$, under Ar. The solution was warmed to $0\text{ }^{\circ}\text{C}$ and then re-cooled to $-78\text{ }^{\circ}\text{C}$. A solution of (1*R**,2*S**)-methyl 2-(2-(*tert*-butoxy)-2-oxoethyl)cyclohexanecarboxylate (**43**) (1.10 g, 4.30 mmol) in anhydrous THF (5 mL) was added, dropwise, and stirring continued for 45 min at $-78\text{ }^{\circ}\text{C}$. Next, a solution of 5-methyl-2(5*H*)-furanone (**52**) (294 mg, 0.30 mmol) in anhydrous THF (5 mL) was added, dropwise, and stirring continued for 1 h at $-78\text{ }^{\circ}\text{C}$. Finally, KO*t*-Bu (1.00 g, 9.00 mmol) was added. The reaction mixture was warmed to $-40\text{ }^{\circ}\text{C}$, stirred for a further 3 h and then quenched with sat. aq. NH_4Cl (20 mL). An extraction into EtOAc (2 x 40 mL) was completed and the combined organic layers were dried (MgSO_4), filtered and concentrated *in vacuo* to yield a crude yellow oily solid. Multiple purifications by flash column chromatography yielded (3*R*,3*aR*,4*R*,4*aR*,8*aR*,9*aR*)-*tert*-butyl 3-methyl-1,9-dioxododecahydronaphtho[2,3-*c*]furan-4-carboxylate (**54**) (47.5 mg, 0.15 mmol, 5%), (3*R*,3*aS*,4*R*,4*aR*,8*aR*,9*aS*)-*tert*-butyl 3-methyl-1,9-dioxododecahydronaphtho[2,3-*c*]furan-4-carboxylate (**55**) (117 mg, 0.36 mmol, 12%) and (3*R*,3*aS*,4*S*,4*aR*,8*aR*,9*aS*)-*tert*-butyl 3-methyl-1,9-dioxododecahydronaphtho[2,3-*c*]furan-4-carboxylate (**56**) (47.5 mg, 0.15 mmol, 5%) as white solids.

Data for (3*R*,3*aR*,4*R*,4*aR*,8*aR*,9*aR*)-*tert*-butyl 3-methyl-1,9-dioxododecahydronaphtho[2,3-*c*]furan-4-carboxylate (**54**):



¹H NMR (600 MHz, CDCl₃) δ 4.53 (1H, q, *J* = 6.4, C³HMe), 3.64 (1H, d, *J* = 7.9, C^{9a}H), 2.84 (1H, dd, *J* = 11.7, 7.9, C^{3a}H), 2.37 (1H, dd, *J* = 11.7, 11.3, C⁴H), 2.14-2.11 (1H, m, C⁸HH), 1.97 (1H, td, *J* = 11.2, 3.6, C^{8a}H), 1.82-1.79 (1H, m, C⁶HH), 1.79-1.71 (2H, m, C⁵HH & C⁷HH), 1.71-1.63 (1H, m, C^{4a}H), 1.49 (9H, s, C(CH₃)₃), 1.33 (3H, d, *J* = 6.4, C³HCH₃), 1.20-1.15 (4H, m, C⁵HH, C⁶HH, C⁷HH & C⁸HH); ¹³C NMR (150 MHz, CDCl₃) δ 201.9 (C⁹=O), 172.5 (C=OO^tBu), 171.1 (C¹=O), 82.4 (C(CH₃)₃), 79.5 (C³HMe), 51.9 (C⁴H), 51.6 (C^{8a}H), 51.5 (C^{9a}H), 47.6 (C^{3a}H), 42.5 (C^{4a}H), 31.5 (C⁵H₂), 28.3 (C(CH₃)₃), 25.1 (C⁸H₂), 25.1 (C⁶H₂), 24.8 (C⁷H₂), 19.4 (C³HCH₃); IR (thin film) 2925 (C-H), 2853 (C-H), 1776 (C=O), 1714 (C=O), 1700 (C=O), 1205 (C-O), 1153, 1138, 1001, 845, 750, 577 cm⁻¹; *m/z* (EI) 322 (100%, [M]⁺); HRMS (EI) calcd for C₁₈H₂₆O₅ [M]⁺ 322.1775, observed 322.1776.

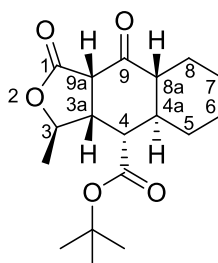
Data for (3*R*,3*aS*,4*R*,4*aR*,8*aR*,9*aS*)-*tert*-butyl 3-methyl-1,9-dioxododecahydronaphtho[2,3-*c*]furan-4-carboxylate (**55**):



¹H NMR (600 MHz, CDCl₃) δ 4.24 (1H, dd, *J* = 10.2, 6.0, C³HMe), 3.77 (1H, d, *J* = 8.3, C^{9a}H), 2.71-2.66 (1H, m, C^{8a}H), 2.51 (1H, d, *J* = 4.9, C⁴H), 2.01-1.96 (1H, m, C⁸HH), 1.84-1.72 (4H, m, C^{4a}H, C⁵HH, C⁶HH & C⁷HH), 1.50 (9H, s, C(CH₃)₃), 1.42 (3H, d, *J* = 6.0, C³HCH₃), 1.33-1.23 (2H, m, C⁵HH & C⁸HH), 1.22-1.14 (2H, m, C⁶HH & C⁷HH); ¹³C NMR (150 MHz, CDCl₃) δ 204.0 (C⁹=O), 172.0 (C=OO^tBu),

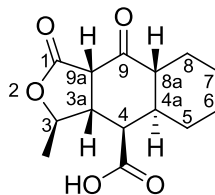
171.1 (C¹=O), 82.5 (C(CH₃)₃), 77.6 (C³HMe), 54.5 (C^{9a}H), 48.4 (C^{3a}H), 48.1 (C^{8a}H), 44.1 (C⁴H), 41.0 (C^{4a}H), 31.4 (C⁵H₂), 28.3 (C(CH₃)₃), 25.7 (C⁸H₂), 25.5 (C⁶H₂), 25.0 (C⁷H₂), 19.1 (C³HCH₃); IR (thin film) 2988 (C-H), 2918 (C-H), 2855 (C-H), 1790 (C=O), 1727 (C=O), 1705 (C=O), 1198 (C-O), 1197, 1133, 1061, 913, 835 cm⁻¹; m/z (CI) 267 (100%, [M-C₄H₉]⁺); HRMS (CI) calcd for C₁₈H₂₇O₅ [M+H]⁺ 323.1853, observed 323.1855.

Data for (3*R*,3*aS*,4*S*,4*aR*,8*aR*,9*aS*)-*tert*-butyl 3-methyl-1,9-dioxododecahydronaphtho[2,3-*c*]furan-4-carboxylate (**56**):



¹H NMR (600 MHz, CDCl₃) δ 4.54 (1H, dq, *J* = 10.2, 6.0, C³HMe), 3.48 (1H, d, *J* = 8.7, C^{9a}H), 2.94 (1H, ddd, *J* = 10.2, 8.7, 5.3, C^{3a}H), 2.81 (1H, dd, *J* = 11.5, 5.3, C⁴H), 2.08 (1H, td, *J* = 11.8, 3.2, C^{8a}H), 1.96-1.88 (3H, m, C^{4a}H, C⁵HH & C⁸HH), 1.84-1.80 (1H, m, C⁶HH), 1.75-1.71 (1H, m, C⁷HH), 1.48 (9H, s, C(CH₃)₃), 1.36 (3H, d, *J* = 6.0, C³HCH₃), 1.39-1.34 (1H, m, C⁸HH), 1.26-1.17 (2H, m, C⁶HH & C⁷HH), 1.13-1.05 (1H, m, C⁵HH); ¹³C NMR (150 MHz, CDCl₃) δ 203.0 (C⁹=O), 171.6 (C=OO^tBu), 170.2 (C¹=O), 82.5 (C(CH₃)₃), 77.3 (C³HMe), 56.3 (C^{9a}H), 52.4 (C^{8a}H), 48.0 (C^{3a}H & C⁴H), 41.5 (C^{4a}H), 32.0 (C⁵H₂), 28.3 (C(CH₃)₃), 25.1 (C⁸H₂), 24.9 (C⁶H₂), 24.8 (C⁷H₂), 20.3 (C³HCH₃); IR (thin film) 2978 (C-H), 2933 (C-H), 2857 (C-H), 1784 (C=O), 1717 (C=O), 1367, 1194 (C-O), 1146, 1066, 985, 751 cm⁻¹; m/z (CI) 267 (100%, [M-C₄H₉]⁺); HRMS (CI) calcd for C₁₈H₂₇O₅ [M+H]⁺ 323.1853, observed 323.1856.

(3*R*,3*aS*,4*R*,4*aR*,8*aR*,9*aS*)-3-Methyl-1,9-dioxododecahydronaphtho[2,3-*c*]furan-4-carboxylic acid (57**)**

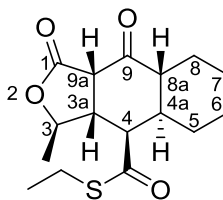


TFA (0.5 mL) was added dropwise to a stirred solution of (3*R*,3*aS*,4*R*,4*aR*,8*aR*,9*aS*)-*tert*-butyl 3-methyl-1,9-dioxododecahydronaphtho[2,3-*c*]furan-4-carboxylate (**55**) (86.0 mg, 0.27 mmol) in CH₂Cl₂ (0.5 mL) at 0 °C, under Ar. The reaction mixture was stirred at 20 °C for 16 h before being concentrated *in vacuo*. The residue was azeotroped with toluene to yield (3*R*,3*aS*,4*R*,4*aR*,8*aR*,9*aS*)-3-methyl-1,9-dioxododecahydronaphtho[2,3-*c*]furan-4-carboxylic acid (**57**) (69.8 mg, 0.26 mmol, 99%) as a white solid; ¹H NMR (600 MHz, MeOH-*d*₄) δ 4.39 (1H, td, *J* = 11.7, 6, C³HMe), 3.82 (1H, d, *J* = 8.7, C^{9*a*}H), 2.87 (1H, dd, *J* = 10.4, 8.7, C^{3*a*}H), 2.76 (1H, td, *J* = 11.7, 3.4, C^{8*a*}H), 2.71 (1H, d, *J* = 4.9, C⁴H), 1.97 (1H, dddd, *J* = 12.4, 11.7, 4.9, 3.8, C^{4*a*}H), 1.96-1.92 (1H, m, C⁸HH), 1.87-1.82 (1H, m, C⁵HH), 1.81-1.74 (2H, m, C⁶HH & C⁷HH), 1.42 (3H, d, *J* = 6.0, C³HCH₃), 1.40-1.36 (1H, m, C⁵HH), 1.31-1.21 (3H, m, C⁶HH, C⁷HH & C⁸HH); ¹³C NMR (150 MHz, MeOH-*d*₄) δ 206.3 (C⁹=O), 176.3 (C=OOH), 173.7 (C¹=O), 79.6 (C³HMe), 49.6 (C^{3*a*}H), 49.2 (C^{8*a*}H), 49.0 (C^{9*a*}H), 44.0 (C⁴H), 41.5 (C^{4*a*}H), 32.5 (C⁵H₂), 26.7 (C⁸H₂), 26.5 (C⁶H₂), 26.1 (C⁷H₂), 18.9 (C³HCH₃); IR (thin film) 2928 (C-H), 2859 (C-H), 1775 (C=O), 1702 (C=O), 1581, 1416, 1201 (C-O), 1052 cm⁻¹; *m/z* (EI) 267 (100%, [M+H]⁺); HRMS (EI) calcd for C₁₄H₁₈O₅ [M+H]⁺ 266.1149, observed 266.1150.

(3*R*,3*aR*,4*R*,4*aR*,8*aR*,9*aS*)-S-Ethyl

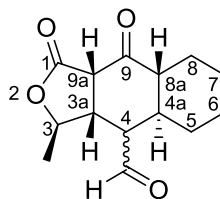
3-methyl-1,9-

dioxododecahydronaphtho[2,3-*c*]furan-4-carbothioate (58**)**



DCC (149 mg, 0.72 mmol) was added to a stirred solution of (3*R*,3*aS*,4*R*,4*aR*,8*aR*,9*aS*)-3-methyl-1,9-dioxododecahydronaphtho[2,3-*c*]furan-4-carboxylic acid (**57**) (160 mg, 0.60 mmol), ethanethiol (173 μ L, 2.40 mmol) and DMAP (37.0 mg, cat.) in CH₂Cl₂ (5 mL) at 0 °C, under Ar. The reaction mixture was stirred at 20 °C for 16 h before being filtered under vacuum to remove the precipitate. The filtrate solvents were concentrated *in vacuo* to yield a crude colourless oil. Purification by flash column chromatography (0-2% Et₂O/CH₂Cl₂) yielded (3*R*,3*aR*,4*R*,4*aR*,8*aR*,9*aS*)-*S*-ethyl 3-methyl-1,9-dioxododecahydronaphtho[2,3-*c*]furan-4-carbothioate (**58**) (128 mg, 0.41 mmol, 69%) as a white solid; R_f 0.64 (8% Et₂O/CH₂Cl₂); ¹H NMR (600 MHz, CDCl₃) δ 4.24 (1H, dq, *J* = 10.5, 6.0, C³HMe), 3.73 (1H, d, *J* = 8.7, C^{9*a*}H), 2.96 (1H, q, *J* = 6.5, SCHHCH₃), 2.92 (1H, q, *J* = 6.5, SCHHCH₃), 2.84 (1H, td, *J* = 11.9, 3.4, C^{8*a*}H), 2.75 (1H, d, *J* = 4.5, C⁴H), 2.65 (1H, dd, *J* = 10.5, 8.7, C^{3*a*}H), 2.00-1.95 (1H, m, C⁸HH), 1.86-1.74 (4H, m, C^{4*a*}H, C⁵HH, C⁶HH & C⁷HH), 1.44 (3H, d, *J* = 6.0, C³HCH₃), 1.40-1.32 (1H, m, C⁵HH), 1.30 (3H, t, *J* = 7.3, SCH₂CH₃), 1.28-1.11 (3H, m, C⁶HH, C⁷HH & C⁸HH); ¹³C NMR (150 MHz, CDCl₃) δ 203.8 (C⁹=O), 200.3 (C=OSET), 170.7 (C¹=O), 77.3 (C³HMe), 54.7 (C^{9*a*}H), 50.6 (C⁴H), 48.8 (C^{8*a*}H), 48.3 (C^{3*a*}H), 41.8 (C^{4*a*}H), 31.4 (C⁵H₂), 25.7 (C⁸H₂), 25.3 (C⁶H₂), 24.8 (C⁷H₂), 24.1 (CH₂CH₃), 18.9 (C³HCH₃), 14.6 (CH₂CH₃); IR (thin film) 2930 (C-H), 2854 (C-H), 1785 (C=O), 1708 (C=O), 1672, 1197 (C-O), 1059, 958 cm⁻¹; m/z (EI) 252 (100%, [M-SEt-Me+OH]⁺); HRMS (EI) calcd for C₁₆H₂₂O₄S [M+H]⁺ 310.1233, observed 310.1233.

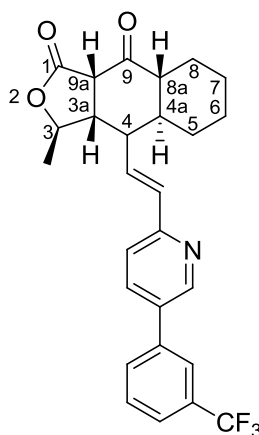
(3*R*,3*aS*,4*aS*,8*aR*,9*aS*)-3-Methyl-1,9-dioxododecahydronaphtho[2,3-*c*]furan-4-carbaldehyde (59**)**



Neat triethylsilane (263 μ L, 1.65 mmol) was added to a stirred suspension of (3*R*,3*aR*,4*R*,4*aR*,8*aR*,9*aS*)-*S*-ethyl 3-methyl-1,9-dioxododecahydronaphtho[2,3-

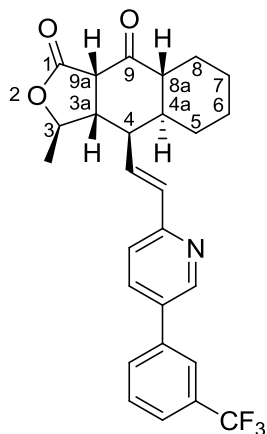
c]furan-4-carbothioate (**58**) (128 mg, 0.41 mmol), palladium on carbon (10%) (44.0 mg, 0.04 mmol) and MgSO₄ (to dry) in degassed acetone (5 mL) under Ar. The reaction mixture was stirred at 20 °C for 16 h before it was filtered over celite and concentrated *in vacuo*. Purification by flash column chromatography (0-2% Et₂O/CH₂Cl₂) gave partial racemisation at C⁴ to yield (3*R*,3*aS*,4*aS*,8*aR*,9*aS*)-3-methyl-1,9-dioxododecahydronaphtho[2,3-*c*]furan-4-carbaldehyde (**59**) (4*S*:4*R*; 1:0.16) (50 mg, 0.20 mmol, 48%) as a colourless film; R_f 0.44 (8% Et₂O/CH₂Cl₂); ¹H NMR (600 MHz, CDCl₃) δ 10.14 (1H, s, 4*S*-CHO), 4.29 (1H, dq, *J* = 10.2, 6.0, 4*S*-C³HMe), 3.67 (1H, d, *J* = 8.7, 4*S*-C^{9*a*}H), 2.88 (1H, dd, *J* = 10.2, 8.7, 4*S*-C^{3*a*}H), 2.80 (1H, d, *J* = 4.9, 4*S*-C⁴H), 2.20 (1H, ddd, *J* = 12.4, 12.0, 3.4, 4*S*-C^{8*a*}H), 2.09-1.96 (3H, m, 4*S*-C^{4*a*}H, 4*S*-C⁵HH & 4*S*-C⁸HH), 1.88-1.81 (2H, m, 4*S*-C⁶HH & 4*S*-C⁷HH), 1.68 (1H, qd, *J* = 12.4, 3.4, 4*S*-C⁵HH), 1.42 (3H, d, *J* = 6.0, C³HCH₃), 1.36-1.32 (1H, m, 4*S*-C⁸HH), 1.23-1.17 (2H, m, 4*S*-C⁶HH & 4*S*-C⁷HH); ¹³C NMR (150 MHz, CDCl₃) δ 202.8 (4*S*-C⁹=O), 202.7 (4*S*-CHO), 170.5 (4*S*-C¹=O), 77.2 (4*S*-C³HMe), 54.5 (4*S*-C^{9*a*}H), 49.4 (4*S*-C^{8*a*}H), 49.1 (4*S*-C⁴H), 44.9 (4*S*-C^{3*a*}H), 41.6 (4*S*-C^{4*a*}H), 30.7 (4*S*-C⁵H₂), 26.0 (4*S*-C⁸H₂), 25.3 (4*S*-C⁶H₂), 24.8 (4*S*-C⁷H₂), 19.1 (4*S*-C³HCH₃).

(3*R*,3*aS*,4*aS*,8*aR*,9*aS*)-3-Methyl-4-((*E*)-2-(5-(3-(trifluoromethyl)phenyl)pyridin-2-yl)vinyl)octahydronaphtho[2,3-*c*]furan-1,9(3*H*,9*aH*)-dione (60**)**



n-BuLi (1.6 M in hexanes) (150 μ L, 0.24 mmol) was added dropwise to a stirred solution of diethyl (5-(3-(trifluoromethyl)phenyl)pyridin-2-yl)methylphosphonate (**28**) (75 mg, 0.20 mmol) in anhydrous THF (1 mL) at 0 $^{\circ}$ C, under Ar. The solution was stirred at 0 $^{\circ}$ C for 10 min before (3*R*,3*aS*,4*aS*,8*aR*,9*aS*)-3-methyl-1,9-dioxododecahydronaphtho[2,3-*c*]furan-4-carbaldehyde (**59**) (50 mg, 0.20 mmol) was added. The reaction mixture was stirred at 0 $^{\circ}$ C for 45 min and then quenched with sat. aq. NH₄Cl (5 mL). An extraction into EtOAc (10 mL) was completed and the organic layer was dried (MgSO₄), filtered and concentrated *in vacuo* to yield a crude yellow oil. Purification by flash column chromatography (0-15% Et₂O/CH₂Cl₂) and then (20-35% Et₂O/toluene) yielded (3*R*,3*aS*,4*R*,4*aS*,8*aR*,9*aS*)-3-methyl-4-((*E*)-2-(5-(3-(trifluoromethyl)phenyl)pyridin-2-yl)vinyl)octahydronaphtho[2,3-*c*]furan-1,9(3*H*,9*aH*)-dione (**61**) (39 mg, 0.08 mmol, 41%) and (3*R*,3*aS*,4*S*,4*aS*,8*aR*,9*aS*)-3-methyl-4-((*E*)-2-(5-(3-(trifluoromethyl)phenyl)pyridin-2-yl)vinyl)octahydronaphtho[2,3-*c*]furan-1,9(3*H*,9*aH*)-dione (**62**) (14 mg, 0.03 mmol, 15%) as white solids.

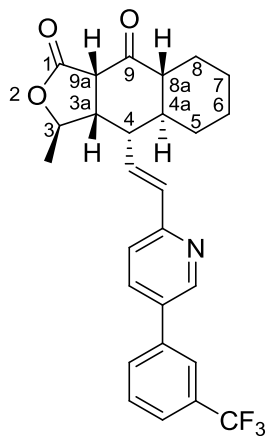
Data for (3*R*,3*aS*,4*R*,4*aS*,8*aR*,9*aS*)-3-methyl-4-((*E*)-2-(5-(3-(trifluoromethyl)phenyl)pyridin-2-yl)vinyl)octahydronaphtho[2,3-*c*]furan-1,9(3*H*,9*aH*)-dione (**61**):



$[\alpha]_D^{20} = +14$ (MeOH); ¹H NMR (600 MHz, CDCl₃) δ 8.82 (1H, d, *J* = 2.3, CHN), 7.89 (1H, dd, *J* = 8.3, 2.3, CHCCHN), 7.82 (1H, s, CHCCF₃), 7.78 (1H, d, *J* = 7.5, CHCCHCCF₃), 7.68 (1H, d, *J* = 7.5, CHCHCCF₃), 7.62 (1H, t, *J* = 7.9, CHCHCCF₃), 7.35 (1H, d, *J* = 7.9, CHCN), 7.10 (1H, dd, *J* = 15.4, 9.8, CH=CH),

6.66 (1H, d, $J = 15.4$, CH=CH), 4.42 (1H, dq, $J = 10.2$, 6.0, C³HMe), 3.66 (1H, d, $J = 8.7$, C^{9a}H), 2.71 (1H, dd, $J = 10.2$, 8.7, C^{3a}H), 2.59 (1H, dd, $J = 9.6$, 4.0, C⁴H), 2.44 (1H, td, $J = 12.0$, 3.6, C^{8a}H), 2.05-1.99 (1H, m, C⁸HH), 1.88 (1H, tt, $J = 12.3$, 4, C^{4a}H), 1.82-1.77 (1H, m, C⁷HH), 1.77-1.72 (1H, m, C⁶HH), 1.71-1.66 (1H, m, C⁵HH), 1.48 (3H, d, $J = 6.0$, C³HCH₃), 1.46-1.40 (1H, m, C⁵HH), 1.40-1.34 (1H, m, C⁸HH), 1.23-1.17 (2H, m, C⁶HH & C⁷HH); ¹³C NMR (150 MHz, CDCl₃) δ 203.8 (C⁹=O), 170.9 (C¹=O), 154.0 (CN), 148.3 (CHN), 138.4 (CCHCCF₃), 135.3 (CHCCHN), 134.2 (CCHN), 132.8 (CH=CH), 132.4 (CH=CH), 131.7 (q, $J = 32.8$, CCF₃), 130.3 (CHCCHCCF₃), 129.8 (CHCHCCF₃), 125.0 (q, $J = 4.0$, CHCHCCF₃), 123.8 (q, $J = 4.0$, CCHCCF₃), 122.3 (d, $J = 247.6$, CF₃), 122.3 (CHCN), 78.0 (C³HMe), 54.1 (C^{9a}H), 51.8 (C^{3a}H), 48.3 (C^{8a}H), 42.2 (C^{4a}H), 41.1 (C⁴H), 31.8 (C⁵H₂), 25.5 (C⁸H₂), 25.4 (C⁶H₂), 24.9 (C⁷H₂), 19.2 (C³HCH₃); IR (thin film) 2921 (C-H), 2852 (C-H), 1783 (C=O), 1719 (C=O), 1447, 1335, 1265, 1167 (C-O), 1127, 804, 730 cm⁻¹; m/z (ES+) 470 (100%, [M+H]⁺); HRMS (ES+) calcd for C₂₇H₂₇NO₃F₃ [M+H]⁺ 470.1943, observed 470.1920.

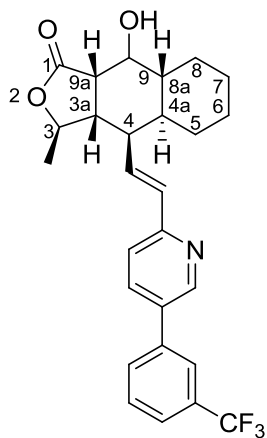
Data for (3*R*,3*aS*,4*S*,4*aS*,8*aR*,9*aS*)-3-methyl-4-((*E*)-2-(5-(3-(trifluoromethyl)phenyl)pyridin-2-yl)vinyl)octahydronaphtho[2,3-*c*]furan-1,9(3*H*,9*aH*)-dione (**62**):



¹H NMR (600 MHz, CDCl₃) δ 8.80 (1H, d, $J = 2.4$, CHN), 7.87 (1H, dd, $J = 8.1$, 2.4, CHCCHN), 7.81 (1H, s, CHCCF₃), 7.76 (1H, d, $J = 7.9$, CHCCHCCF₃), 7.67 (1H, d, $J = 7.9$, CHCHCCF₃), 7.61 (1H, t, $J = 7.9$, CHCHCCF₃), 7.31 (1H, d, $J = 8.1$, CHCN), 6.66 (1H, d, $J = 15.4$, CH=CH), 6.60 (1H, dd, $J = 15.4$, 9.4, CH=CH), 4.57

(1H, dq, $J = 9.4, 6.0$, C³HMe), 3.58 (1H, d, $J = 7.9$, C^{9a}H), 2.90-2.83 (2H, m, C^{3a}H & C⁴H), 2.18 (1H, td, $J = 11.6, 3.2$, C^{8a}H), 1.99-1.92 (2H, m, C⁵HH & C⁸HH), 1.86-1.81 (1H, m, C⁶HH), 1.78-1.69 (2H, m, C^{4a}H & C⁷HH), 1.44 (3H, d, $J = 6.0$, C³HCH₃), 1.42-1.38 (1H, m, C⁸HH), 1.24-1.16 (2H, m, C⁶HH & C⁷HH), 1.11-1.01 (1H, m, C⁵HH); ¹³C NMR (150 MHz, CDCl₃) δ 203.9 (C⁹=O), 170.8 (C¹=O), 153.9 (CN), 148.4 (CHN), 138.5 (CCHCCF₃), 135.2 (CHCCHN), 134.5 (CH=CH), 134.1 (CCHN), 131.9 (CH=CH), 131.7 (q, $J = 32.1$, CCF₃), 130.3 (CHCCHCCF₃), 129.8 (CHCHCCF₃), 124.9 (q, $J = 3.8$, CHCHCCF₃), 123.8 (q, $J = 3.8$, CCHCCF₃), 124.1 (d, $J = 271.7$, CF₃), 122.0 (CHCN), 77.3 (C³HMe), 56.7 (C^{9a}H), 53.1 (C^{8a}H), 52.5 (C^{3a}H), 45.5 (C⁴H), 43.3 (C^{4a}H), 33.1 (C⁵H₂), 25.3 (C⁸H₂), 25.0 (C⁶H₂), 24.8 (C⁷H₂), 21.9 (C³HCH₃); IR (thin film) 2922 (C-H), 2855 (C-H), 1781 (C=O), 1714 (C=O), 1440, 1335, 1268, 1123 (C-O), 1074, 810, 703 cm⁻¹; m/z (EI) 469 (100%, [M]⁺); HRMS (EI) calcd for C₂₇H₂₆NO₃F₃ [M]⁺ 469.1859, observed 469.1859.

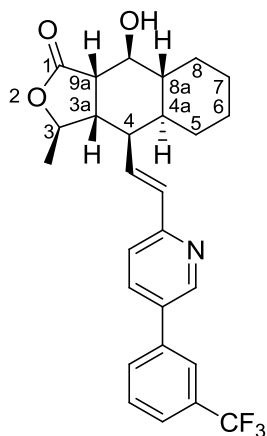
(3R,3aS,4R,4aS,8aR,9aS)-9-Hydroxy-3-methyl-4-((E)-2-(5-(3-(trifluoromethyl)phenyl)pyridin-2-yl)vinyl)decahydronaphtho[2,3-c]furan-1(3H)-one (63)



NaBH₄ (2.13 mg, 0.06 mmol) was added to a stirred solution of (3R,3aS,4R,4aS,8aR,9aS)-3-methyl-4-((E)-2-(5-(3-(trifluoromethyl)phenyl)pyridin-2-yl)vinyl)octahydronaphtho[2,3-c]furan-1,9(3H,9aH)-dione (**61**) (24.0 mg, 0.05 mmol) in anhydrous THF (2 mL) and MeOH (2 mL) at 0 °C, under Ar. The reaction mixture was stirred at 0 °C for 15 min and then quenched with sat. aq. NH₄Cl (0.5

mL). An extraction into Et₂O (5 mL) was completed and the organic layer was dried (MgSO₄), filtered and concentrated *in vacuo* to yield a crude yellow gum. Purification by flash column chromatography (0-2% Et₂O/CH₂Cl₂) yielded (3*R*,3*aS*,4*R*,4*aS*,8*aR*,9*R*,9*aS*)-9-hydroxy-3-methyl-4-((*E*)-2-(5-(3-(trifluoromethyl)phenyl)pyridin-2-yl)vinyl)decahydronaphtho[2,3-*c*]furan-1(3*H*)-one (**63**) as a mixture of isomers. Purification by preparative thin layer chromatography (0-2% Et₂O/CH₂Cl₂) yielded (3*R*,3*aS*,4*R*,4*aS*,8*aR*,9*R*,9*aS*)-9-hydroxy-3-methyl-4-((*E*)-2-(5-(3-(trifluoromethyl)phenyl)pyridin-2-yl)vinyl)decahydronaphtho[2,3-*c*]furan-1(3*H*)-one (**64**) (9 mg, 0.02 mmol, 38%) and (3*R*,3*aS*,4*R*,4*aS*,8*aR*,9*S*,9*aS*)-9-hydroxy-3-methyl-4-((*E*)-2-(5-(3-(trifluoromethyl)phenyl)pyridin-2-yl)vinyl)decahydronaphtho[2,3-*c*]furan-1(3*H*)-one (**65**) (7 mg, 0.02 mmol, 29%) as white solids.

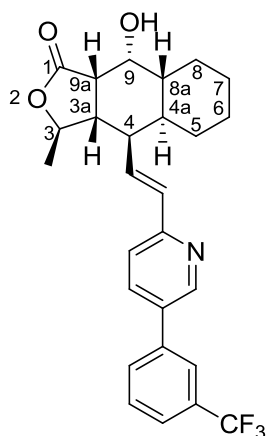
Data for (3*R*,3*aS*,4*R*,4*aS*,8*aR*,9*R*,9*aS*)-9-hydroxy-3-methyl-4-((*E*)-2-(5-(3-(trifluoromethyl)phenyl)pyridin-2-yl)vinyl)decahydronaphtho[2,3-*c*]furan-1(3*H*)-one (**64**):



¹H NMR (600 MHz, CDCl₃) δ 8.80 (1H, d, *J* = 1.9, *CHN*), 7.86 (1H, dd, *J* = 8.1, 1.9, *CHCCHN*), 7.82 (1H, s, *CHCCF*₃), 7.77 (1H, d, *J* = 7.5, *CHCCHCCF*₃), 7.66 (1H, d, *J* = 7.5, *CHCHCCF*₃), 7.61 (1H, t, *J* = 7.9, *CHCHCCF*₃), 7.35 (1H, d, *J* = 8.1, *CHCN*), 6.88 (1H, dd, *J* = 15.4, 9.8, *CH=CH*), 6.55 (1H, d, *J* = 15.4, *CH=CH*), 4.54 (1H, dq, *J* = 10.4, 6.0, *C*³*HMe*), 3.47 (1H, ddd, *J* = 10.9, 9.8, 1.1, *C*⁹*HOH*), 2.74 (1H, dd, *J* = 9.8, 7.9, *C*^{9*a*}*H*), 2.54 (1H, d, *J* = 1.9, *OH*), 2.40 (1H, dd, *J* = 9.6, 4.0, *C*⁴*H*), 2.36-2.30 (2H, m, *C*^{3*a*}*H* & *C*⁸*HH*), 1.78-1.72 (2H, m, *C*⁶*HH* & *C*⁷*HH*), 1.58-

1.49 (3H, m, C^{4a}H, C⁵HH & C^{8a}H), 1.47 (1H, d, *J* = 6.0, C³HCH₃), 1.32-1.16 (4H, m, C⁵HH, C⁶HH, C⁷HH & C⁸HH); ¹³C NMR (150 MHz, CDCl₃) δ 177.9 (C¹=O), 154.6 (CN), 148.1 (CHN), 131.8 (CCHCCF₃), 131.5 (CHCCHN), 131.3 (CH=CH), 130.9 (q, *J* = 32.1, CCF₃), 130.3 (CH=CH & CHCCHCCF₃), 129.9 (CCHN), 129.8 (CHCHCCF₃), 124.9 (q, *J* = 3.6, CHCHCCF₃), 123.8 (q, *J* = 3.6, CCHCCF₃), 124.1 (d, *J* = 272.1, CF₃), 121.6 (CHCN), 78.5 (C³HMe), 73.2 (C⁹HOH), 49.5 (C^{3a}H), 47.7 (C^{9a}H), 41.1 (C⁴H), 40.2 (C^{4a}H), 38.7 (C^{8a}H), 32.1 (C⁵H₂), 31.2 (C⁸H₂), 26.1 (C⁶H₂), 25.5 (C⁷H₂), 19.5 (C³HCH₃); IR (thin film) 2921 (C-H), 2851 (C-H), 1764 (C=O), 1440, 1334, 1267, 1166 (C-O), 1124, 1075, 1051, 804, 755 cm⁻¹; m/z (ES+) 472 (100%, [M]⁺); HRMS (EI) calcd for C₂₇H₂₈NO₃F₃ [M-H]⁺ 471.2016, observed 471.2016.

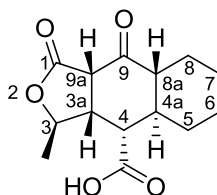
Data for (3*R*,3*aS*,4*R*,4*aS*,8*aR*,9*S*,9*aS*)-9-hydroxy-3-methyl-4-((*E*)-2-(5-(3-(trifluoromethyl)phenyl)pyridin-2-yl)vinyl)decahydronaphtho[2,3-*c*]furan-1(3*H*)-one (**65**):



¹H NMR (600 MHz, CDCl₃) δ 8.79 (1H, d, *J* = 1.9, CHN), 7.85 (1H, dd, *J* = 8.1, 1.9, CHCCHN), 7.81 (1H, s, CHCCF₃), 7.76 (1H, d, *J* = 7.5, CHCHCCF₃), 7.66 (1H, d, *J* = 7.5, CHCCHCCF₃), 7.61 (1H, t, *J* = 7.9, CHCHCCF₃), 7.32 (1H, d, *J* = 8.3, CHCN), 6.87 (1H, dd, *J* = 15.4, 10.2, CH=CH), 6.52 (1H, d, *J* = 15.4, CH=CH), 4.74 (1H, dq, *J* = 10.5, 6.0, C³HMe), 4.09 (1H, td, *J* = 4.9, 2.3, C⁹H), 2.93 (1H, dd, *J* = 8.3, 4.9, C^{9a}H), 2.48 (1H, dd, *J* = 10.2, 4.2, C⁴H), 2.21 (1H, dd, *J* = 10.5, 8.3, C^{3a}H), 2.11 (1H, d, *J* = 4.9, OH), 1.92 (1H, tt, *J* = 11.7, 4.5, C^{4a}H), 1.78-1.70 (2H, m, C⁶HH & C⁷HH), 1.59-1.54 (3H, m, C⁵HH, C⁸HH & C^{8a}H), 1.51-1.44 (1H, m, C⁸HH), 1.44

(3H, d, $J = 6.0$, C^3HCH_3), 1.31-1.19 (3H, m, C^5HH , C^6HH & C^7HH); ^{13}C NMR (150 MHz, $CDCl_3$) δ 177.4 ($C^1=O$), 154.7 (CN), 148.1 (CHN), 138.6 ($CCHCCF_3$), 135.4 (CH=CH), 135.1 (CHCCHN), 133.7 (CCHN), 131.7 (q, $J = 32.1$, CCF_3), 130.8 (CH=CH), 130.3 (CHCCHCCF₃), 129.8 (CHCHCCF₃), 124.8 (q, $J = 4.0$, CHCHCCF₃), 123.8 (q, $J = 4.0$, CCHCCF₃), 124.1 (d, $J = 271.7$, CF_3), 121.9 (CHCN), 79.7 (C^3HMe), 69.0 (C^9HOH), 48.4 ($C^{3a}H$), 45.8 ($C^{9a}H$), 41.3 (C^4H), 38.4 ($C^{8a}H_2$), 31.7 ($C^{4a}H$), 31.4 (C^5H_2), 28.9 (C^8H_2), 26.4 (C^6H_2), 26.1 (C^7H_2), 19.3 (C^3HCH_3); IR (thin film) 2924 (C-H), 2853 (C-H), 1761 (C=O), 1440, 1334, 1267, 1165 (C-O), 1124, 1075, 1050, 803, 700 cm^{-1} ; m/z (ES+) 472 (100%, $[M]^+$); HRMS (ES+) calcd for $C_{27}H_{29}NO_3F_3$ $[M]^+$ 472.2100, observed 472.2089.

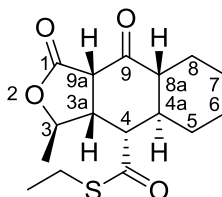
(3R,3aS,4S,4aR,8aR,9aS)-3-Methyl-1,9-dioxododecahydronaphtho[2,3-c]furan-4-carboxylic acid (66)



TFA (0.3 mL) was added dropwise to a stirred solution of (3R,3aS,4S,4aR,8aR,9aS)-*tert*-butyl 3-methyl-1,9-dioxododecahydronaphtho[2,3-c]furan-4-carboxylate (**56**) (29.0 mg, 0.09 mmol) in CH_2Cl_2 (0.3 mL) at 0 °C, under Ar. The reaction mixture was stirred at 20 °C for 16 h before being concentrated *in vacuo*. The residue was azeotroped with toluene to yield (3R,3aS,4S,4aR,8aR,9aS)-3-methyl-1,9-dioxododecahydronaphtho[2,3-c]furan-4-carboxylic acid (**66**) (24 mg, 0.09 mmol, 99%) as a white solid; 1H NMR (600 MHz, MeOH- d_4) δ 4.50 (1H, dq, $J = 10.2$, 6.0, C^3HMe), 3.74 (1H, d, $J = 8.7$, $C^{9a}H$), 3.08 (1H, dd, $J = 10.2$, 5.8, $C^{3a}H$), 2.99 (1H, td, $J = 11.5$, 5.8, C^4H), 2.30 (1H, td, $J = 11.6$, 3.2, $C^{8a}H$), 2.01-1.96 (1H, m, C^5HH), 1.91 (1H, dtd, $J = 11.9$, 11.5, 3.4, $C^{4a}H$), 1.90-1.86 (1H, m, C^8HH), 1.84-1.79 (1H, m, C^6HH), 1.76-1.71 (1H, m, C^7HH), 1.34 (3H, d, $J = 6.0$, C^3HCH_3), 1.39-1.31 (1H, m, C^8HH), 1.33-1.23 (2H, m, C^6HH & C^7HH), 1.17-1.10 (1H, m, C^8HH); ^{13}C NMR (150 MHz, MeOH- d_4) δ 205.7 ($C^9=O$), 175.5 ($C=OOH$), 172.9 ($C^1=O$), 78.8 (C^3HMe), 52.5 ($C^{8a}H$), 49.6 ($C^{3a}H$), 47.5

(C⁴H), 42.1 (C^{4a}H), 33.2 (C⁵H₂), 26.2 (C⁸H₂), 25.9 (C⁶H₂), 25.8 (C⁷H₂), 20.1 (C³HCH₃), *N.B.* Peak for C^{9a}H under solvent peak; IR (thin film) 2929 (C-H), 2858 (C-H), 1778 (C=O), 1707 (C=O), 1320, 1190 (C-O), 1067, 752, 668 cm⁻¹; m/z (EI) 266 (100%, [M]⁺); HRMS (EI) calcd for C₁₄H₁₈O₅ [M]⁺ 266.1149, observed 266.1148.

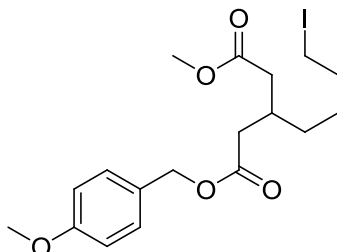
(3*R*,3*aR*,4*S*,4*aR*,8*aR*,9*aS*)-S-Ethyl 3-methyl-1,9-dioxododecahydronaphtho[2,3-*c*]furan-4-carbothioate (67)



EDCI (12.9 mg, 0.08 mmol) was added to a stirred solution of (3*R*,3*aS*,4*S*,4*aR*,8*aR*,9*aS*)-3-methyl-1,9-dioxododecahydronaphtho[2,3-*c*]furan-4-carboxylic acid (**66**) (14.7 mg, 0.06 mmol), ethanethiol (15.9 μ L, 0.22 mmol) and DMAP (0.37 mg, cat.) in CH₂Cl₂ (1 mL) at 0 °C, under Ar. The reaction mixture was stirred at 20 °C for 3 h before being diluted with CH₂Cl₂ (5 mL), washed (H₂O), dried (MgSO₄), filtered and concentrated *in vacuo* to yield a crude colourless oil. Purification by flash column chromatography (0-10% Et₂O/CH₂Cl₂) yielded (3*R*,3*aR*,4*S*,4*aR*,8*aR*,9*aS*)-S-ethyl 3-methyl-1,9-dioxododecahydronaphtho[2,3-*c*]furan-4-carbothioate (**67**) (4 mg, 0.01 mmol, 23%) as a white solid; ¹H NMR (600 MHz, CDCl₃) δ 4.53 (1H, dq, *J* = 10.2, 6.0, C³HMe), 3.51 (1H, d, *J* = 8.7, C^{9a}H), 3.13 (1H, dd, *J* = 10.5, 5.3, C⁴H), 2.99 (1H, td, *J* = 9.3, 5.5, C^{3a}H), 2.94 (1H, q, *J* = 7.5, SCH₂CH₃), 2.14-2.07 (2H, m, C^{4a}H & C^{8a}H), 1.97-1.92 (1H, m, C⁸HH), 1.89-1.81 (2H, m, C⁶HH & C⁷HH), 1.75-1.70 (1H, m, C⁵HH), 1.42-1.35 (1H, m, C⁸HH), 1.29 (3H, t, *J* = 7.5, SCH₂CH₃), 1.26 (3H, d, *J* = 6.0, C³HCH₃), 1.24-1.17 (2H, m, C⁶HH & C⁷HH), 1.13-1.06 (1H, m, C⁵HH); ¹³C NMR (150 MHz, CDCl₃) δ 202.4 (C⁹=O), 199.7 (C=OSet), 169.8 (C¹=O), 77.6 (C³HMe), 56.1 (C^{9a}H), 55.7 (C⁴H), 52.3 (C^{8a}H), 48.8 (C^{3a}H), 41.4 (C^{4a}H), 31.9 (C⁵H₂), 25.0 (C⁸H₂), 24.8 (C⁶H₂), 24.8 (C⁷H₂), 23.9 (CH₂CH₃), 20.3 (C³HCH₃), 14.7 (CH₂CH₃); IR (thin film) 2930 (C-H), 2855 (C-H), 1774 (C=O), 1714 (C=O), 1678 (C=O), 1262, 1196 (C-O), 1098, 960,

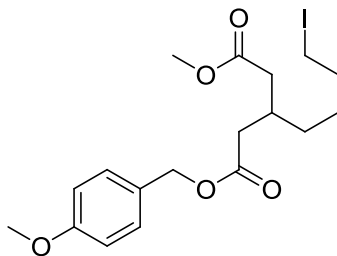
729 cm^{-1} ; m/z (EI) 252 (100%, $[\text{M}-\text{SEt}-\text{Me}+\text{OH}]^+$); HRMS (EI) calcd for $\text{C}_{16}\text{H}_{22}\text{O}_4\text{S}$ $[\text{M}+\text{H}]^+$ 310.1233, observed 310.1231.

1-(4-Methoxybenzyl) 5-methyl 3-(4-iodobutyl)pentanedioate (68)



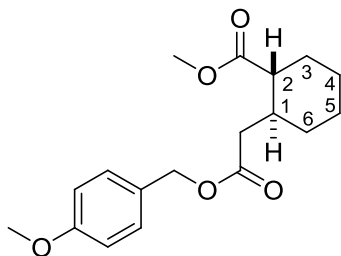
n-BuLi (2.5 M in hexanes) (15.6 mL, 39.0 mmol) was added dropwise to a stirred solution of DIPA (5.56 mL, 39.0 mmol) in anhydrous 2-MeTHF (30 mL) at $-78\text{ }^{\circ}\text{C}$, under N_2 . The reaction mixture was stirred at $-78\text{ }^{\circ}\text{C}$ for 15 min before 4-methoxybenzyl acetate (6.39 mL, 39.0 mmol) was added dropwise and stirring continued for 30 min at $-78\text{ }^{\circ}\text{C}$. Next, a solution of **43** (5.23 g, 19.51 mmol) in anhydrous 2-MeTHF (10 mL) was added and stirring continued for 45 min at $-78\text{ }^{\circ}\text{C}$. Finally, solid $\text{KO}t\text{-Bu}$ (4.38 g, 39.0 mmol) was added. The reaction mixture was stirred for a further 1 h and then quenched with sat. aq. NH_4Cl (100 mL). An extraction into 2-MeTHF (2 x 100 mL) was completed and the combined organic layers were dried (hydrophobic frit) and concentrated *in vacuo* to yield a crude yellow oil. Purification by automated column chromatography (0-30% EtOAc/cyclohexane) yielded 1-(4-methoxybenzyl) 5-methyl 3-(4-iodobutyl)pentanedioate (**68**) (1.81 g, 4.04 mmol, 21%) as a colourless oil and some impure *rac*-methyl 2-(2-((4-methoxybenzyl)oxy)-2-oxoethyl)cyclohexanecarboxylate (**69**). Further purification by MDAP (MeCN/ H_2O with an $(\text{NH}_4)\text{HCO}_3$ modifier) yielded **69** (32 mg, 0.1 mmol, 0.5%).

Data for 1-(4-methoxybenzyl) 5-methyl 3-(4-iodobutyl)pentanedioate (**68**):



^1H NMR (400 MHz, Acetone- d_6) δ 7.35 (2H, d, J = 8.6, 2 x Ar-CH), 6.94 (2H, d, J = 8.7, 2 x Ar-CH), 5.06 (2H, s, Bn- CH_2), 3.82 (3H, s, Bn- OCH_3), 3.63 (3H, s, COOCH_3), 3.26 (2H, d, J = 6.8, CH_2I), 2.43-2.30 (5H, m, CH_2COOMe , CH_2COOBn & $\text{CHCH}_2\text{COOMe}$), 1.83-1.75 (2H, m, $\text{CH}_2\text{CH}_2\text{I}$), 1.48-1.35 (4H, m, 2 x CH_2); ^{13}C NMR (100 MHz, Acetone- d_6) δ 172.3 (C=OOMe), 171.7 (C=OObn), 159.8 (Ar-COMe), 130.0 (2 x Ar-CH), 128.6 (Ar-C CH_2), 113.8 (2 x Ar-CH), 65.4 (Bn- CH_2), 54.7 (Ar- OCH_3), 50.7 (COOCH_3), 38.1 ($\text{CH}_2\text{C}=\text{O}$), 37.8 ($\text{CH}_2\text{C}=\text{O}$), 33.4 ($\text{CH}_2\text{CH}_2\text{I}$), 32.4 ($\text{CHCH}_2\text{COOMe}$), 31.9 (CH_2), 27.2 (CH_2), 6.5 (CH_2I); IR (thin film) 2936 (C-H), 2838 (C-H), 1731 (C=O), 1613 (ArC-C), 1515 (ArC-C), 1247 (C-O), 1172, 1150, 1033, 823 cm^{-1} ; m/z (ES+) 466 (100%, $\text{M}[\text{NH}_4]^+$); HRMS (EI) calcd for $\text{C}_{18}\text{H}_{25}\text{O}_5\text{I}$ $[\text{M}+\text{H}]^+$ 448.0741, observed 448.0756.

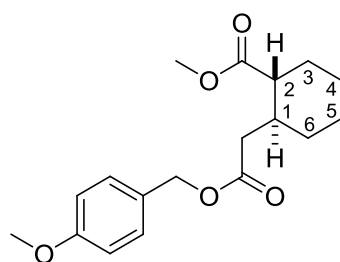
Data for *rac*-Methyl 2-(2-((4-methoxybenzyl)oxy)-2-oxoethyl)cyclohexanecarboxylate (**69**):



^1H NMR (400 MHz, Acetone- d_6) δ 7.33 (2H, d, J = 8.7, 2 x Ar-CH), 6.94 (2H, d, J = 8.7, 2 x Ar-CH), 5.04 (2H, s, Bn- CH_2), 3.81 (3H, s, Bn- OCH_3), 3.62 (3H, s, COOCH_3), 2.38 (1H, dd, J = 15.0, 3.7, C^2H), 2.21-2.12 (1H, m, C^1H), 2.12 (2H, d, J = 14.9, CH_2COOBn), 1.92-1.85 (1H, m, C^3HH), 1.84-1.77 (1H, m, C^6HH), 1.76-1.67 (2H, m, C^4HH & C^5HH), 1.50-1.39 (1H, m, C^3HH), 1.33-1.23 (2H, m, C^4HH & C^5HH), 1.14-1.03 (1H, m, C^6HH); ^{13}C NMR (100 MHz, Acetone- d_6) δ 174.9 (C=OOMe), 171.4 (C=OObn), 159.7 (Ar-COMe), 129.9 (2 x Ar-CH), 128.6 (Ar-

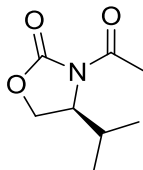
CCH₂), 113.7 (2 x Ar-CH), 65.3 (Bn-CH₂), 54.7 (Ar-OCH₃), 50.7 (COOCH₃), 48.4 (C²H), 39.1 (C¹H), 36.1 (CH₂C=O), 31.0 (C⁶H₂), 29.7 (C³H₂), 25.3 (C⁵H₂), 25.0 (C⁴H₂); IR (thin film) 2933 (C-H), 2857 (C-H), 1730 (C=O), 1613 (ArC-C), 1515 (ArC-C), 1447, 1247 (C-O), 1151, 1105, 1032, 976, 822 cm⁻¹; m/z (ES+) 320 (100%, [M+H]⁺); HRMS (EI) calcd for C₁₈H₂₄O₅ [M+H]⁺ 320.1618, observed 320.1613.

(1*R,2*S**)-Methyl 2-(2-((4-methoxybenzyl)oxy)-2-oxoethyl)cyclohexanecarboxylate (69)**



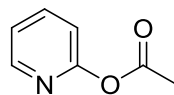
LDA (2 M in THF/pentane/ethylbenzene) (2.52 mL, 5.04 mmol) was added dropwise to a stirred solution of 1-(4-methoxybenzyl) 5-methyl 3-(4-iodobutyl)pentanedioate (**68**) (1.41 g, 3.15 mmol) in anhydrous 2-MeTHF (7 mL) at -78 °C, under N₂. The reaction mixture was stirred at -78 °C for 3 h and then quenched with sat. aq. NH₄Cl (10 mL). An extraction into 2-MeTHF (25 mL) was completed and the organic layer was dried (hydrophobic frit) and concentrated *in vacuo* to yield a crude yellow oil. Purification by automated column chromatography (0-25% *t*-BME/cyclohexane) yielded *rac*-methyl 2-(2-((4-methoxybenzyl)oxy)-2-oxoethyl)cyclohexanecarboxylate (**69**) (917 mg, 2.86 mmol, 91%) as a colourless oil. See data above.

(*S*)-3-Acetyl-4-isopropylloxazolidin-2-one (70)



n-BuLi (1.6 M in hexanes) (5.81 mL, 9.29 mmol) was added dropwise to a stirred solution of (*S*)-4-isopropylloxazolidin-2-one (1.00 g, 7.74 mmol) in anhydrous 2-MeTHF (20 mL) at -78 °C, under N₂. The reaction mixture was stirred at -78 °C for 30 min before acetyl chloride (1 M in CH₂Cl₂) (9.29 mL, 9.29 mmol) was added. The reaction mixture was stirred for a further 30 min and then quenched with sat. aq. NH₄Cl (10 mL). An extraction into 2-MeTHF (2 x 20 mL) was completed and the organic layer was dried (hydrophobic frit) and concentrated *in vacuo* to yield a crude yellow oil. Purification by automated column chromatography (0-50% EtOAc/cyclohexane) yielded (*S*)-3-acetyl-4-isopropylloxazolidin-2-one (**70**) (1.18 g, 6.90 mmol, 89%) as a colourless oil; ¹H NMR (400 MHz, Acetone-d₆) δ 4.46 (1H, ddd, *J* = 8.2, 3.8, 3.0, CHN), 4.38 (1H, dd, *J* = 8.9, 8.2, CHHCHN), 4.32 (1H, dd, *J* = 8.9, 3.0, CHHCHN), 2.43 (3H, s, CH₃), 2.33 (1H, td, *J* = 7.0, 3.8, CH(CH₃)₂), 0.93 (3H, d, *J* = 7.0, CH(CH₃)₂), 0.88 (3H, d, *J* = 7.0, CH(CH₃)₂); ¹³C NMR (100 MHz, Acetone-d₆) δ 169.4 (C=O), 154.3 (C=OCH₃), 63.3 (CH₂), 58.2 (CHN), 28.6 (CH(CH₃)₂), 22.8 (C=OCH₃), 17.1 (CH(CH₃)₂), 14.1 (CH(CH₃)₂); IR (thin film) 2964 (C-H), 1776 (C=O), 1697 (C-O), 1373, 1302, 1205, 1150 (C-O), 1062, 968, 773, 620 cm⁻¹; *m/z* (ES⁺) 172 (100%, [M+H]⁺); HRMS (EI) calcd for C₈H₁₃NO₃ [M]⁺ 171.0890, observed 171.0899.

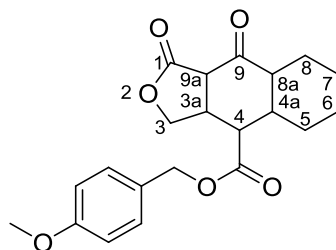
Pyridin-2-yl acetate¹⁵² (**71**)



Acetyl chloride (1 M in CH₂Cl₂) (21.0 mL, 21.0 mmol) was added dropwise to a stirred solution of pyridin-2(1H)-one (2.00 g, 21.0 mmol) and pyridine (1.70 mL, 21.0 mmol) in CH₂Cl₂ (50 mL) at 0 °C, under N₂. The reaction mixture was stirred at 20 °C for 2 h before being concentrated *in vacuo* to half its volume. The organic layer was washed with sat. aq. brine (10 mL), dried (hydrophobic frit) and

concentrated *in vacuo* to yield a crude yellow oil. Purification by automated column chromatography (0-100% EtOAc/cyclohexane) yielded pyridin-2-yl acetate (**71**) (937 mg, 6.8 mmol, 33%) as a colourless oil; ^1H NMR (600 MHz, CDCl_3) δ 8.43 (1H, ddd, $J = 4.9, 2.0, 0.9$, CHCHCN), 7.81 (1H, ddd, $J = 8.1, 7.4, 2.0$, CHN), 7.25 (1H, ddd, $J = 7.4, 4.9, 0.9$, CHCN), 7.10 (1H, dt, $J = 8.1, 0.9$, CHCHN), 2.36 (3H, s, CH_3); ^{13}C NMR (150 MHz, CDCl_3) δ 169.0 (C=O), 157.8 (CN), 148.5 (CHCHCN), 139.6 (CHN), 122.1 (CHCN), 116.5 (CHCHN), 21.2 (CH_3); IR (thin film) 2955 (C-H), 1643 (ArC-C), 1595 (ArC-C), 1539 (ArC-C), 1464 (ArC-N), 1426 (ArC-N), 1224, 1155 (C-O), 989, 770, 726, 560, 514 cm^{-1} ; m/z (ES+) 138 (100%, $[\text{M}+\text{H}]^+$). Data agrees with that reported by Usami *et al.*¹⁵²

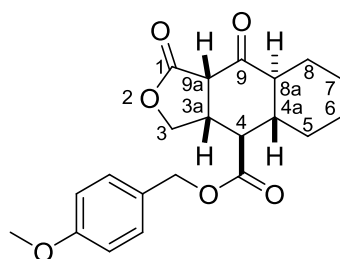
***rac*-4-Methoxybenzyl 1,9-dioxododecahydronaphtho[2,3-*c*]furan-4-carboxylate (**72**)**



n-BuLi (1.6 M in hexanes) (3.76 mL, 6.01 mmol) was added dropwise to a stirred solution of distilled TMP (1.02 mL, 6.01 mmol) in anhydrous 2-MeTHF (5 mL) stirred at $-78\text{ }^\circ\text{C}$, under N_2 . The solution was warmed to $0\text{ }^\circ\text{C}$ and then re-cooled to $-78\text{ }^\circ\text{C}$. A solution of (1*R**,2*S**)-methyl 2-(2-((4-methoxybenzyl)oxy)-2-oxoethyl)cyclohexanecarboxylate (**69**) (917 mg, 2.86 mmol) in anhydrous 2-MeTHF (5 mL) was added dropwise and stirring continued for 45 min at $-78\text{ }^\circ\text{C}$. Next, neat furan-2(5H)-one (0.12 mL, 1.72 mmol) was added and stirring continued for 2 h at $-78\text{ }^\circ\text{C}$. Finally, solid KO*t*-Bu (674 mg, 6.01 mmol) was added. The reaction mixture was warmed to $-40\text{ }^\circ\text{C}$, stirred for a further 3 h and then quenched with sat. aq. NH_4Cl (20 mL). An extraction into 2-MeTHF (20 mL) was completed and the organic layer was dried (hydrophobic frit) and concentrated *in vacuo* to yield a crude yellow oil with white precipitate. Purification by automated column chromatography (0-50% EtOAc/cyclohexane) yielded several crude samples of

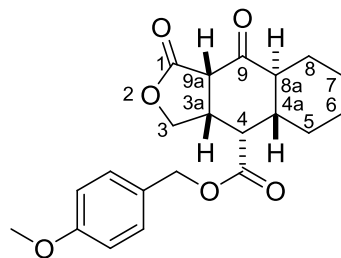
varying stereoisomers. Further purifications by MDAP (MeCN/H₂O with an (NH₄)HCO₃ modifier) yielded (3a*S**,4*R**,4a*S**,8a*S**,9a*S**)-4-methoxybenzyl 1,9-dioxododecahydronaphtho[2,3-*c*]furan-4-carboxylate (**73**) (20 mg, 0.05 mmol, 2%) and (3a*S**,4*S**,4a*S**,8a*S**,9a*S**)-4-methoxybenzyl 1,9-dioxododecahydronaphtho[2,3-*c*]furan-4-carboxylate (**74**) (20 mg, 0.05 mmol, 2%) as white solids.

Data for (3a*S**,4*R**,4a*S**,8a*S**,9a*S**)-4-methoxybenzyl 1,9-dioxododecahydronaphtho[2,3-*c*]furan-4-carboxylate (**73**):



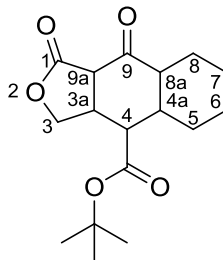
¹H NMR (600 MHz, CDCl₃) δ 7.31 (2H, d, *J* = 8.7, 2 x Ar-CH), 6.92 (2H, d, *J* = 8.7, 2 x Ar-CH), 5.17 (1H, d, *J* = 11.9, Bn-CHH), 5.13 (1H, d, *J* = 11.9, Bn-CHH), 4.16 (1H, d, *J* = 1.3, C³HH), 4.16 (1H, d, *J* = 3.8, C³HH), 3.84 (3H, s, Bn-OCH₃), 3.50 (1H, d, *J* = 7.6, C^{9a}H), 3.19 (1H, dddd, *J* = 11.4, 7.6, 3.8, 1.3, C^{3a}H), 2.56 (1H, t, *J* = 11.4, C⁴H), 2.17-2.12 (1H, m, C⁸HH), 2.04-1.98 (1H, m, C^{8a}H), 1.84-1.63 (4H, m, C^{4a}H, C⁵HH, C⁶HH & C⁷HH), 1.26-1.10 (4H, m, C⁵HH, C⁶HH, C⁷HH & C⁸HH); ¹³C NMR (150 MHz, CDCl₃) δ 201.4 (C⁹=O), 172.8 (C=OOBn), 171.1 (C¹=O), 160.0 (Ar-COMe), 130.3 (2 x Ar-CH), 127.3 (Ar-CCH₂), 114.1 (2 x Ar-CH), 70.3 (C³H₂), 67.0 (Bn-CH₂), 55.3 (Ar-OCH₃), 53.2 (C^{9a}H), 51.1 (C^{8a}H), 50.2 (C⁴H), 42.7 (C^{4a}H), 42.5 (C^{3a}H), 31.6 (C⁵H₂), 25.0 (C⁸H₂), 24.9 (C⁶H₂), 24.6 (C⁷H₂); IR (thin film) 2932 (C-H), 2857 (C-H), 1778 (C=O), 1723 (C-O), 1613 (ArC-C), 1515 (ArC-C), 1247, 1163 (C-O), 1029, 996, 916, 823, 733 cm⁻¹; *m/z* (ES⁺) 390 (100%, M[NH₄⁺]⁺); HRMS (EI) calcd for C₂₁H₂₄O₆ [M+H]⁺ 372.1567, observed 372.1569.

Data for (3a*S**,4*S**,4a*S**,8a*S**,9a*S**)-4-methoxybenzyl 1,9-dioxododecahydronaphtho[2,3-*c*]furan-4-carboxylate (**74**):



^1H NMR (600 MHz, CDCl_3) δ 7.33 (2H, d, $J = 8.7$, 2 x Ar-CH), 6.93 (2H, d, $J = 8.7$, 2 x Ar-CH), 5.18 (1H, d, $J = 11.8$, Bn-CHH), 5.14 (1H, d, $J = 11.8$, Bn-CHH), 4.38 (1H, dd, $J = 9.1$, 8.2, C^3HH), 3.95 (1H, dd, $J = 10.6$, 9.1, C^3HH), 3.84 (3H, s, Bn-OCH₃), 3.73 (1H, d, $J = 8.8$, C^{9a}H), 3.26 (1H, dddd, $J = 10.6$, 8.8, 8.2, 1.2, C^{3a}H), 2.68 (1H, dd, $J = 4.9$, 1.2, C^4H), 2.61 (1H, td, $J = 12.0$, 3.7, C^{8a}H), 2.04-1.99 (1H, m, C^8HH), 1.92-1.86 (1H, m, C^{4a}H), 1.81-1.70 (3H, m, C^5HH , C^6HH & C^7HH), 1.34-1.26 (1H, m, C^8HH), 1.23-1.08 (3H, m, C^5HH , C^6HH & C^7HH); ^{13}C NMR (150 MHz, CDCl_3) δ 203.3 ($\text{C}^9=\text{O}$), 172.6 ($\text{C}=\text{OOBn}$), 171.4 ($\text{C}^1=\text{O}$), 160.0 (Ar-COMe), 130.5 (2 x Ar-CH), 127.2 (Ar-CCH₂), 114.1 (2 x Ar-CH), 69.2 (C^3H_2), 66.9 (Bn-CH₂), 55.3 (Ar-OCH₃), 52.6 (C^{9a}H), 48.1 (C^{8a}H), 44.0 (C^4H), 40.4 (C^{4a}H), 40.0 (C^{3a}H), 31.2 (C^5H_2), 25.7 (C^8H_2), 25.5 (C^6H_2), 24.6 (C^7H_2); IR (thin film) 2933 (C-H), 2858 (C-H), 1790 (C=O), 1721 (C=O), 1613 (ArC-C), 1515 (ArC-C), 1448 (ArC-C), 1303 (C-O), 1249 (C-O), 1202, 1169, 1032, 948, 823, 731 cm^{-1} ; m/z (ES+) 390 (100%, $[\text{M}+\text{H}]^+$); HRMS (EI) calcd for $\text{C}_{21}\text{H}_{24}\text{O}_6$ $[\text{M}+\text{H}]^+$ 372.1567, observed 372.1568.

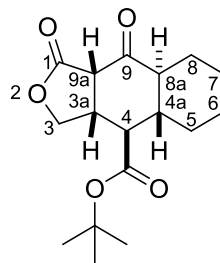
***rac-tert*-Butyl 1,9-dioxododecahydronaphtho[2,3-*c*]furan-4-carboxylate (44)**



n-BuLi (2.7 M in heptanes) (12.8 mL, 34.5 mmol) was added dropwise to a stirred solution of distilled TMP (5.87 mL, 34.5 mmol) in anhydrous 2-MeTHF (40 mL) at -78 °C, under N_2 . The solution was warmed to 0 °C and then re-cooled to -78 °C. A

solution of (1*R**,2*S**)-methyl 2-(2-(*tert*-butoxy)-2-oxoethyl)cyclohexanecarboxylate (**43**) (4.21 g, 16.4 mmol) in anhydrous 2-MeTHF (40 mL) was added dropwise and stirring continued for 30 min at -78 °C. Next, neat furan-2(5H)-one (0.58 mL, 8.21 mmol) was added dropwise. The reaction mixture was stirred for a further 3 h, quenched with sat. aq. NH₄Cl (50 mL) and diluted with H₂O (25 mL). An extraction into EtOAc (2 x 50 mL) was completed and the combined organic layers were washed with sat. aq. brine (30 mL), dried (hydrophobic frit) and concentrated *in vacuo* to yield a crude yellow oil with white precipitate. Purification by automated column chromatography (0-100% EtOAc/cyclohexane) yielded (3*aS**,4*R*,4*aS**,8*aS**,9*aS**)-*tert*-butyl 1,9-dioxododecahydronaphtho[2,3-*c*]furan-4-carboxylate (**45**) (663 mg, 2.15 mmol, 26%) and (3*aS**,4*R**,4*aR**,8*aR**,9*aS**)-*tert*-butyl 1,9-dioxododecahydronaphtho[2,3-*c*]furan-4-carboxylate (**47**) (644 mg, 2.09 mmol, 25%) as white solids. Further purification by MDAP (MeCN/H₂O with an (NH₄)HCO₃ modifier) yielded (3*aS**,4*R**,4*aS**,8*aS**,9*aS**)-*tert*-butyl 1,9-dioxododecahydronaphtho[2,3-*c*]furan-4-carboxylate (**75**) (25 mg, 0.04 mmol, 1%) as a white solid.

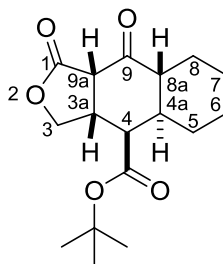
Data for (3*aS**,4*R**,4*aS**,8*aS**,9*aS**)-*tert*-butyl 1,9-dioxododecahydronaphtho[2,3-*c*]furan-4-carboxylate (**45**):



¹H NMR (600 MHz, CDCl₃) δ 4.22 (1H, d, *J* = 3.8, C³HH), 4.21 (1H, s, C³HH), 3.49 (1H, d, *J* = 7.5, C^{9a}H), 3.15 (1H, ddd, *J* = 11.5, 7.5, 3.8, C^{3a}H), 2.41 (1H, t, *J* = 11.5, C⁴H), 2.14-2.10 (1H, m, C⁸HH), 2.01-1.96 (1H, m, C^{8a}H), 1.82-1.66 (4H, m, C^{4a}H, C⁵HH, C⁶HH & C⁷HH), 1.48 (9H, s, C(CH₃)₃), 1.46-1.41 (1H, m, C⁸HH), 1.25-1.12 (3H, m, C⁵HH, C⁶HH & C⁷HH); ¹³C NMR (150 MHz, CDCl₃) δ 201.9 (C⁹=O), 172.4 (C=OO^tBu), 171.5 (C¹=O), 82.5 (C(CH₃)₃), 70.5 (C³H₂), 53.3 (C^{9a}H), 51.3 (C^{8a}H), 51.0 (C⁴H), 42.8 (C^{4a}H), 42.8 (C^{3a}H), 31.5 (C⁸H₂), 28.2 (C(CH₃)₃), 25.1 (C⁵H₂), 25.0

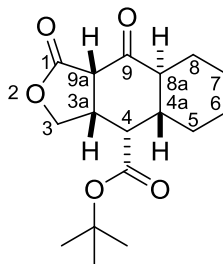
(C⁶H₂), 24.8 (C⁷H₂); IR (thin film) 2974 (C-H), 2929 (C-H), 2856 (C-H), 1795 (C=O), 1715 (C=O), 1367 (C-H), 1244 (C-O), 1157, 1021, 845 cm⁻¹; m/z (ES+) 326 (100%, M[NH₄⁺]⁺); HRMS (EI) calcd for C₁₇H₂₄O₅ [M+H]⁺ 308.1618, observed 308.1613.

Data for (3a*S**,4*R**,4a*R**,8a*R**,9a*S**)-*tert*-butyl 1,9-dioxododecahydronaphtho[2,3-*c*]furan-4-carboxylate (**47**):



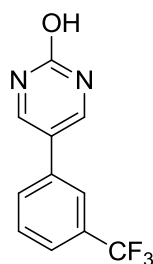
¹H NMR (600 MHz, CDCl₃) δ 4.39 (1H, t, *J* = 8.3, C³HH), 3.94 (1H, t, *J* = 9.8, C³HH), 3.72 (1H, d, *J* = 8.7, C^{9a}H), 3.25 (1H, ddd, *J* = 9.8, 8.7, 8.3, C^{3a}H), 2.66 (1H, td, *J* = 12.0, 3.6, C^{8a}H), 2.53 (1H, d, *J* = 4.5, C⁴H), 2.03 (1H, d, *J* = 14.7, C⁸HH), 1.85 (1H, tdd, *J* = 12.0, 4.5, 3.4, C^{4a}H), 1.84-1.76 (3H, m, C⁵HH, C⁶HH & C⁷HH), 1.50 (9H, s, C(CH₃)₃), 1.49-1.42 (1H, m, C⁸HH), 1.36-1.15 (3H, m, C⁵HH, C⁶HH & C⁷HH); ¹³C NMR (150 MHz, CDCl₃) δ 203.8 (C⁹=O), 172.0 (C=OO^tBu), 171.8 (C¹=O), 82.5 (C(CH₃)₃), 69.5 (C³H₂), 52.9 (C^{9a}H), 48.2 (C^{8a}H), 44.9 (C⁴H), 40.6 (C^{4a}H), 40.3 (C^{3a}H), 31.4 (C⁸H₂), 28.3 (C(CH₃)₃), 25.9 (C⁵H₂), 25.7 (C⁶H₂), 25.1 (C⁷H₂); IR (thin film) 2926 (C-H), 2850 (C-H), 1778 (C=O), 1715 (C=O), 1698 (C=O), 1365 (C-H), 1204 (C-O), 1138, 1002, 845 cm⁻¹; m/z (ES+) 326 (100%, M[NH₄⁺]⁺); HRMS (ES-) calcd for C₁₇H₂₃O₅ [M-H]⁺ 307.1545, observed 307.1546.

Data for (3a*S**,4*R**,4a*S**,8a*S**,9a*S**)-*tert*-butyl 1,9-dioxododecahydronaphtho[2,3-*c*]furan-4-carboxylate (**75**):



^1H NMR (600 MHz, CDCl_3) δ 4.27 (1H, dd, $J = 9.8, 7.8$, C^3HH), 4.18 (1H, dd, $J = 11.2, 9.8$, C^3HH), 3.43 (1H, d, $J = 8.2$, C^{9a}H), 3.38 (1H, dddd, $J = 11.4, 8.2, 7.8, 5.2$, C^{3a}H), 2.84 (1H, dd, $J = 11.3, 5.2$, C^4H), 2.13 (1H, td, $J = 11.7, 3.0$, C^{8a}H), 2.00-1.90 (2H, m, C^{4a}H & C^8HH), 1.90-1.82 (2H, m, C^6HH & C^7HH), 1.82-1.75 (1H, m, C^5HH), 1.50 (9H, s, $\text{C}(\text{CH}_3)_3$), 1.48-1.37 (1H, m, C^8HH), 1.29-1.17 (3H, m, C^5HH , C^6HH & C^7HH); ^{13}C NMR (150 MHz, CDCl_3) δ 202.8 ($\text{C}^9=\text{O}$), 171.4 ($\text{C}=\text{OO}^t\text{Bu}$), 171.0 ($\text{C}^1=\text{O}$), 82.4 ($\text{C}(\text{CH}_3)_3$), 68.4 (C^3H_2), 54.3 (C^{9a}H), 52.3 (C^{8a}H), 48.3 (C^4H), 41.1 (C^{4a}H), 40.6 (C^{3a}H), 32.1 (C^8H_2), 28.3 ($\text{C}(\text{CH}_3)_3$), 25.2 (C^5H_2), 25.0 (C^6H_2), 24.7 (C^7H_2); IR (thin film) 2974 (C-H), 2929 (C-H), 2856 (C-H), 1795 (C=O), 1715 (C=O), 1367 (C-H), 1244 (C-O), 1157, 1021, 845 cm^{-1} ; m/z (ES+) 326 (100%, $\text{M}[\text{NH}_4^+]^+$); HRMS (EI) calcd for $\text{C}_{17}\text{H}_{24}\text{O}_5$ $[\text{M}]^+$ 308.1618, observed 308.1614.

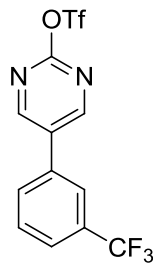
5-(3-(Trifluoromethyl)phenyl)pyrimidin-2-ol (76)



A solution of 5-bromopyrimidin-2-ol (2.00 g, 11.4 mmol), (3-(trifluoromethyl)phenyl)boronic acid (2.60 g, 13.7 mmol), $\text{PdCl}_2(\text{dppf})$ (0.04 g, 0.06 mmol) and K_2CO_3 (4.74 g, 34.3 mmol) in a deoxygenated mixture of $i\text{PrOH}$ (15 mL) and H_2O (3 mL) was heated in a sealed microwave vessel at 120 $^\circ\text{C}$ for 30 min using a Biotage Initiator 60. Once cooled, the reaction mixture was diluted with H_2O (10 mL). An extraction into EtOAc (25 mL) was completed and the organic layer was dried (hydrophobic frit) and concentrated *in vacuo* to yield a crude black oily solid. Purification by automated column chromatography (0-25% EtOAc/3:1

EtOAc:EtOH) yielded 5-(3-(trifluoromethyl)phenyl)pyrimidin-2-ol (**76**) (200 mg, 0.83 mmol, 7%) as a brown solid; ^1H NMR (400 MHz, MeOH- d_4) δ 8.67 (2H, s, 2 x CHN), 7.91-7.89 (1H, m, CCHCCF₃), 7.88-7.84 (1H, m, CHCHCCF₃), 7.70 (1H, d, J = 1.2, CHCCHCCF₃), 7.69-7.68 (1H, m, CHCHCCF₃); ^{13}C NMR (150 MHz, CDCl₃) δ 158.5 (COH), 135.7 (2 x CHN), 132.7 (CCHCCF₃), 131.3 (q, J = 32.2, CCF₃), 130.6 (CHCCHCCF₃), 129.2 (CHCHCCF₃), 125.6 (q, J = 3.6, CCHCCF₃), 123.6 (q, J = 3.6, CHCHCCF₃), 118.8 (CCHN), 123.9 (d, J = 271.8, CF₃); IR (thin film) 1693, 1477 (ArC-C), 1381 (ArC-C), 1328 (ArC-N), 1275 (ArC-N), 1222 (C-O), 1164, 1122, 1077, 1048, 1011, 930, 804, 705 cm^{-1} ; m/z (ES⁺) 241 (100%, [M+H]⁺); HRMS (ES⁺) calcd for C₁₁H₈N₂OF₃ [M+H]⁺ 241.0589, observed 241.0585.

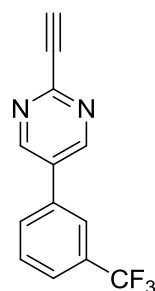
5-(3-(Trifluoromethyl)phenyl)pyrimidin-2-yl trifluoromethanesulfonate (**77**)



N,N-Bis(trifluoromethylsulfonyl)aniline (1.44 g, 3.71 mmol) was added to a stirred solution of 5-(3-(trifluoromethyl)phenyl)pyrimidin-2-ol (**76**) (0.89 g, 3.71 mmol) and K₂CO₃ (1.54 g, 11.1 mmol) in DMF (10 mL) under N₂. The reaction mixture was stirred at 20 °C for 1 h and then quenched with sat. aq. NH₄Cl (5 mL). An extraction into 2-MeTHF (2 x 10 mL) was completed and the combined organic layers were dried (hydrophobic frit) and concentrated *in vacuo* to yield a crude brown oil. Purification by automated column chromatography (0-25% MeOH/*t*-BME) yielded a crude orange oil. Further purification by automated column chromatography (0-25% EtOAc/cyclohexane) yielded a still crude yellow oil. Finally, purification by MDAP (MeCN/H₂O with an (NH₄)HCO₃ modifier) yielded 5-(3-(trifluoromethyl)phenyl)pyrimidin-2-yl trifluoromethanesulfonate (**77**) (96.3 mg, 0.26 mmol, 7%) as a colourless oil; ^1H NMR (400 MHz, MeOH- d_4) δ 9.20 (2H, s, 2 x CHN), 8.10 (1H, s, CCHCCF₃), 8.04 (1H, d, J = 7.8, CHCHCCF₃), 7.85 (1H, d, J

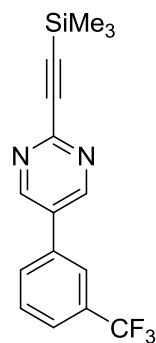
= 7.8, CHCCHCCF₃), 7.78 (1H, d, *J* = 7.8, CHCHCCF₃); ¹³C NMR (100 MHz, MeOH-d₄) δ 159.1 (2 x CHN), 158.0 (OCN), 133.8 (CHCCHCCF₃), 133.7 (CCHCCF₃), 131.5 (q, *J* = 32.8, CCF₃), 130.9 (CHCHCCF₃), 130.1 (CCHN), 125.8 (q, *J* = 3.6, CHCHCCF₃), 123.8 (q, *J* = 3.6, CCHCCF₃), 124.0 (d, *J* = 271.5, CF₃), 113.1 (d, *J* = 271.8, SCF₃); IR (thin film) 3382, 2490, 1414 (ArC-C), 1337 (ArC-C), 1287 (ArC-N), 1214 (C-F), 1127 (S=O), 902 cm⁻¹; m/z (ES+) 373 (86%, [M+H]⁺); HRMS (EI) calcd for C₁₂H₆N₂O₃F₆ [M]⁺ 371.9998, observed 371.9996.

2-Ethynyl-5-(3-(trifluoromethyl)phenyl)pyrimidines (79)



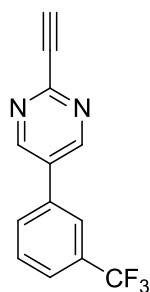
A solution of 5-(3-(trifluoromethyl)phenyl)pyrimidin-2-yl trifluoromethanesulfonate (**77**) (95.0 mg, 0.26 mmol), ethynyltrimethylsilane (0.07 mL, 0.51 mmol), PdCl₂(PPh₃)₂ (9.00 mg, 0.01 mmol), CuI (2.43 mg, 0.01 mmol) and NEt₃ (0.12 mL, 0.77 mmol) in DMSO (0.2 mL) was heated in a sealed microwave vessel at 100 °C for 10 min using a Biotage Initiator 60. Based on LCMS analysis the desired intermediate, 5-(3-(trifluoromethyl)phenyl)-2-((trimethylsilyl)ethynyl)pyrimidine (**78**), had been formed. A solution of NaOH in MeOH (1M, 0.25 mL) was added. The reaction mixture was stirred for 1 h before being acidified with aq. HCl and then basified with solid K₂CO₃. An extraction into *t*-BME (2 x 5 mL) was completed and the combined organic layers dried (hydrophobic frit) and concentrated *in vacuo* to yield 2-ethynyl-5-(3-(trifluoromethyl)phenyl)pyrimidine (**79**) as a crude colourless oil. Purification by MDAP (MeCN/H₂O with a formic acid modifier) yielded no product. The formation of the intermediate and the desired product was assumed based on LCMS analysis.

Data for 5-(3-(trifluoromethyl)phenyl)-2-((trimethylsilyl)ethynyl)pyrimidine (**78**):



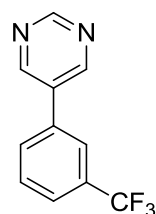
LCMS (System B) Rt. 1.39 min (64%) ES +ve m/z 321 (M+H)⁺

Data for 2-ethynyl-5-(3-(trifluoromethyl)phenyl)pyrimidine (**79**):



LCMS (System B) Rt. 1.04 min (11%) ES +ve m/z 249 (M+H)⁺

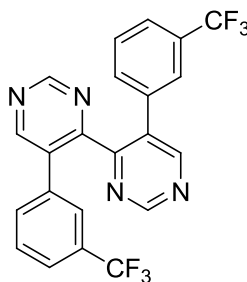
5-(3-(Trifluoromethyl)phenyl)pyrimidine (**80**)



A solution of 5-bromopyrimidine (100 mg, 0.63 mmol), (3-(trifluoromethyl)phenyl)boronic acid (155 mg, 0.82 mmol), PdCl₂(dppf) (23.0 mg, 0.03 mmol) and K₃PO₄ (267 mg, 1.26 mmol) in deoxygenated iPrOH (2 mL) and H₂O (0.5 mL) was heated in a Biotage Initiator 60 to 120 °C for 1 h. Once cooled, the reaction mixture was diluted with H₂O (2 mL). An extraction into EtOAc (5 mL) was completed and the organic layer was dried (hydrophobic frit) and concentrated *in vacuo* to yield a crude brown oily solid. Purification by automated column chromatography (0-100% EtOAc/cyclohexane) yielded 5-(3-(trifluoromethyl)phenyl)pyrimidine (**80**) (143 mg, 0.60 mmol, 96%) as a yellow solid;

^1H NMR (400 MHz, CDCl_3) δ 9.29 (1H, s, NCHN), 9.00 (2H, s, 2 x CHN), 7.87-7.83 (1H, m, CCHCCF₃), 7.82-7.74 (2H, m, CHCHCCF₃ & CHCCHCCF₃), 7.69 (1H, t, J = 7.7, CHCHCCF₃); ^{13}C NMR (150 MHz, CDCl_3) δ 160.5 (NCN), 157.7 (2 x CHN), 140.4 (CCHCCF₃), 133.4 (q, J = 32.2, CCF₃), 132.9 (CCHN), 130.6 (CHCCHCCF₃), 129.2 (CHCHCCF₃), 128.2 (q, J = 3.6, CCHCCF₃), 126.4 (q, J = 3.6, CHCHCCF₃), 124.0 (d, J = 271.8, CF₃); IR (thin film) 1559 (ArC-C), 1407 (ArC-C), 1335 (ArC-N), 1275 (ArC-N), 1172, 1118, 803, 722, 699 cm^{-1} ; m/z (ES+) 225 (97%, $[\text{M}+\text{H}]^+$); HRMS (ES+) calcd for $\text{C}_{11}\text{H}_8\text{N}_2\text{F}_3$ $[\text{M}+\text{H}]^+$ 225.0649, observed 225.0640.

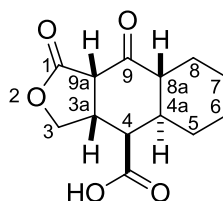
5,5'-Bis(3-(trifluoromethyl)phenyl)-4,4'-bipyrimidine (**81**)



n-BuLi (1.6 M in hexanes) (0.89 mL, 1.43 mmol) was added to a stirred solution of distilled TMP (0.24 mL, 1.43 mmol) in anhydrous 2-MeTHF (1 mL) at -78 °C, under N_2 . The solution was warmed to 0 °C and then re-cooled to -78 °C. A solution of 5-(3-(trifluoromethyl)phenyl)pyrimidine (**80**) (80.0 mg, 0.36 mmol) in anhydrous 2-MeTHF (1 mL) was added dropwise and stirring continued for 2 h at -78 °C. Next, a solution of I_2 (362 mg, 1.43 mmol) in anhydrous 2-MeTHF (1 mL) was added dropwise. The reaction mixture was stirred for a further 1 h and then quenched with sat. aq. NH_4Cl (5 mL). An extraction into 2-MeTHF (2 x 5 mL) was completed and the combined organic layers were dried (hydrophobic frit) and concentrated *in vacuo* to yield a crude brown solid. Purification by automated column chromatography (0-100% EtOAc/cyclohexane) yielded 5,5'-bis(3-(trifluoromethyl)phenyl)-4,4'-bipyrimidine (**81**) (43 mg, 0.10 mmol, 27%) as an orange solid; ^1H NMR (400 MHz, Acetone- d_6) δ 9.38 (2H, s, 2 x NCHN), 8.90 (2H, s, 2 x CHN), 7.67 (2H, d, J = 7.8, 2 x CHCCHCCF₃), 7.48 (2H, t, J = 7.8, 2 x

CHCHCCF₃), 7.12-7.06 (4H, m, 2 x CCHCCF₃ & CHCHCCF₃); ¹³C NMR (150 MHz, CDCl₃) δ 165.9 (NCCN), 163.7 (2 x NCHN), 163.1 (2 x CCHN), 139.7 (2 x CCHCCF₃), 137.6 (CHCCHCCF₃), 137.2 (CCHN), 137.1 (CHCHCCF₃), 136.2 (q, *J* = 32.2, 2 x CCF₃), 134.8 (q, *J* = 3.6, 2 x CCHCCF₃), 130.6 (q, *J* = 3.6, 2 x CHCHCCF₃), 128.9 (q, *J* = 180, 2 x CF₃); IR (thin film) 1571 (ArC-C), 1420 (ArC-C), 1335 (ArC-N), 1213 (ArC-N), 1170, 1118, 905, 808, 702, 597, 521 cm⁻¹; *m/z* (ES⁺) 447 (100%, [M+H]⁺); HRMS (ES⁺) calcd for C₂₂H₁₃N₄F₆ [M+H]⁺ 447.1044, observed 447.1040.

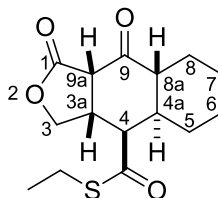
(3a*S,4*R**,4a*R**,8a*R**,9a*S**)-1,9-Dioxododecahydronaphtho[2,3-*c*]furan-4-carboxylic acid (**82**)**



TFA (0.3 mL) was added dropwise to a stirred solution of (3a*S**,4*R**,4a*R**,8a*R**,9a*S**)-*tert*-butyl 1,9-dioxododecahydronaphtho[2,3-*c*]furan-4-carboxylate (**47**) (50.0 mg, 0.16 mmol) in anhydrous CH₂Cl₂ (0.3 mL) at 0 °C, under Ar. The reaction mixture was stirred at RT for 16 h before being concentrated *in vacuo*. The residue was azeotroped with toluene to yield (3a*S**,4*R**,4a*R**,8a*R**,9a*S**)-1,9-dioxododecahydronaphtho[2,3-*c*]furan-4-carboxylic acid (**82**) (40.0 mg, 0.16 mmol, 99%) as a white solid; ¹H NMR (600 MHz, MeOH-d₄) δ 4.43 (1H, dd, *J* = 9.2, 8.3, C³HH), 4.05 (1H, dd, *J* = 9.8, 9.2, C³HH), 3.75 (1H, d, *J* = 9.0, C^{9a}H), 3.37 (1H, ddd, *J* = 9.8, 9.0, 8.3, C^{3a}H), 2.72 (1H, d, *J* = 4.9, C⁴H), 2.69-2.64 (1H, m, C^{8a}H), 1.98-1.95 (1H, m, C⁸HH), 1.98 (1H, dddd, *J* = 13.2, 12.0, 4.9, 3.0, C^{4a}H), 1.87-1.82 (1H, m, C⁵HH), 1.82-1.75 (2H, m, C⁶HH & C⁷HH), 1.44-1.35 (1H, m, C⁵HH), 1.32-1.21 (3H, m, C⁶HH, C⁷HH & C⁸HH); ¹³C NMR (150 MHz, MeOH-d₄) δ 206.3 (C⁹=O), 176.4 (C=OOH), 174.6 (C¹=O), 71.3 (C³H₂), 54.1 (C^{9a}H), 49.4 (C^{8a}H), 44.9 (C⁴H), 41.2 (C^{3a}H), 41.0 (C^{4a}H), 32.5 (C⁵H₂), 27.0 (C⁸H₂), 26.7 (C⁶H₂), 26.3 (C⁷H₂); IR (thin film) 2936 (C-H), 2857 (C-H), 1759 (C=O), 1701

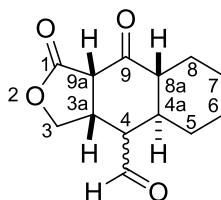
(C=O), 1170, 1000, 839, 800, 719, 645, 549 cm^{-1} ; m/z (ES+) 253 (100%, $[\text{M}+\text{H}]^+$); HRMS (ES-) calcd for $\text{C}_{13}\text{H}_{15}\text{O}_5$ $[\text{M}-\text{H}]^+$ 251.0920, observed 251.0919.

(3a*R,4*R**,4a*R**,8a*R**,9a*S**)-S-Ethyl 1,9-dioxododecahydronaphtho[2,3-c]furan-4-carbothioate (**83**)**



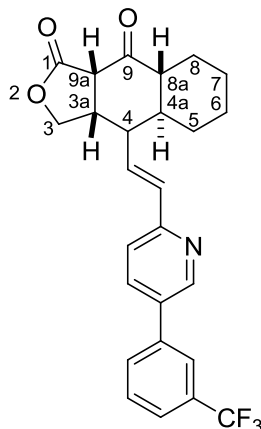
DCC (29.7 mg, 0.14 mmol) was added to a stirred solution of (3a*S**,4*R**,4a*R**,8a*R**,9a*S**)-1,9-dioxododecahydronaphtho[2,3-c]furan-4-carboxylic acid (**82**) (30.0 mg, 0.12 mmol), ethanethiol (26.0 μL , 0.36 mmol) and DMAP (7.00 mg, cat.) in DMF (1 mL) at 0 $^{\circ}\text{C}$, under Ar. The reaction mixture was stirred at 20 $^{\circ}\text{C}$ for 2 h before being diluted with CH_2Cl_2 (10 mL) and washed with H_2O (2 x 5 mL). The organic layer was dried (MgSO_4), filtered and concentrated *in vacuo* to yield a crude pink solid. Purification by column chromatography (0-50% Et_2O /Pet. Ether) yielded (3a*R**,4*R**,4a*R**,8a*R**,9a*S**)-S-ethyl 1,9-dioxododecahydronaphtho[2,3-c]furan-4-carbothioate (**83**) (10.5 mg, 0.035 mmol, 29%) as a white solid; ^1H NMR (600 MHz, CDCl_3) δ 4.38 (1H, dd, $J = 9.0, 8.1$, C^3HH), 3.93 (1H, dd, $J = 10.8, 9.0$, C^3HH), 3.68 (1H, d, $J = 8.7$, C^{9a}H), 3.19 (1H, ddd, $J = 10.9, 8.7, 8.1$, C^{3a}H), 2.94 (2H, qd, $J = 7.5, 2.6$, CH_2CH_3), 2.79 (1H, td, $J = 12.2, 12.0, 3.8$, C^{8a}H), 2.78 (1H, d, $J = 4.5$, C^4H), 2.02-1.97 (1H, m, C^8HH), 1.87 (1H, dddd, $J = 12.2, 12.0, 4.5, 3.8$, C^{4a}H), 1.83-1.75 (3H, m, C^5HH , C^6HH & C^7HH), 1.40-1.32 (1H, m, C^8HH), 1.30 (3H, t, $J = 7.5$, CH_2CH_3), 1.28-1.21 (1H, m, C^5HH), 1.21-1.15 (2H, m, C^6HH & C^7HH); ^{13}C NMR (150 MHz, CDCl_3) δ 203.7 ($\text{C}^9=\text{O}$), 200.4 ($\text{C}=\text{OEt}$), 171.5 ($\text{C}^1=\text{O}$), 69.1 (C^3H_2), 53.1 (C^{9a}H), 51.4 (C^4H), 48.4 (C^{8a}H), 41.2 (C^{4a}H), 40.7 (C^{3a}H), 31.5 (C^5H_2), 25.7 (C^8H_2), 25.6 (C^6H_2), 24.8 (C^7H_2), 24.1 (CH_2CH_3), 14.6 (CH_2CH_3); IR (thin film) 2931 (C-H), 2887 (C-H), 1793 (C=O), 1708 (C=O), 1672 (C=O), 1203, 1137, 982, 897 cm^{-1} ; m/z (ES+) 297 (100%, $[\text{M}+\text{H}]^+$); HRMS (ES-) calcd for $\text{C}_{15}\text{H}_{19}\text{O}_4\text{S}$ $[\text{M}-\text{H}]^+$ 295.1003, observed 295.1004.

(3aS*,4aS*,8aR*,9aS*)-1,9-Dioxododecahydronaphtho[2,3-c]furan-4-carbaldehyde (84)



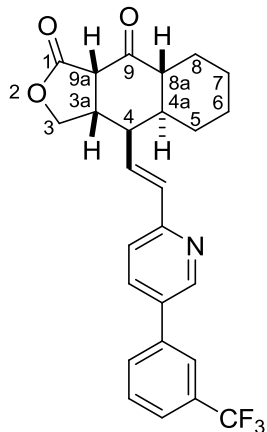
Neat triethylsilane (15 μ L, 0.09 mmol) was added to a stirred suspension of (3aR*,4R*,4aR*,8aR*,9aS*)-S-ethyl 1,9-dioxododecahydronaphtho[2,3-c]furan-4-carbothioate (**83**) (10.0 mg, 0.03 mmol), palladium on carbon (4.00 mg, 0.003 mmol) in degassed acetone (0.2 mL). The reaction mixture was stirred at 20 $^{\circ}$ C for 16 h before being filtered over celite and concentrated *in vacuo*. Purification by flash column chromatography (0-2% Et₂O/CH₂Cl₂) gave partial racemisation at C⁴ to yield (3aS*,4aS*,8aR*,9aS*)-1,9-dioxododecahydronaphtho[2,3-c]furan-4-carbaldehyde (**84**) (4S:4R; 0.7:1) (7.00 mg, 0.03 mmol, 99%) as a white solid; ¹H NMR (600 MHz, CDCl₃) δ 10.11 (1H, s, 4S-CHO), 9.90 (1H, d, *J* = 1.5, 4R-CHO), 4.47-4.44 (1H, m, 4R-C³HH), 4.38 (1H, dd, *J* = 9.0, 7.9, 4S-C³HH), 4.04-3.96 (2H, m, 4R-C³HH & 4S-C³HH), 3.61 (1H, d, *J* = 9.0, 4S-C^{9a}H), 3.47-3.40 (3H, m, 4R-C^{9a}H, 4R-C^{3a}H & 4S-C^{3a}H), 3.09 (1H, dd, *J* = 11.7, 3.0, 4R-C⁴H), 2.83 (1H, d, *J* = 4.5, 4S-C⁴H), 2.22 (1H, td, *J* = 11.7, 3.4, 4R-C^{8a}H), 2.17 (1H, td, *J* = 11.7, 3.8, 4S-C^{8a}H), 2.11-1.94 (6H, m, 4R-C^{4a}H, 4S-C^{4a}H, 4R-C⁷HH, 4S-C⁷HH, 4R-C⁸HH & 4S-C⁸HH), 1.90-1.74 (3H, m, 4R-C⁵HH, 4R-C⁷HH & 4S-C⁷HH), 1.71-1.63 (1H, m, 4S-C⁵HH), 1.47-1.39 (1H, m, 4R-C⁸HH), 1.37-1.15 (7H, m, 4R-C⁵HH, 4S-C⁵HH, 4R-C⁶HH, 4S-C⁶HH, 4R-C⁷HH, 4S-C⁷HH & 4S-C⁸HH); ¹³C NMR (150 MHz, CDCl₃) δ 202.8 (4S-C⁹=O), 202.8 (4R-C⁹=O), 202.6 (4R-CHO), 201.3 (4S-CHO), 171.4 (4R-C¹=O), 171.0 (4S-C¹=O), 69.4 (4R-C³H₂), 68.0 (4S-C³H₂), 54.0 (4S-C^{9a}H), 52.9 (4S-C⁴H), 52.9 (4R-C^{9a}H), 52.6 (4S-C^{8a}H), 50.0 (4R-C⁴H), 49.4 (4R-C^{8a}H), 41.0 (4R-C^{4a}H), 40.2 (4S-C^{4a}H), 39.0 (4S-C^{3a}H), 36.8 (4R-C^{3a}H), 32.0 (4S-C⁵H₂), 30.6 (4R-C⁵H₂), 26.0 (4R-C⁸H₂), 25.7 (4S-C⁸H₂), 24.9 (4S-C⁶H₂ & 4R-C⁶H₂), 24.8 (4R-C⁷H₂), 24.6 (4S-C⁷H₂); IR (thin film) 2928 (C-H), 2858 (C-H), 1779 (C=O), 1705 (C=O), 1208, 1165, 1120, 1016, 750 cm⁻¹; *m/z* (ES⁺) 237 (100%, [M+H]⁺); HRMS (EI) calcd for C₁₃H₁₆O₄ [M-H]⁺ 236.1043, observed 236.1044.

(3aS*,4aS*,8aR*,9aS*)-4-((E)-2-(5-(3-(Trifluoromethyl)phenyl)pyridin-2-yl)vinyl)octahydronaphtho[2,3-c]furan-1,9(3H,9aH)-dione (85)



n-BuLi (1.6 M in hexanes) (144 μ L, 0.23 mmol) was added dropwise to a stirred solution of diethyl ((5-(3-(trifluoromethyl)phenyl)pyridin-2-yl)methyl)phosphonate (**28**) (79.0 mg, 0.21 mmol) in anhydrous THF (1 mL) at 0 °C, under Ar. The solution was stirred at 0 °C for 10 min before a solution of (3aS*,4aS*,8aR*,9aS*)-1,9-dioxododecahydronaphtho[2,3-c]furan-4-carbaldehyde (**84**) (50 mg, 0.21 mmol) in anhydrous THF (1 mL) was added. The reaction mixture was stirred at 0 °C for 45 min and then quenched with sat. aq. NH₄Cl (10 mL). An extraction into EtOAc (2 x 5 mL) was completed and the combined organic layers were dried (MgSO₄), filtered and concentrated *in vacuo* to yield a crude yellow gum. Purification by flash column chromatography (0-2% Et₂O/CH₂Cl₂) yielded (3aS*,4aS*,8aR*,9aS*)-4-((E)-2-(5-(3-(trifluoromethyl)phenyl)pyridin-2-yl)vinyl)octahydronaphtho[2,3-c]furan-1,9(3H,9aH)-dione (**85**) as a mixture of isomers. Purification by preparative TLC (0-2% Et₂O/CH₂Cl₂) yielded (3aS*,4R*,4aS*,8aR*,9aS*)-4-((E)-2-(5-(3-(trifluoromethyl)phenyl)pyridin-2-yl)vinyl)octahydronaphtho[2,3-c]furan-1,9(3H,9aH)-dione (**86**) (47.3 mg, 0.10 mmol, 49%) and (3aS*,4S*,4aS*,8aR*,9aS*)-4-((E)-2-(5-(3-(trifluoromethyl)phenyl)pyridin-2-yl)vinyl)octahydronaphtho[2,3-c]furan-1,9(3H,9aH)-dione (**87**) (24.5 mg, 0.05 mmol, 26%) as white solids.

Data for (3a*S**,4*R**,4a*S**,8a*R**,9a*S**)-4-((*E*)-2-(5-(3-(trifluoromethyl)phenyl)pyridin-2-yl)vinyl)octahydronaphtho[2,3-*c*]furan-1,9(3*H*,9a*H*)-dione (**86**):

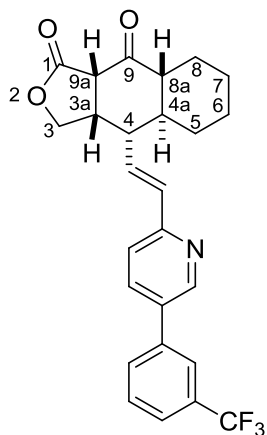


^1H NMR (600 MHz, CDCl_3) δ 8.82 (1H, s, CHN), 7.88 (1H, dd, $J = 7.9, 2.3$, CHCCHN), 7.82 (1H, s, CHCCF₃), 7.77 (1H, d, $J = 7.9$, CHCCHCCF₃), 7.67 (1H, d, $J = 7.5$, CHCHCCF₃), 7.62 (1H, t, $J = 7.5$, CHCHCCF₃), 7.34 (1H, d, $J = 8.3$, CHCN), 7.08 (1H, dd, $J = 15.4, 9.8$, CH=CH), 6.65 (1H, d, $J = 15.1$, CH=CH), 4.47 (1H, t, $J = 8.5$, C³HH), 4.11 (1H, t, $J = 9.8$, C³HH), 3.61 (1H, d, $J = 9.0$, C^{9a}H), 3.23 (1H, ddd, $J = 9.8, 9.0, 8.5$, C^{3a}H), 2.60 (1H, dd, $J = 9.8, 3.6$, C⁴H), 2.42 (1H, td, $J = 12.2, 3.6$, C^{8a}H), 2.07-2.02 (1H, m, C⁸HH), 1.91 (1H, tt, $J = 12.2, 3.6$, C^{4a}H), 1.83-1.78 (1H, m, C⁷HH), 1.78-1.73 (1H, m, C⁶HH), 1.72-1.67 (1H, m, C⁵HH), 1.48-1.40 (2H, m, C⁸HH), 1.40-1.34 (1H, m, C⁵HH), 1.23-1.15 (2H, m, C⁶HH & C⁷HH); ^{13}C NMR (150 MHz, CDCl_3) δ 203.8 (C⁹=O), 171.6 (C¹=O), 154.0 (CN), 148.2 (CHN), 138.4 (CCHCCF₃), 135.3 (CHCCHN), 134.2 (CCHN), 132.7 (CH=CH), 132.4 (CH=CH), 131.8 (q, $J = 32.1$, CCF₃), 130.3 (CHCCHCCF₃), 129.8 (CHCHCCF₃), 125.0 (q, $J = 3.6$, CCHCCF₃), 123.8 (q, $J = 3.6$, CHCHCCF₃), 124.1 (d, $J = 271.7$, CF₃), 122.3 (CHCN), 70.0 (C³H₂), 52.5 (C^{9a}H), 48.5 (C^{8a}H), 43.5 (C^{3a}H), 42.1 (C⁴H), 41.6 (C^{4a}H), 31.7 (C⁵H₂), 25.8 (C⁸H₂), 25.5 (C⁶H₂), 25.0 (C⁷H₂); IR (thin film) 2930 (C-H), 2855 (C-H), 1784 (C=O), 1708 (C=O), 1478, 1440, 1335, 1164, 1124, 1018, 755 cm^{-1} ; m/z (ES⁺) 456 (100%, [M+H]⁺); HRMS (ES⁻) calcd for C₂₆H₂₃NO₃F₃ [M-H]⁺ 454.1631, observed 454.1630.

Purification by chiral column chromatography gave (+)-(3a*S*,4*R*,4a*S*,8a*R*,9a*S*)-4-((*E*)-2-(5-(3-(trifluoromethyl)phenyl)pyridin-2-yl)vinyl)octahydronaphtho[2,3-*c*]furan-

1,9(3H,9aH)-dione ((+)-**86**) with an $[\alpha]_D^{25} = +13.2$ (MeOH) and (-)-(3a*S*,4*R*,4a*S*,8a*R*,9a*S*)-4-((*E*)-2-(5-(3-(trifluoromethyl)phenyl)pyridin-2-yl)vinyl)octahydronaphtho[2,3-*c*]furan-1,9(3H,9aH)-dione ((-)-**86**) with an $[\alpha]_D^{25} = -13.4$ (MeOH).

Data for (3a*S**,4*S**,4a*S**,8a*R**,9a*S**)-4-((*E*)-2-(5-(3-(trifluoromethyl)phenyl)pyridin-2-yl)vinyl)octahydronaphtho[2,3-*c*]furan-1,9(3H,9aH)-dione (**87**):

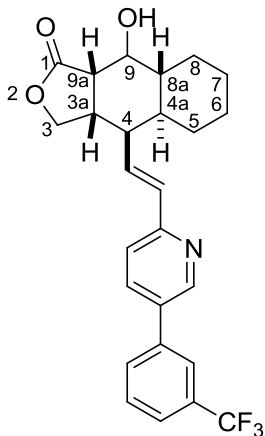


^1H NMR (600 MHz, CDCl_3) δ 8.79 (1H, d, $J = 2.3$, CHN), 7.87 (1H, dd, $J = 8.1, 2.3$, CHCCHN), 7.81 (1H, s, CHCCF₃), 7.76 (1H, d, $J = 7.5$, CHCCHCCF₃), 7.67 (1H, d, $J = 7.5$, CHCHCCF₃), 7.61 (1H, t, $J = 7.5$, CHCHCCF₃), 7.32 (1H, d, $J = 8.3$, CHCN), 6.70 (1H, d, $J = 15.4$, CH=CH), 6.49 (1H, dd, $J = 15.4, 9.8$, CH=CH), 4.43 (1H, dd, $J = 9.0, 8.3$, C³HH), 4.15 (1H, dd, $J = 11.7, 9.0$, C³HH), 3.51 (1H, d, $J = 8.7$, C^{9a}H), 3.32 (1H, dddd, $J = 11.7, 8.7, 8.3, 5.6$, C^{3a}H), 2.87 (1H, ddd, $J = 11.3, 9.8, 5.6$, C⁴H), 2.21 (1H, td, $J = 11.7, 3.0$, C^{8a}H), 2.00-1.93 (2H, m, C⁵HH & C⁸HH), 1.87-1.82 (1H, m, C⁷HH), 1.75 (2H, qd, $J = 11.3, 3.4$, C^{4a}H & C⁶HH), 1.49-1.40 (1H, m, C⁸HH), 1.28-1.15 (2H, m, C⁶HH & C⁷HH), 1.13-1.05 (1H, m, C⁵HH); ^{13}C NMR (150 MHz, CDCl_3) δ 203.8 (C⁹=O), 171.7 (C¹=O), 153.9 (CN), 148.2 (CHN), 138.4 (CCHCCF₃), 135.2 (CHCCHN), 134.2 (CCHN), 133.2 (CH=CH), 132.4 (CH=CH), 131.8 (q, $J = 32.1$, CCF₃), 130.3 (CHCCHCCF₃), 129.8 (CHCHCCF₃), 125.0 (q, $J = 3.6$, CHCHCCF₃), 123.8 (q, $J = 3.6$, CCHCCF₃), 124.7 (d, $J = 272.0$, CF₃), 122.0 (CHCN), 68.2 (C³H₂), 54.7 (C^{9a}H), 52.9 (C^{8a}H), 45.3 (C⁴H), 44.6 (C^{3a}H), 42.9 (C^{4a}H), 33.0 (C⁵H₂), 25.2 (C⁸H₂), 24.9 (C⁶H₂), 24.8 (C⁷H₂); IR (thin film) 2923 (C-H), 2853 (C-H), 1782 (C=O), 1703 (C=O), 1333, 1160, 1119, 1074,

1010, 801, 699 cm^{-1} ; m/z (ES+) 456 (100%, $[\text{M}+\text{H}]^+$); HRMS (ES⁻) calcd for $\text{C}_{26}\text{H}_{23}\text{NO}_3\text{F}_3$ $[\text{M}-\text{H}]^+$ 454.1616, observed 454.1630.

Purification by chiral column chromatography gave (+)-(3aS,4S,4aS,8aR,9aS)-4-((E)-2-(5-(3-(trifluoromethyl)phenyl)pyridin-2-yl)vinyl)octahydronaphtho[2,3-c]furan-1,9(3H,9aH)-dione ((+)-**87**) with an $[\alpha]_{\text{D}}^{25} = +30.4$ (MeOH) and (-)-(3aS,4S,4aS,8aR,9aS)-4-((E)-2-(5-(3-(trifluoromethyl)phenyl)pyridin-2-yl)vinyl)octahydronaphtho[2,3-c]furan-1,9(3H,9aH)-dione ((-)-**87**) with an $[\alpha]_{\text{D}}^{25} = -31.6$ (MeOH).

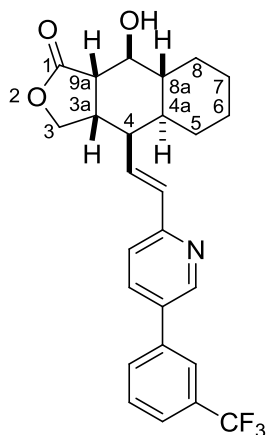
(3aS*,4R*,4aS*,8aR*,9aS*)-9-Hydroxy-4-((E)-2-(5-(3-(trifluoromethyl)phenyl)pyridin-2-yl)vinyl)decahydronaphtho[2,3-c]furan-1(3H)-one (88)



NaBH_4 (0.58 mg, 0.015 mmol) was added to a stirred solution of (3aS*,4R*,4aS*,8aR*,9aS*)-4-((E)-2-(5-(3-(trifluoromethyl)phenyl)pyridin-2-yl)vinyl)octahydronaphtho[2,3-c]furan-1,9(3H,9aH)-dione (**86**) (6.4 mg, 0.014 mmol) in anhydrous THF (0.5 mL) and MeOH (0.5 mL) at 0 °C, under Ar. The reaction mixture was stirred at 0 °C for 15 min and then quenched with sat. aq. NH_4Cl (0.5 mL). An extraction into Et_2O (5 mL) was completed and the organic layer was dried (MgSO_4), filtered and concentrated *in vacuo* to yield a crude yellow gum. Purification by flash column chromatography (0-2% $\text{Et}_2\text{O}/\text{CH}_2\text{Cl}_2$) yielded (3aS*,4R*,4aS*,8aR*,9aS*)-9-hydroxy-4-((E)-2-(5-(3-(trifluoromethyl)phenyl)pyridin-2-yl)vinyl)decahydronaphtho[2,3-c]furan-1(3H)-one

(**88**) as a mixture of isomers. Purification by preparative TLC (0-2% Et₂O/CH₂Cl₂) yielded (3aS*,4R*,4aS*,8aR*,9S*,9aS*)-9-hydroxy-4-((E)-2-(5-(3-(trifluoromethyl)phenyl)pyridin-2-yl)vinyl)decahydronaphtho[2,3-c]furan-1(3H)-one (**89**) (1.56 mg, 0.0034 mmol, 24%) and (3aS*,4R*,4aS*,8aR*,9R*,9aS*)-9-hydroxy-4-((E)-2-(5-(3-(trifluoromethyl)phenyl)pyridin-2-yl)vinyl)decahydronaphtho[2,3-c]furan-1(3H)-one (**90**) (0.48 mg, 0.001 mmol, 8%) as white solids.

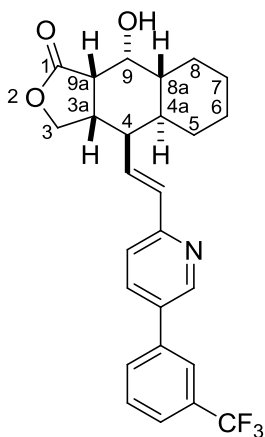
Data for (3aS*,4R*,4aS*,8aR*,9S*,9aS*)-9-hydroxy-4-((E)-2-(5-(3-(trifluoromethyl)phenyl)pyridin-2-yl)vinyl)decahydronaphtho[2,3-c]furan-1(3H)-one (**89**):



¹H NMR (600 MHz, CDCl₃) δ 8.80 (1H, d, *J* = 1.9, CHN), 7.86 (1H, dd, *J* = 7.9, 1.9, CHCCHN), 7.81 (1H, s, CHCCF₃), 7.77 (1H, d, *J* = 7.5, CHCCHCCF₃), 7.66 (1H, d, *J* = 7.5, CHCHCCF₃), 7.61 (1H, t, *J* = 7.5, CHCHCCF₃), 7.34 (1H, d, *J* = 8.3, CHCN), 6.89 (1H, dd, *J* = 15.2, 10.0, CH=CH), 6.54 (1H, d, *J* = 15.2, CH=CH), 4.44 (1H, t, *J* = 8.7, C³HH), 4.17 (1H, dd, *J* = 11.7, 8.7, C³HH), 3.46 (1H, t, *J* = 10.0, C⁹H), 2.87 (1H, dt, *J* = 11.3, 8.7, C^{3a}H), 2.69 (1H, dd, *J* = 9.6, 8.1, C^{9a}H), 2.50 (1H, d, *J* = 1.5, OH), 2.41 (1H, dd, *J* = 9.8, 3.8, C⁴H), 2.36-2.31 (1H, m, C⁸HH), 1.78-1.72 (2H, m, C⁶HH & C⁷HH), 1.55-1.45 (3H, m, C^{4a}H, C⁵HH & C^{8a}H), 1.37-1.17 (4H, m, C⁵HH, C⁶HH, C⁷HH & C⁸HH); ¹³C NMR (150 MHz, CDCl₃) δ 178.6 (C¹=O), 154.6 (CN), 148.2 (CHN), 138.6 (CCHCCF₃), 135.1 (CHCCHN), 134.4 (CH=CH), 133.8 (CCHN), 131.6 (CH=CH), 131.7 (q, *J* = 32.1, CCF₃), 130.3 (CHCCHCCF₃), 129.8 (CHCHCCF₃), 124.9 (q, *J* = 3.6, CHCHCCF₃), 123.8 (q, *J* = 3.6, CCHCCF₃), 124.1 (d, *J* = 272.4, CF₃), 121.7 (CHCN), 72.9 (C⁹H), 70.0 (C³H₂), 46.0 (C^{9a}H),

41.4 ($C^{3a}H$), 41.3 (C^4H), 38.8 ($C^{4a}H$), 38.3 ($C^{8a}H$), 31.1 (C^5H_2), 29.0 (C^6H_2 & C^7H_2), 26.1 (C^8H_2); IR (thin film) 2924 (C-H), 2853 (C-H), 1773 (C=O), 1441, 1334, 1266, 1165, 1123, 1010, 753 cm^{-1} ; m/z (ES+) 458 (100%, $[M+H]^+$); HRMS (ES+) calcd for $C_{26}H_{27}NO_3F_3$ $[M]^+$ 458.1943, observed 458.1947.

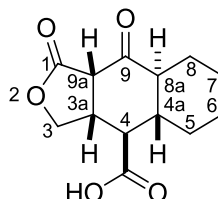
Data for (3a*S**,4*R**,4a*S**,8a*R**,9*R**,9a*S**)-9-hydroxy-4-((*E*)-2-(5-(3-(trifluoromethyl)phenyl)pyridin-2-yl)vinyl)decahydronaphtho[2,3-*c*]furan-1(3*H*)-one (90):



1H NMR (600 MHz, $CDCl_3$) δ 8.79 (1H, d, $J = 2.3$, CHN), 7.85 (1H, dd, $J = 8.3, 2.3$, $CHCCHN$), 7.81 (1H, s, $CHCCF_3$), 7.76 (1H, d, $J = 7.5$, $CHCHCCF_3$), 7.66 (1H, d, $J = 7.9$, $CHCCHCCF_3$), 7.61 (1H, t, $J = 7.9$, $CHCHCCF_3$), 7.31 (1H, d, $J = 7.9$, $CHCN$), 6.88 (1H, dd, $J = 15.4, 9.8$, $CH=CH$), 6.52 (1H, d, $J = 15.4$, $CH=CH$), 4.36 (2H, d, $J = 9.8$, C^3H_2), 4.11 (1H, t, $J = 4.3$, C^9H), 2.87 (1H, dd, $J = 8.3, 4.9$, $C^{9a}H$), 2.74 (1H, td, $J = 9.8, 8.3$, $C^{3a}H$), 2.51 (1H, dd, $J = 9.8, 5.3$, C^4H), 2.00 (1H, d, $J = 4.5$, OH), 1.99-1.94 (1H, m, $C^{4a}H$), 1.79-1.70 (2H, m, C^7HH & C^8HH), 1.61-1.55 (2H, m, C^5HH , C^6HH & $C^{8a}H$), 1.32-1.20 (4H, m, C^5HH , C^6HH , C^7HH & C^8HH); ^{13}C NMR (150 MHz, $CDCl_3$) δ 178.2 ($C^1=O$), 154.7 (CN), 148.2 (CHN), 138.6 ($CCHCCF_3$), 135.1 ($CHCCHN$ & $CH=CH$), 133.7 (CCHN), 131.0 ($CH=CH$), 130.9 (q, $J = 32.8$, CCF_3), 130.3 ($CHCCHCCF_3$), 129.8 ($CHCHCCF_3$), 124.8 (q, $J = 3.8$, $CHCHCCF_3$), 123.8 (q, $J = 3.8$, $CCHCCF_3$), 124.1 (d, $J = 272.4$, CF_3), 121.9 (CHCN), 71.4 (C^3H_2), 69.2 (C^9HOH), 44.1 ($C^{9a}H$), 41.5 (C^4H), 40.3 ($C^{3a}H$), 38.6 ($C^{8a}H_2$), 31.5 ($C^{4a}H$), 29.8 (C^5H_2), 28.9 (C^8H_2), 26.4 (C^6H_2), 26.1 (C^7H_2); IR (thin film) 2925 (C-H), 2854 (C-H), 1755 (C=O), 1334, 1266, 1165, 1126, 1010, 753 cm^{-1}

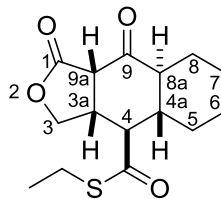
¹; m/z (ES+) 458 (100%, [M+H]⁺); HRMS (ES+) calcd for C₂₆H₂₇NO₃F₃ [M]⁺ 458.1943, observed 458.1951.

(3aS*,4R*,4aS*,8aS*,9aS*)-1,9-Dioxododecahydronaphtho[2,3-c]furan-4-carboxylic acid (91)



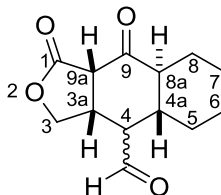
TFA (3.00 mL, 38.9 mmol) was added to a stirred solution of (3aS*,4R*,4aS*,8aS*,9aS*)-*tert*-butyl 1,9-dioxododecahydronaphtho[2,3-c]furan-4-carboxylate (**45**) (1.09 g, 3.53 mmol) in CH₂Cl₂ (6 mL) at 0 °C, under N₂. The reaction mixture was stirred at 20 °C for 16 h before being concentrated *in vacuo*. The residue was azeotroped with toluene (25 mL) to yield a crude pink solid. Purification by trituration (CH₂Cl₂) yielded (3aS*,4R*,4aS*,8aS*,9aS*)-1,9-dioxododecahydronaphtho[2,3-c]furan-4-carboxylic acid (**91**) (441 mg, 1.75 mmol, 49%) as a white solid; ¹H NMR (600 MHz, CDCl₃) δ 4.33 (1H, dd, *J* = 9.8, C³HH), 4.27 (1H, dd, *J* = 9.8, 4.5, C³HH), 3.55 (1H, d, *J* = 7.9, C^{9a}H), 3.22 (1H, ddd, *J* = 11.8, 7.4, 4.5, C^{3a}H), 2.57 (1H, t, *J* = 11.5, C^{3a}H), 2.19-2.12 (1H, m, C⁸HH), 2.06-2.01 (1H, m, C^{8a}H), 1.89-1.82 (2H, m, C⁶HH & C⁷HH), 1.81-1.73 (2H, m, C⁵HH & C^{4a}H), 1.26-1.18 (4H, m, C⁵HH, C⁶HH, C⁷HH & C⁸HH); ¹³C NMR (150 MHz, CDCl₃) δ 201.5 (C⁹=O), 177.5 (C=OOH), 171.2 (C¹=O), 70.6 (C³H₂), 53.2 (C^{9a}H), 51.1 (C⁴H), 49.9 (C^{8a}H), 42.5 (C^{3a}H), 42.4 (C^{4a}H), 31.8 (C⁵H₂), 25.1 (C⁸H₂), 25.0 (C⁶H₂), 24.7 (C⁷H₂); IR (thin film) 2930 (C-H), 2869 (C-H), 1779 (C=O), 1705 (C=O), 1171, 1166, 1018 cm⁻¹; m/z (ES+) 253 (100%, [M+H]⁺); HRMS (EI) calcd for C₁₃H₁₆O₅ [M]⁺ 252.0992, observed 252.0982.

(3aR*,4R*,4aS*,8aS*,9aS*)-S-Ethyl 1,9-dioxododecahydronaphtho[2,3-c]furan-4-carbothioate (92)



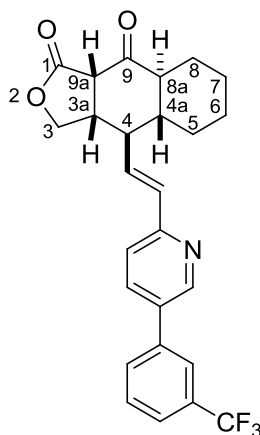
EDCI (502 mg, 2.62 mmol) was added to a stirred solution of (3aS*,4R*,4aS*,8aS*,9aS*)-1,9-dioxododecahydronaphtho[2,3-c]furan-4-carboxylic acid (**91**) (440 mg, 1.74 mmol), ethanethiol (0.52 mL, 6.98 mmol) and DMAP (21.3 mg, 0.17 mmol) in CH₂Cl₂ (20 mL) under N₂. The reaction mixture was stirred at 20 °C for 2 h and then quenched with sat. aq. NH₄Cl (10 mL). An extraction into CH₂Cl₂ (10 mL) was completed and the organic layer was dried (hydrophobic frit) and concentrated *in vacuo* to yield (3aR*,4R*,4aS*,8aS*,9aS*)-S-ethyl 1,9-dioxododecahydronaphtho[2,3-c]furan-4-carbothioate (**92**) (482 mg, 1.62 mmol, 93%) as an off-white solid; ¹H NMR (600 MHz, CDCl₃) δ 4.38 (1H, d, *J* = 9.6, C³HH), 4.18 (1H, dd, *J* = 9.6, 4.7, C³HH), 3.51 (1H, d, *J* = 7.5, C^{9a}H), 3.21 (1H, ddd, *J* = 11.6, 7.4, 4.7, C^{3a}H), 3.02-2.89 (2H, m, CH₂CH₃), 2.70 (1H, t, *J* = 11.1, C⁴H), 2.15-2.10 (1H, m, C³HH), 2.02 (1H, td, *J* = 11.2, 3.2, C^{8a}H), 1.85-1.69 (4H, m, C^{4a}H, C⁵HH, C⁶HH & C⁷HH), 1.30-1.27 (3H, m, CH₂CH₃), 1.27-1.09 (4H, m, C⁵HH, C⁶HH, C⁷HH & C⁸HH); ¹³C NMR (150 MHz, CDCl₃) δ 201.9 (C⁹=O), 201.6 (C=OSET), 171.4 (C¹=O), 70.6 (C³H₂), 54.9 (C^{9a}H), 51.1 (C⁴H), 49.7 (C^{8a}H), 41.9 (C^{4a}H), 39.1 (C^{3a}H), 31.8 (C⁵H₂), 25.1 (C⁸H₂), 25.0 (C⁶H₂), 24.7 (C⁷H₂), 24.6 (CH₂CH₃), 14.2 (CH₂CH₃); IR (thin film) 2930 (C-H), 2876 (C-H), 1783 (C=O), 1706 (C=O), 1671 (C=O), 1448, 1362, 1203, 1137, 1012, 981, 896 cm⁻¹; *m/z* (ES⁺) 297 (100%, [M+H]⁺); HRMS (EI) calcd for C₁₅H₂₀O₄S [M]⁺ 296.1077, observed 296.1076.

(3aS*,4aR*,8aS*,9aS*)-1,9-dioxododecahydronaphtho[2,3-c]furan-4-carbaldehyde (93**)**



Neat triethylsilane (1.02 mL, 6.41 mmol) was added to a stirred solution of (3aR*,4R*,4aS*,8aS*,9aS*)-S-ethyl 1,9-dioxododecahydronaphtho[2,3-c]furan-4-carbothioate (**92**) (475 mg, 1.60 mmol), palladium on carbon (171 mg, 1.60 mmol) and MgSO₄ (to dry) in anhydrous, degassed acetone (25 mL) under N₂. The reaction mixture was stirred at 20 °C for 16 h before being filtered over celite and concentrated *in vacuo*. Purification by flash column chromatography (0-100% EtOAc/cyclohexane) gave partial racemisation at C⁴ to yield (3aS*,4aR*,8aS*,9aS*)-1,9-dioxododecahydronaphtho[2,3-c]furan-4-carbaldehyde (**93**) (4S*:4R*, 1:6) (130 mg, 0.55 mmol, 34%) as a colourless oil; ¹H NMR (600 MHz, CDCl₃) δ 9.90-9.89 (1H, m, 4S*-CHO), 9.83 (1H, d, *J* = 2.8, 4R*-CHO), 4.26 (1H, dd, *J* = 9.8, 4.7, 4R-C³HH), 4.20 (1H, d, *J* = 9.6, 4R*-C³HH), 3.56 (1H, d, *J* = 7.8, 4R*-C^{9a}H), 3.22 (1H, ddd, *J* = 11.6, 7.5, 4.5, 4R*-C^{3a}H), 2.57 (1H, td, *J* = 11.4, 2.9, 4R*-C⁴H), 2.18-2.11 (2H, m, 4R*-C⁸HH & 4R*-C^{8a}H), 2.04-1.97 (2H, m, 4R*-C⁶HH & 4R*-C⁷HH), 1.89-1.77 (2H, m, 4R*-C⁵HH & 4R*-C^{4a}H), 1.40-1.35 (1H, m, 4R*-C⁸HH), 1.32-1.19 (3H, m, 4R*-C⁵HH, 4R*-C⁶HH & 4R*-C⁷HH); ¹³C NMR (150 MHz, CDCl₃) δ 201.6 (4R*-C⁹=O), 201.3 (4R*-CHO), 168.7 (4R*-C¹=O), 70.4 (4R*-C³H₂), 54.8 (4R*-C⁴H), 52.9 (4R*-C^{9a}H), 51.1 (4R*-C^{8a}H), 41.8 (4R*-C^{4a}H), 39.1 (4R*-C^{3a}H), 31.7 (4R*-C⁵H₂), 24.9 (4R*-C⁸H₂ & 4R*-C⁶H₂), 24.5 (4R*-C⁷H₂), 19.1 (4R*-C³HCH₃); IR (thin film) 2927 (C-H), 2855 (C-H), 1770 (C=O), 1713 (C=O), 1125, 730 cm⁻¹; m/z (ES+) 237 (100%, [M+H]⁺); HRMS (EI) calcd for C₁₃H₁₆O₄ [M]⁺ 236.1043, observed 236.1049.

(3aS*,4R*,4aR*,8aS*,9aS*)-4-((E)-2-(5-(3-(Trifluoromethyl)phenyl)pyridin-2-yl)vinyl)octahydronaphtho[2,3-c]furan-1,9(3H,9aH)-dione (94)

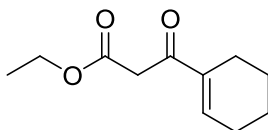


n-BuLi (2.7 M in heptanes) (0.25 mL, 0.66 mmol) was added dropwise to a stirred solution of diethyl (5-(3-(trifluoromethyl)phenyl)pyridin-2-yl)methylphosphonate (**28**) (226 mg, 0.60 mmol) in anhydrous 2-MeTHF (10 mL) at 0 °C, under N₂. The solution was stirred at 0 °C for 10 min before a solution of (3a*S**,4a*R**,8a*S**,9a*S**)-1,9-dioxododecahydronaphtho[2,3-*c*]furan-4-carbaldehyde (**93**) (130 mg, 0.55 mmol) in anhydrous 2-MeTHF (10 mL) was added. The reaction mixture was stirred at 0 °C for a further 1 h and then quenched with sat. aq. NH₄Cl (5 mL). An extraction into EtOAc (10 mL) was completed and the organic phase was washed with sat. aq. brine (5 mL), dried (hydrophobic frit) and concentrated *in vacuo* to yield a crude yellow gum. Purification by automated column chromatography (0-100% EtOAc/cyclohexane) yielded (3a*S**,4*R**,4a*R**,8a*S**,9a*S**)-4-((*E*)-2-(5-(3-(trifluoromethyl)phenyl)pyridin-2-yl)vinyl)octahydronaphtho[2,3-*c*]furan-1,9(3*H*,9a*H*)-dione (**94**) (76.0 mg, 0.17 mmol, 25 %) as a yellow glass; ¹H NMR (600 MHz, CDCl₃) δ 8.82 (1H, d, *J* = 2.0, *CHN*), 7.90 (1H, dd, *J* = 8.1, 2.4, *CHCCHN*), 7.83 (1H, s, *CHCCF*₃), 7.78 (1H, d, *J* = 7.6, *CHCCHCCF*₃), 7.69 (1H, d, *J* = 7.8, *CHCHCCF*₃), 7.63 (1H, t, *J* = 7.6, *CHCHCCF*₃), 7.36 (1H, dd, *J* = 8.2, 0.6, *CHCN*), 6.70 (1H, d, *J* = 15.4, *CH=CH*), 6.56 (1H, dd, *J* = 15.4, 9.4, *CH=CH*), 4.37 (1H, d, *J* = 9.4, *C*³*HH*), 4.20 (1H, dd, *J* = 9.4, 4.8, *C*³*HH*), 3.58 (1H, d, *J* = 7.4, *C*^{9a}*H*), 2.85 (1H, ddd, *J* = 11.1, 7.4, 4.8, *C*^{3a}*H*), 2.34 (1H, td, *J* = 11.1, 9.4, *C*⁴*H*), 2.20-2.08 (1H, m, *C*^{8a}*H* & *C*⁸*HH*), 2.02-1.94 (1H, m, *C*⁵*HH*), 1.86-1.66 (2H, m, *C*⁶*HH* & *C*⁷*HH*), 1.56 (1H, qd, *J* = 11.2, 3.4, *C*^{4a}*H*), 1.34-1.00 (4H, m, *C*⁵*HH*, *C*⁶*HH*, *C*⁷*HH* & *C*⁸*HH*); ¹³C NMR (150 MHz, CDCl₃) δ 203.0 (*C*⁹=O), 172.1 (*C*¹=O), 152.6

(CN), 147.8 (CHN), 138.2 (CCHCCF₃), 134.7 (CHCCHN), 134.4 (CCHN), 134.3 (CH=CH), 131.9 (CH=CH), 131.8 (q, *J* = 32.1, CCF₃), 130.3 (CHCCHCCF₃), 129.9 (CHCHCCF₃), 125.1 (q, *J* = 3.6, CHCHCCF₃), 123.9 (q, *J* = 3.6, CCHCCF₃), 124.0 (d, *J* = 272.0, CF₃), 122.5 (CHCN), 70.5 (C³H₂), 53.9 (C^{9a}H), 52.0 (C^{8a}H), 48.2 (C⁴H), 44.5 (C^{3a}H), 44.4 (C^{4a}H), 32.7 (C⁵H₂), 25.4 (C⁸H₂), 25.3 (C⁶H₂), 24.9 (C⁷H₂); IR (thin film) 2930 (C-H), 2858 (C-H), 1772 (C=O), 1706 (C=O), 1335, 1167, 1119, 1072, 998, 971, 810 cm⁻¹; m/z (ES+) 455 (100%, [M+H]⁺); HRMS (EI) calcd for C₂₆H₂₄O₃F₃N [M+H]⁺ 455.17028, observed 455.17029.

Purification by chiral column chromatography gave (+)-(3a*S*,4*R*,4a*R*,8a*S*,9a*S*)-4-((*E*)-2-(5-(3-(trifluoromethyl)phenyl)pyridin-2-yl)vinyl)octahydronaphtho[2,3-*c*]furan-1,9(3*H*,9a*H*)-dione ((+)-**94**) with an [α]_D²⁵ = +31.4 (MeOH) and (-)-(3a*S*,4*R*,4a*R*,8a*S*,9a*S*)-4-((*E*)-2-(5-(3-(trifluoromethyl)phenyl)pyridin-2-yl)vinyl)octahydronaphtho[2,3-*c*]furan-1,9(3*H*,9a*H*)-dione ((-)-**94**) with an [α]_D²⁵ = -31.3 (MeOH).

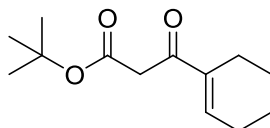
Ethyl 3-cyclohexenyl-3-oxopropanoate (**95**)



A solution of 1-(cyclohex-1-en-1-yl)ethanone (1.04 mL, 8.05 mmol) and diethyl carbonate (2.93 mL, 24.2 mmol) in *t*-BME (5 mL) was added dropwise to a stirred solution of KO*t*-Bu (1 M in THF) (16.1 mL, 16.1 mmol) under N₂. The reaction mixture was stirred at 20 °C for 16 hr and then quenched with sat. aq. NH₄Cl (10 mL). An extraction into *t*-BME (2 x 30 mL) was completed and the combined organic layers were dried (hydrophobic frit) and concentrated *in vacuo* to yield a crude orange oil. Purification by automated column chromatography (0-100% *t*-BME/cyclohexane) yielded ethyl 3-cyclohexenyl-3-oxopropanoate (**95**) (441 mg, 2.25 mmol, 28%) as a yellow oil. Some of the product existed in the enol form; ¹H NMR (400 MHz, CDCl₃) δ 12.13 (<1H, s, Enol-OH), 6.92-6.89 (1H, m, C=CH), 6.82-6.78 (<1H, m, Enol-C=CH), 5.13-5.11 (<1H, m, Enol-HC=COH), 4.22 (<2H, q,

$J = 7.2$, Enol- CH_2CH_3), 4.20 (2H, q, $J = 7.2$, CH_2CH_3), 3.68 (2H, s, $\text{C}=\text{OCH}_2\text{C}=\text{O}$), 2.32-2.20 (<6H, m, $\text{CH}_2\text{C}=\text{CH}$, $\text{C}=\text{CHCH}_2$ & Enol- $\text{CH}_2\text{C}=\text{CH}$), 2.17-2.12 (<2H, m, Enol- $\text{C}=\text{CHCH}_2$), 1.7-1.59 (<8H, m, 2 x CH_2 & 2 x Enol- CH_2), 1.31 (<3H, t, $J = 7.1$, Enol- CH_2CH_3), 1.28 (3H, t, $J = 7.1$, CH_2CH_3); ^{13}C NMR (150 MHz, CDCl_3) δ 193.6 ($\text{C}=\text{O}$), 168.6 ($\text{C}=\text{OOEt}$), 142.6 ($\text{CH}=\text{C}$), 139.2 ($\text{CH}=\text{C}$), 62.0 (OCH_2CH_3), 44.9 ($\text{C}=\text{OCH}_2\text{C}=\text{O}$), 26.5 ($\text{C}=\text{CHCH}_2$), 23.2 ($\text{CH}_2\text{C}=\text{CH}$), 21.9 (CH_2), 21.6 (CH_2), 13.8 (OCH_2CH_3); IR (thin film) 2933 (C-H), 2864 (C-H), 1731 ($\text{C}=\text{O}$), 1664 ($\text{C}=\text{O}$), 1187, 1031 cm^{-1} ; m/z (ES+) 197 (100%, $[\text{M}+\text{H}]^+$); HRMS (EI) calcd for $\text{C}_{11}\text{H}_{16}\text{O}_3$ $[\text{M}]^+$ 196.1094, observed 196.1095.

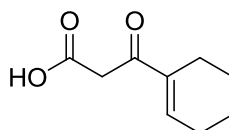
***tert*-Butyl 3-cyclohexenyl-3-oxopropanoate¹⁵³ (96)**



n-BuLi (1.6 M in hexanes) (12.3 mL, 19.6 mmol) was added dropwise to a stirred solution of DIPA (2.80 mL, 19.6 mmol) in anhydrous 2-MeTHF (20 mL) at 0 °C, under N_2 . The reaction mixture was stirred at 0 °C for 20 min and then cooled to -78 °C. Next, *tert*-butyl acetate (2.87 mL, 21.4 mmol) was added dropwise and stirring continued for 10 min at -78 °C. Finally, a solution of methyl cyclohex-1-enecarboxylate (0.47 mL, 3.57 mmol) in anhydrous 2-MeTHF (20 mL) was added. The reaction mixture was stirred at -78 °C for 4 h and then quenched with sat. aq. NH_4Cl (10 mL). An extraction into 2-MeTHF (2 x 30 mL) was completed and the combined organic layers were dried (hydrophobic frit) and concentrated *in vacuo* to yield a crude yellow oil. Purification by automated column chromatography (0-25% EtOAc/cyclohexane) yielded *tert*-butyl 3-cyclohexenyl-3-oxopropanoate (**96**) (757 mg, 3.38 mmol, 95%) as a colourless oil; ^1H NMR (400 MHz, Acetone- d_6) δ 7.00-6.95 (1H, m, $\text{C}=\text{CH}$), 3.61 (2H, s, $\text{C}=\text{OCH}_2\text{C}=\text{O}$), 2.31-2.24 (2H, m, $\text{CHHC}=\text{CH}$ & $\text{C}=\text{CHCHH}$), 2.22-2.16 (2H, m, 2 x CHH), 1.65-1.60 (4H, m, $\text{CHHC}=\text{CH}$, $\text{C}=\text{CHCHH}$ & 2 x CHH), 1.43 (9H, s, $\text{C}(\text{CH}_3)_3$); ^{13}C NMR (150 MHz, CDCl_3) δ 194.1 ($\text{C}=\text{O}$), 167.5 ($\text{C}=\text{OOEt}$), 142.1 ($\text{CH}=\text{C}$), 139.1 ($\text{CH}=\text{C}$), 81.6 ($\text{OC}(\text{CH}_3)_3$), 46.1 ($\text{C}=\text{OCH}_2\text{C}=\text{O}$), 28.0 ($\text{OC}(\text{CH}_3)_3$), 26.3 ($\text{C}=\text{CHCH}_2$), 23.1 ($\text{CH}_2\text{C}=\text{CH}$), 21.9 (CH_2),

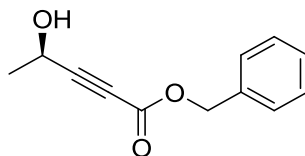
21.6 (CH₂); IR (thin film) 2975 (C-H), 2933 (C-H), 2862 (C-H), 1728 (C=O), 1668 (C=O), 1367, 1249, 1144, 962, 840 cm⁻¹; m/z (ES+) 225 (100%, [M+H]⁺); HRMS (EI) calcd for C₁₃H₂₀O₃ [M]⁺ 224.1407, observed 224.1412. Data agrees with that reported by Lavallée *et al.*¹⁵³

3-Cyclohexenyl-3-oxopropanoic acid (**97**)



TFA (1.25 mL, 16.2 mmol) was added to a stirred solution of *tert*-butyl 3-cyclohexenyl-3-oxopropanoate (**96**) (750 mg, 3.35 mmol) in CH₂Cl₂ (8 mL) under N₂. The reaction mixture was stirred at 20 °C for 2 h before being concentrated *in vacuo*. Purification by automated column chromatography (0-100% EtOAc/cyclohexane) yielded 3-cyclohexenyl-3-oxopropanoic acid (**97**) (465 mg, 2.77 mmol, 83%) as a colourless oil; ¹H NMR (400 MHz, Acetone-d₆) δ 4.87-4.80 (1H, m, C=CH), 3.12-3.08 (2H, m, C=OCH₂C=O), 2.88-2.81 (1H, m, CHHC=CH), 2.26-2.19 (1H, m, C=CHCHH), 1.89-1.77 (3H, m, CHHC=CH & 2 x CHH), 1.56 (1H, qt, *J* = 13.1, 3.6, CHH), 1.47-1.40 (1H, m, C=CHCHH), 1.33-1.20 (1H, m, CHH); m/z (ES+) 169 (100%, [M+H]⁺).

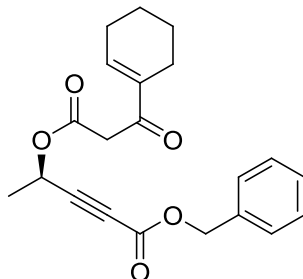
(*R*)-Benzyl 4-hydroxybut-2-ynoate¹⁴¹ (**98**)



HMDS (3.52 mL, 16.8 mmol) was added to a stirred solution of (*R*)-but-3-yn-2-ol (2.40 mL, 30.5 mmol) in anhydrous 2-MeTHF (15 mL), with a drop of H₂SO₄ added, under N₂. The reaction mixture was stirred at 70 °C for 16 h. Once cool, the reaction mixture was further cooled to -40 °C, *n*-BuLi (2.7 M in heptanes) (11.3 mL, 30.5 mmol) was added dropwise and stirring was continued for 1.5 h at -40 °C. The solution was then added, *via* cannular, to a stirred solution of benzyl chloroformate (5.23 mL, 36.6 mmol) in anhydrous 2-MeTHF (15 mL) and stirring was continued

for a further 30 min. Finally, aq. H₂SO₄ (6N, 12 mL) was added dropwise. The reaction mixture was stirred at 20 °C for a further 1 h. An extraction into *t*-BME (2 x 50 mL) was completed and the combined organic layers were washed with NH₄OH (50 mL) and sat. aq. brine (50 mL), dried (hydrophobic frit) and concentrated *in vacuo* to yield a crude brown oil. Purification by automated column chromatography (0-25% EtOAc/cyclohexane) yielded (*R*)-benzyl 4-hydroxypent-2-ynoate (**98**) (3.42 g, 16.8 mmol, 55%) as a colourless oil; ¹H NMR (400 MHz, CDCl₃) δ 7.41-7.38 (5H, m, 5 x Ar-CH), 5.23 (2H, s, Bz-CH₂), 4.65 (1H, qd, *J* = 6.7, 5.6, CHOH), 2.20 (1H, d, *J* = 5.6, CHOH), 1.52 (3H, d, *J* = 6.7, CH₃); ¹³C NMR (150 MHz, CDCl₃) δ 153.4 (C=O), 134.8 (Ar-C), 128.8 (2 x Ar-CH), 128.8 (2 x Ar-CH), 128.7 (Ar-CH), 89.0 (C≡C), 81.2 (CHOH), 75.8 (C≡C), 67.9 (Bz-CH₂), 23.4 (CH₃); IR (thin film) 2237, 1706 (C=O), 1373, 1232, 1056, 748, 697 cm⁻¹; *m/z* (ES⁺) 222 (100%, [M+H]⁺); HRMS (EI) calcd for C₁₂H₁₂O₃ [M]⁺ 204.0781, observed 204.0740. Data agrees with that reported by Fu *et al.*¹⁴¹

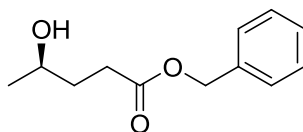
(*R*)-Benzyl 4-(3-cyclohexenyl-3-oxopropanoyloxy)pent-2-ynoate (99)



NBS (72.6 mg, 0.41 mmol) was added to a stirred solution of (*R*)-benzyl 4-hydroxypent-2-ynoate (**98**) (416 mg, 2.04 mmol) and ethyl 3-cyclohexenyl-3-oxopropanoate (**95**) (400 mg, 2.04 mmol) in toluene (8 mL) under N₂. The reaction mixture was stirred at 90 °C for 16 h, in a flask with a distillation arm attached, before being concentrated *in vacuo*. Purification by automated column chromatography (0-50% *t*-BME/cyclohexane) yielded a crude colourless oil. Further purification by MDAP (MeCN/H₂O with a formic acid modifier) yielded (*R*)-benzyl 4-(3-cyclohexenyl-3-oxopropanoyloxy)pent-2-ynoate (**99**) (27 mg, 0.076 mmol, 4%) as a colourless oil; ¹H NMR (400 MHz, CDCl₃) δ 7.41-7.37 (5H, m, 5 x

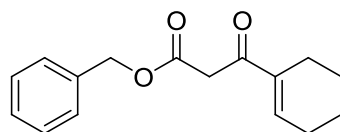
Ar-CH), 6.90-6.87 (1H, m, C=CH), 5.61 (1H, q, $J = 6.7$, OCHCH₃), 5.22 (2H, s, Bz-CH₂), 3.72 (2H, s, C=OCH₂C=O), 2.31-2.23 (4H, m, 2 x CH₂), 1.68-1.59 (4H, m, 2 x CH₂), 1.58 (3H, d, $J = 6.7$, CH₃); IR (thin film) 2938 (C-H), 2870 (C-H), 2856 (C-H), 1721 (C=O), 1656 (C=O), 1258, 1216, 1161, 1081, 733 cm⁻¹; m/z (ES+) 355 (100%, [M+H]⁺); HRMS (CI) calcd for C₂₁H₂₃O₅ [M+H]⁺ 355.1540, observed 355.1542.

(R)-Benzyl 4-hydroxypentanoate (100)



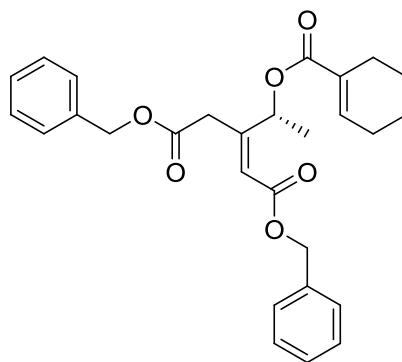
A solution of (*R*)-benzyl 4-hydroxypent-2-ynoate (**98**) (1.50 g, 7.34 mmol) in EtOH (20 mL) was added to Lindlar catalyst (120 mg, 1.13 mmol) and quinoline (0.26 mL, 2.20 mmol) under N₂. The reaction mixture was stirred under H₂ at 20 °C for 16 h. The reaction mixture was diluted with EtOAc (20 mL), filtered over celite and concentrated *in vacuo*. Purification by automated column chromatography (0-50% *t*-BME/cyclohexane) yielded (*R*)-benzyl 4-hydroxypentanoate (**100**) (712 mg, 3.42 mmol, 47%) as a colourless oil; ¹H NMR (400 MHz, CDCl₃) δ 7.40-7.34 (5H, m, 5 x Ar-CH), 5.15 (2H, s, Bz-CH₂), 3.91-3.81 (1H, m, CHOH), 2.53 (1H, dd, $J = 7.2, 0.5$, CHHC=O), 2.51 (1H, d, $J = 7.1$, CHHC=O), 1.88 (1H, td, $J = 7.4, 4.3$, COHCHH), 1.84 (1H, td, $J = 7.4, 4.3$, COHCHH), 1.23 (3H, d, $J = 6.2$, CH₃); ¹³C NMR (150 MHz, CDCl₃) δ 177.5 (C=O), 141.0 (Ar-C), 128.7 (2 x Ar-CH), 127.9 (Ar-CH), 127.2 (2 x Ar-CH), 77.4 (CHOH), 65.5 (Bz-CH₂), 29.9 (CH₂), 29.2 (CH₂), 21.2 (CH₃); IR (thin film) 3409 (br, OH), 2977 (C-H), 2932 (C-H), 2874 (C-H), 1760 (C=O), 1453, 1385, 1343, 1171, 1040, 1020, 940, 736, 698 cm⁻¹; m/z (ES+) 209 (100%, [M+H]⁺); HRMS (CI) calcd for C₁₂H₁₇O₃ [M+H]⁺ 209.1172, observed 209.1170.

Benzyl 3-cyclohexenyl-3-oxopropanoate (101)



NEt₃ (0.21 mL, 1.49 mmol) was added to a stirred solution of (*R*)-benzyl 4-hydroxypent-2-ynoate (**98**) (153 mg, 0.74 mmol) and ethyl 3-(cyclohex-1-en-1-yl)-3-oxopropanoate (**95**) (146 mg, 0.74 mmol) in toluene (3 mL) under N₂. The reaction mixture was stirred at 110 °C for 18 h, in a flask attached to a distillation arm, before being quenched with H₂O (10 mL). An extraction into EtOAc (2 x 20 mL) was completed and the combined organic layers were washed with sat. aq. brine (5mL), dried (hydrophobic frit) and concentrated *in vacuo* to yield a crude colourless oil. Purification by MDAP (MeCN/H₂O with an (NH₄)HCO₃ modifier) yielded benzyl 3-cyclohexenyl-3-oxopropanoate (**101**) (125 mg, 0.46 mmol, 65%) as a colourless oil; ¹H NMR (400 MHz, CDCl₃) δ 7.41-7.34 (5H, m, 5 x Ar-CH), 6.90-6.86 (1H, m, C=CH), 5.20 (2H, s, Bz-CH₂), 3.75 (2H, s, C=OCH₂C=O), 2.28-2.22 (4H, m, CH₂C=CH & C=CHCH₂), 1.68-1.56 (2H, m, 2 x CH₂); m/z (ES+) 259 (100%, [M+H]⁺).

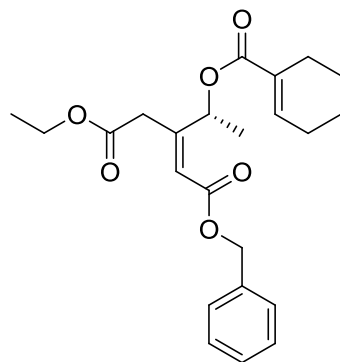
(*R,Z*)-Dibenzyl 3-(1-(cyclohex-1-enecarbonyloxy)ethyl)pent-2-enedioate (102)



Cs₂CO₃ (139 mg, 0.43 mmol) was added to a stirred solution of (*R*)-benzyl 4-hydroxypent-2-ynoate (**98**) (87.0 mg, 0.43 mmol) and benzyl 3-cyclohexenyl-3-oxopropanoate (**101**) (110 mg, 0.43 mmol) in EtOAc (10 mL) under N₂. The reaction mixture was stirred at 20 °C for 16 h and then quenched with H₂O (25 mL) and extracted into EtOAc (50 mL). The organic layer was washed with sat. aq. brine (25 mL), dried (hydrophobic frit) and concentrated *in vacuo* to yield a crude orange oil. Purification by automated column chromatography (0-25% EtOAc/cyclohexane) yielded a crude red oil. Further purification by MDAP

(MeCN/H₂O with an (NH₄)HCO₃ modifier) yielded (*R,Z*)-dibenzyl 3-(1-(cyclohex-1-enecarbonyloxy)ethyl)pent-2-enedioate (**102**) (13 mg, 0.028 mmol, 7%) as a yellow solid; ¹H NMR (400 MHz, CDCl₃) δ 7.40-7.32 (10H, m, 10 x Ar-CH), 7.00 (1H, dquin, *J* = 3.8, 2.1, C=CH), 6.16 (1H, s, C=CHC=O), 5.47 (1H, qd, *J* = 6.5, 1.0, OCHCH₃), 5.14 (2H, s, Bz-CH₂), 5.12 (2H, s, Bz-CH₂), 3.84 (1H, d, *J* = 16.6, CHHC=CH), 3.74 (1H, d, *J* = 16.6, CHHC=CH), 2.27-2.15 (4H, m, 2 x CH₂), 1.69-1.56 (4H, m, 2 x CH₂), 1.40 (3H, d, *J* = 6.5, CHCH₃); ¹³C NMR (100 MHz, CDCl₃) δ 169.5 (C=CHC=O), 166.1 (CC=OO), 165.7 (CCH₂C=O), 152.3 (C=CHC=O), 140.6 (Cyc-C=CH), 135.8 (2 x Bz-C), 130.0 (6 Cyc-C=CH), 128.6, 128.5, 128.4, 128.3, 128.2, 128.1 (10 x Ar-CH), 119.1 (C=CHC=O), 72.6 (CHCH₃), 66.7 (Bz-CH₂), 66.2 (Bz-CH₂), 34.5 (CCH₂C=O), 25.8 (CH₂), 24.0 (CH₂), 22.0 (CH₂), 21.4 (CH₂), 19.3 (CHCH₃); IR (thin film) 2936 (C-H), 1715 (C=O), 1233, 1149, 744, 698 cm⁻¹; m/z (ES+) 462 (100%, [M+H]⁺); HRMS (EI) calcd for C₂₈H₃₀O₆ [M]⁺ 462.2034, observed 462.2035.

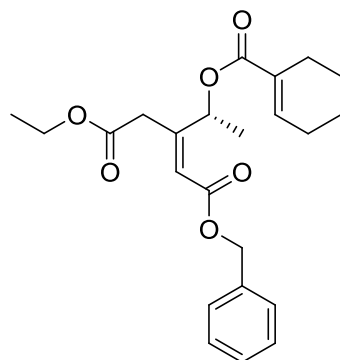
(*R,Z*)-1-Benzyl 5-ethyl 3-(1-(cyclohex-1-enecarbonyloxy)ethyl)pent-2-enedioate (103)



Cs₂CO₃ (498 mg, 1.53 mmol) was added to a stirred solution of (*R*)-benzyl 4-hydroxypent-2-ynoate (**98**) (312 mg, 1.53 mmol) and ethyl 3-cyclohexenyl-3-oxopropanoate (**95**) (300 mg, 1.53 mmol) in EtOAc (12 mL) under N₂. The reaction mixture was stirred at 20 °C for 16 h and then quenched with H₂O (15 mL). An extraction into EtOAc (2 x 30 mL) was completed and the combined organic layers were washed with sat. aq. brine (10 mL), dried (hydrophobic frit) and concentrated *in vacuo* to yield a crude orange oil. Purification by automated column

chromatography (0-50% EtOAc/cyclohexane) yielded a crude yellow oil. Further purification by MDAP (MeCN/H₂O with a formic acid modifier) yielded a 1:1 mixture of (*R,Z*)-1-benzyl 5-ethyl 3-(1-(cyclohex-1-enecarbonyloxy)ethyl)pent-2-enedioate (**103**) and (*R,E*)-5-benzyl 1-ethyl 3-(1-(cyclohex-1-enecarbonyloxy)ethyl)pent-2-enedioate (**104**) (42 mg, 0.10 mmol, 7%) and (*R*)-benzyl 4-(2-cyclohexenyl-2-oxoethyl)-5-methyl-2-oxo-2,5-dihydrofuran-3-carboxylate (**105**) (12 mg, 0.03 mmol, 2%). The 1:1 mixture was purified further by chiral column chromatography to yield (*R,Z*)-1-benzyl 5-ethyl 3-(1-(cyclohex-1-enecarbonyloxy)ethyl)pent-2-enedioate (**103**) (18 mg, 0.04 mmol, 3%) and (*R,E*)-5-benzyl 1-ethyl 3-(1-(cyclohex-1-enecarbonyloxy)ethyl)pent-2-enedioate (**104**) (18 mg, 0.04 mmol, 3%) as white solids.

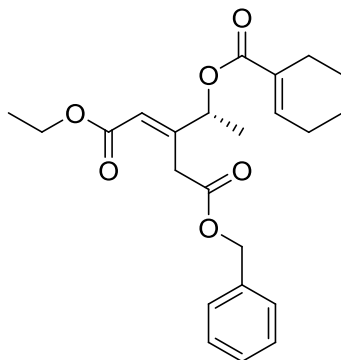
Data for (*R,Z*)-1-benzyl 5-ethyl 3-(1-(cyclohex-1-enecarbonyloxy)ethyl)pent-2-enedioate (**103**):



¹H NMR (400 MHz, CDCl₃) δ 7.40-7.32 (5H, m, 5 x Ar-CH), 7.02 (1H, dt, *J* = 3.8, 2.0, C=CH), 6.15 (1H, s, C=CHC=O), 5.47 (1H, qd, *J* = 6.8, 0.8, OCHCH₃), 5.17 (2H, s, Bz-CH₂), 4.13 (2H, q, *J* = 7.2, OCH₂CH₃), 3.78 (1H, d, *J* = 16.4, CHHC=CH), 3.68 (1H, d, *J* = 16.4, CHHC=CH), 2.30-2.18 (4H, m, 2 x CH₂), 1.72-1.57 (4H, m, 2 x CH₂), 1.42 (3H, d, *J* = 6.5, CHCH₃), 1.25 (3H, t, *J* = 7.2, CH₂CH₃); ¹³C NMR (150 MHz, CDCl₃) δ 169.6 (CCH₂C=O), 166.1 (CC=OO), 165.7 (C=CHC=O), 152.6 (C=CHC=O), 140.5 (Cyc-C=CH), 135.8 (Bz-C), 130.1 (Cyc-C=CH), 128.6 (2 x Ar-CH), 128.4 (Ar-CH), 128.3 (2 x Ar-CH), 118.9 (C=CHC=O), 72.6 (CHCH₃), 66.1 (Bz-CH₂), 60.9 (CH₂CH₃), 34.6 (CCH₂C=O), 25.8 (CH₂), 24.1 (CH₂), 22.0 (CH₂), 21.4 (CH₂), 19.0 (CHCH₃), 14.1 (CH₂CH₃); IR (thin film) 2933

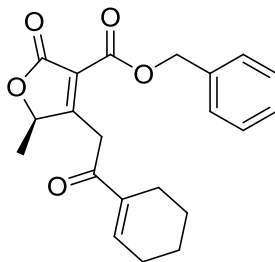
(C-H), 1708 (C=O), 1648 (C=O), 1230, 1146, 1033, 743, 697 cm^{-1} ; m/z (ES+) 401 (100%, $[\text{M}+\text{H}]^+$); HRMS (EI) calcd for $\text{C}_{23}\text{H}_{28}\text{O}_6$ $[\text{M}]^+$ 400.1880, observed 400.1885.

Data for (*R,E*)-5-benzyl 1-ethyl 3-(1-(cyclohex-1-enecarbonyloxy)ethyl)pent-2-enedioate (**104**):



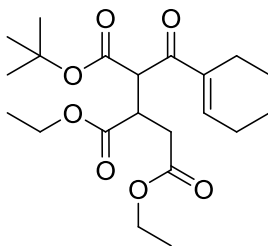
^1H NMR (400 MHz, CDCl_3) δ 7.41-7.32 (5H, m, 5 x Ar-CH), 7.01 (1H, tt, $J = 3.8, 1.8$, C=CH), 6.10 (1H, s, C=CHC=O), 5.47 (1H, qd, $J = 6.5, 1.0$, OCHCH₃), 5.14 (2H, s, Bz-CH₂), 4.15 (2H, qd, $J = 7.1, 0.5$, OCH₂CH₃), 3.82 (1H, d, $J = 16.6$, CHHC=CH), 3.72 (1H, d, $J = 16.6$, CHHC=CH), 2.29-2.16 (4H, m, 2 x CH₂), 1.70-1.56 (4H, m, 2 x CH₂), 1.40 (3H, d, $J = 6.8$, CHCH₃), 1.26 (3H, t, $J = 7.2$, CH₂CH₃); ^{13}C NMR (150 MHz, CDCl_3) δ 169.6 (CCH₂C=O), 166.2 (CC=OO), 165.9 (C=CHC=O), 151.5 (C=CHC=O), 140.5 (Cyc-C=CH), 135.8 (Bz-C), 130.1 (Cyc-C=CH), 128.5 (2 x Ar-CH), 128.1 (Ar-CH), 128.1 (2 x Ar-CH), 119.6 (C=CHC=O), 72.7 (CHCH₃), 66.7 (Bz-CH₂), 60.3 (CH₂CH₃), 34.4 (CCH₂C=O), 25.8 (CH₂), 24.1 (CH₂), 22.0 (CH₂), 21.4 (CH₂), 19.0 (CHCH₃), 14.2 (CH₂CH₃); IR (thin film) 2934 (C-H), 1708 (C=O), 1648 (C=O), 1230, 1146, 1070, 1034, 742, 697 cm^{-1} ; m/z (ES+) 401 (100%, $[\text{M}+\text{H}]^+$); HRMS (EI) calcd for $\text{C}_{23}\text{H}_{28}\text{O}_6$ $[\text{M}]^+$ 400.1880, observed 400.1885.

Data for (*R*)-benzyl 4-(2-cyclohexenyl-2-oxoethyl)-5-methyl-2-oxo-2,5-dihydrofuran-3-carboxylate (**105**):



^1H NMR (600 MHz, CDCl_3) δ 7.42-7.32 (5H, m, 5 x Ar-CH), 6.80-6.77 (1H, m, C=CH), 5.26 (1H, q, $J = 6.8$, OCHCH $_3$), 5.16 (2H, s, Bz-CH $_2$), 3.70 (1H, d, $J = 17.0$, CCHHC=O), 3.44 (1H, d, $J = 17.0$, CCHHC=O), 2.33-2.30 (2H, m, CH $_2$ C=CH), 2.27-2.21 (2H, m, C=CHCH $_2$), 1.71-1.61 (4H, m, 2 x CH $_2$), 1.49 (3H, d, $J = 6.9$, CHCH $_3$); ^{13}C NMR (150 MHz, CDCl_3) δ 190.3 (CH $_2$ C=O), 169.1 (CH=CC=O), 167.3 (CC=OOCH $_2$), 163.8 (C=CC=OO), 147.7 (Cyc-C=CH), 139.2 (Cyc-C=CH), 134.9 (Bz-C), 130.5 (C=OCC=O), 128.8 (2 x Ar-CH), 128.7 (Ar-CH), 128.4 (2 x Ar-CH), 78.9 (CHCH $_3$), 67.6 (Bz-CH $_2$), 32.7 (CCH $_2$ C=O), 26.4 (C=CHCH $_2$), 22.5 (CH $_2$ C=CH), 21.5 (CH $_2$), 21.4 (CH $_2$), 17.8 (CHCH $_3$); IR (thin film) 2941 (C-H), 1722 (C=O), 1230, 1154, 738, 697 cm^{-1} ; m/z (ES $^+$) 401 (100%, [M+H] $^+$); HRMS (CI) calcd for $\text{C}_{21}\text{H}_{23}\text{O}_5$ [M+H] $^+$ 355.1540, observed 355.1544.

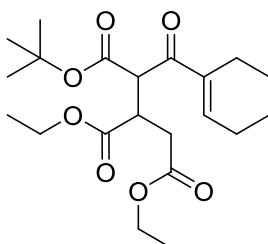
3-*tert*-Butyl 1,2-diethyl 4-oxodecahydronaphthalene-1,2,3-tricarboxylate (106)



Cs_2CO_3 (291 mg, 0.89 mmol) was added to a stirred solution of diethyl maleate (0.13 mL, 0.89 mmol) and *tert*-butyl 3-cyclohexenyl-3-oxopropanoate (**96**) (200 mg, 0.89 mmol) in EtOAc (4 mL) under N_2 . The reaction mixture was stirred at 20 °C for 20 h and then quenched with H_2O (10 mL). An extraction into EtOAc (2 x 20 mL) was completed and the combined organic layers were washed with sat. aq. brine (10 mL), dried (hydrophobic frit) and concentrated *in vacuo* to yield a crude yellow oil. Purification by automated column chromatography (0-25% *t*-BME/cyclohexane)

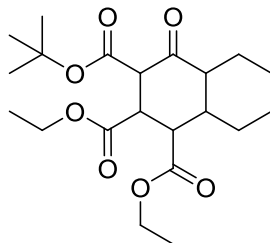
yielded a still crude colourless oil. Further purification by MDAP (MeCN/H₂O with an (NH₄)HCO₃ modifier) yielded 3-*tert*-butyl 1,2-diethyl 4-oxodecahydronaphthalene-1,2,3-tricarboxylate (**106**) (86 mg, 0.22 mmol, 24%) as a colourless oil and (1*S**,2*S**,3*R**,4*aS**,8*aR**)-3-*tert*-butyl 1,2-diethyl 4-oxodecahydronaphthalene-1,2,3-tricarboxylate (**107**) (13 mg, 0.03 mmol, 4%) as a white solid.

Data for 3-*tert*-butyl 1,2-diethyl 4-oxodecahydronaphthalene-1,2,3-tricarboxylate (**106**):



¹H NMR (600 MHz, CDCl₃) δ 4.24-4.13 (4H, m, 2 x OCH₂H₃), 3.66 (1H, t, *J* = 12.5, CHCO₂Et), 3.32 (1H, dd, *J* = 12.5, 3.9, CHCO₂Et), 3.26 (1H, d, *J* = 12.5, CHCO₂^tBu), 2.70-2.67 (1H, m, C=OCH), 2.60-2.55 (1H, m, CHCHCO₂Et), 2.31-2.27 (1H, m, CHH), 1.81-1.76 (1H, m, CHH), 1.53 (9H, s, C(CH₃)₃), 1.52-1.50 (1H, m, CHH), 1.49-1.41 (2H, m, CHH & CHH), 1.34-1.17 (8H, m, 2 x CHH & 2 x OCH₂H₃), 1.07 (1H, qd, *J* = 12.9, 3.3, CHH); ¹³C NMR (150 MHz, CDCl₃) δ 204.2 (C=O), 172.9 (C=OOEt), 171.8 (C=OOEt), 167.4 (C=OO^tBu), 81.9 (C(CH₃)₃), 61.4 (CO₂CH₂CH₃), 61.0 (CO₂CH₂CH₃), 59.1 (C=OCHC=O), 49.2 (C=OCHCH), 47.4 (C=OCHCH), 42.9 (CHCO₂CH₂CH₃), 40.8 (CHCO₂CH₂CH₃), 28.0 (C(CH₃)₃), 25.9 (CH₂), 25.3 (CH₂), 25.2 (CH₂), 21.4 (CH₂), 14.2 (CO₂CH₂CH₃), 14.1 (CO₂CH₂CH₃); IR (thin film) 2977 (C-H), 2933 (C-H), 1729 (C=O), 1671 (C=O), 1368, 1146, 1028, 843 cm⁻¹; *m/z* (ES+) 397 (100%, [M+H]⁺); HRMS (ES+) calcd for C₂₁H₃₃O₇ [M+H]⁺ 397.2226, observed 397.2228.

Data for (1*S**,2*S**,3*R**,4*aS**,8*aR**)-3-*tert*-butyl 1,2-diethyl 4-oxodecahydronaphthalene-1,2,3-tricarboxylate (**107**):



^1H NMR (600 MHz, CDCl_3) δ 4.24-4.13 (4H, m, 2 x OCH_2H_3), 3.66 (1H, t, $J = 12.5$, CHCO_2Et), 3.32 (1H, dd, $J = 12.5$, 3.9, CHCO_2Et), 3.26 (1H, d, $J = 12.5$, CHCO_2^tBu), 2.70-2.67 (1H, m, $\text{C}=\text{OCH}$), 2.60-2.55 (1H, m, CHCHCO_2Et), 2.31-2.27 (1H, m, CHH), 1.81-1.76 (1H, m, CHH), 1.53 (9H, s, $\text{C}(\text{CH}_3)_3$), 1.52-1.50 (1H, m, CHH), 1.49-1.41 (2H, m, CHH & CHH), 1.34-1.17 (8H, m, 2 x CHH & 2 x OCH_2H_3), 1.07 (1H, qd, $J = 12.9$, 3.3, CHH); ^{13}C NMR (150 MHz, CDCl_3) δ 204.2 ($\text{C}=\text{O}$), 172.9 ($\text{C}=\text{OOEt}$), 171.8 ($\text{C}=\text{OOEt}$), 167.4 ($\text{C}=\text{OO}^t\text{Bu}$), 81.9 ($\text{C}(\text{CH}_3)_3$), 61.4 ($\text{CO}_2\text{CH}_2\text{CH}_3$), 61.0 ($\text{CO}_2\text{CH}_2\text{CH}_3$), 59.1 ($\text{C}=\text{OCHC}=\text{O}$), 49.2 ($\text{C}=\text{OCHCH}$), 47.4 ($\text{C}=\text{OCHCH}$), 42.9 ($\text{CHCO}_2\text{CH}_2\text{CH}_3$), 40.8 ($\text{CHCO}_2\text{CH}_2\text{CH}_3$), 28.0 ($\text{C}(\text{CH}_3)_3$), 25.9 (CH_2), 25.3 (CH_2), 25.2 (CH_2), 21.4 (CH_2), 14.2 ($\text{CO}_2\text{CH}_2\text{CH}_3$), 14.1 ($\text{CO}_2\text{CH}_2\text{CH}_3$); IR (thin film) 2936 (C-H), 1729 (C=O), 1368, 1264, 1144, 1058, 1031, 847 cm^{-1} ; m/z (ES+) 397 (100%, $[\text{M}+\text{H}]^+$); HRMS (EI) calcd for $\text{C}_{21}\text{H}_{32}\text{O}_7$ $[\text{M}]^+$ 396.2143, observed 396.2142.

Biology

Biological testing of compounds was completed in collaboration with Prof. Rachel Chambers' research group at the Centre for Inflammation and Tissue Repair (UCL, Division of Medicine). Calcium mobilisation assay work was assisted by Dr. Natalia Smoktunowicz and Dr. Manuela Plate.

Materials and Methods

Reagents:

Thrombin, extracted from human plasma, was purchased from Calbiochem (Merck Biosciences, UK). PAR-1 agonist peptide and reverse peptide were supplied by

Bachem. The RWJ-58259 sample used as standard was synthesised by Dr. Eifion Robinson (University College London).

Cell Culture:

Primary human lung fibroblasts (pHLFs), grown from explant cultures of normal adult lung tissue, were a gift from Dr Robin J McAnulty (University College London). Cells were maintained in DMEM at 37 °C (10% CO₂) supplemented with glutamine (4 mM), penicillin, streptomycin, and 10% (v/v) FBS (all from Invitrogen) and were below passage 10 when used for experiments.

Measurement of Intracellular Ca²⁺ Levels:

pHLFs were seeded in clear-bottom, black, 96-well microplates at a density of 10,000 cells/well for 48 h and then quiesced for 24 h. Intracellular Ca²⁺ levels were assessed using the Fluo-4 AM kit (Invitrogen, UK) according to the manufacturer's instructions. The dye was dissolved in assay buffer (20 mM HEPES in HBSS) supplemented with 2.5 mM probenecid. Wells were aspirated and solutions of test compounds (3 mM in DMSO) were added. Serial dilution using dye buffer solution was done to give the desired final concentrations (100 µL per well). For positive controls, the equivalent volume of DMSO only was diluted in the dye buffer solution and added to the relevant wells. The cells were then incubated again at 37 °C (10% CO₂) for 30 min and at ambient conditions, in the dark, for 30 min. Cells were then stimulated by addition of a solution of thrombin in assay buffer (50 µL, 10 nM). Change in intracellular Ca²⁺ concentration was monitored in real-time using a fluorescent imaging plate reader (FLIPR® Tetra System, Molecular Devices, Inc). Measurements were taken every 1 sec for 1 min, then every 6 sec for a further 2 min. Experiments were performed in three replicates, on the same plate, at least twice. The data was plotted as change in relative fluorescence units (RFU) or as percentage inhibition.¹⁵⁴

References

1. Behr J. The Diagnosis and Treatment of Idiopathic Pulmonary Fibrosis. *Dtsch Arztebl Int.* 2013;110(51-52):875-881.
2. Travis WD, Costabel U, Hansell DM, et al. An Official American Thoracic Society/European Respiratory Society Statement: Update of the International Multidisciplinary Classification of the Idiopathic Interstitial Pneumonias. *Am J Resp Crit Care Med.* 2013;188(6):733-748.
3. King Jr TE, Pardo A, Selman M. Idiopathic pulmonary fibrosis. *Lancet.*378:1949-1961.
4. Idiopathic Pulmonary Fibrosis. *What is Idiopathic Pulmonary Fibrosis (IPF)?* <http://www.chss.org.uk/wp-content/uploads/ipf.jpg>.
5. Diagnosis and Initial Management of Nonmalignant Diseases Related to Asbestos. *Am J Respir Crit Care Med.* 2004;170(6):691-715.
6. Kishimoto T, Kato K, Arakawa H, Ashizawa K, Inai K, Takeshima Y. Clinical, Radiological, and Pathological Investigation of Asbestosis. *Int J Environ Res Public Health.* 2011;8(3):899-912.
7. Akira M, Yamamoto S, Inoue Y, Sakatani M. High-Resolution CT of Asbestosis and Idiopathic Pulmonary Fibrosis. *Am J Roentgenol.* 2003;181(1):163-169.
8. Ross RM. The clinical diagnosis of asbestosis in this century requires more than a chest radiograph. *Chest.* 2003;124(3):1120-1128.
9. Goswami E, Craven V, Dahlstrom D, Alexander D, Mowat F. Domestic Asbestos Exposure: A Review of Epidemiologic and Exposure Data. *Int J Environ Res Public Health.* 2013;10(11):5629-5670.
10. Idiopathic pulmonary fibrosis (IPF) cases linked with asbestos exposure [press release]. Munich: European Lung Foundation2014.
11. Sverzellati N. Highlights of HRCT imaging in IPF. *Respir Res.* 2013;14(Suppl 1):S3.
12. Spagnolo P, Tonelli R, Cocconcelli E, Stefani A, Richeldi L. Idiopathic pulmonary fibrosis: diagnostic pitfalls and therapeutic challenges. *Multidiscip Respir Med.* 2012;7(1):42.

13. Navaratnam V, Fleming KM, West J, et al. The rising incidence of idiopathic pulmonary fibrosis in the UK. *Thorax*. 2011;66(6):462-467.
14. Maher T. Does cancer get too much attention? 2014. <http://www.bbc.co.uk/news/health-29363887>.
15. Pardo A, Selman M. Idiopathic pulmonary fibrosis: new insights in its pathogenesis. *Int J Biochem Cell Biol*. 2002;34(12):1534-1538.
16. Loomis-King H, Flaherty KR, Moore BB. Pathogenesis, current treatments and future directions for idiopathic pulmonary fibrosis. *Curr Opin Pharmacol*. 2013;13(3):377-385.
17. Gunther A, Korfei M, Mahavadi P, von der Beck D, Ruppert C, Markart P. Unravelling the progressive pathophysiology of idiopathic pulmonary fibrosis. *Eur Respir Rev*. 2012;21(124):152-160.
18. Barkauskas CE, Noble PW. Cellular mechanisms of tissue fibrosis. 7. New insights into the cellular mechanisms of pulmonary fibrosis. *Am J Physiol Cell Physiol*. 2014;306(11):C987-996.
19. Hoyles RK, du Bois RM. Treatment of idiopathic pulmonary fibrosis: a European perspective. *Clin Pulm Med*. 2006;13(1):17-24.
20. Prednisone. <http://www.drugs.com/monograph/prednisone.html>.
21. Maltzman JS, Koretzky GA. Azathioprine: old drug, new actions. *J Clin Invest*. 2003;111(8):1122-1124.
22. Aitio M-L. N-acetylcysteine – passe-partout or much ado about nothing? *Brit J Clin Pharmacol*. 2006;61(1):5-15.
23. Behr J, Degenkolb B, Krombach F, Vogelmeier C. Intracellular glutathione and bronchoalveolar cells in fibrosing alveolitis: effects of N-acetylcysteine. *Eur Respir J*. 2002;19(5):906-911.
24. Demedts M, Behr J, Buhl R, et al. High-Dose Acetylcysteine in Idiopathic Pulmonary Fibrosis. *New Engl J Med*. 2005;353(21):2229-2242.
25. Woodcock H, Maher T. The treatment of idiopathic pulmonary fibrosis. *F1000Prime Rep*. 2014;6(16).
26. G. R, K.J. A, T.E. KJ, J.A L, F.J M. Prednisone, Azathioprine, and N-Acetylcysteine for Pulmonary Fibrosis. *N Engl J Med*. 2012;366(21):1968-1977.
27. Randomized Trial of Acetylcysteine in Idiopathic Pulmonary Fibrosis. *N Engl J Med*. 2014;370(22):2093-2101.

28. Noth I, Anstrom KJ, Calvert SB, et al. A placebo-controlled randomized trial of warfarin in idiopathic pulmonary fibrosis. *Am J Respir Crit Care Med.* 2012;186(1):88-95.
29. Malouf MA, Hopkins P, Snell G, Glanville AR. An investigator-driven study of everolimus in surgical lung biopsy confirmed idiopathic pulmonary fibrosis. *Respirology.* 2011;16(5):776-783.
30. Raghu G, Million-Rousseau R, Morganti A, Perchenet L, Behr J. Macitentan for the treatment of idiopathic pulmonary fibrosis: the randomised controlled MUSIC trial. *Eur Respir J.* 2013;42(6):1622-1632.
31. Douglas WW, Ryu JH, Schroeder DR. Idiopathic Pulmonary Fibrosis. *Am J Resp Crit Care.* 2000;161(4):1172-1178.
32. George TJ, Arnaoutakis GJ, Shah AS. Lung transplant in idiopathic pulmonary fibrosis. *Arch Surg.* 2011;146(10):1204-1209.
33. Regulatory watch : First drug for idiopathic pulmonary fibrosis approved in Japan. *Nat Rev Drug Discov.* 2008;7(12):966-967.
34. Gan Y, Herzog E, Gomer R. Pirfenidone treatment of idiopathic pulmonary fibrosis. *Ther Clin Risk Manag.* 2011;7:39-47.
35. China SFDA Approves F647/pirfenidone for the Treatment of Idiopathic Pulmonary Fibrosis [press release]. Evaluate2011.
36. Crestani B. A first step against idiopathic pulmonary fibrosis. *European Respiratory Review.* 2011;20(121):130-131.
37. Noble PW, Albera C, Bradford WZ, et al. Pirfenidone in patients with idiopathic pulmonary fibrosis (CAPACITY): two randomised trials. *Lancet.* 2011;377(9779):1760-1769.
38. King TE, Bradford WZ, Castro-Bernardini S, et al. A Phase 3 Trial of Pirfenidone in Patients with Idiopathic Pulmonary Fibrosis. *New Engl J Med.* 2014;370(22):2083-2092.
39. Designation For Pirfenidone, An Investigational Treatment For IPF [press release]. Market Watch2014.
40. Jiang C, Huang H, Liu J, Wang Y, Lu Z, Xu Z. Adverse Events of Pirfenidone for the Treatment of Pulmonary Fibrosis: A Meta-Analysis of Randomized Controlled Trials. *PLoS ONE.* 2012;7(10):e47024.
41. Onoue S, Seto Y, Kato M, Aoki Y, Kojo Y, Yamada S. Inhalable powder formulation of pirfenidone with reduced phototoxic risk for treatment of pulmonary fibrosis. *Pharm Res.* 2013;30(6):1586-1596.

42. Carroll J. Foiled in U.S., InterMune wins EU approval for pirfenidone. 2011; <http://www.fiercebiotech.com/press-releases/intermune-receives-european-union-approval-esbriet-pirfenidone>.
43. Antoniu SA. Nintedanib (BIBF 1120) for IPF: a tomorrow therapy? *Multidiscip Respir Med*. 2012;7(1):41.
44. Noble PW, Barkauskas CE, Jiang D. Pulmonary fibrosis: patterns and perpetrators. *J Clin Invest*. 2012;122(8):2756-2762.
45. Richeldi L, du Bois RM, Raghu G, et al. Efficacy and Safety of Nintedanib in Idiopathic Pulmonary Fibrosis. *New Engl J Med*. 2014;370(22):2071-2082.
46. Ryerson CJ, Collard HR. Hot off the breath: a big step forward for idiopathic pulmonary fibrosis. *Thorax*. 2014.
47. FibroGen Announces One-Year Data Supporting the Safety and Efficacy Profile of FG-3019 in Patients with Idiopathic Pulmonary Fibrosis [press release]. 2014.
48. Rafii R, Juarez MM, Albertson TE, Chan AL. A review of current and novel therapies for idiopathic pulmonary fibrosis. *J Thorac Dis*. 2013;5(1):48-73.
49. Garde D. FibroGen lines up a \$125M IPO to shoulder its way into the IPF race. 2014. <http://www.fiercebiotech.com/story/fibrogen-lines-125m-ipo-shoulder-its-way-ipf-race/2014-10-01>.
50. Macfarlane SR, Seatter MJ, Kanke T, Hunter GD, Plevin R. Proteinase-Activated Receptors. *Pharmacol Rev*. 2001;53(2):245-282.
51. Coughlin SR. Thrombin signalling and protease-activated receptors. *Nature*. 2000;407(6801):258-264.
52. Chen J, Ishii M, Wang L, Ishii K, Coughlin SR. Thrombin receptor activation. Confirmation of the intramolecular tethered liganding hypothesis and discovery of an alternative intermolecular liganding mode. *J Biol Chem*. 1994;269(23):16041-16045.
53. Ramachandran R, Noorbakhsh F, DeFea K, Hollenberg MD. Targeting proteinase-activated receptors: therapeutic potential and challenges. *Nat Rev Drug Discov*. 2012;11(1):69-86.
54. Lin H, Liu AP, Smith TH, Trejo J. Cofactoring and Dimerization of Proteinase-Activated Receptors. *Pharmacol Rev*. 2013;65(4):1198-1213.
55. Kaneider NC, Leger AJ, Agarwal A, et al. 'Role reversal' for the receptor PAR1 in sepsis-induced vascular damage. *Nat Immunol*. 2007;8(12):1303-1312.

56. McLaughlin JN, Patterson MM, Malik AB. Protease-activated receptor-3 (PAR3) regulates PAR1 signaling by receptor dimerization. *Proc Natl Acad Sci USA*. 2007;104(13):5662-5667.
57. Leger AJ, Jacques SL, Badar J, et al. Blocking the Protease-Activated Receptor 1-4 Heterodimer in Platelet-Mediated Thrombosis. *Circulation*. 2006;113(9):1244-1254.
58. Nakanishi-Matsui M, Zheng Y-W, Sulciner DJ, Weiss EJ, Ludeman MJ, Coughlin SR. PAR3 is a cofactor for PAR4 activation by thrombin. *Nature*. 2000;404(6778):609-613.
59. Bah A, Chen Z, Bush-Pelc LA, Mathews FS, Di Cera E. Crystal structures of murine thrombin in complex with the extracellular fragments of murine protease-activated receptors PAR3 and PAR4. *P Natl Acad Sci USA*. 2007;104(28):11603-11608.
60. Kahn ML, Nakanishi-Matsui M, Shapiro MJ, Ishihara H, Coughlin SR. Protease-activated receptors 1 and 4 mediate activation of human platelets by thrombin. *J Clin Invest*. 1999;103(6):879-887.
61. Chackalamannil S, Xia Y. Thrombin receptor (PAR-1) antagonists as novel antithrombotic agents. *Expert Opin Ther Pat*. 2006;16(4):493-505.
62. Chackalamannil S. Thrombin receptor (protease activated receptor-1) antagonists as potent antithrombotic agents with strong antiplatelet effects. *J Med Chem*. 2006;49(18):5389-5403.
63. Howell DCJ, Johns RH, Lasky JA, et al. Absence of Proteinase-Activated Receptor-1 Signaling Affords Protection from Bleomycin-Induced Lung Inflammation and Fibrosis. *Am J Pathol*. 2005;166(5):1353-1365.
64. C. HD, Laurent GJ, Chambers RC. Role of thrombin and its major cellular receptor, protease-activated receptor-1, in pulmonary fibrosis. *Biochem Soc Trans*. 2002;30(2):211-216.
65. Lin C, Duitman J, Daalhuisen J, et al. Targeting protease activated receptor-1 with P1pal-12 limits bleomycin-induced pulmonary fibrosis. *Thorax*. 2014;69(2):152-160.
66. Schwarz MI, King TE. *Interstitial Lung Disease*. People's Medical Publishing House; 2010.
67. Andrade-Gordon P, Maryanoff BE, Derian CK, et al. Design, synthesis, and biological characterization of a peptide-mimetic antagonist for a tethered-ligand receptor. *P Natl Acad Sci USA*. 1999;96(22):12257-12262.
68. Zhang H-C, Derian CK, Andrade-Gordon P, et al. Discovery and Optimization of a Novel Series of Thrombin Receptor (PAR-1)

- Antagonists: Potent, Selective Peptide Mimetics Based on Indole and Indazole Templates. *J Med Chem.* 2001;44(7):1021-1024.
69. Ahn HS, Foster C, Boykow G, et al. Binding of a thrombin receptor tethered ligand analogue to human platelet thrombin receptor. *Mol Pharmacol.* 1997;51(2):350-356.
 70. Andrade-Gordon P, Derian CK, Maryanoff BE, et al. Administration of a Potent Antagonist of Protease-Activated Receptor-1 (PAR-1) Attenuates Vascular Restenosis Following Balloon Angioplasty in Rats. *J Pharmacol Exp Ther.* 2001;298(1):34-42.
 71. Damiano BP, Derian CK, Maryanoff BE, Zhang HC, Gordon PA. RWJ-58259: a selective antagonist of protease activated receptor-1. *Cardiovasc Drug Rev.* 2003;21(4):313-326.
 72. Suzuki S, Kotake M, Miyamoto M, Kawahara T, Inventors. 2-Iminopyrrolidine Derivatives. 2002.
 73. Matsuoka T, Kogushi M, Kawata T, et al. Inhibitory effect of E5555, an orally active thrombin receptor antagonist, on intimal hyperplasia following balloon injury. *J Am Coll Cardiol.* 2004;43(5s1):A68.
 74. Kogushi M, Matsuoka T, Kuramochi H, et al. Oral administration of the thrombin receptor antagonist E5555 (atopaxar) attenuates intimal thickening following balloon injury in rats. *Eur J Pharmacol.* 2011;666(1-3):158-164.
 75. Kogushi M, Matsuoka T, Kawata T, et al. The novel and orally active thrombin receptor antagonist E5555 (Atopaxar) inhibits arterial thrombosis without affecting bleeding time in guinea pigs. *Eur J Pharmacol.* 2011;657(1-3):131-137.
 76. Ueno M, Ferreiro JL, Angiolillo DJ. Mechanism of action and clinical development of platelet thrombin receptor antagonists. *Expert Rev Cardiovasc Ther.* 2010;8(8):1191-1200.
 77. M. Takeuchi MK, S. Kitamura, R. Hagino, H. Ozawa, H. Tanaka. Pharmacodynamics and safety of a novel Protease Activated Receptor-1 antagonist E5555 for healthy volunteers. ECS Congress; 2007; Vienna, Austria.
 78. Goto S, Ogawa H, Takeuchi M, Flather MD, Bhatt DL, Investigators JL. Double-blind, placebo-controlled Phase II studies of the protease-activated receptor 1 antagonist E5555 (atopaxar) in Japanese patients with acute coronary syndrome or high-risk coronary artery disease. *Eur Heart J.* 2010;31(21):2601-2613.

79. Diltiazem. <http://www.drugs.com/diltiazem.html>.
80. Metformin. <http://www.drugs.com/metformin.html>.
81. Kimura N, Masuda S, Tanihara Y, et al. Metformin is a superior substrate for renal organic cation transporter OCT2 rather than hepatic OCT1. *Drug Metab Pharmacokinet.* 2005;20(5):379-386.
82. Serebruany VL, Kogushi M, Dastros-Pitei D, Flather M, Bhatt DL. The in-vitro effects of E5555, a protease-activated receptor (PAR)-1 antagonist, on platelet biomarkers in healthy volunteers and patients with coronary artery disease. *Thromb Haemostasis.* 2009;102(7):111-119.
83. Doller D, Chackalamannil S, Czarniecki M, McQuade R, Ruperto V. Design, synthesis, and structure-activity relationship studies of himbacine derived muscarinic receptor antagonists. *Bioorg Med Chem Lett.* 1999;9(6):901-906.
84. Chackalamannil S, Asberob T, Xia Y, Doller D, Clasby MC, Czarniecki MF, Inventors. Thrombin Receptor Antagonists. 1999.
85. Chackalamannil S, Xia Y, Greenlee WJ, et al. Discovery of potent orally active thrombin receptor (protease activated receptor 1) antagonists as novel antithrombotic agents. *J Med Chem.* 2005;48(19):5884-5887.
86. Xia Y, Chackalamannil S, Clasby M, et al. Himbacine derived thrombin receptor (PAR-1) antagonists: SAR of the pyridine ring. *Bioorg Med Chem Lett.* 2007;17(16):4509-4513.
87. Clasby MC, Chackalamannil S, Czarniecki M, et al. Metabolism-based identification of a potent thrombin receptor antagonist. *J Med Chem.* 2007;50(1):129-138.
88. Chelliah MV, Chackalamannil S, Xia Y, et al. Heterotricyclic himbacine analogs as potent, orally active thrombin receptor (protease activated receptor-1) antagonists. *J Med Chem.* 2007;50(21):5147-5160.
89. Chackalamannil S, Wang YG, Greenlee WJ, et al. Discovery of a novel, orally active himbacine-based thrombin receptor antagonist (SCH 530348) with potent antiplatelet activity. *J Med Chem.* 2008;51(11):3061-3064.
90. Kosoglou T, Reyderman L, Tiessen R, et al. Trap-induced platelet aggregation following single and multiple rising oral doses of SCH 530348, a novel thrombin receptor antagonist, in healthy volunteers. 2009.
91. Reyderman L, Kosoglou T, Kasserra C, et al. Lack of ethnic differences in the pharmacodynamics (PD) and pharmacokinetics

- (PK) of SCH 530348, a novel oral antiplatelet agent, in Japanese and Caucasian subjects. *Clin Pharmacol Ther.* 2009;85(S1):S21 PI-41.
92. Kosoglou T, Reyderman L, Kasserra C, et al. Optimizing dose of the novel thrombin receptor antagonist SCH 530348 based on pharmacodynamics and pharmacokinetics in healthy subjects. *Clin Pharmacol Ther.* 2008;83(S1):S55 PII-42.
 93. Reyderman L, Kosoglou T, Tseng J, et al. The effect of food and antacid on pharmacokinetics (PK) of SCH 530348 in healthy subjects. *Clin Pharmacol Ther.* 2009;85(S1):S21 PI-42.
 94. Becker RC, Moliterno DJ, Jennings LK, et al. Safety and tolerability of SCH 530348 in patients undergoing non-urgent percutaneous coronary intervention: a randomised, double-blind, placebo-controlled phase II study. *Lancet.* 2009;373:919-928.
 95. Goto S, Yamaguchi T, Ikeda Y, Kato K, Yamaguchi H, Jensen P. Safety and Exploratory Efficacy of the Novel Thrombin Receptor (PAR-1) Antagonist SCH530348 for Non-ST-Segment Elevation Acute Coronary Syndrome. *J Atheroscler Thromb.* 2010;17(2):156-164.
 96. Shinohara Y, Goto S, Shimizu K, Jensen P. A phase II safety study of novel antiplatelet agent, SCH 530348, in Japanese patients with prior ischemic stroke. 2008;3(S1):138 PO101-193.
 97. Harrington RA, VdWF, Armstrong PW, Aylward P, Park B, Veltri E, Mahaffey KW, Moliterno DJ, Strony J, Wallentin L, White HD, Diaz R, Aylward P, Huber K, Van de Werf F, Nicolau JC, Armstrong PW, Prieto JC, Isaza D, Widimsky P, Grande P, Nieminen M, Montalescot G, Bode C, Wong L, Ofner P, Lewis BS, Ambrosio G, Valgimigli M, Ogawa H, Yamaguchi T, Jukema JW, Cornel JH, White HD, Nordrehaug JE, Ruzylo W, Providencia L, Tan HC, Dalby A, Seung-Jung P, Betriu A, Cequier A, Held C, Pfisterer M, Chen MF, Timurkaynak T, Storey RF, Chen E, Harrington RA, Hudson MP, Lincoff AM, Mahaffey KW, Morrow DA, Tricoci P, Whellan D. The Thrombin Receptor Antagonist for Clinical Event Reduction in Acute Coronary Syndrome (TRA*CER) trial: study design and rationale. *Am Heart J.* 2009;158(3):327-334.
 98. Morrow DA, Scirica BM, Fox KAA, et al. Evaluation of a novel antiplatelet agent for secondary prevention in patients with a history of atherosclerotic disease: Design and rationale for the Thrombin-Receptor Antagonist in Secondary Prevention of

- Atherothrombotic Ischemic Events (TRA 2°P)-TIMI 50 trial. *Am Heart J*.158(3):335-341.e333.
99. Tricoci P, Huang Z, Held C, et al. Thrombin-receptor antagonist vorapaxar in acute coronary syndromes. *N Engl J Med*. 2012;366(1):20-33.
 100. Bonaca MP, Scirica BM, Creager MA, et al. Vorapaxar in patients with peripheral artery disease: results from TRA2°P-TIMI 50. *Circulation*. 2013;127(14):1522-1529, 1529e1521-1526.
 101. FDA approves Zontivity to reduce the risk of heart attacks and stroke in high-risk patients [press release]. FDA2014.
 102. Zontivity. <http://www.zontivity.com/>.
 103. Ahn H-S, Arik L, Boykow G, et al. Structure-activity relationships of pyrroloquinazolines as thrombin receptor antagonists. *Bioorg Med Chem Lett*. 1999;9(14):2073-2078.
 104. Chackalamannil S, Doller D, Eagen K, et al. Potent, low molecular weight thrombin receptor antagonists. *Bioorg Med Chem Lett*. 2001;11(21):2851-2853.
 105. Barrow JC, Nantermet PG, Selnick HG, et al. Discovery and initial structure–activity relationships of trisubstituted ureas as thrombin receptor (PAR-1) antagonists. *Bioorg Med Chem Lett*. 2001;11(20):2691-2696.
 106. Nantermet PG, Barrow JC, Lundell GF, et al. Discovery of a nonpeptidic small molecule antagonist of the human platelet thrombin receptor (PAR-1). *Bioorg Med Chem Lett*. 2002;12(3):319-323.
 107. Severino B, Fiorino F, Perissutti E, et al. Synthesis and pharmacological evaluation of peptide-mimetic protease-activated receptor-1 antagonists containing novel heterocyclic scaffolds. *Bioorg Med Chem*. 2008;16(11):6009-6020.
 108. Ventosa-Andrés P, Valdivielso ÁM, Pappos I, García-López MT, Tsopanoglou NE, Herranz R. Design, synthesis and biological evaluation of new peptide-based ureas and thioureas as potential antagonists of the thrombin receptor PAR1. *Eur J Med Chem*. 2012;58:98-111.
 109. Lee S, Song J-H, Park CM, et al. Discovery of Octahydroindenes as PAR1 Antagonists. *Med Chem Lett*. 2013;4(11):1054-1058.
 110. Perez M, Lamothe M, Maraval C, et al. Discovery of Novel Protease Activated Receptors 1 Antagonists with Potent Antithrombotic Activity in Vivo. *J Med Chem*. 2009;52(19):5826-5836.

111. Planty B, Pujol C, Lamothe M, et al. Exploration of a new series of PAR1 antagonists. *Bioorg Med Chem Lett*. 2010;20(5):1735-1739.
112. Létienne R, Leparq-Panissié A, Calmettes Y, Nadal-Wollbold F, Perez M, Le Grand B. Antithrombotic activity of F16618, a new PAR1 antagonist evaluated in extracorporeal arterio-venous shunt in the rat. *Biochem Pharmacol*. 2010;79(11):1616-1621.
113. Fukunaga R, Hirano K, Hirano M, et al. Upregulation of proteinase-activated receptors and hypercontractile responses precede development of arterial lesions after balloon injury. *Am J Physiol-Heart C*. 2006;291(5):H2388-H2395.
114. Bocquet A, Létienne R, Sablayrolles S, De Vries L, Perez M, Le Grand B. Effects of a new PAR1 antagonist, F16618, on smooth muscle cell contraction. *Eur J Pharmacol*. 2009;611(1–3):60-63.
115. Kai Y, Hirano K, Maeda Y, Nishimura J, Sasaki T, Kanaide H. Prevention of the Hypercontractile Response to Thrombin by Proteinase-Activated Receptor-1 Antagonist in Subarachnoid Hemorrhage. *Stroke*. 2007;38(12):3259-3265.
116. Rilatt I, Mirabel E, Grand BL, Perez M. Discovery and SAR of small molecule PAR1 antagonists. *Bioorg Med Chem Lett*. 2010;20(3):903-906.
117. Deng X, Mercer PF, Scotton CJ, Gilchrist A, Chambers RC. Thrombin Induces Fibroblast CCL2/JE Production and Release via Coupling of PAR1 to Gαq and Cooperation between ERK1/2 and Rho Kinase Signaling Pathways. *Mol Biol Cell*. 2008;19(6):2520-2533.
118. Asteriti S, Daniele S, Porchia F, et al. Modulation of PAR1 signaling by benzimidazole compounds. *Brit J Pharmacol*. 2012;167(1):80-94.
119. Dowal L, Sim DS, Dilks JR, et al. Identification of an antithrombotic allosteric modulator that acts through helix 8 of PAR1. *P Natl Acad Sci USA*. 2011;108(7):2951-2956.
120. Dockendorff C, Aisiku O, VerPlank L, et al. Discovery of 1,3-Diaminobenzenes as Selective Inhibitors of Platelet Activation at the PAR1 Receptor. *Med Chem Lett*. 2012;3(3):232-237.
121. Ortiz-Stern A.
122. Grimmett MR. Ring Syntheses Involving Formation of Two Bonds: [4+1] Fragments. *Imidazole and Benzimidazole Synthesis*. San Diego: Academic Press; 1997:63-102.

123. Algul O, Kaessler A, Apcin Y, Yilmaz A, Jose J. Comparative studies on conventional and microwave synthesis of some benzimidazole, benzothiazole and indole derivatives and testing on inhibition of hyaluronidase. *Molecules*. 2008;13(4):736-748.
124. Le Z-G, Chen Z-C, Hu Y, Zheng Q-G. Organic Reactions in Ionic liquids: N-Alkylation of Phthalimide and Several Nitrogen Heterocycles. *Synthesis*. 2004(02):208-212.
125. Kogushi M, Inventor. Pharmaceutical composition, use of 2-iminopyrrolidine derivative for production of pharmaceutical composition, and kit for treatment or amelioration of heart diseases. 2010.
126. Rinner U, Lentsch C, Aichinger C. Syntheses of Galbulimima Alkaloids. *Synthesis*. 2010:3763-3784.
127. Casey M, McCarthy R. A New Strategy for the Synthesis of Himbacine. *Synlett*. 2011(6):801-804.
128. Breuning M, Steiner M. Convenient Multigram Synthesis of (*R*)-Homopipericolic Acid Methyl Ester. *Synthesis*. 2006(08):1386-1389.
129. Bull JA, Charette AB. Improved Procedure for the Synthesis of gem-Diiodoalkanes by the Alkylation of Diiodomethane. Scope and Limitations. *J Org Chem*. 2008;73(20):8097-8100.
130. Yamaguchi M, Tsukamoto M, Hirao I. A highly stereoselective synthesis of carbocyclic compounds by the michael induced intramolecular alkylation a stereocontrol of extracyclic chiral centers. *Tetrahedron Lett*. 1985;26(14):1723-1726.
131. Harcken C, Brückner R, Rank E. Total Syntheses of (-)-Grandinolide and (-)-Sapranthin by the Sharpless Asymmetric Dihydroxylation of Methyl trans-3-Pentenoate: Elucidation of the Stereostructure of (-)-Sapranthin. *Chem Eur J*. 1998;4(11):2342-2352.
132. Fukuyama T, Lin SC, Li L. Facile reduction of ethyl thiol esters to aldehydes: application to a total synthesis of (+)-neothramycin A methyl ether. *J Am Chem Soc*. 1990;112(19):7050-7051.
133. Zhang C, Srinivasan Y, Arlow DH, et al. High-resolution crystal structure of human protease-activated receptor 1. *Nature*. 2012;492(7429):387-392.
134. Tan J, Akakura M, Yamamoto H. The Supersilyl Group as a Carboxylic Acid Protecting Group: Application to Highly Stereoselective Aldol and Mannich Reactions. *Angew Chem Int Edit*. 2013;52(28):7198-7202.

135. Nakanishi J, Tatamidani H, Fukumoto Y, Chatani N. A New Synthesis of Aldehydes by the Palladium-Catalyzed Reaction of 2-Pyridinyl Esters with Hydrosilanes. *Synlett*. 2006(06):869-872.
136. Priefer R, Farrell PG, Harpp DN. Effective synthetic routes to cubylcarbinol derivatives. *Synthesis*. 2002:2671.
137. Perner RJ, Lee C-H, Jiang M, et al. Synthesis and biological evaluation of 6,7-disubstituted 4-aminopyrido[2,3-d]pyrimidines as adenosine kinase inhibitors. *Bioorg Med Chem Lett*. 2005;15(11):2803-2807.
138. Yamaguchi Y, Ochi T, Wakamiya T, Matsubara Y, Yoshida Z-i. New Fluorophores with Rod-Shaped Polycyano π -Conjugated Structures: Synthesis and Photophysical Properties. *Org Lett*. 2006;8(4):717-720.
139. Ibrahim N, Chevot F, Legraverend M. Regioselective Sonogashira cross-coupling reactions of 6-chloro-2,8-diiodo-9-THP-9H-purine with alkyne derivatives. *Tetrahedron Lett*. 2011;52(2):305-307.
140. Fallahi-Sichani M, Honarnejad S, Heiser LM, Gray JW, Sorger PK. Metrics other than potency reveal systematic variation in responses to cancer drugs. *Nat Chem Biol*. 2013;9(11):708-714.
141. Fu X, Yin J, Thiruvengadam TK, McAllister TL, Tann C-H, Colon C. Improved Large-Scale Synthesis of (*R*)-Benzyl 4-Hydroxyl-2-pentynoate from (*R*)-3-Butyn-2-ol. *Org Process Res Dev*. 2002;6(3):308-310.
142. Ramachandran SA, Kharul RK, Marque S, et al. Synthetic Studies toward Highly Functionalized 5 β -Lanosterol Derivatives: A Versatile Approach Utilizing Anionic Cycloaddition. *J Org Chem*. 2006;71(16):6149-6156.
143. Algul O Fau - Kaessler A, Kaessler A Fau - Apcin Y, Apcin Y Fau - Yilmaz A, Yilmaz A Fau - Jose J, J J. - Comparative studies on conventional and microwave synthesis of some benzimidazole, benzothiazole and indole derivatives and testing on inhibition of hyaluronidase. *Molecules*. 2008;13(4):736-748.
144. Matsushita H, Lee S-H, Joung M, Clapham B, Janda KD. Smart cleavage reactions: the synthesis of benzimidazoles and benzothiazoles from polymer-bound esters. *Tetrahedron Lett*. 2004;45(2):313-316.
145. Cetinkaya B, Cetinkaya E, A. Chamizo J, et al. Synthesis and structures of 1,3,1',3'-tetrabenzyl-2,2'-biimidazolidinylidenes (electron-rich alkenes), their amination intermediates and their

- degradation products. *J Chem Soc Perk T 1*. 1998(13):2047-2054.
146. Nieto CT, Salgado MM, Domínguez SH, Díez D, Garrido NM. Rapid access with diversity to enantiopure flexible PNA monomers following asymmetric orthogonal strategies. *Tetrahedron-Asymmetr*. 2014;25(13–14):1046-1060.
 147. Tufariello JJ, Trybulski EJ. Synthetic approach to the skeleton of histrionicotoxin. *J Org Chem*. 1974;39(23):3378-3384.
 148. Zhou Z, Larouche D, Bennett SM. Reactions of some alkynyl halides with Samarium(II) iodide. *Tetrahedron*. 1995;51(43):11623-11644.
 149. Scarborough RM, Toder BH, Smith AB. A stereospecific total synthesis of (.+.-)-methylenomycin A and its epimer, (.+.-)-epimethylenomycin A. *J Am Chem Soc*. 1980;102(11):3904-3913.
 150. Takahata H, Uchida Y, Momose T. New Synthesis of All Four Isomers of 3-Hydroxy-4-methyl- γ -butyrolactone by Stereoselective Intramolecular Lactonization. Application to Asymmetric Synthesis of Biologically Active Compounds. *J Org Chem*. 1994;59(24):7201-7208.
 151. Takadoi M, Katoh T, Ishiwata A, Terashima S. Synthetic studies of himbacine, a potent antagonist of the muscarinic M2 subtype receptor 1. Stereoselective total synthesis and antagonistic activity of enantiomeric pairs of himbacine and (2'S,6'R)-diepihimbacine, 4-epihimbacine, and novel himbacine congeners. *Tetrahedron*. 2002;58(50):9903-9923.
 152. Usami K, Isobe M. Low-temperature photooxygenation of coelenterate luciferin analog synthesis and proof of 1,2-dioxetanone as luminescence intermediate. *Tetrahedron*. 1996;52(37):12061-12090.
 153. Lavallée J-F, Spino C, Ruel R, Hogan KT, Deslongchamps P. Stereoselective synthesis of cis-decalins via Diels–Alder and double Michael addition of substituted Nazarov reagents. *Can J Chemistry*. 1992;70(5):1406-1426.
 154. Ortiz-Stern A, Deng X, Smoktunowicz N, Mercer PF, Chambers RC. PAR-1-dependent and PAR-independent pro-inflammatory signaling in human lung fibroblasts exposed to thrombin. *J Cell Physiol*. 2012;227(11):3575-3584.